Imperial College London
Department of Medicine

Metabolic Profiling of ASS1 Negative and ASS1 Positive Glioblastoma Subtypes to Identify Novel Targets for Therapy

Julia Kerstin Langer

July 2016

Supervised by Dr. Nelofer Syed
and Dr. Elizabeth Want

Submitted in part fulfilment of the requirements for the degree of
Doctor of Philosophy in Medicine of Imperial College London
and the Diploma of Imperial College London

Abstract

Glioblastoma multiforme (GBM) are the most common and most malignant brain tumours. Despite treatment advances, average survival remains unacceptably low with 15-months [49], hence novel therapies are desperately needed. Cellular metabolism plays a central role in cancers. Sensitivity towards arginine-deprivation via treatment with pegylated arginine deiminase (ADI-PEG20) therapy has been identified in GBM, arresting proliferation in methylated arginino-succinate-synthetase-1^{M} (ASS1^{M}) and not unmethylated ASS1 (ASS1^{U}) GBM cells [126]. Advances of biochemical techniques and analysis have facilitated therapeutic target identification as well as biomarker discovery [45] [80].

Complimentary analysis via gas-chromatography coupled with mass spectrometry and ^{1}hydrogen nuclear-magnetic-resonance spectrometry of *in vitro* GBM cells identified distinct metabolic profiles in ASS1 subtypes. Intracellular and extracellular analysis of GBM cells exposed to ADI-PEG20 treatment elucidated metabolic perturbations in the arginine, creatine, glycolytic, uridine, citric acid, thymine and glutamine pathways, induced by arginine deprivation.

Transcriptional analysis of perturbed pathways elucidated differentially altered enzymatic expression in ASS1 GBM subtypes upon ADI-PEG20 treatment. Significantly modulated enzymes included transcriptional downregulation of thymidylate synthase (TYMS) in ASS1^{M} GBM cells, whereas ASS1^{U} remained unaltered. Significantly altered enzymatic mRNA expression also identified modulation of glutamic pyruvate transaminase 2 (GPT2) in ASS1^{M} cells, as well as thymidine kinase 2 (TK2) and alanine-glyoxylate aminotransferase 2 (AGXT2) in ASS1^{U} GBM.

Targeting the *de novo* thymine and creatine metabolic pathway, demonstrated that phytic acid (IP6) arrested proliferation in GBM cells, whereas creatine supplementation boosted proliferation. IP6 arrested proliferation in a time- and dose-dependent manner, irrespective of ASS1 status. Combining IP6 and ADI-PEG20, showed arrested proliferation was enhanced, compared to either treatment alone in ASS1^{M} GBM cells.

Acknowledgements

My sincere gratitude to project supervisors Dr. Nelofer Syed and Dr. Elizabeth Want for the opportunity of conducting research with them and their support throughout my PhD. I would also like to thank collaborators, Prof. Eric Chan-Chun Yong (National University of Singapore), Dr. Yanjun Hong and Dr. Henrik Antti (Umea University).

Further, special thanks to Dr. Fernando Abaitua Elustondo, Dr. Boling Qiao and Dr. Combiz Khozoie, Alexander Renziehausen, Dr. Sabrina Lamour, Dr. Lina Moeren, Dr. Michael Kyriakides, Dr. Gabriel Valbuena and Dr. Chiara Marini Bettolo for their guidance, help and continual encouragement.

I sincerely thank my family and friends, especially Angela de Manzanos and Zhana Kuncheva and Reinhard Fellmann for their support.

Sincere gratitude goes to Anabelle Grassini, Wendy Fulcher and Kevin O'Neill. Special thanks also to Mohammad Awad and Dr. Ilaria Bravi. This PhD project was made possible through the Grassini studentship and supported by the Brain Tumour Research Campaign, registered charity no. 295895. Further thanks to the Imperial College International office for enabling the international research exchange with Prof. Eric Chan at the National University of Singapore.

Declaration of Originality

I hereby certify that the present thesis is in full the work of the author, with the work of others appropriately acknowledged.

Copyright Declaration

The copyright of this thesis rests with the author and is made available under a Creative Commons Attribution Non-Commercial No Derivatives licence. Researchers are free to copy, distribute or transmit the thesis on the condition that they attribute it, that they do not use it for commercial purposes and that they do not alter, transform or build upon it. For any reuse or redistribution, researchers must make clear to others the licence terms of this work.

Contents

1 Introduction **18**

1.1 Glioblastoma multiforme overview 18

1.1.1 Prevalence of GBM 19

1.1.2 Clinical challenges in diagnosing and treating GBM 19

1.2 Cancer and metabolism 23

1.2.1 Overview of cancer metabolism 23

1.2.2 Oncometabolites 25

1.2.3 Arginine, ASS1 and arginine deprivation therapy by ADI-PEG20 30

1.3 Metabolomics 35

1.3.1 Metabolomics overview and applications to GBM . 35

1.3.2 GC/TOF MS 38

1.3.3 ^{1}H NMR 40

1.3.4 Chemometrics 42

1.4 Hypothesis and study aims 44

1.5 Objectives 44

2 Methods and Materials **45**

2.1 Tissue culture 45

2.1.1 Cell lines and culture conditions 45

2.1.2 Drugs and reagents 46

2.1.3 Cell proliferation assay 46

2.1.4 Luciferase assay 46

2.1.5 Cell culture experiments for GC/TOF MS 47

2.1.6 Cell culture experiments for ^{1}H NMR 47

2.2 GC/TOF MS 49

2.2.1 Sample preparation, metabolite extraction, derivatisation 49

2.2.2 GC/TOF MS analysis and instrumental setting . . 50
2.2.3 Data processing 51
2.2.4 Compound identification 51
2.2.5 Statistical analysis 51
2.3 ^{1}H NMR 53
2.3.1 Sample preparation and metabolite extraction . . . 53
2.3.2 ^{1}H NMR analysis and instrumental settings 53
2.3.3 Data processing 54
2.3.4 Statistical analysis 54
2.4 Transcriptional investigations (RT-QPCR) 56
2.4.1 RNA extraction from cultured cells and quantification 56
2.4.2 Reverse transcription and cDNA conversion 56
2.4.3 Quantitative real-time PCR and analysis 56

3 Results: Metabolic characterisation of ASS1 GBM subtypes 59
3.1 Introduction 59
3.1.1 Aims 60
3.1.2 Objectives 60
3.2 Results 61
3.2.1 Establishment of conditions for cell culture experimentation 61
3.2.2 GC/TOF MS: Metabolic characterisation of ASS1 GBM subtypes 63
3.2.3 Profiling via GC/TOF MS 64
3.2.4 GC/TOF MS: Distinct basal metabolic profile of ASS1 subtypes in GBM cell lines as determined by PCA and PLS-DA 66
3.2.5 Arginine deprivation alters global metabolic profile of ASS1^{M} GBM cell lines 70
3.2.6 ^{1}H NMR: Complementary metabolic characterisation of ASS1 GBM subtypes 79
3.2.7 Experimental parameters 79

3.2.8 ^{1}H NMR validates global GC/TOF MS observations: Distinct basal metabolic profile of ASS1 subtypes in GBM cell lines . . . 81
3.2.9 ^{1}H NMR: Metabolic alteration upon ADI-PEG20 treatment . . . 86
3.2.10 Validation of trends in ASS1 GBM subtypes via ^{1}H NMR analysis . . . 91
3.2.11 Experimental parameters . . . 91
3.2.12 ^{1}H NMR: Validation of global basal level trends in ASS1 subtypes . . . 94
3.3 Discussion . . . 108
3.3.1 Basal profiles present limited metabolic differences amongst ASS1 subtypes in GBM cell lines . . . 108
3.3.2 Arginine deprivation via ADI-PEG20 alters global metabolic profile in ASS1^{M} GBM cell lines . . . 110
3.3.3 Modulation of arginine, glycolytic, citric acid, thymine and glutamine pathway in GBM cell lines upon ADI-PEG20 treatment . . . 114
3.3.4 Metabolic techniques for studying ADI-PEG20 treatment response . . . 115
3.3.5 Study limitations . . . 116
3.3.6 Conclusions . . . 117

4 Results: Transcriptional studies and metabolic pathway investigations 118
4.1 Introduction . . . 118
4.1.1 Aims . . . 120
4.1.2 Objectives . . . 120
4.2 Results . . . 121
4.2.1 Transcriptional expression of enzymes associated with altered GBM metabolism . . . 121
4.2.2 Biological interpretation . . . 123
4.2.3 Validating TYMS transcriptional expression . . . 128
4.2.4 Basal levels of TYMS in ASS1^{M} and ASS1^{U} GBM subtypes . . . 128

4.2.5 Downregulation of TYMS in ASS1^{M} subtypes upon ADI-PEG20 treatment . . . 129
4.3 Discussion . . . 131
4.3.1 Arginine deprivation alters transcriptional expression of metabolic enzymes in ASS1 subtypes . . . 131
4.3.2 Systematic database and literature review presents enzymatic roles in cancers and metabolic inhibitors 132
4.3.3 RT-QPCR validates transcriptional down-regulation of TYMS upon ADI-PEG20 treatment in ASS1^{M} cells . . . 133
4.3.4 Study limitations . . . 137
4.3.5 Conclusions . . . 137

5 Results: IP6 arrests proliferation and enhances effect of ADI-PEG20 in ASS1^{M} GBM cells, while creatine promotes proliferation 139
5.1 Introduction . . . 139
5.1.1 Aims . . . 141
5.1.2 Objectives . . . 141
5.2 Results . . . 142
5.2.1 IP6 arrests proliferation of GBM cell lines . . . 142
5.2.2 Enhanced effect of ADI-PEG20 via IP6 in ASS1^{M} cell lines . . . 144
5.2.3 Combination of ADI-PEG20 and IP6 potentiates further down-regulation of TYMS . . . 147
5.2.4 Arginine deprivation via ADI-PEG20 compromises the creatine pathway . . . 149
5.3 Discussion . . . 156
5.3.1 IP6 arrests proliferation in GBM cell lines . . . 156
5.3.2 IP6 and ADI-PEG20 combination enhance arrested proliferation in ASS1^{M} cells but not ASS1^{U} . . . 157
5.3.3 Combination treatment down-regulates TYMS mRNA expression in ASS1^{M} GBM cells . . . 157
5.3.4 Creatine stimulates proliferation, yet mechanism can not be attributed to ATP changes . . . 158
5.3.5 Study limitations . . . 160

5.3.6 Conclusions 161
5.3.7 Future work 163

6 Final discussion and concluding remarks 165
6.1 Summary of main findings 165
6.1.1 Metabolic characterisation of ASS1 GBM subtypes 166
6.1.2 Transcriptional studies and metabolic pathway investigations 167
6.1.3 IP6 arrests proliferation and enhances effect of ADI-PEG20 in $ASS1^{M}$ GBM cells, while creatine promotes proliferation 168
6.1.4 Future directions 170
6.1.5 Concluding remarks 172

A Appendix 192
A.1 Appendix to section 2.2: Data set for GC/TOF MS analysis 192
A.2 Appendix to section A.2: GC/TOF MS: Metabolic characterisation of ASS1 GBM subtypes 223
A.3 Appendix to section 3.2.6: ^{1}H NMR: Complementary metabolic characterisation of ASS1 GBM subtypes 225
A.4 Appendix to section 3.2.10: Validation of trends in ASS1 GBM subtypes via ^{1}H NMR analysis 229

List of Tables

1.1 Overview of metabolites associated with cancers 29

2.1 Standards of GC/TOF MS analysis 50
2.2 Primers for QPCR 58

3.1 GC/TOF MS: Putative discriminant metabolites of ASS1 subtypes 69
3.2 GC/TOF MS: Putative discriminant metabolites of untreated control versus ADI-PEG20 treated $ASS1^{M}$ cell extract 75
3.3 GC/TOF MS: Putative discriminant metabolites of untreated control versus ADI-PEG20 treated $ASS1^{M}$ cell media 76
3.4 GC/TOF MS: Putative discriminant metabolites of control versus ADI-PEG20 treated $ASS1^{U}$ cells 77
3.5 GC/TOF MS: Putative discriminant metabolites of control versus ADI-PEG20 treated astrocyte cells 78
3.6 ^{1}H NMR: Discriminant metabolites amongst ASS1 subtypes at basal level 86
3.7 ^{1}H NMR: Discriminant metabolites amongst ASS1 subtypes 90
3.8 ^{1}H NMR validation: Discriminant metabolites amongst ASS1 subtypes at basal levels 100
3.9 ^{1}H NMR validation: Discriminant metabolites amongst $ASS1^{M}$ cells 106
3.10 ^{1}H NMR validation: Discriminant metabolites amongst $ASS1^{U}$ cells 107
3.11 ^{1}H NMR validation: Discriminant metabolites amongst Non-GBM cells 107

3.12 Comparative summary: Putative discriminant metabolites of GC/TOF MS and ^{1}H NMR analysis 109
3.13 ASS1^{M} comparative summary: Putative discriminant metabolites of GC/TOF MS and ^{1}H NMR analysis . . . 111
3.14 ASS1^{U} comparative summary: Putative discriminant metabolites of GC/TOF MS and ^{1}H NMR analysis 112
3.15 Astrocyte comparative summary: Putative discriminant metabolites of GC/TOF MS and ^{1}H NMR analysis . . . 113

4.1 Overview of enzyme pathway, catalytic reaction and protein expression 126
4.2 Synthesis of literature review: biological interpretation . 127

A.1 Raw data of GC/TOF MS: media 193
A.2 Raw data of GC/TOF MS: extract 215

List of Figures

1.1 MRI and histology form part of clinical standard for GBM diagnosis 20
1.2 Stupp [124] protocol forms standard of clinical treatment in GBM 22
1.3 Biochemical shift towards aerobic glycolysis in GBM cells via Warburg effect 24
1.4 Features of oncometabolite 2-hydroxuglutarate in glioma 26
1.5 Metabolic cycle of arginine 31
1.6 ADI-PEG20 in clinical trials 34
1.7 Overview of work flow and experimental techniques use for metabolomic profiling 37
1.8 Schematic overview of basic GC/TOF MS instrumentation 39
1.9 Schematic overview of basic ^{1}H NMR instrumentation . 41
1.10 Overview of principal component analysis 43

3.1 GBM cell proliferation and sensitivity to ADI-PEG20 . . 62
3.2 Cell count determination in ASS1 GBM subtypes for GC/TOF MS analysis 63
3.3 GC/TOF MS: highlighting quality control 65
3.4 GC/TOF MS: Distinct metabolic profile of ASS1 subtypes at basal levels 67
3.5 GC/TOF MS: PLS-DA and permutation test of ASS1^{M} and ASS1^{U} extracts at basal levels 68
3.6 GC/TOF MS: Global metabolic alteration upon ADI-PEG20 treatment in ASS1^{M} GBM cell line profiles . . . 71
3.7 GC/TOF MS: Representative PLS-DA and permutation test plot of cell extract in presence of ADI-PEG20 73
3.8 Cell count determination at 48 hours in ASS1 GBM subtypes for ^{1}H NMR analysis 80

3.9 ^{1}H NMR: Control of ADI-PEG20 treatment effect via arginine and citrulline 81
3.10 ^{1}H NMR: basal metabolic profile 82
3.11 ^{1}H NMR: OPLS-DA correlation coefficient plot of cell extract from ASS1 subtypes 84
3.12 ^{1}H NMR: OPLS-DA correlation coefficient plot of media from ASS1 subtypes 85
3.13 ^{1}H NMR: metabolic profile upon ADI-PEG20 treatment 87
3.14 ^{1}H NMR of cell extract: OPLS-DA correlation coefficient plot of ASS1^{M} control versus treatment 88
3.15 ^{1}H NMR of cell media: OPLS-DA correlation coefficient plot of GBM control versus treatment 89
3.16 Cell count determination at 48 hours in ASS1 GBM subtypes for ^{1}H NMR validation 92
3.17 Representative CPMG and 1D NOESY ^{1}H NMR spectra 93
3.18 ^{1}H NMR validation: Internal control of ADI-PEG20 effect 94
3.19 ^{1}H NMR validation: PCA of metabolic profiles in media 95
3.20 ^{1}H NMR validation: PCA of basal metabolic profiles . . 96
3.21 ^{1}H NMR validation of extract: OPLS-DA correlation coefficient plot 98
3.22 ^{1}H NMR validation: OPLS-DA correlation coefficient plot of media from ASS1 subtypes 99
3.23 ^{1}H NMR validation: PCA of extract group comparison upon ADI-PEG20 treatment 102
3.24 ^{1}H NMR validation: PCA of media group comparison upon ADI-PEG20 treatment 103
3.25 Representative ^{1}H NMR: OPLS-DA correlation coefficient plot of cell extract upon treatment 104
3.26 Representative ^{1}H NMR: OPLS-DA correlation coefficient plot of cell media upon treatment 105

4.1 ASS1^{M} RT-QPCR: ADI-PEG20 modulates expression of enzymes associated with citric acid, glycolytic and thymine pathways in ASS1^{M} cells 122

4.2 $ASS1^{U}$ RT-QPCR: ADI-PEG20 modulates expression of enzymes associated with citric acid, glycolytic and thymine pathways in $ASS1^{U}$ cells 123
4.3 Basal mRNA expression of TYMS determined by RT-QPCR 129
4.4 RT-QPCR expression of TYMS upon ADI-PEG20 treatment 130
4.5 TYMS and thymine synthesis pathway 136

5.1 IP6 titration: SRB proliferation assay 143
5.2 IP6 and ADI-PEG20 combination treatment: SRB proliferation assay 146
5.3 RT-QPCR: Transcriptional down-regulation of TYMS in $ASS1^{M}$, yet not $ASS1^{U}$ GBM cells upon IP6 and ADI-PEG20 combination treatment. 148
5.4 ^{1}H NMR: Fold-decrease of creatine in $ASS1^{M}$ GBM cells 150
5.5 Creatine metabolism via arginine and glycine 151
5.6 GC/TOF MS: Fold-increase of glycine in $ASS1^{M}$ GBM cells 152
5.7 Creatine supplementation boost proliferation in GBM cell: creatine titration and SRB proliferation assay . . . 154
5.8 Luciferase assay: ATP content is not enhanced by creatine supplementation in GBM cells 155

A.1 GC/TOF MS: PLS-DA and permutation test of $ASS1^{M}$ and $ASS1^{U}$ media at basal levels 223
A.2 GC/TOF MS: Cell extract PLS-DA plots and permutation validation upon ADI-PEG20 treatment 224
A.3 GC/TOF MS: Cell media PLS-DA plots and permutation validation upon ADI-PEG20 treatment 224
A.4 Extract ^{1}H NMR: OPLS-DA correlation coefficient plot of $ASS1^{U}$ control versus treatment 225
A.5 Extract ^{1}H NMR: OPLS-DA correlation coefficient plot of non-GBM control versus treatment 226
A.6 Media ^{1}H NMR: OPLS-DA correlation coefficient plot of $ASS1^{U}$ control versus treatment 227

A.7 Media ^{1}H NMR: OPLS-DA correlation coefficient plot of non-GBM control versus treatment 228
A.8 ^{1}H NMR validation: OPLS-DA correlation coefficient plot of U87 extract 229
A.9 ^{1}H NMR validation: OPLS-DA correlation coefficient plot of U118 extract 230
A.10 ^{1}H NMR validation: OPLS-DA correlation coefficient plot of GAMG extract 231
A.11 ^{1}H NMR validation: OPLS-DA correlation coefficient plot of LN229 extract 232
A.12 ^{1}H NMR validation: OPLS-DA correlation coefficient plot of U87 media 233
A.13 ^{1}H NMR validation: OPLS-DA correlation coefficient plot of U118 media 234
A.14 ^{1}H NMR validation: OPLS-DA correlation coefficient plot of GAMG media 235
A.15 ^{1}H NMR validation: OPLS-DA correlation coefficient plot of LN229 media 236
A.16 ^{1}H NMR validation: OPLS-DA correlation coefficient plot of astrocyte media 237

Nomenclature

Abbrevations

^{1}H NMR	1-hydrogen nuclear magnetic resonance
ADI-PEG20	Arginine Deiminase-Polyethylene Glycol-20
ASL	Argininosuccinate lyase
ASS1^{M}	methylated argininosuccinate synthetase 1
ASS1^{U}	unmethylated argininosuccinate synthetase 1
ASS1	Argininosuccinate synthetase 1
ATCC	American Type Tissue Culture Collection
BBB	Blood-brain-barrier
cDNA	Complementary DNA
CPMG	Carr-Purcell Meiboom-Gill spin echo pulse programme
CV	Coefficient of variation
D_2O	Deuterium oxide
DMEM	Dulbecco's Modified Eagle Medium
DMSO	Dimethylsulphoxide
DNA	Deoxyribonucleic acid
dNTP	Deoxynucleoside triphosphates
DSMZ	German Collection of Microorganisms and Cell Cultures
dTMP	Deoxythymidylate monophosphate
DTT	Dithiothreitol
dTTP	Deoxythymidine triphosphate
dUMP	Deoxyuridine monophosphate
EDTA	Ethylenediaminetetraacetic acid
FBS	Foetal bovine serum
FID	Free induction decay
GBM	Glioblastoma multiforme
GC/TOF MS	Gas-chromatography time-of-flight / mass-spectrometry
H_20	Distilled water
HIF1	Hypoxia-inducible factor-1
IDH	Isocitrate dehydrogenase
IP6	Phytic acid
M-MLV	Moloney murine leukemia virus
MGMT	O-6-methylguanine-DNA methyltransferase
mRNA	Messenger ribonucleic acid
MSTFA	N-methyl-n-(trimethylsilyl)-trifluoroacetamide
NAN_3	Sodium azide

NS	Not statistically significant
OD	Optical density
OPLS-DA	Orthogonal projection to latent structures discriminatory analysis
PBS	Phosphate buffered saline
PCA	Principal component analysis
PCR	Polymerase chain reaction
PLS-DA	Projections to latent structures discriminatory analysis
RT	Room temperature
RT-QPCR	Reverse transcriptase-quantitative PCR
SD	Standard deviation
SEM	Standard error of mean
SRB	Sulphorhodamine B
TCA	Tricholoracetic acid
TK	Thymidine kinase
TMZ	Temozolomide
Tris	tris(hydroxymethyl)aminomethane
TSP	3-(Trimethylsilyl)propionic-2,2,3,3-d_4-acid sodium salt
TYMS	Thymidylate synthase
VIP	Variable importance in projection

Letters, Symbols and Units

μg	Micrograms
μl	Microlitre
μm	Micrometre
g	Grams
n	Number
p	p-value
ppm	Parts per million
r	Correlation coefficient
rpm	Rotations per minute
s	Seconds
K	Kelvin
M	Molar
mg	Milligrams
MHz	Megahertz
min	Minutes
mM	Millimolar
mm	Millimetre
ns	Number of acquired scans
Q_2	Parameter for predictive ability of multivariate model

1. Introduction

1.1. Glioblastoma multiforme overview

Glioblastoma multiforme (GBM) are the most common and most malignant brain tumours. Treatment consists of surgery, radio- and temozolomide chemo-therapy [124], however average survival remains unacceptably low with only 15-months [49]. Novel therapies overcoming treatment challenges (section 1.1.2), including tumour heterogeneity, treatment resistances and difficulty in achieving complete resection [90], are desperately needed.

Cellular metabolism plays a central role in cancers (section 1.2), and sensitivity towards arginine-deprivation via ADI-PEG20 therapy has been identified in a subset of GBM cells [126] (section 1.2.3). Metabolic therapies are particularly attractive for use in GBM, overcoming some of the treatment challenges, such as the blood-brain-barrier, by acting systemically. Advances in biochemical techniques, including GC/TOF MS and ^{1}H NMR, and chemometric analysis (section 1.3) have facilitated metabolic studies, making this a strong approach for therapeutic target identification and biomarker discovery [45], [80] (section 1.3).

1.1.1. Prevalence of GBM

Annual incidence of GBM is low compared to other cancers, with 3 per 100,000 in the population [14], yet disease progression is fast and mortality is high with an average survival of only 15-months [49]. The majority of GBM arise *de novo*, whereas 5% of cases have clinical history of progression from low grade gliomas and are referred to as secondary GBM [98].

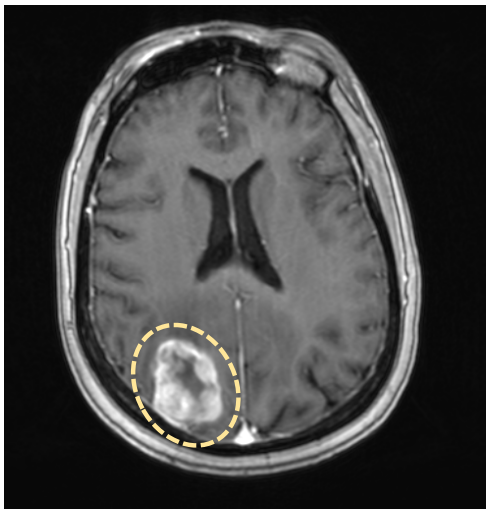
GBM can occur at any age, yet *de novo* tumours predominantly arise in patients in their 60's, and secondary GBM in people in their 40's [98]. In the UK, brain tumours make-up 2% of all cancers, yet the prognosis for malignant brain tumours is dismal with a one-year survival of 30% for both males and females, and five-year survival of 15% in England and Wales [85].

Major direct causes leading to development of GBM have not been identified. Only for a small subset of patients have previous ionising radiation exposure, for example through childhood cancer treatment, and this has been associated as a risk factor [120]. Smoking, diet, head injury, viral infections and mobile phone use have however not demonstrated to be significant contributing factors [93], [49]. In less than 10% of gliomas, rare genetic pathologies, including Li Fraumeni syndrome, type 1- and 2- neurofibromatosis, Turcot- and Cowden-syndrome, predispose individuals [110], yet numbers contributing towards total GBM incidence are low.

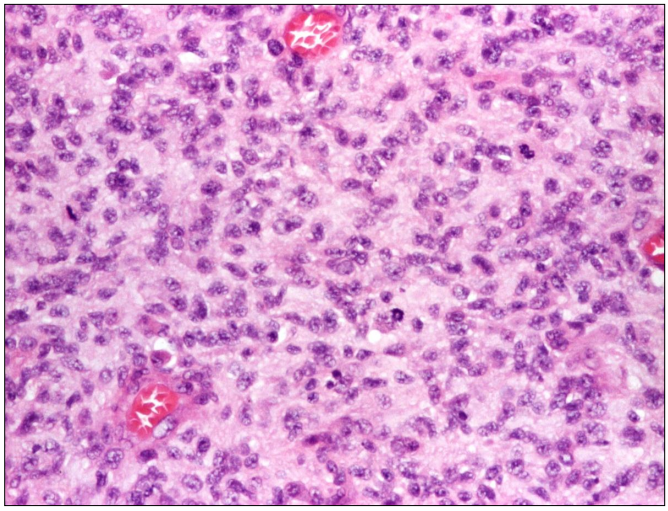
1.1.2. Clinical challenges in diagnosing and treating GBM

The clinical standard for diagnosis of GBM continues to rely on magnetic resonance imaging (MRI) and histopathological tumour-staging according to World Health Organisation (WHO) classification (figure 1.1).

Histologically features of GBM have been described as cells of astrocytic lineage with heterogenous populations, mitotic species, diffuse cell infiltration, as well as manifestation of necrosis and angiogenesis [94] (example of histological GBM tissue section shown in caption *b.* of figure 1.1).



(a)



(b)

Figure 1.1.: MRI and histology form part of clinical standard for GBM diagnosis. GBM diagnosis consists of MRI imaging and histopathological tissue staining from biopsies or excised tumour. (a) Pre-operative MRI of GBM, with tumour circled in yellow. Courtesy of Mr. Mohammed Awad and Mr. Kevin O'Neill. (b) Histopathological tissue section of GBM showing heterogenous cell populations, mitotic species and diffuse cell infiltration. Courtesy of Dr. Ilaria Bravi.

Clinical standard of treatment follows the Stupp protocol [124] (overview in figure 1.2), focusing on surgical resection, cycles of radio-therapy and chemo-therapy via temozolomide. Introduction of the Stupp protocol significantly improved treatment outcome, yet successes are limited with an increase in median survival from 11% to 27% compared to radiotherapy and surgery alone [124]. Surgical resection continues to be the most life-enhancing measure [124], with *aggressive* resection showing enhanced survival compared to *complete* resection. Despite these advances, 85% of recurrences are found at sites of resection [103] and tumour excision remains challenging through the diffuse nature of GBM cells and presence of CD133+ cells, which are highly resistant to apoptotic death [160].

Temozolomide (TMZ) is a DNA-alkylating agent which exerts it's action by methylating the O^6 position of the nucleobase guanine [42]. Compared to radio-therapy and surgery alone, addition of TMZ improved median survival by 3.5 months [33]. Despite the significant clinical advances made through TMZ administration, resistances have been found to occur, linked to methylation of O^6-methylguanine-DNA methyltransferase (MGMT), which reverts TMZ-induced methylation [14],[55]. Subsequently prognosis, response rate and survival of patients with methylation of the MGMT gene is higher than those with non-methylated MGMT [44].

Other chemo-therapies including the biodegradable, drug-emulting carmustine wafers implanted during surgery, have been employed in order to overcome challenges of the blood-brain-barrier (BBB). Unfortunately carmustine wafers have not translated into wide-spread clinical success, as their use has also been linked to infections [86].
Second-line chemotherapies also remain unsatisfactory and no standard of treatment has been determined [44]. In the United States, bevacizumab, an anti-VEGF monoclonal antibody, has been employed, however in view of limited survival improvement the European Medicines Agency did not approve use in Europe [109].

Chemo-therapies in clinical trials for GBM include small molecules, antibodies, platelet-derived growth factor receptors, and other inhibitors [110]. Electric field therapies are also being tested, with clinical studies of elec-

tric field treatment showing acceptable toxicity [125], yet only improved treatment through a few weeks of delay in GBM disease progression [116]. Increasingly metabolic therapies for GBM are also reaching clinical testing. Ongoing clinical trials include metabolic treatment through the ketogenic diet and ADI-PEG20 combination treatment [129](detail on ADI-PEG20 in section 1.2.3), where results are keenly awaited. Early case-studies applying the ketogenic diet, a high-fat, high-protein and low-carbohydrate diet, show this approach may be effective in controlling some disease progression [119] and further results are awaited.

Clinical failures in GBM can be attributed to several factors, including the heterogeneity of these tumours and lack of effective therapies. In view of these challenges, in order to enhance patient outcome, strategies should seek to better target and personalise therapies, using combination treatments that exert multiple inhibitory actions [59], and identify novel therapies with significant and prolonged impact.

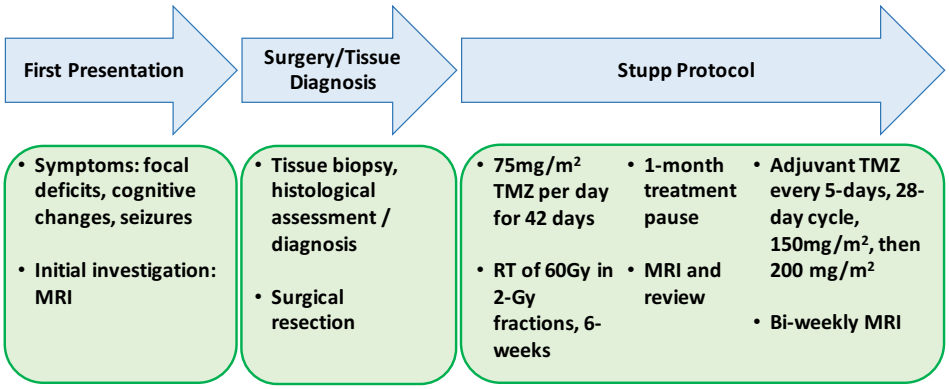


Figure 1.2.: Stupp [124] protocol forms standard of clinical treatment in GBM. Diagram provides simplified overview of GBM patient clinical treatment. Initial symptoms are investigated by MRI, followed by biopsy or direct surgical resection, leading on to cycles of chemotherapy via temozolomide (TMZ) and radio-therapy (RT) of 60 Gray units (Gy).

1.2. Cancer and metabolism

1.2.1. Overview of cancer metabolism

Cellular metabolism plays a central role in GBM. Fundamental metabolic characteristics such as the Warburg effect [144] and enzymatic alterations have enabled GBM and other cancer cells to acquire features utilised to sustain proliferation and resist certain therapies. Studying and understanding these metabolic characteristics has enabled their exploitation for clinical purposes (section 1.2.2), including cancer diagnosis and disease staging.

The Warburg effect [144] (figure 1.3), first recognised in the 1920's, is the most widely known metabolic perturbation, whereby normal cellular energy production via oxidative phosphorylation shifts towards aerobic glycolysis, which is biochemically a more energy-costly process than oxidative phosphorylation [73]. Compared to normal cells, the Warburg effect characterises cancer cells through increased glucose consumption, glycolysis and lactate production [137]. The precise mechanism by which the Warburg effect contributes towards cancer cell survival remains to be elucidated, however increased energy access, promotion of biosynthetic pathway flux, tissue architecture disruption and facilitated signal transduction have been presented [78].

Outside of the Warburg effect, further metabolic alterations have been identified to play an important role in GBM, including enzymatic mutations in isocitrate dehydrogenase 1 (IDH1), succinate dehydrogenase (SDH), fumarate hydratase (FH) and epigenetic alterations of argininго-succinate synthetase 1 (ASS1) [95], [126] (further details section 1.2.2 and 1.2.3).

Metabolic cancer characteristics already exploited clinically for visualising patient tumours include ^{18}F-deoxyglucose positron emission tomography (FDG-PET) imaging, whereby increased glucose uptake of tumours is used to determine cancer staging and distinguish the tumour from normal cells [137]. Further labelled metabolites also used for imagine including chlorine, acetate, methionine and amino-acid analogues, that have been used to show altered uptake in cancers [50], though wide-spread clinical application remains ellusive.

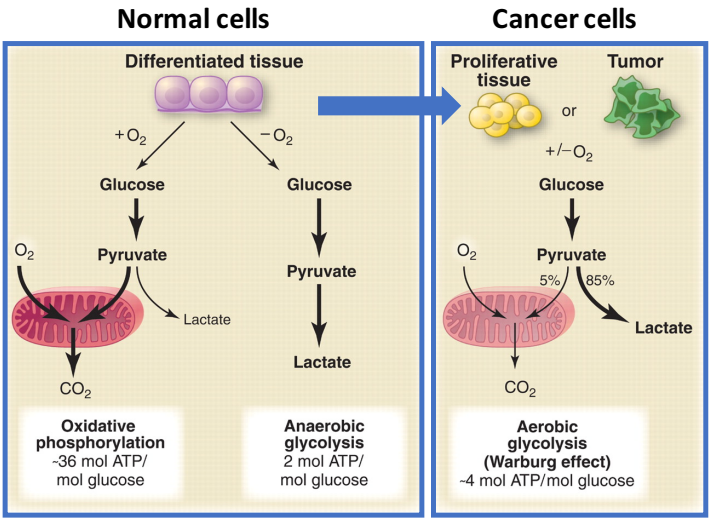


Figure 1.3.: Biochemical shift towards aerobic glycolysis in GBM cells via Warburg effect. Cellular metabolism is central to GBM, with the Warburg effect [144] being one of the most widely known biochemical changes that occur in cancer cells. Normal cellular energy production shifts from oxidative phosphorylation towards aerobic glycolysis, resulting in a metabolic cancer phenotype marked by increased glucose intake, glycolysis and lactate production. Figure adapted from Vander Heiden *et al.* (2009) [137].

1.2.2. Oncometabolites

Cancer cells display altered metabolic features and requirements compared to normal cells. Central changes include altered nutrient consumption as well as production of certain metabolites, required to support cellular growth, proliferative demand and cell survival [137]. The term oncometabolites has been used to describe metabolites associated with cancers, with 2-hydroxyglutarate (2HG) as one of the most prominent and extensively studied oncometabolites, associated with altered gene transcription [135]. Further important metabolic perturbations in cancers include glutamine, fumarate, succinate, serine, asparagine and arginine (overview in figure 1.1, and arginine is discussed in section 1.2.3).

Production of the oncometabolite 2HG is the result of mutations found in enzymes IDH1 and IDH2 [156]. In normal cells these two enzymes produce alpha-ketoglutarate (α-KG), however when these mutations are present 2HG is produced instead [156]. It was been found that in a subset of gliomas 2HG impacts DNA and histone methylation, altering gene transcription including hypoxia inducible factor-1-alpha (HIF1α), contributing towards tumourigenesis and this cancer phenotype [135] (figure 1.4).

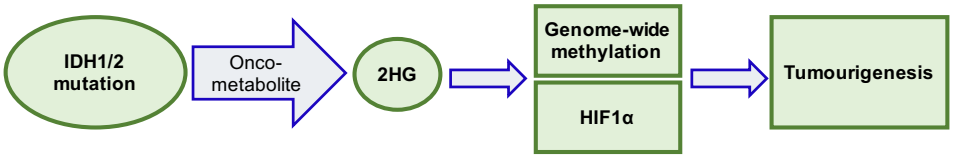


Figure 1.4.: Features of oncometabolite 2-hydroxuglutarate in glioma. In normal cells enzymes isocitrate dehydrogenase-1 (IDH1) and isocitrate dehydrogenase-2 (IDH2) produce alpha-ketoglutarate (α-KG), yet in gliomas mutated IDH1 and IDH2 produce the oncometabolite 2-hydroxuglutarate (2HG), resulting in genome-wide changes of histone and DNA methylation and increased hypoxia inducible factor-1-alpha (HIF1α), contributing towards tumorigenesis and cancer phenotype.

Glutamine addiction, with a dependency on extra-cellular glutamine, has been demonstrated in several cancers, despite this being a non-essential amino-acid, that can be synthesised intracellularly [148] [91]. Mechanisms have been in part attributed to the role of glutamine as a nitrogen donor, required for synthesis of nucleotides and amino-acids [91]. Further mechanism include a role in facilitating animo-acid update, as well as sustained activation of cell-cycle regulator mTOR [148].

Fumarate and succinate accumulation has been attributed to mutations of TCA cycle enzymes fumarate hydratase (FH) and succinate dehydrogenase (SDH) in several cancers [157], [95]. Screening for these enzymes has found clinical application for detecting familial predisposition to cancer and metastatic phenotypes [48].

Serine is a non-essential amino-acid, metabolised by the mitochondrial enzyme serine hydroxyl-methyl-transferase 2 (SHMT2), to glycine, which is

required for nucleotide synthesis [76]. Over-expression of SHMT2 has been identified in several cancers and been associated with poor prognosis [76]. Further, over-expression of serine metabolism enzymes has been demonstrated in melanoma, colorectal and breast cancer [106], [95].

Asparagine dependency of acute lymphoblastic leukaemia (ALL) and some acute myeloblastic leukaemia (AML) cells has translated into some clinical successes, particularly for childhood ALL. Despite some reported side effects [54], up to 90% of children with ALL are now treatable since introduction of l-asparaginase into chemotherapy regimes [95]. Underlying mechanisms of this dependency for extracellular asparagine is due to lack of the enzyme asparagine synthase [112].

Targeting genes associated with oncometablites and exploitation of metabolic features in cancers demonstrates great clinical utility. Key therapeutic-drugs already employed for cancers include use of anti-pyrimidine 5-fluorouracil, anti-asparagine l-asparaginase, anti-folate methotrexate [95] and further application has also been demonstrated for imaging, as outlined in section 1.2.1.

As the clinical significance of oncometabolites is increasingly being recognised, further advances have been made in understanding the role that important metabolic perturbations including the glutamine, serine, proline, asparagine and arginine metabolism have in cancer. Further understanding underlying mechanisms and vulnerabilities of the cancer metabolism will ultimately lead to novel diagnostic, prognostic and treatment approaches.

Table 1.1.: Overview of metabolites associated with cancers. Cancer cells display characteristic metabolic phenotypes. Elucidating metabolic perturbations as well as understanding underlying mechanisms and vulnerabilities has great potential for clinical exploitation by developing novel diagnostic, prognostic and treatment approaches.

Metabolite	**Associated enzyme or pathway**	**Abbreviation**	**Significance in cancer**	*Source*
2-hydroxy-glutarate	isocitrate dehydrogenase 1 and 2	IDH1 and IDH2	DNA and histone methylation and transcriptional induction of HIF1α	[156], [135]
Glutamine	target of rampamycin complex 1	TOR kinase	nitrogen donor for nucleotide and amino-acid synthesis and mTOR cell cycle regulator activation	[148], [91]
Fumarate	fumarate hydratase	FH	screening for familial cancer predisposition	[157], [95], [48]
Succinate	succinate dehydrogenase	SDH	as above	[157], [95], [48]
Serine	serine hydroxyl-methyl-transferase 2	SHMT2	association with poor prognosis	[76]
Asparagine	asparagine synthase	ASNS	enhanced clinical outcome via l-asparaginase in chemotherapy for childhood leukaemia	[112], [54]
Arginine	argininosuccinate synthetase-1 and argininosuccinate lyase	ASS1 and ASL	loss of ASS1 renders cells sensitive to arginine-deprivation therapy	[126], [39], [4]

1.2.3. Arginine, ASS1 and arginine deprivation therapy by ADI-PEG20

Arginine is a semi-essential amino-acid and epigenetic investigations by Syed *et al.* [126] have identified metabolic alterations in GBM, whereby 30% of *de novo* GBM tumours display methylation-dependent silencing of the arginino-succinate-synthetase-1 (ASS1) gene. ASS1 is the rate-limiting enzyme of *de novo* intra-cellular arginine synthesis, central to the arginine metabolism (see figure 1.7) and links to multiple important metabolic pathways, including the tricarboxylic acid (TCA) cycle, nitric oxide pathway, urea cycle, energy storage, creatine and polyamine synthesis [51].

Arginine is synthesised by ASS1 together with arginino-succinate-lyase (ASL) in a two-step process, from citrulline [39]. It is a semi-essential amino-acid as during periods of rapid proliferation, such as childhood growth and in certain cancers, there is a high cellular demand that can not be met through endogenous synthesis, hence requiring extracellular supply [39].
Cells which display methylation-specific silencing of the ASS1 gene ($ASS1^{M}$) are auxotrophic for arginine, making them dependent on extra-cellular arginine supplies, whereas unmethylated ASS1 cells ($ASS1^{U}$) can synthesise their own arginine to meet cellular demands [39].

Identifying these two ASS1 subtypes is of great clinical significance. Studies by Syed *et al.* [126] demonstrate that methylation of ASS1 is associated with significantly worse prognosis in GBM, and further studies in other cancers also conclude that ASS1 is a tumour suppressor [71], [4], [62]. Importantly, $ASS1^{M}$ GBM can be targeted with arginine-deprivation therapy [122].

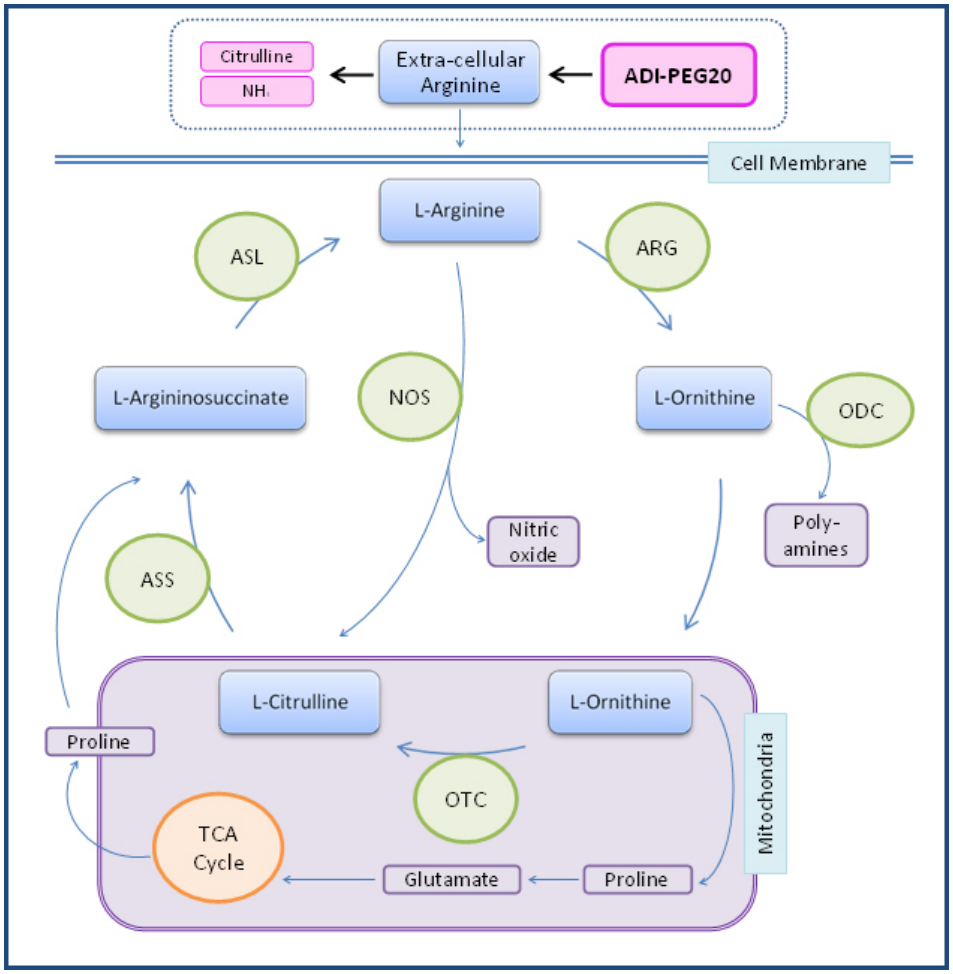


Figure 1.5.: Metabolic cycle of arginine. $ASS1^{U}$ GBM synthesise arginine from citrulline, whereas $ASS1^{M}$ GBM are reliant on extracellular arginine supplies. ADI-PEG20 degrades extra-cellular arginine, reducing this to citrulline and ammonia. Key: arginase (ARG), ornithine-decarboxylase (ODC), ornithine transcarbamoylase (OTC), ASS1, argininosuccinate lyase (ASL) and nitric oxide synthase (NOS), tricarboxylic acid (TCA) cycle. Figure adapted from Haines *et al.* [51], Delage *et al.* [29] and Shen *et al.* [122]

Arginine-deprivation therapy via ADI-PEG20 has demonstrated clinical application for several cancers (see figure 1.6) and is a strong candidate for anticancer therapy in $ASS1^{M}$ GBM tumours. Early clinical trials for glioma are ongoing, and to date, 19 clinical trials are registered under the US National Institute for Health (www.clinicaltrials.gov) for ADI-PEG20 in other cancers including melanoma, mesothelioma, gastrointestinal cancer, non-small cell lung-cancer and hepatocellular carcinoma [95], [104]. It should be noted, that of the completed clinical trials (see figure 1.6), had tumours been stratified for ASS1 methylation status, rather than expression via immunohistochemistry or no stratification, then the response rate may have been improved by targeting tumours that are susceptible to ADI-PEG20.

As ADI-PEG20 degrades blood arginine systemically, this feature further makes it an attractive therapy in GBM, overcoming challenges associated with the blood-brain-barrier [122]. Further, clinical trials for both hepatoma and melanoma have shown ADI-PEG20 to be well tolerated with low toxicities [38]. Compared to other amino acid degrading therapies, such as l-asparaginase, ADI-PEG20 has not been associated with side effects such as hepatitis, pancreatitis or neurotoxicity [104].

ADI-PEG20 comprises of the active ingredient arginine deiminase, which can be isolated from *Mycoplasma* and further pegylated, hence reducing antigenicity and enhancing serum half-life [36]. The enzyme exerts it's action, catabolising arginine to citrulline and ammonia, hence depleting extracellular arginine and subsequently depriving intracellular availability in $ASS1^{M}$ cells, which lack ability for endogenous arginine synthesis [122]. As a result of metabolic stress, arrest in proliferation ensues, cells undergo macroautophagy, and during prolonged arginine starvation periods this leads to caspase-independent apoptosis [122], [126].

The precise mechanism by which arginine starvation sends cells into metabolic distress, induces macroautophagy, nuclear DNA leakage and arrests proliferation is not completely understood. Macroautophagy is known to occur in response to starvation of several nutrients in a bid to maintain homeostasis, whereby cells recycle their organelles to liberate building-blocks and energy [37]. Despite early autophagy (24-48 hours) being a protective response to

cellular distress caused by arginine starvation in $ASS1^{M}$ cells, it has been found that later (above 48 hours) and excessive autophagy plays a role in regulating cell death [128].

As ADI-PEG20 progresses towards the clinic for GBM, one of the major future challenges will be identifying ADI-PEG20 sensitive tumours using imaging or biomarks [152]. Metabolic profiling approaches and advances in technologies will facilitate characterisation and identification of ASS1 subtypes in GBM and other cancers.

Cancers in Clinical Trials	Stage of Clinical Trial	Combination Treatment	ASS1 status stratification	Response Rate
Hepatocellular carcinoma	Phase III (recruiting)	With best supportive care	No	NA
Mesothelioma	Phase II (complete)	NA	IHC ASS1 deficiency	46% stable disease and partial metabolic response in ASS1-
Melanoma	Phase II (complete)	NA	No (only for monitoring)	11% partial response in ASS1- only
Small cell lung carcinoma	Phase II (ongoing)	NA	IHC ASS1 deficiency or <5%	NA
Non-Hodgkin's Lymphoma	Phase II (recruiting)	NA	No	NA
Acute Myeloid Leukemia	Phase II (recruiting)	NA	No	NA
Mesothelioma and non-squamous non-small cell lung carcinoma	Phase I (recruiting)	With pemetrexed and cisplatin	IHC ASS1 deficiency	NA
Prostate	Phase I (recruiting)	NA	No	NA
Pancreatic	Phase I (pre-recruitment)	With Paxitaxel and Gemcitabine	No	NA
Gastrointestinal	Phase I (pre-recruitment)	With leucovorin and FOLFOX	No	NA
Breast (HER2-)	Phase I (recruiting)	With doxorubicin	IHC ASS1 deficiency <25%	NA

Figure 1.6.: ADI-PEG20 in clinical trials. ADI-PEG20 is a strong candidate for use in GBM, as it has already entered late stages of clinical trials (phase II and III) for several cancer types (www.clinicaltrials.gov). Few of these trials (outlined in red) have stratified for ASS1 expression, whilst this is key for targeting the therapy. Importantly, not only the immuno-histological chemistry (IHC) expression, but specifically the methylation status is important for stratifying treatment. Response rates of trials highlighted in red may have been improved if ASS1 methylation status had been determined for selectively targeting patients that have $ASS1^{M}$ tumours. In comparison to other amino acid degrading therapies, such as l-asparaginase, ADI-PEG20 has not been associated with side effects such as hepatitis, pancreatitis or neurotoxicity [104].

1.3. Metabolomics

1.3.1. Metabolomics overview and applications to GBM

Metabolites are the ultimate products of cellular processes, reflecting alterations that may occur intra-cellularly at genetic, transcriptional and protein level, as well as extra-cellularly, including environmental factors and diet [40]. Metabolomics is a powerful tool used for studying metabolites, with successful application to basic research, preclinical and clinical studies for elucidating biomarkers [101], [80].

Instrument run work processes include extraction of metabolites from biological samples, instrumental run, followed by computation data processing and analysis, as well a biological interpretation, drawing on openly accessible spectral libraries and databases (overview figure 1.7). Mass-spectrometry coupled with gas-chromatography (section 1.3.2) and ^{1}H NMR (section 1.3.3) have become the most widely applied and established instrumental platforms used for metabolomic research and will be focused on in this thesis, yet further platforms also exist, including liquid chromatography-MS (LC MS) and high-performance liquid chromatography MS (HPLC MS).

As with genomics and proteomics, advances in computational technologies have facilitated processing and analysing large data sets acquired in metabolomic studies. For example, a single sample analysed by GC/TOF MS may yield over 1200 compounds in one run [99], demanding advanced computational and statistical analysis. One of the key features of metabolomic studies is the untargeted profiling approach, whereby multivariate statistical methods (section 1.3.4) are applied as hypothesis-generating tools, contrasting targeted biochemical analysis [47].

Despite the powerful research and clinical potential of metabolomic approaches, relatively few studies have been made in GBM. Cuperlovic-Culf *et al.* [27] applied ^{1}H NMR profiling to GBM, identifying four distinct GBM subtypes, linked to prognostic gene expression markers including IDH1, as well as cancer metabolic markers choline, lactate and glutamine. Wibom *et al.* [145] also highlight prognostic potential, identifying metabolic markers linked to early radiotherapy treatment response as well as detecting glucose,

glutamate, myo-inositol to be associated with tumour tissue compared to non-tumour tissue. Studies by Chinnaiyan *et al.* [24] used metabolomic approaches to differentiate low- and high-grade gliomas, yet clinical utility for guiding drug-treatment remains limited.

Taken together, these studies in GBM and other cancers demonstrate successes of metabolomic application for discovering novel treatment approaches, as well as prognostic markers. To date, no studies have been published looking at ASS1 subtypes in GBM, despite the great potential for characterising these heterogenous populations, guiding treatment approaches and identifying new targets for therapy.

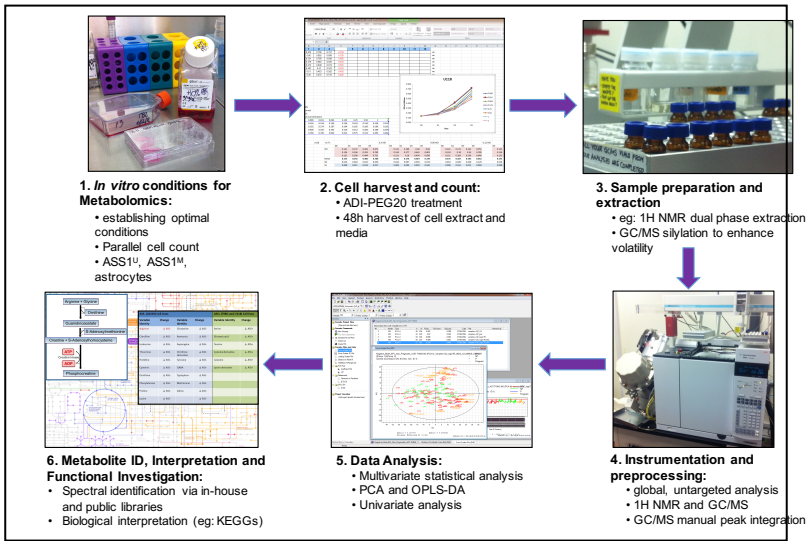


Figure 1.7.: Overview of work-flow and experimental techniques use for metabolomic profiling. Simplified overview of work-flow for metabolomic analysis as applied to ASS1 GBM cell lines. Cells were cultured *in vitro*, harvested at 48-hours, followed by sample preparation, instumental run, data analysis and biological interpretation.

1.3.2. GC/TOF MS

GC/TOF MS has been widely used for metabolomic profiling studies due to its high sensitivity, which can go down to picomolar scale [107], reproducibility and powerful peak resolution, compared to other analytical platforms [99]. Utilising electron impact ionisation, analytes are converted to positively and negatively charged ions and carried under a high-temperature vacuum gas-phase [22]. This is followed by collision of the eluted analyte under a high-energy electron beam, fragmenting the analyte, allowing for measurement of mass-to-size ratio (m/z) via a mass analyser [22] (overview of instrumentation in figure 1.8).

Prior to GC/MS analytical run most metabolites require chemical derivatisation, which is important as it helps enhance analyte volatility and chemical stability at high temperatures during analysis and improves chromatographic detectability [35].
Derivatisation is a process by which the analyte is transformed into a derivative, which is a chemical product of similar chemical structure. More specifically, certain functional groups (eg: O-H, COOH, N-H and S-H) within the analyte are modified, resulting in altered properties, including chemical reactivity, solubility, boiling point and melting point [70], [52]. These modified properties improve GC/MS chromatographic behaviour and can be exploited for quantification and analyte separation.
Silylation, acylation and alkylation are the main derivatisation reactions used in for GC analysis. Silylation, via methoxamine and N-methyl-n-(trimethylsilyl)-trifluoroacetamide (MSTFA) is the most commonly applied reaction, whereby reagents react with and modify active hydrogens in the analyte [118].

The underlying principle of GC/MS is that different metabolites have distinct chemical properties and the speed by which they travel through the column are used to determine m/z ratios for identification [6]. Subsequently metabolites can rapidly be identified in large electron ionisation spectral libraries including the National Institute of Standards and Technology (NIST) [9] (further description of methodology in section 2.2). GC/TOF MS is particularly suited for studying compounds of low molecular weight,

that are volatile and thermally stable [31], [22].

Limitations of GC/TOF MS include extensive sample preparation and high temperatures for compound derivatisation, loss of non-volative and high-molecular weight metabolites as well as long analytical times of up to 1-hour per sample, restricting high-throughput application [35].
Compared to other MS platforms such as tandem MS, GC/TOF MS is however a cost-effective and easily applicable platform [97]. Further, analytical platforms such as LC MS and HPLC MS are limited by alterations in ionisation efficiency and co-eluting compounds, restricting application between different instruments and use of mass spectral libraries [132], [154].

Combining GC/TOF MS with other instrumentation such as ^{1}H NMR can strengthen analytical coverage and these two techniques have been highlighted to compliment each other in metabolomic studies [117].

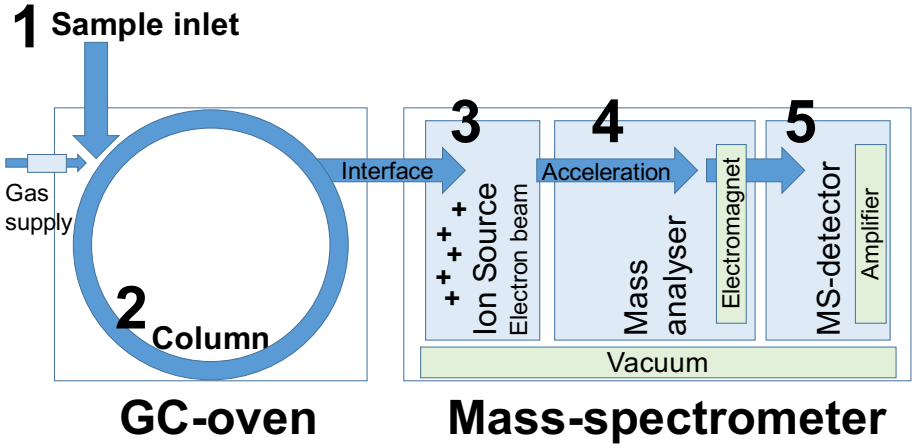


Figure 1.8.: Schematic overview of basic GC/TOF MS instrumentation. Basic components of GC/TOF MS instrumentation, whereby 1. samples are inserted into the gas-chromatography (GC) oven, 2. separated in the gas-chromatography column, enter the mass-spectrometer component where 3. analytes are ionised (converted to positively and negatively charged ions) and accelerated, carried under a vacuum gas, fragmented under an electron beam, 4. deflected, passing through the mass analyser and 5. measured by mass-to-size ration (m/z) in the mass detector.

1.3.3. ^{1}H NMR

^{1}H NMR is a robust, reproducible instrument for non-destructive analysis of complex biological samples. Basic concepts are centred on strong magnetic fields and radio frequency pulses being applied to atomic nuclei of molecules, with changes in resonance frequency being measured [35]. In comparison to other instruments used for metabolomic analysis, ^{1}H NMR requires simple sample preparation and methodological approaches have been well established, with automation allowing for high-throughput analysis [15].

The basic principle of ^{1}H NMR is that atomic nuclei of different biological molecules possess characteristic magnetic spins, which are measurable as resonance frequencies under strong electromagnetic fields [81] (for instrumental overview see figure 1.9). The superconducting electromagnet, cooled to very low temperatures below -200°C, together with a sample probe holder, pulse-programmer, radio-frequency transmitter and signal receiver, form the core elements of ^{1}H NMR instrumentation [15]. When samples are placed in this magnetic field, atomic nuclei with odd number of protons and neutrons absorb electromagnetic radiation, aligning on one axis in the magnetic field [81].
Biological samples are high in hydrogen, which is the most commonly studied isotope in metabolomic NMR studies [35]. In ^{1}H NMR, hydrogen nuclei aligned under the electromagnetic field then shift via application of a radio-frequency pulse by 90° from the axis. As nuclei return or 'relax' into their original position, a current is generated, and this signal, referred to as free induction decay (FID), is detected by the receiver coil of the spectrometer [81]. Signal outputs of FID are presented in the form of peaks, equating to different hydrogen atomic nuclei [58]. FID are visualised on ^{1}H NMR spectra as chemical shifts in parts per million (ppm) and intensities as megahertz (MHz) [81]. The areas under the spectral peak, referred to as integrals, are proportionate to identical protons present in the atomic nuclei, allowing for relative concentrations of metabolites to be measured via ^{1}H NMR [15] (further methodology is also described in section 2.3).

Limitations of ^{1}H NMR include lower sensitivity in terms of metabolite range and signal intensity, compared to other analytical platforms, which can be

overcome by using complimentary techniques such as GC/TOF MS [99]. Clear advantages of ^{1}H NMR are marked by stability in chemical shifts, ease of quantification and application for obtaining more detailed chemical structural information [99], [147]. Further, ^{1}H NMR also involves simpler sample preparation, less time-intensive instrumental run optimisation and the non-destructive analytical nature allowing for sample storage and re-analysis [99], [127], [147].

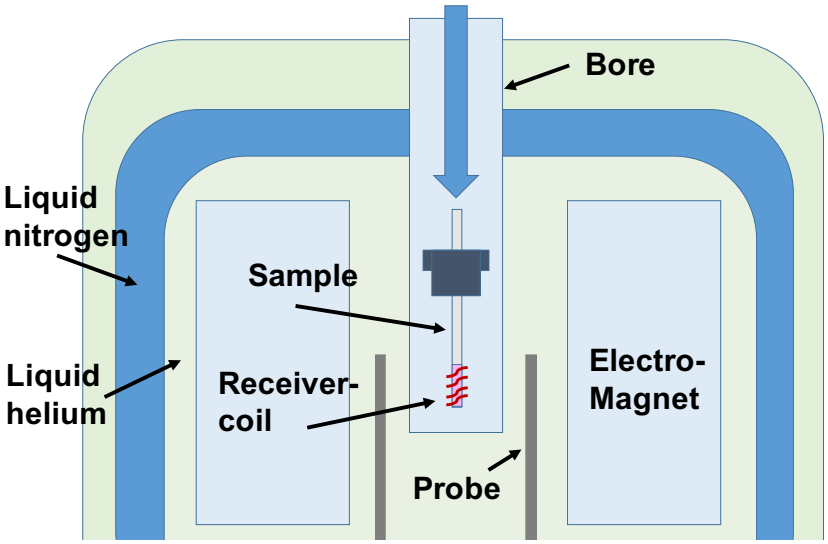


Figure 1.9.: Schematic overview of basic ^{1}H NMR instrumentation. Basic components of ^{1}H NMR instrumentation, whereby samples held in a probe are individually inserted through the bore and transported to the centre of the magnet, where signal is detected by the probe via the receiver coil. Helium cools the superconducting coils and the liquid nitrogen insulates the helium.

1.3.4. Chemometrics

GC/TOF MS, ^{1}H NMR and other analytical platforms used for metabolomic analysis yield information-rich data sets, that have demanded application and development of chemometric tools, requiring advanced computational power. Work-flows include data pre-processing, binning (whereby data-points are grouped in 'bins') and alignment, normalisation, removal of noise (eg: cutting the water signal peak), followed by multivariate statistical analysis with both supervised and unsupervised methods [153] (see also figure 1.7).

Multivariate statistics

Multivariate statistics are employed for analysis of metabolomic data, as they deconvolute and enhance information recovery from data-rich information sets. Further, metabolic patterns and relationships can be revealed through the simplified weighted approaches applied in multivariate statistics, using both unsupervised and supervised methods [41], [6].

Principal component analysis (PCA) is the most widely applied unsupervised method for metabolomic data, whereby no class information (eg: treated or untreated groups) is attributed [6] (see figure 1.10 for overview). Spectroscopic data has several dimensions and PCA is employed to enhance visualisation and highlight patterns [63].
Underpinning principles rely on 'orthogonal linear transformation' of data, whereby data from several dimensions is compressed into 'principal components', reducing dimensionality and complexity [155]. The principal components explain variance in the data matrix, whereby the first component explains the greatest variance and the second principal component explains the second largest variance, which can be projected on planes and visualised as data points on 'score plots' [150] (further descriptions of statistical analysis found also in section 2.3.4 and 2.2.5).

For supervised methods, partial-least squares discriminant analysis (PLS-DA) and orthogonal partial-least squares discriminant analysis (OPLS-DA) are widely applied to metabolomic data, whereby class information (eg:

treatment group) are allocated to highlight features associated with sample groups [151], [6]. Separation is forced between groups and this method is used to investigate more subtle differences between groups [41].
As with PCA, data is also transformed and projected onto new planes and visualised as data scores plots. Main differences between OPLS-DA and PLS-DA is that OPLS-DA has an added feature, incorporating a filter, whereby more subtle differences can be detected between groups. As over-fitting can occur, both these supervised methods require model validation, with established approaches including permutation validation, where class information is randomised and compared to the original model [114] (further descriptions of statistical analysis found in section 2.3.4 and 2.2.5).

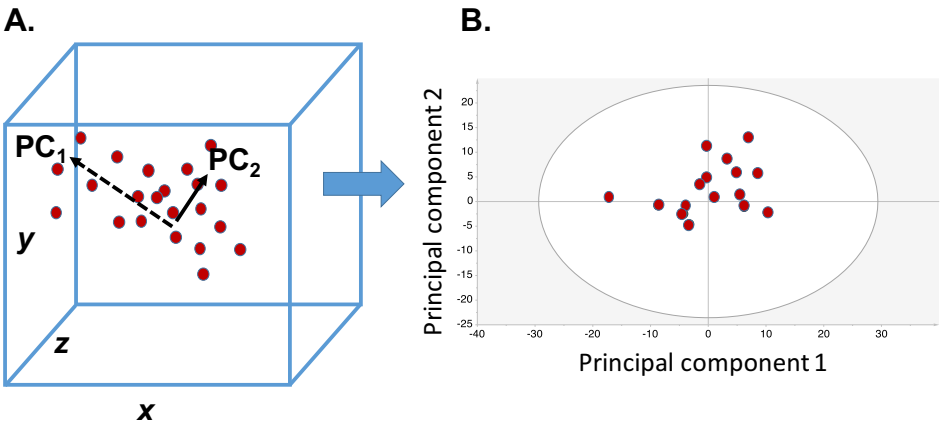


Figure 1.10.: Overview of principal component analysis. Principal component analysis (PCA) reduces dimensionality of three-dimensional data by compressing data into principal components. (A.) PC_1 (dashed arrow) and PC_2 (solid arrow) describe most of the variance in a dataset. These principal components are then projected on planes and visualised as (B.) score plots.

1.4. Hypothesis and study aims

With arginine playing a central role in GBM metabolism, it was hypothesised that metabolic consequences of arginine deprivation via ADI-PEG20 would be highlighted through an untargeted metabolic approach, helping to identify novel treatment approaches.
Overall aims of this PhD project were to (*i*) characterise and determine the metabolic profiles of ASS1 GBM subtypes with non-invasive methods, (*ii*) compare and elucidate metabolic alterations upon arginine deprivation therapy and (*iii*) identify novel treatment approaches in GBM.

1.5. Objectives

1. Profiling global metabolic phenotypes of $ASS1^{M}$ and $ASS1^{U}$ GBM cell lines at basal levels (no ADI-PEG20 treatment) and in the presence of ADI-PEG20 via GC/TOF MS and ^{1}H NMR, applying multivariate statistical analysis (using unsupervised PCA and supervised PLS-DA and OPLS-DA) to intracellular and extracellular samples.

2. Comparing transcriptional expression of enzymes associated with altered metabolic pathways via RT-QPCR, both in the absence and presence of ADI-PEG20, followed by biological interpretation, drawing on public databases and literature, focusing on novel therapeutic approaches for GBM.

3. Challenging GBM cell lines *in vitro* with dose-titrations of novel therapies identified, assessing effects on proliferation via SRB analysis, as well as functionally validating findings via RT-QPCR enzymatic transcriptional expression.

2. Methods and Materials

2.1. Tissue culture

2.1.1. Cell lines and culture conditions

Established glioblastoma (GBM) cell lines were obtained from the German Collection of Microorganisms and Cell Cultures (DMSZ)(GAMG, SNB19) and the American Type Tissue Culture Collection (ATCC)(U87, U118, LN229) and maintained in Dulbecco's Modified Eagle Medium (DMEM, low glucose, l-glutamine)(Invitrogen, Paisley) supplemented with 10% foetal bovine serum (Invitrogen, Paisley).

Human astrocytes (ScienCell, CA, USA) were cultured in astrocyte medium, supplemented with 2% foetal bovine serum (FBS) and 1% astrocyte growth supplement (ScienCell, CA, USA). Cells were incubated in an Heraeus, HERAcell 150 incubator (Thermo Fisher Scientific) at an atmosphere of 5% CO_2 at 37°C. Cells were cryopreserved under liquid nitrogen in 90% FBS and 10% dimethylsulphoxide (DMSO)(Sigma-Aldrich, St. Lois, MO, USA).

Adherent cells were subcultured, removing overlying medium and washing the monolayer briefly with phosphate buffered saline (PBS)(Invitrogen, Paisley, UK). Cells were incubated with 0.25% trypsin with 1mM Ethylenediaminetetraacetic acid (EDTA)(Invitrogen, Paisley, UK) at 37°C for 2-3 minutes and detached from the culture flasks by gentle agitation. Trypsin was neutralised by adding three volumes of complete media and media with cells were pipetted 2-3 times to ensure detachment and single cell suspension. As required, cell numbers were determined via use of a haemocytometer chamber (Neubauer Improved, DE), using 0.4% trypan blue solution (Sigma-Aldrich, St. Lois, MO, USA). Cells were diluted into complete medium and seeded in culture flasks or plates.

2.1.2. Drugs and reagents

Arginine deiminase formulated with polyethylene glycol (ADI-PEG20) was obtained from Polaris Pharmaceuticals Inc. (San Diego, CA, USA) and diluted (0-2μg per ml) into media. L-citrulline (Sigma-Aldrich, St. Lois, MO, USA) was dissolved in PBS and diluted in media (1mM). Phytic acid sodium salt hydrate (IP6)(Sigma-Aldrich, St. Lois, MO, USA) was dissolved into media, pH adjusted to 7.4, and further diluted (0-33mM) into media. Creatine (Sigma-Aldrich, St. Lois, MO, USA) was dissolved in media and diluted to $0.1 - 10\mu$M.

2.1.3. Cell proliferation assay

Cell growth and growth inhibition was tested with the sulphorhodamine B (SRB) colourimetric assay [139]. Cells were seeded at 2x10^3 in triplicate wells on 96-well plates (Corning, NY, USA) for each treatment condition and time-points. 24-hours after seeding media was removed and drug treatments were added in fresh media. Once time-point were reached, cells were fixed with 50% trichloroacetic acid (TCA)(Sigma-Aldrich, St. Lois, MO, USA) for 1-hour at 4°C. Plates were then washed with water and allowed to air-dry. The plates were subsequently stained with 0.4% SRB (Sigma-Aldrich, St. Lois, MO, USA) dissolved in 1% acetic acid (Sigma-Aldrich, St. Lois, MO, USA) for 1 hour. Unbound dye was removed from cells by washing with 1% acetic acid and plates were air dried. Cell-bound dye was solubilised in 10mmol/l Tris (pH=10.5) for 1 hour on a shaker, and colourimetric absorbance was measured at a wavelength of 490nm on a microplate reader (Elx800 BioTek, Invitrogen, UK). Averages of replicates were taken and background absorbance was subtracted. Repeat experiments were performed three times. For mean comparisons of groups the T-test was used, where p-values of below 0.05 were considered significant.

2.1.4. Luciferase assay

Cellular adenosine triphosphate (ATP) concentrations were determined via firefly luciferase assay [84], using the Promega Luciferase Assay System (Promega Corporation, WI, USA). Cells were seeded at 2x10^3 in triplicate wells on white walled and clear base 96-well plates (Corning, NY, USA) for each treatment condition, exposing cells to $0.1 - 10\mu$M creatine and

lysed at day 5. Luciferase activity was measured according to manufacturer's instructions. In brief, cell media was carefully removed, cells were PBS washed, incubated with lysis buffer (Promega Luciferase Assay System (Promega Corporation, WI, USA)) and incubated with luciferase assay reagent and luminescence was immediately read using the 96-well microplate luminometer (GloMax 96 Micro, Promega Corporation, WI, USA).

2.1.5. Cell culture experiments for GC/TOF MS

Cells (SNB19, U87, astrocytes) were each seeded in replicate ($n = 12$) at $8x10^4$ per well in a 6-well dish (Corning, NY, USA). 24-hours post seeding, media was removed and cells were washed with 2ml PBS. Control and ADI-PEG20 ($1\mu g/ml$) treated cells were cultured in medium containing, 1mM citrulline and 10% FBS. ADI-PEG20 treated and control media ($n = 3$) were also prepared and incubated in the absence of cells. 24- and 48-hours post treatment replicate samples for each condition ($n = 3$) were harvested, collecting cell media and adherent cells for GC/TOF MS metabolomic analysis. Further replicates ($n = 3$) of each condition were collected for total cell count determination.

Removed media samples were centrifuge-spun to remove cellular debris and rapidly frozen and stored at $-80°C$ until subsequent analysis. The adherent cell monolayer was washed twice with 2ml PBS and cells were quenched with 1ml ice-cold methanol (Sigma-Aldrich, St. Lois, MO, USA) for 3-5 minutes, keeping the plates on ice. Cells were removed by scraping, followed by the cell and methanol suspension being transferred to microcentrifuge tubes on dry ice, followed by storage at $-80°C$ until further analysis.

2.1.6. Cell culture experiments for ^{1}H NMR

Cells (SNB19, GAMG, LN229, U87, U118, astrocytes) were seeded in replicate ($n = 12$) at a density of $1.1x10^6$ cells per 10-cm tissue culture dish (Corning, NY, USA). 24-hours post seeding, media was removed and cells were washed in PBS. Control and ADI-PEG20 ($1\mu g/ml$) treated cells were cultured in medium containing, 1mM citrulline and 10% FBS. 48-hours post treatment replicate samples ($n = 6$ per condition) were harvested, collecting cell media and adherent cells. Further replicates ($n = 3$) of each condition

were collected for total cell count determination.

Removed media samples were centrifuge-spun to remove cellular debris and rapidly frozen and stored at $-80°C$ until subsequent analysis. The adherent cell monolayer was washed twice with 2ml PBS and cells were quenched with 1.8ml ice-cold methanol (Sigma-Aldrich, St. Lois, MO, USA) for 3-5 minutes, keeping the plates on ice. Cells were removed by scraping, followed by the cell and methanol suspension being transferred to microcentrifuge tubes on dry ice. Samples were subsequently dried overnight in a vacuum concentrator (Speedvac, Eppendorf, DE) at 45°C, followed by storage at $-80°C$ until further analysis.

2.2. GC/TOF MS

2.2.1. Sample preparation, metabolite extraction, derivatisation

Cell media and extract samples for GC/TOF MS analysis were prepared with the reference to the protocol of Chan *et. al.* [22]. Samples were randomised, defrosted at room temperature and vortexed.

For the cell media fraction, 200μl were transferred to individual microcentrifuge tubes. A quality control was prepared from a pool of each sample, and 200μl were transferred to individual microcentrifuge tubes. 1.5ml of methanol was added to each sample, mixed for 5 minutes for protein precipitation and spun at 10,000g for 10 minutes at 4°C to pellet precipitated protein. 1.3ml of supernatant was transferred to individual silylated glass tubes.
For the cellular fraction, 200μl cell lysate was transferred to individual microcentrifuge tubes and 1.3ml extraction mixture [(water:MeOH [2:10]), analytical grade, Sigma-Alrich, St. Louis, MO, USA], giving a final methanol concentration of 80% together with the cell lysate. Samples were vortexed for 5 minutes for cellular disruption and extracted on ice for 20 minutes, following centrifugation at 4°C at 17,500g for 10 minutes. 1.4ml supernatant was transferred to silylated glass tubes.
Both individual and pooled standards (table 2.1) were prepared, making a stock solution in water (10mg/ml). Individual samples were diluted in methanol (0.005mg/ml), and 100μl were transferred to silylated glass tubes. Pooled standards were diluted to 300μl water containing metabolite standards (table 2.1) and 200μl methanol.

All samples and standards were evaporated to dryness at 40°C under nitrogen gas in a concentration evaporator (Turbovap LV, Biotage, Uppsalla, Sweden). Toluene [(100μl, anhydrous)(Sigma-Alrich, St. Louis, MO, USA)] was added to each sample, vortexed for 1min and dried under a concentration evaporator, ensuring complete removal of water. Methoximation was performed, adding 50μl of MOX [(2% methoxamine hydrochloride in pyridine), Sigma-Alrich, St. Louis, MO, USA] per sample, vortex mixing for 1min and incubation at 60°C for 2h.

Table 2.1.: Standard stocks were prepared in water (10mg/ml) and diluted to 0.05mg/ml.

Standard	Source
L-proline	Fluka Biochemika (Sigma-Aldrich, St. Lois, MO, USA)
L-alanine	Fluka Biochemika (Sigma-Aldrich, St. Lois, MO, USA)
L-glutamic acid	Fluka Biochemika (Sigma-Aldrich, St. Lois, MO, USA)
L-glutamine	Fluka Biochemika (Sigma-Aldrich, St. Lois, MO, USA)
L-methionine	Fluka Biochemika (Sigma-Aldrich, St. Lois, MO, USA)
D-glucose	Supelco (Sigma-Aldrich, St. Lois, MO, USA)
D-alpha-hydroxyglutaric acid	Sigma-Aldrich, St. Lois, MO, USA
D-lactic acid	Sigma-Aldrich, St. Lois, MO, USA
Ammonium formate	AnalR (Sigma-Aldrich, St. Lois, MO, USA)

Following methoximation, samples were derivatised, adding 100μl MSTFA (N-methyl-n-(trimethylsilyl)-trifluoroacetamide), Sigma-Alrich, St. Louis, MO, USA] per sample, vortex mixing for 2min and incubation for 1h at 60°C to enhance volatility and stability of metabolites. Samples were next vortexed for 2min, spun at 17,500g for 5min at room temperature and transferred to the GC/TOF MS autosampler vials for analysis.

2.2.2. GC/TOF MS analysis and instrumental setting

Samples were subjected to GC/TOF MS on a Pegasus GC-TOFMS (Leco Corp., St Joseph, MI, USA), connected with an Agilent 7890 gas chromatograph, using a fused silica capillary column (Agilent J and W Scientific), with 0.25μm thickness and open split interface. Under helium as carrier gas, samples were injected, with constant temperatures (220°C), transfer (280°C), ion source (250°C) and flow (1.5ml/min) for injection, with an injection volume of 1μl.

Primary oven temperatures were programmed at 70°C for 0.2min, raised to 270°C for 5min and further increased to 310°C for 11min. 70 eV electron beams were used for the ionisation, and masses were recorded from 40 to 600 m/z at a rate of 20 spectra/sec with the detector voltage set at 1800 V.

2.2.3. Data processing

Gas chromatographs were baseline corrected, de-convoluted, noise-reduced, smoothed, library matched and areas were calculated with ChromaTOF software (LecoCorp. v 4.4). Signal-to-noise above 150 ratio were analysed and chromatographs were normalised to cell count or total peak area prior to statistical analysis.

2.2.4. Compound identification

Putative analyte identities were found by comparing MS spectra with the retention index (RI) of the US National Institute of Science and Technology (NIST) library, as well as the Fiehn library, Golm Metabolome Database, Human Metabolome Database and in-house databases. Spectral peaks with similarity indexes (SI) of 60% or above were used as a cut-off for preliminary identification and matching putative metabolites with spectral libraries (NIST). Mass spectra were further visually inspected and retention times (RT) were verified with spectral libraries (NIST and in-house). Metabolic peaks with coefficient variation higher than 30% in the QCs were also used as a cut-off and excluded from further analysis.

2.2.5. Statistical analysis

Normalised data was imported into SIMCA (v 12.0, Umetrics, Umea, Sweden) for multivariate analysis. Data was scaled with standard unit variance (peak heights divided by standard deviation) and principle component analysis (PCA) was performed for identifying clustering trends and potential outliers subject to exclusion, based on sample processing errors or instrumental drift. First all data was included for PCA, followed by select grouping (eg: treatment versus non-treatment) for both PCA and partial least squares discriminant analysis (PLS-DA).

The validity of the model was verified for overfitting, using randomised permutation tests (100 permutations) and visualising model validation plots. Criteria for validation included Q_2 values of permuted data sets being higher than Q_2 values of original data sets. Further criteria included a regression line of Q_2 values from data sets trending towards zero or negative values.
Discriminant lists of potential metabolites accounting for data separation

between groups were generated from the PLS-DA analysis, using variable importance in projection (VIP) for rankings, with cut-off values at 1.0. Univariate statistics (T-tests) were applied, to determine significance between groups, as well as Bonferroni-correction as a conservative measure of significance. Fold-changes were also calculated between groups.

Select metabolites were further interpreted in their biological context, with the use of the Human Metabolome Database (HMDB), Kyoto Encyclopedia of Genes and Genomes database (KEGG) or literature searches.

2.3. ^{1}H NMR

2.3.1. Sample preparation and metabolite extraction

The cell media and cell pellet were prepared with reference to the protocol of Beckonert *et al* [15]. For the cell pellet, 500μl cold HPLC grade methanol (Sigma-Aldrich, St. Lois, MO, USA) was added to each randomised sample and vortexed for 30 seconds. Subsequently 130μl HPLC grade water (Sigma-Aldrich, St. Lois, MO, USA) were added to the samples, followed by a 30 second vortex and 20 minute incubation on ice. Samples were spun at 13,000 rpm for 10 minutes, and the supernatant was transferred to new microcentrifuge tubes on ice. This procedure was then repeated with the remaining cell pellet, adding 500μl methanol, followed by water and transfer of the supernatant. Samples were concentrated and dried over-night in the a vacuum concentrator (Speedvac, Eppendorf, DE) at 45°C, followed by storage at −80°C until further analysis or direct use.

On the day of ^{1}H NMR analysis, dried extracts were reconstituted with 600μl phosphate buffer [0.2M , 0.043M , 7:3 deuterium oxide:water, 0.01% 3-(Trimethylsilyl)propionic-2,2,3,3-d4 acid sodium salt (TSP)(all Sigma-Aldrich, St. Lois, MO, USA), pH adjusted to 7.4], vortexed and centrifuged at 13,000rpm for 5 minutes. 550μl of supernatant was transferred to 5mm NMR tubes (Sigma-Aldrich, St. Lois, MO, USA) for subsequent analysis.

For the cell media, samples were taken from −80°C and left to thaw at room temperature. Samples were vortexed to resuspend any precipitate and then 550μl media were transferred to microcentrifuge tubes with 50μl deuterium oxide containing 0.01% TSP. The solution was mixed by vortexing, followed by a 13,000 rpm spin for 5 minutes. Subsequently 550μl were transferred to 5mm NMR tubes for analysis.

2.3.2. ^{1}H NMR analysis and instrumental settings

^{1}H NMR spectra were acquired on a Bruker Avance-600 spectrometer (MA, USA [600.1 MHz, 1H frequency]) at a temperature of 300 K, with the use of a Bruker TXI probe and an automated sample handing carousel (BACS-60 autosampler, Bruker). Topspin version 3.0 software (Bruker, MA, USA) was

used for instrumental control and spectral processing.

The one-dimensional ^{1}H NMR spectra were acquired using both Carr-Purcell-Meiboom-Gill (CPMG) and Nuclear Overhauser enhancement spectroscopy (NOESY) [87] pulse sequence, with fixed spin-spin relaxation delay (relaxation delay- 90°-[t1-900-mixing time-900]-acquire). Shimming, water suppression and 90° pulse were set for the first sample, and these parameters were applied to subsequent samples. TSP was used as a reference compound for chemical shift.

Individual spectra were acquired with 256 scans into 12 data points with a spectral width of 20ppm, relaxation delay of 3 sec and acquisition time of 4.5 sec. Broadening factor of 0.3Hz was also applied prior to Fourier transformation.

2.3.3. Data processing

The spectra were imported and processed in MATLAB (Mathworks, Inc. MA, USA) with in-house software (developed by Dr. Timothy Ebbels and Dr. Hector Keun), where data was phase corrected, referenced to TSP at 0 ppm and baseline corrected. Following individual review in Topsin (version 3.0 software, Bruker, MA, USA), TSP and water peaks were removed. Spectra were next aligned and subjected to probablistic quotient normalisation with the use of in-house MATLAB scripts (courtesy Dr. Kirill Veselkov).

2.3.4. Statistical analysis

As described in GC/TOF MS statistical analysis section (2.2.5), processed ^{1}H NMR spectral data was imported into SIMCA (v 12.0, Umetrics, Umea, Sweden) for multivariate analysis. In brief, data was scaled with standard unit variance, subjected to PCA analysis for identifying clustering trends, and groups (eg: treatment versus non-treatment) were compared.

Spectra were further analysed, importing data into MATLAB (Mathworks, Inc. MA, USA) for orthogonal partial least squares discriminant analysis

(OPLS-DA), facilitating visualisation of discriminant spectral peaks from ^{1}H NMR analysis. OPLS-DA loading plots displayed direction of variation (eg: treatment versus non-treatment) and strength of correlation, according to colourimetric scale (eg: red indicating high correlation and blue indiating low correlation), as determined by correlation coefficient R_2 values.
The validity of the OPLS-DA model was verified via Q^2 values, where higher values indicated increased model strength and negative values were criteria for exclusion due to poor predictive capability.

Discriminant ^{1}H NMR spectra peaks detected via OPLS-DA analysis were extracted manually and metabolite identities were assigned with reference to in-house databases and use of NMR suite profiler software (Chenomx, v8.1, Alberta, Canada).
Fold-changes were calculated and univariate statistics (T-tests) were applied, to determine significance between groups, followed by biological interpretation with reference to the Human Metabolome Database (HMDB), Kyoto Encyclopedia of Genes and Genomes database (KEGG) or literature searches.

2.4. Transcriptional investigations (RT-QPCR)

2.4.1. RNA extraction from cultured cells and quantification

Cells were washed with PBS, collected and stored at −80°C until subsequent extraction. RNA was extracted using the RNeasy Mini Kit (Qiagen, Crawley, UK) according to the manufacture's protocol. Briefly, 600μl RNeasy lysis buffer (RLT), containing guanidine salts for protein denaturation, was added to cell samples. Cells were then homogenised, shearing genomic DNA and cellular components with a 20-gauge needle (5-10 times), followed by a mix with 600μl of 70% ethanol. Samples were then transferred to silica columns and spun with a bench top centrifuge (Eppendorf 5417 R, Hamburg, DE), allowing RNA to bind to the column. Columns were then washed with RW1 buffer, treated with a DNAse digestion (Qiagen, Crawley, UK), followed by a further RW1 wash and two washes with RPE buffer. RNA was eluted in 50μl RNAse free water, concentrations were quantified and purity was assessed with the NanoVue 4282 Spectrophotometer (Fischer-Scientific, UK). Absorbance was measured at 260 and 280nm. Samples were kept on ice and used immediately for complementary DNA (cDNA) conversion or storage at −80°C.

2.4.2. Reverse transcription and cDNA conversion

cDNA was synthesised according to the M-MLV Reverse Transcriptase protocol (Promega, WI, USA). In brief, 2μg RNA was added to 1μg random primers (Invitrogen, Paisley, UK) and a total of 15μl water. The mix was heated to 70°C for 5 minutes to melt secondary structures in the template and chilled to 4°C. A mix containing the 5x reverse transcriptase buffer, deoxynucleoside triphosphates (dNTPs), ribonuclease inhibitors, M-MLV enzyme and water were added to the RNA sample, mixed and incubated for 60 minutes at 37°C. Samples were used immediately or stored at −20°C.

2.4.3. Quantitative real-time PCR and analysis

40ng cDNA was added for the amplification of each gene in triplicate on a 96-well QPCR plate. For every sample the target and reference gene (TBP1) were tested. QPCR was performed with 2xSYBR Green Fast mix (Invitrogen, Paisley, UK), 0.1μl forward and reverse primers (Invitrogen,

Paisley, UK), DEPC treated water. Primer sequences were taken from the qPrimerDepot database (https://primerdepot.nci.nih.gov) and sequences are listed in table 2.2.

QPCR was performed using the Bio-Rad CFX96 Detection System instrument and software (Bio-Rad, Hemel Hempstead, UK). The following cycling conditions were used to amplify all genes: 95°C for 10 minutes, 50 cycles of 95°C denaturation (15 seconds) and 60°C annealing (1 minute), followed by an extension at 65°C (5 seconds) and final extension to 95°C. Threshold cycle values (Cτ) were calculated with use of the Bio-Rad CFX Manager 3.1 and target genes were normalised to the reference gene (TBP1).

Table 2.2.: Primer sequences, annealing temperature (Tm, Celcius and PCR product size, forward (F), reverse (R).

Primer	Target Gene	Direction ($5' - 3'$)	Primer Sequence	Tm (°C)	Product size (base pairs)
1	TYMS	F	GCAGTTGGTCAACTCCCTGT	60	109
		R	AGAGAAGAAGGGGACTTGGG	60	
2	TK1	F	TCCAGTGCAGCCACAATTAC	60	100
		R	CTGTCATAGGCATCGACGAG	60	
3	TK2	F	GATCCAGTCAAACCATTCCG	60	102
		R	TCGATTCACAGCGCAAGATA	60	
4	LDHA	F	GGAGATCCATCATCTCTCCC	60	98
		R	GGCCTGTGCCATCAGTATCT	60	
5	PDHA1	F	TTTGCAAAATTACGGGATGC	60	97
		R	TCATGAGGAAGATGCTCGC	60	
6	CS	F	AATTCGTGGAGGAAGCACTG	60	97
		R	ATGGCTTTACTTACTGCGGC	60	
7	SDHA	F	TTTTCCCACAACCTTCTTGC	60	97
		R	AGAACATCGGAACTGCGACT	60	
8	FH	F	CTCGCTTCAAGATGCCAAA	60	108
		R	AGTATTATGGCGCCCAGACC	60	
9	MDH2	F	GGGCTGTTCTTCAGGAGAAGT	60	98
		R	AGCTTCAGCACCTCGGC	60	
10	ASS1	F	ATTGACATCGTGGAGAACCG	60	101
		R	GCCTCGATGTCTAAATGAGCA	60	
11	TBP1	F	TATAATCCCAAGCGGTTTGC	60	170
		R	GCTGGAAAACCCAACTTCTG	60	

3. Results: Metabolic characterisation of ASS1 GBM subtypes

3.1. Introduction

Understanding arginine-depleting agents in a metabolic context as well as identifying metrics have been presented as key questions for the success of arginine-depleting agents in cancer treatment [128]. As described in section 1, 30% of *de novo* GBM tumours are $ASS1^{M}$ (Syed *et al.* [126]), rendering these cells auxotrophic for arginine. Further, in $ASS1^{U}$ cells, ASS1 is the rate-limiting enzyme of *de novo* synthesis. Arginine links into multiple important metabolic processes, including the TCA cycle, NO pathway and polyamine synthesis. ADI-PEG20 is a strong therapeutic candidate for GBM, degrading blood arginine systemically, thereby overcoming challenges of the BBB, and it is currently in late stage clinical trials for several cancers [104].

3.1.1. Aims

Metabolic profiling via GC/TOF MS and ^{1}H NMR, was applied to *in vitro* GBM cell lines in the absence of treatment and presence of ADI-PEG20 treatment. The aim of these studies was to (*i*) characterise ASS1 subtypes, (*ii*) compare and elucidate metabolic alterations induced upon arginine deprivation therapy in GBM cell lines, as well as a (*iii*) identifying cellular vulnerabilities that could lead to novel treatment approaches.

3.1.2. Objectives

1. Characterising metabolic profiles of ASS1^{M} (SNB19, GAMG, LN229) and ASS1^{U} (U87, U118) cell lines via GC/TOF MS and ^{1}H NMR at basal levels and in response to arginine deprivation via ADI-PEG20 *in vitro*.

2. Comparing global metabolic profiles amongst cell lines of ASS1 subtypes at basal levels and upon ADI-PEG20 treatment, using untargeted PCA statistical analysis.

3. Elucidating and identifying specific differences amongst groups in both intracellular and extracellular (growth media) fractions of GBM cells, using OPLS-DA and PLS-DA statistical analysis as well as spectral libraries to determine metabolite identities.

3.2. Results

3.2.1. Establishment of conditions for cell culture experimentation

Proliferation of ASS1 GBM subtypes upon arginine deprivation via ADI-PEG20

Optimal ADI-PEG20 treatment conditions and harvest time-points were determined in GBM cell lines, for capturing early consequences of arginine deprivation treatment. Cells were subjected to ADI-PEG20 titration of 0-2μg/ml (ADI-PEG20 is concentrated in saline solution and does not require DMSO or other drug vehicle). Cells were further harvested at different time-points (day 0-5) and subjected to SRB proliferation analysis.

In line with previous findings by Syed *et al.* [126], SRB analysis (figure 3.1) confirmed that proliferation of ASS1$^{\mathrm{M}}$ GBM cell lines is arrested upon ADI-PEG20 treatment and ASS1$^{\mathrm{U}}$ cells continue to proliferate. Additionally, a slight dose-dependent effect was also observed in ASS1$^{\mathrm{M}}$ cells, which became pronounced from 1μg/ml on day 5.
A dosage of 1μg/ml and time-points between day 1 and 3 were chosen for subsequent experiments, as this was the lowest dose that suppressed growth in all ASS1$^{\mathrm{M}}$ cells, whilst also capturing control and ASS1$^{\mathrm{M}}$ cells before they reached confluency.

In the non-GBM line (astrocytes), which have methylation of ASS1, ADI-PEG20 was found to arrest proliferation. GBM stem from the same cell lineage as astrocytes and are the closest non-malignant control. These results were interpreted with the consideration that astrocyte cell lines have their limitations in representing true physiological conditions (eg: evidence by non-malignant cells not proliferating at the same rate as malignant cells *in vivo*). Highlighting the need for better *in vitro* controls in the wider research community, astrocytes were however included in subsequent studies as a non-GBM control, accepting their limitation and interpreting results accordingly with this consideration.

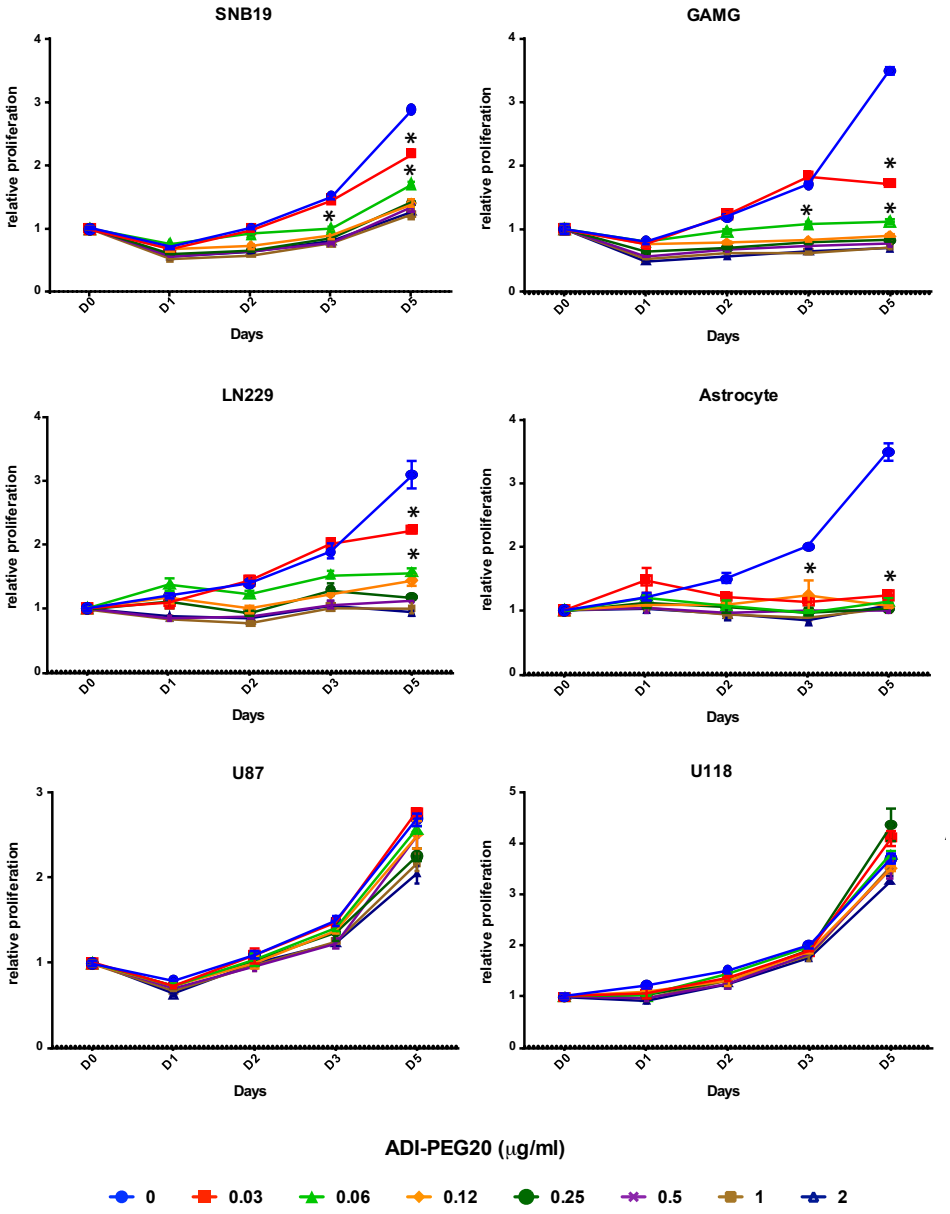


Figure 3.1.: GBM cell proliferation and sensitivity to ADI-PEG20. Dose-response curves of ADI-PEG20 treated (0-2μg/ml) GBM cell lines. SRB proliferation assay shows ASS1$^{\mathrm{M}}$ are sensitive to ADI-PEG20 as demonstrated by arrested proliferation from day 1, whereas ASS1$^{\mathrm{U}}$ continue to proliferate, making use of their capacity to synthesise arginine. ADI-PEG20 concentrations of 1μg/ml and early time-points of 24-48 hours were selected for subsequent experiments as this was the dose and time where ADI-PEG20 suppressed growth in ASS1$^{\mathrm{M}}$ cells, whilst capturing ASS1$^{\mathrm{U}}$ before they reached confluency. Cells were plated in triplicate and values shown are averages with standard error. Optical densities were read at 490nm and units are relative to day 0. ASS1$^{\mathrm{M}}$ (LN229, GAMG, SNB19), ASS1$^{\mathrm{U}}$(U87 and U118), and non-GBM (astrocyte) cells. Error bars represent standard error $*p < 0.05$.

3.2.2. GC/TOF MS: Metabolic characterisation of ASS1 GBM subtypes

Experimental parameters

Establishing cell count at harvest for GC/TOF MS analysis

Having determined via SRB assay that ADI-PEG20 concentration at 1μg/ml and a cell harvest window between day 1 and 3 (section 3.2.1) to be suitable for analysis, cell culture time-points and cell count were more precisely determined for GC/TOF MS. Cell count was assessed at 24 and 48 hours of treatment for GBM cell lines (figure 3.2). Harvest at 48 hours was chosen for subsequent analysis, as viable cell count was significantly decreased in ASS1^{M} (SNB19) cells upon ADI-PEG20 treatment. These results also further validated the SRB results (section 3.2.1), showing that ADI-PEG20 arrests proliferation in ASS1^{M} cells and not ASS1^{U} cells. Viable cell count also decrease in astrocytes, as expected, based on SRB results.

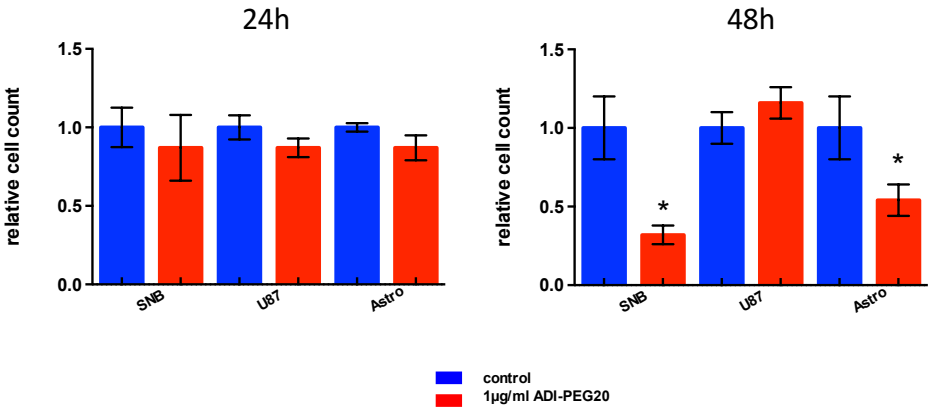
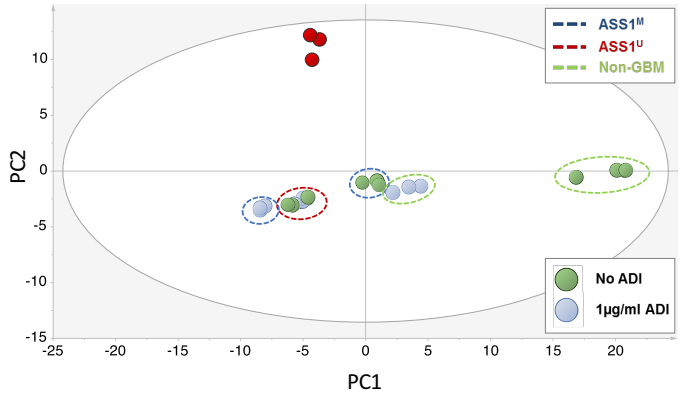


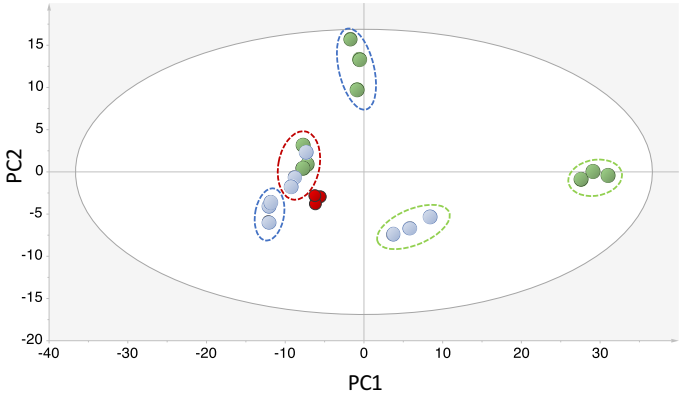
Figure 3.2.: Cell count determination in ASS1 GBM subtypes for GC/TOF MS analysis. ASS1^{M} (SNB19), ASS1^{U}(U87), and non-GBM control (astrocyte) cells ($n = 3$) were harvested at 24 and 48 hours in the presence and absence of ADI-PEG20 (1μg/ml) for GC/TOF MS analysis. Viable cells were counted with use of trypan blue and a haemocytometer, showing at 48 hours viable cell count of ASS1^{M} cells significantly decreased, whereas no significant change was observed in ASS1^{U} cells. Values shown are relative to control and error bars represent standard error $*p < 0.05$.

3.2.3. Profiling via GC/TOF MS

GC/TOF MS detected a total of 4,389 distinct metabolites in cell extract and 9,366 in cell media samples. Peaks with high variance (CV>30% in QCs) were removed and 2,310 metabolites featured in cell extract and 5,775 in cell media were imported into SIMCA for further statistical analysis. Close clustering of QC samples (figure 3.3), as indicated by grouping of all individual QC samples in the same region of the PCA scores plot, demonstrated consistency and robustness in instrumental run (i.e. no significant analytical variability) as well as sample preparation and processing. Clustering of sample groups (eg: non-treated cell line), via PCA analysis also demonstrated reproducibility amongst biological replicates for both cell extract and cell media samples.



(a)

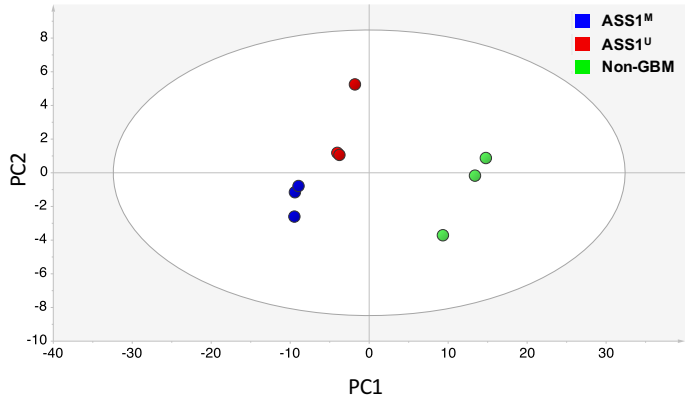


(b)

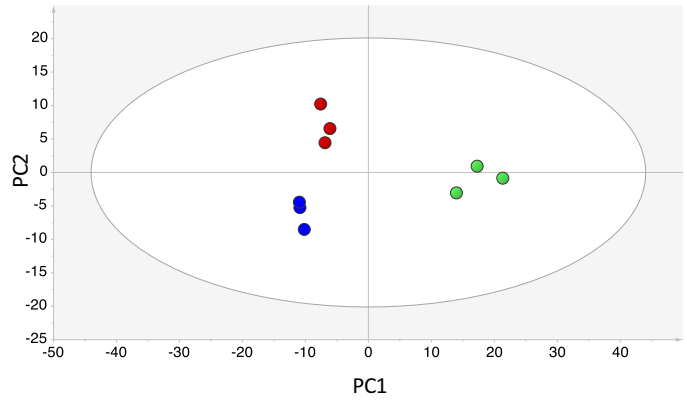
Figure 3.3.: GC/TOF MS highlighting quality control. This figure focuses on the quality control, to verify the consistency and robustness of the GC/TOF MS instrumental run, which is demonstrated by the PCA scores plot (PC1 vs PC2) showing clustering of quality controls (red circles, consisting of all pooled samples) amongst analysed metabolic profiles of GBM (SNB19, U87), and astrocyte cells (n=3) harvested at 48 hours in the presence and absence of ADI-PEG20 (1μg/ml). Individual cell lines are presented in subsequent figures. (a) Cell extract; R^2=0.945, Q^2=0.931 and (b) Cell media; R^2=0.799, Q^2=0.719.

3.2.4. GC/TOF MS: Distinct basal metabolic profile of ASS1 subtypes in GBM cell lines as determined by PCA and PLS-DA

PCA analysis showed that under normal growth conditions (absence of ADI-PEG20 treatment, here forth also referred to as basal levels), the global metabolic profile of GBM (SNB19 and U87) cells differed from non-GBM (astrocyte) cells in both extract (figure 3.4a) and cell media (figure 3.4b) fractions. There was a further separation between global profiles of $ASS1^{M}$ and $ASS1^{U}$ GBM subtypes. These results were also reflected in both the cell extract and cell media component.



(a)



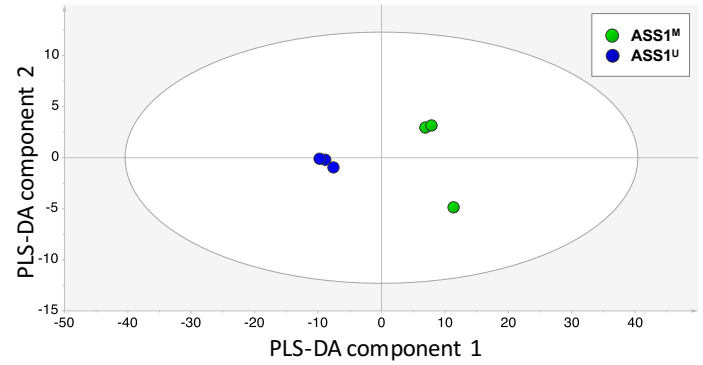
(b)

Figure 3.4.: GC/TOF MS: Distinct metabolic profile of ASS1 subtypes at basal levels. PCA scores plot (PC1 vs PC2), showing distinct global metabolic profile of $ASS1^{M}$ (SNB19), $ASS1^{U}$(U87), and non-GBM (astrocyte) cells ($n = 3$) harvested at 48 hours in absence of ADI-PEG20 and analysed via GC/TOF MS. Spectral peaks were normalised to cell count. (a) Cell extract; R^2=0.942, Q^2=0.881 and (b) Cell media; R^2=0.787, Q^2=0.635.

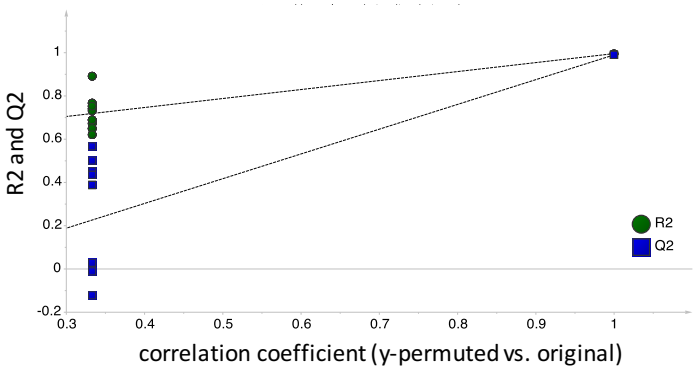
PLS-DA highlights discriminant metabolites between ASS1 subtypes analysed via GC/TOF MS

Differences between metabolic profiles of ASS1 subtypes ($ASS1^{M}$ versus $ASS1^{U}$) were further explored using PLS-DA, with PLS-DA models being validated by permutation tests. For the cell extract fraction (figure 3.5), $ASS1^{M}$ versus $ASS1^{U}$ group comparisons passed model validation criteria, where (i) Q^2 values of permuted data were higher than those of the original

data sets and (*ii*) Q^2 values intersected the y-axis below zero. For the cell media fraction (appendix figure A.1), PLS-DA did not pass model validation and were hence excluded from further analysis.



(a)



(b)

Figure 3.5.: GC/TOF MS: PLS-DA and permutation test of $ASS1^M$ and $ASS1^U$ extracts at basal levels. (a) PLS-DA was used to investigate the metabolic profiles of $ASS1^M$ (SNB19) and $ASS1^U$ (U87) cells from the cell extracts at basal levels. (b) Permutation test (100 permutations) was used for validating PLS-DA model, as determined here, where Q^2 values of permuted data were higher than those of the original data sets and Q^2 values trending towards intersection of the y-axis below zero.

GC/TOF MS: Tabulating basal level discriminant metabolites between ASS1 subtypes

Data from cell extract comparison ($ASS1^{M}$ versus $ASS1^{U}$), which had passed PLS-DA model validation was taken forward, generating a list of putative discriminant metabolites (table 3.1). Metabolites with VIP below 1 and p-values above 0.05 were removed, as described in section 2.2.5.

A total of 7 putative metabolites passed this cut-off criteria in the cell extract fraction and could be attributed to separation between $ASS1^{M}$ and $ASS1^{U}$ cells. Of these discriminant metabolites only 1 metabolite, malonic acid, passed the stringent Bonferroni-correction p-value of 0.00045 (table 3.1). Results tabulated show that when comparing basal extract metabolites of $ASS1^{M}$ and $ASS1^{U}$ cells, the majority of those passing the cut-off criteria were amino acids.

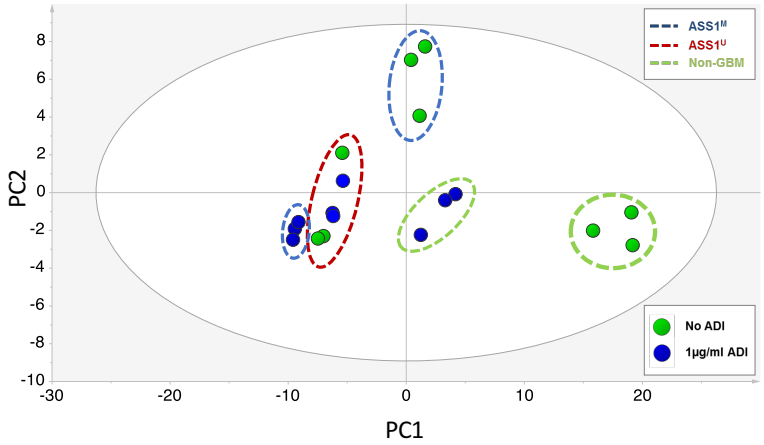
Table 3.1.: GC/TOF MS: Putative discriminant metabolites of ASS1 subtypes. Tabulation of putative differential metabolites derived from PLS-DA model of GC/TOF MS analysis of $ASS1^{M}$ (SNB19) versus $ASS1^{U}$ (U87) cell extract samples. Harvested at 48 hours and normalised to cell count, $*p < 0.00045$ passed Bonferroni correction. Fold-changes are relative to $ASS1^{M}$ (SNB19), all metabolites were ranked according to variable importance in projection (VIP) value and reached a similarity index of at least 60% with spectral libraries.

Sample	Metabolite	VIP	Fold-change	$P - value$
extract	Malonic acid	1.08	2.0	$< 0.00045*$
	L-threonine	1.03	1.8	< 0.01
	Alanine	1.03	3.2	< 0.01
	L-valine	1.00	1.5	< 0.01
	L-proline	1.00	1.8	< 0.05
	Cholesterol	1.00	1.5	< 0.05
	L-leucine	1.00	1.8	< 0.05

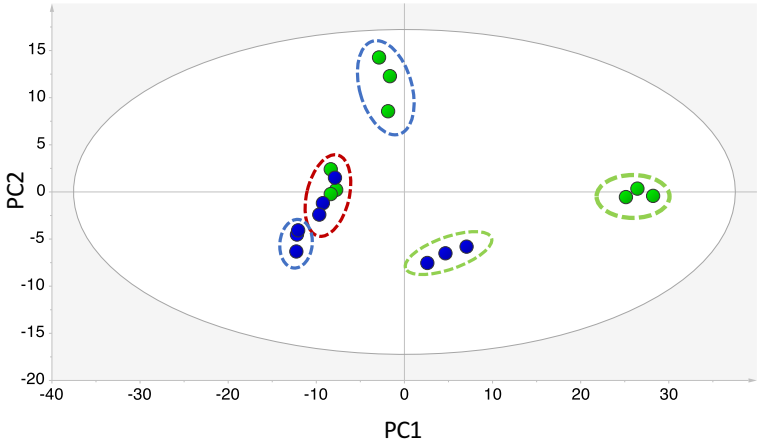
3.2.5. Arginine deprivation alters global metabolic profile of ASS1^{M} GBM cell lines

The effects of ADI-PEG20 on the metabolome of ASS1^{M} and ASS1^{U} GBM cells were next analysed via GC/TOF MS. PCA analysis (figure 3.6) showed that upon ADI-PEG20 treatment, there was a clear separation in the global metabolic profile of ASS1^{M} GBM cells.
This stood in contrast to observations in ASS1^{U} GBM, where there was no separation upon treatment, indicating there were few spectral differences and hence little global alteration in metabolic profile at 48 hours of exposure to ADI-PEG20. Results from SRB analysis in section 3.2.1 had shown that ASS1^{U} cells continue to proliferate in presence of ADI-PEG20. GC/TOF MS analysis provided further information of the cellular processes, showing that any metabolic alterations, such as those that could have been induced as cells start to synthesise arginine were limited in ASS1^{U} cells.

Astrocyte cells, which also display methylation of ASS1 showed separation upon treatment, as expected based on observations from cell count (figure 3.2). These results were seen in both the cell extract and cell media fraction of samples analysed by GC/TOF MS (figure 3.6). It should also be noted that replicate samples clustered closely, indicating similar spectral peaks and good biological reproducibility.



(a)



(b)

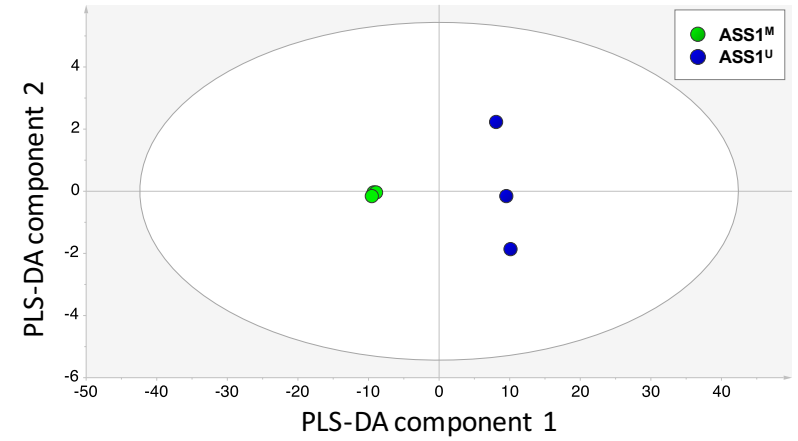
Figure 3.6.: GC/TOF MS: Global metabolic alteration upon ADI-PEG20 treatment in ASS1^{M} GBM cell line profiles. PCA scores plots (PC1 vs PC2) showing alterations in global metabolic profile of ASS1^{M} (SNB19) and non-GBM (astrocyte) cells upon ADI-PEG20 (1μg/ml) treatment. ASS1^{U} (U87) do not show separation upon treatment. Cells were harvested at 48 hours and spectra were normalised to cell count. (a) Cell extract; R^2=0.907, Q^2=0.869 and (b) Cell media; R^2=0.804, Q^2=0.719.

GC/TOF MS: PLS-DA highlights discriminant metabolites between untreated and ADI-PEG20 treated samples

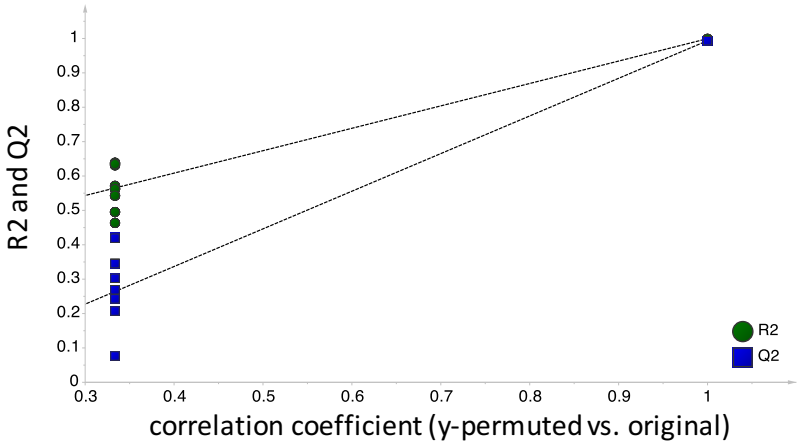
Differences between metabolic profiles of groups (eg: non-treated control versus treatment) were further explored using PLS-DA, with models being

validated by permutation tests (representative figure 3.7).

For the cell extract fraction, PLS-DA models generated from $ASS1^{M}$ (figure 3.7) cells passed model validation and were taken further, tabulating putative discriminant metabolites (see next section). For $ASS1^{U}$ and non-GBM (astrocyte) extracts, samples did not pass model validation as determined by permutation test, as described in materials and methods (section 2.2.5), where Q^2 values of permuted data sets were higher than those of original data sets (appendix figure A.2), and were hence excluded from further analysis.
For the cell media fraction, all group comparisons and models generated passed permutation validation criteria (appendix figure A.3), as determined by Q^2 values of permuted data sets being higher than those of original data sets. Having passed model validation, metabolites were ranked according to VIP value above 1 and p-value below 0.05 (see next section).



(a)



(b)

Figure 3.7.: GC/TOF MS: Representative PLS-DA and permutation test plot of cell extract in presence of ADI-PEG20. Representative plot (SNB19, extract samples) of (a) PLS-DA; R^2=0.958, Q^2=0.994 and (b) Y-permuted model validation (100 permutations) test for group comparison of non-treated versus treated (ADI-PEG20, 1μg/ml) GBM cell lines.

GC/TOF MS: Tabulating discriminant metabolites upon treatment

For groups passing PLS-DA model validation, lists of putative discriminant metabolites were generated, removing metabolites with VIP below 1 and p-values above 0.05 as in section 3.2.4 (see appendix table A.1 and A.2 for raw data list).
In $ASS1^{M}$ (SNB19) GBM cells, 8 putative discriminant metabolites passed the cut-off criteria in the cell extract fraction, and could be attributed to separation between non-treated and treated cells (table 3.2). Of these discriminant metabolites, 5 also reached the Bonferroni $p < 0.00045$. For the cell media fraction, 26 putative metabolites passed this cut-off criteria and 11 also passed the stringent Bonferroni p-value of below 0.0002 (table 3.3).
For $ASS1^{U}$ (U87) GBM cells, in the cell media fraction, 6 putative discriminant metabolites reached the cut-off criteria, and one metabolites, tryptophan, passed the Bonferroni p-value (table 3.4).
In non-GBM (astrocyte) cells, 35 discriminant metabolites shown by PLS-DA reached the cut-off criteria, with one metabolite, malonic acid, passing the stringent Bonferroni p-value (table 3.5).

Regarding the fold-change upon treatment, both in cell extract and media, there was a uniform increase upon treatment in $ASS1^{M}$ GBM. This stood in contrast to observations in $ASS1^{U}$ GBM, where in the media treatment resulted in both increased and decreased fold-changes amongst metabolites. Fold-changes in metabolites of astrocytes followed the same trend as $ASS1^{M}$ GBM.

Table 3.2.: GC/TOF MS: Putative discriminant metabolites of untreated control versus ADI-PEG20 treated ASS1^{M} cell extract. Differential Metabolites derived from PLS-DA model of GC/TOF MS analysis between non-treated ASS1^{M} (SNB19) and ADI-PEG20 treated cells. Fold-changes uniformly show metabolites were higher in treated samples compared to non-treated samples. Harvested at 48 hours and normalised to cell count. For cell extract $*p < 0.00045$ passed Bonferroni value. All metabolites were ranked according to variable importance in projection (VIP) value and reached a similarity index of at least 60% with spectral libraries.

Sample	Metabolite	VIP	Fold-change	$P - value$
extract	Malic acid	1.03	2.9	$< 0.00045*$
	Malonic acid	1.03	3.4	$< 0.00045*$
	Cholesterol	1.03	3.6	$< 0.00045*$
	Glucosamine	1.02	3.4	$< 0.00045*$
	L-Valine	1.01	4.0	$< 0.00045*$
	Galactose	1.01	2.5	< 0.001
	L-Proline	1.01	4.1	< 0.001
	Glycine	1.00	4.1	< 0.01

Table 3.3.: GC/TOF MS: Putative discriminant metabolites of untreated control versus ADI-PEG20 treated ASS1^{M} cell media. Differential Metabolites derived from PLS-DA model of GC/TOF MS analysis between non-treated ASS1^{M} (SNB19) and ADI-PEG20 treated cells. Fold-changes uniformly show metabolites were higher in treated samples compared to non-treated samples. Harvested at 48 hours and normalised to cell count. For cell media $*p < 0.0002$ passed Bonferroni value. All metabolites were ranked according to variable importance in projection (VIP) value and reached a similarity index of at least 60% with spectral libraries.

Sample	Metabolite	VIP	Fold-change	$P - value$
media	Maltose	1.15	4.2	$< 0.0002*$
	D-Galactose	1.15	4.1	$< 0.0002*$
	Pyridine	1.15	3.6	$< 0.0002*$
	Malonic acid	1.14	4.6	$< 0.0002*$
	L-Proline	1.14	3.9	$< 0.0002*$
	L-Valine	1.14	4.4	$< 0.0002*$
	Ribitol	1.14	3.4	$< 0.0002*$
	D-Glucose	1.14	3.9	$< 0.0002*$
	Pyrimidine	1.14	3.8	$< 0.0002*$
	L-Leucine	1.14	4.4	$< 0.0002*$
	Myo-inositol	1.14	3.5	$< 0.0002*$
	L-Isoleucine	1.13	4.6	< 0.001
	Malic acid	1.13	4.2	< 0.001
	Cholesterol	1.13	3.1	< 0.001
	Serine	1.13	3.1	< 0.001
	D-Gluconic acid	1.12	2.9	< 0.001
	Inositol	1.12	3.4	< 0.001
	L-Cysteine	1.12	2.8	< 0.001
	L-Threonine	1.11	3.4	< 0.005
	Phenylalanine	1.11	4.0	< 0.005
	L-Methionine	1.10	4.4	< 0.005
	D-Turanose	1.08	6.4	< 0.005
	L-Aspartic acid	1.08	4.5	< 0.01
	Purine	1.03	4.2	< 0.05
	D-Fructose	1.01	3.7	< 0.05
	L-Asparagine	1.01	4.2	< 0.05

Table 3.4.: GC/TOF MS: Putative discriminant metabolites of control versus ADI-PEG20 treated ASS1^{U} cells. Differential Metabolites derived from PLS-DA model of GC/TOF MS analysis between ASS1^{U} (U87) control and ADI-PEG20 treated cells. Fold-changes show metabolites both increased and decreased upon treatment. Harvested at 48h and normalised to cell count, $*p < 0.0002$ passed Bonferroni correction. All metabolites were ranked according to variable importance in projection (VIP) value and reached a similarity index of at least 60% with spectral libraries.

Sample	Metabolite	VIP	Fold-change	$P - value$
media	Tryptophan	1.56	7.0	$< 0.0002*$
	Maltose	1.48	0.1	< 0.01
	Glycine	1.52	11.0	< 0.01
	Ribitol	1.42	2.3	< 0.01
	Malic acid	1.35	0.8	< 0.01
	D-Galactose	1.33	0.8	< 0.01

Table 3.5.: GC/TOF MS: Putative discriminant metabolites of control versus ADI-PEG20 treated astrocyte cells. Differential Metabolites derived from PLS-DA model of GC/TOF MS analysis between non-GBM (astrocytes) control and ADI-PEG20 treated cells. Fold-changes uniformly show increased metabolites in treated samples compared to non-treated samples. Harvested at 48 hours and normalised to cell count, $*p < 0.0002$ passed Bonferroni correction. All metabolites were ranked according to variable importance in projection (VIP) value and reached a similarity index of at least 60% with spectral libraries.

Sample	Metabolite	VIP	Fold-change	$P - value$
media	Malonic acid	1.14	1.9	$< 0.0002*$
	Inosine	1.14	3.1	< 0.0005
	Glycine	1.13	2.4	< 0.0005
	L-Aspartic acid	1.13	5.4	< 0.0005
	Ribitol	1.13	3.4	< 0.001
	D-Fructose	1.13	3.7	< 0.001
	Tryptophan	1.13	2.9	< 0.001
	L-Methionine	1.12	3.8	< 0.001
	Maltose	1.12	2.0	< 0.005
	L-Asparagine	1.12	8.2	< 0.005
	Myo-inositol	1.12	2.3	< 0.005
	L-homoserine	1.12	3.5	< 0.005
	Cholesterol	1.12	2.1	< 0.005
	D-Gluconic acid	1.11	2.1	< 0.005
	Malic acid	1.11	2.1	< 0.005
	D-Galactose	1.11	2.2	< 0.005
	2-keto-D-gluconic acid	1.10	4.3	< 0.005
	Pyridine	1.10	2.2	< 0.005
	D-Galactose	1.10	2.2	< 0.005
	L-Leucine	1.09	2.8	< 0.005
	Phenylalanine	1.09	2.6	< 0.005
	L-Isoleucine	1.08	2.6	< 0.005
	L-Proline	1.08	2.1	< 0.01
	Glucosamine	1.08	5.8	< 0.01
	Glycoside	1.08	5.2	< 0.01
	Pyrimidine	1.08	2.1	< 0.01
	L-Threonic acid	1.08	2.0	< 0.01
	L-Valine	1.06	2.4	< 0.01
	L-Cysteine	1.06	4.4	< 0.01
	Mannose	1.05	3.7	< 0.05
	D-Glucose	1.04	2.0	< 0.05
	Urea	1.04	1.9	< 0.05
	D-Fructose	1.01	2.1	< 0.05
	Purine	1.01	2.4	< 0.05

3.2.6. ^{1}H NMR: Complementary metabolic characterisation of ASS1 GBM subtypes

3.2.7. Experimental parameters

^{1}H NMR was performed in order to expand the scope of metabolite coverage and validate global trends observed in GC/TOF MS. The strength of using two different analytical instruments lies in the complimentary coverage of metabolites across these platforms [12]. Overlap also exists for some compounds, allowing for validation across two instruments.

Cell count of non-treated and ADI-PEG20 treated cells at 48 hour harvest for ^{1}H NMR analysis

As with the GC/TOF MS (section A.2), parameters for optimal cell culture conditions were established for ^{1}H NMR analysis. This included optimisation of the cell seeding density and ensuring cell harvest yield of at least 1x10^6 at 48 hours, to have sufficient sample volume and biological material for ^{1}H NMR instrumental analysis.

In line with the parameters and cells used in GC/TOF MS analysis, ASS1$^{\mathrm{M}}$ (SNB19), ASS1$^{\mathrm{U}}$ (U87) and non-GBM (astrocyte) cells were harvested at 48 hours and cell count was determined (figure 3.8). In keeping with previous SRB (section 3.2.1) and cell count analysis (section A.2), harvest for ^{1}H NMR analysis at 48 hours confirmed that ADI-PEG20 significantly decreases viable cell count in ASS1$^{\mathrm{M}}$ cells and not ASS1$^{\mathrm{U}}$ cells. As in GC/TOF MS cell harvest, viable cell count in astrocytes decreased upon ADI-PEG20 treatment at 48 hours, however contrary to previous results (section A.2) this was not significant.

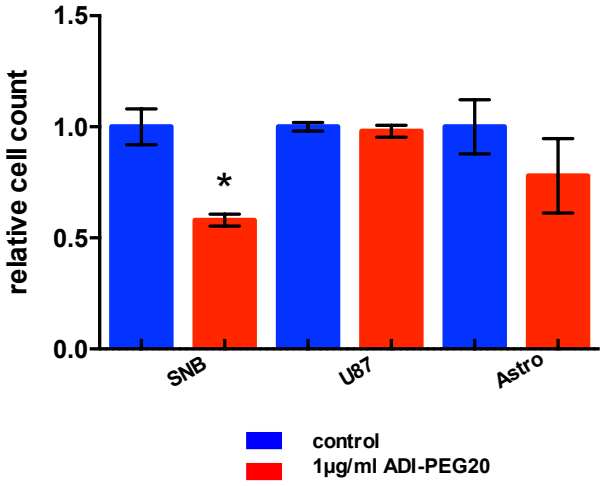


Figure 3.8.: Cell count determination at 48 hours in ASS1 GBM subtypes for ^{1}H NMR analysis. ASS1$^{\mathrm{M}}$ (SNB19), ASS1$^{\mathrm{U}}$(U87), and non-GBM (astrocyte) cells ($n = 3$) were harvested at 48 hours in the presence and absence of ADI-PEG20 (1μg/ml) for ^{1}H NMR analysis. Cells were counted via a haemocytometer with use of trypan blue, showing that at 48 hours viable cell count of ASS1$^{\mathrm{M}}$ cells significantly decreased, whereas no significant change was observed in ASS1$^{\mathrm{U}}$ or non-GBM (astrocyte) cells. Values shown are relative to control and error bars represent standard error $*p < 0.05$.

Profiling via ^{1}H NMR

Data from ^{1}H NMR analysis was normalised via probabilistic quotient normalisation, as this approach has been shown to be more accurate than widespread normalisation approaches used for ^{1}H NMR [32].

Confirmation of ADI-PEG20 treatment effect

In order to validate the expected arginine decrease upon ADI-PEG20 treatment, levels were interrogated. Cell media samples showed that arginine decreased in ADI-PEG20 treated samples, relative to non-treated (control) samples (figure 3.9). The observed decrease was significant, however smaller than anticipated. This could be attributed to the fact that the amino-acid lysine, also a constituent of DMEM media [34], rest at the same spectral region as arginine, making it difficult to distinguish between the spectral

detection of these two amino acids.

Citrulline, one of the by-products released during arginine degradation, was therefore also interrogated. In line with the expected treatment effect, citrulline increased by a fold-change of 1.2 - 1.3 upon treatment (figure 3.9). These results suggest that citrulline is a clearer indicator for detecting ADI-PEG20 effect via ^{1}H NMR, as it rests in a spectral region where there are no other metabolites.

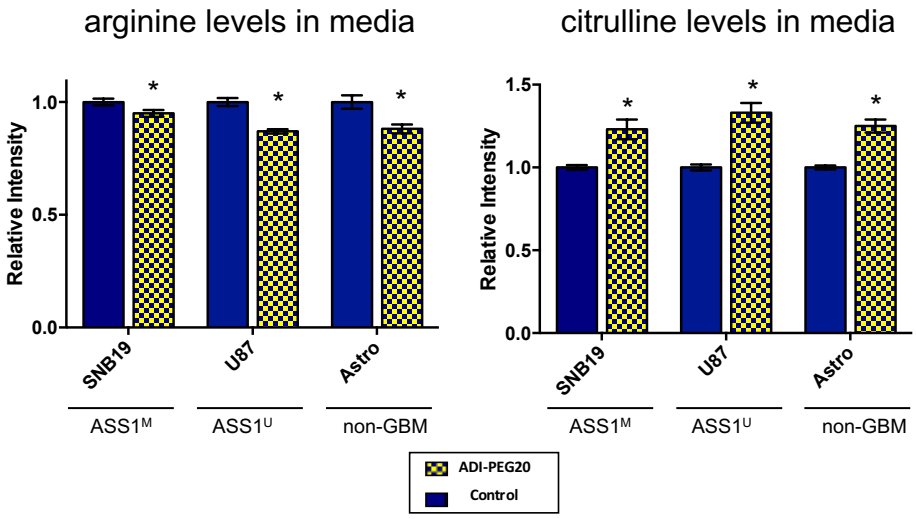
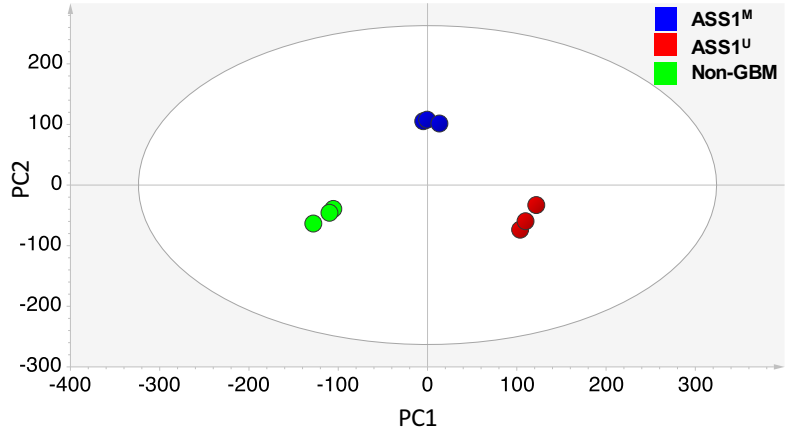


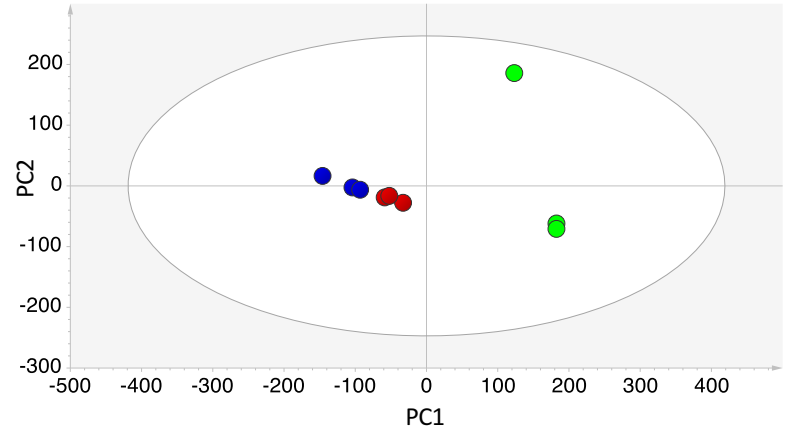
Figure 3.9.: ^{1}H NMR: Control of ADI-PEG20 treatment effect via arginine and citrulline. Arginine decreases and citrulline increases upon ADI-PEG20 treatment (1μg/ml ADI-PEG20). Averages ($n = 3$) of integral intensities calculated at 48 hours in media of untreated control and treated GBM cell line samples. Standard deviation marked with error bars and significance between treated and non-treated lines marked with $*p < 0.05$.

3.2.8. ^{1}H NMR validates global GC/TOF MS observations: Distinct basal metabolic profile of ASS1 subtypes in GBM cell lines

In order to validate global GC/TOF MS findings and enhance the scope of metabolic coverage, PCA was performed on ^{1}H NMR data. PCA showed a separation in the global metabolic profile of ASS1$^{\mathrm{M}}$ and ASS1$^{\mathrm{U}}$ GBM cell lines at basal levels (figure 3.10). These findings validated the global trend observed at basal level in GC/TOF MS analysis.



(a)



(b)

Figure 3.10.: ^{1}H NMR: basal metabolic profile. PCA scores plots (PC1 vs PC2) of ASS1^{M} (SNB19), ASS1^{U} (U87) and non-GBM (astrocyte) cells ($n = 3$), harvested at 48 hours in the absence of ADI-PEG20 treatment and analysed via ^{1}H NMR. As demonstrated by clear separation amongst cells, results in both media and extract show distinct global metabolic profile between ASS1^{U}, ASS1^{M} and non-GBM (astrocyte) cells. Probabilistic quotient normalisation. (a) Cell extract; R^2=0.457, Q^2=0.076 and (b) Cell media; R^2=0.621, Q^2=0.197.

^{1}H NMR: OPLS-DA highlights discriminant metabolites at basal levels

Specific differences between metabolic profiles of ASS1 subtypes ($ASS1^{M}$ versus $ASS1^{U}$) were further explored using OPLS-DA in MATLAB. OPLS-DA is frequently applied to metabolomic data and similar to the PLS-DA model applied in GC/TOF MS analysis (section A.2). Additional features include that more subtle differences can be detected between data-sets of groups, and model visualisation is improved [12] [146].

Discriminant metabolites between ASS1 subtypes were highlighted with OPLS-DA, by showing (*i*) the direction of variation (eg: elevated in $ASS1^{U}$) and (*ii*) strength of correlation, as shown by colourimetric R^2 correlation coefficient indicator (red for high correlation and blue for no correlation). Validity of OPLS-DA models was determined through Q^2 values, with 1 being the highest score and negative Q^2 values disqualifying OPLS-DA models due to lack of predictive power.

Both cell extract (figure 3.11) and cell media (figure 3.12) group comparisons ($ASS1^{M}$ versus $ASS1^{U}$) passed model validation. OPLS-DA highlighted discriminant metabolite peaks and those with high correlation coefficients were extracted. Metabolites were matched with standards in the Chenomx spectral library (Chenomx NMR suite 8.1 Profiler, Canada) and discriminant metabolites are listed in table 3.6.

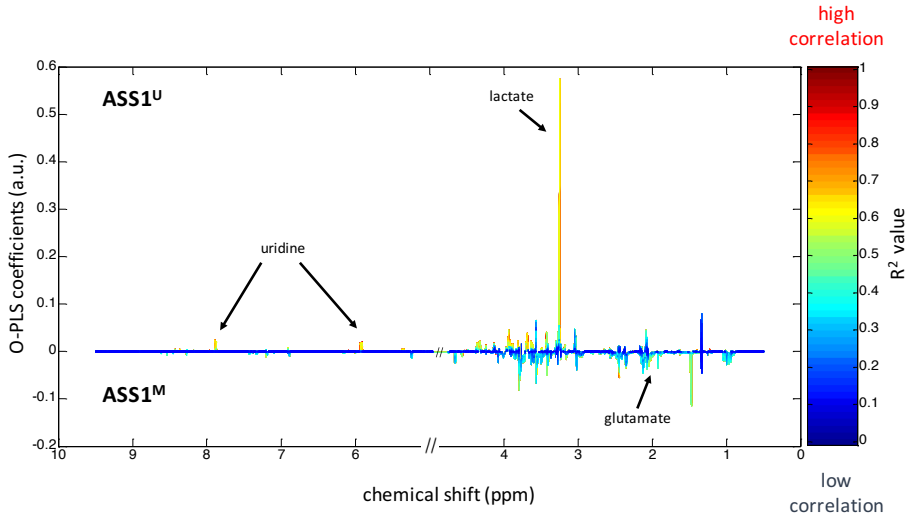


Figure 3.11.: ^{1}H NMR: OPLS-DA correlation coefficient plot of cell extract from ASS1 subtypes. OPLS-DA correlation coefficient plot from ^{1}H NMR spectra. Comparison of ASS1^{M} (SNB19) and ASS1^{U} (U87) GBM cell extract at basal levels (absence of treatment), showing limited discriminatory metabolites as indicated by colour scale of Pearson correlation coefficient R^2, where red indicated strong correlation and blue poor correlation. Upward pointing peaks are positively correlated with ASS1^{U} cells and downward pointing peaks are positively correlated with ASS1^{M}. Metabolites including lactate and uridine were associated with ASS1^{M} cell extract, whereas glutamate was associated with ASS1^{U} cell extract. Probabilistic quotient normalised. Cumulative values R^2=0.889 and Q^2=0.440. Key: A.u (arbitrary units), ppm (parts per million).

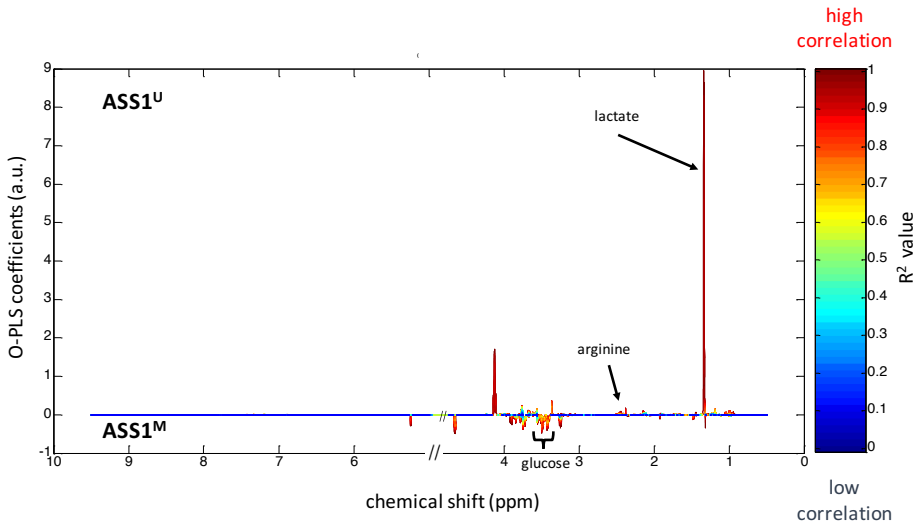


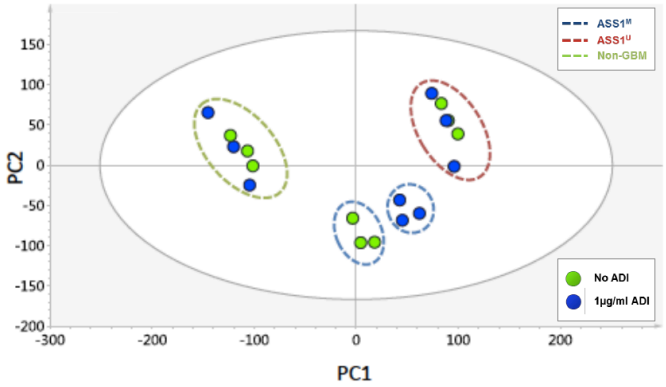
Figure 3.12.: ^{1}H NMR: OPLS-DA correlation coefficient plot of media from ASS1 subtypes. OPLS-DA correlation coefficient plot from ^{1}H NMR spectra. Comparison of ASS1^M (SNB19) and ASS1^U (U87) GBM cell media at basal levels (absence of treatment), showing limited discriminatory metabolites as indicated by colour scale of Pearson correlation coefficient R^2, where red indicated strong correlation and blue poor correlation. Metabolites including glucose were associated with ASS1^M cell media, whereas arginine and lactate were associated with ASS1^U cell media. Upward pointing peaks are positively correlated with ASS1^U cells and downward pointing peaks are positively correlated with ASS1^M. Probabilistic quotient normalised. Cumulative values R^2=0.999 and Q^2=0.889. Key: A.u (arbitrary units), ppm (parts per million).

Table 3.6.: OPLS-DA: discriminant metabolites amongst ASS1 subtypes at basal level. Differential metabolites derived from OPLS-DA model of $ASS1^{M}$ (SNB19) and $ASS1^{U}$ (U87) cell extract and media comparison at basal levels (absence of treatment) from ^{1}H NMR analysis. Metabolites listed were positively correlated with ASS1 subtypes.

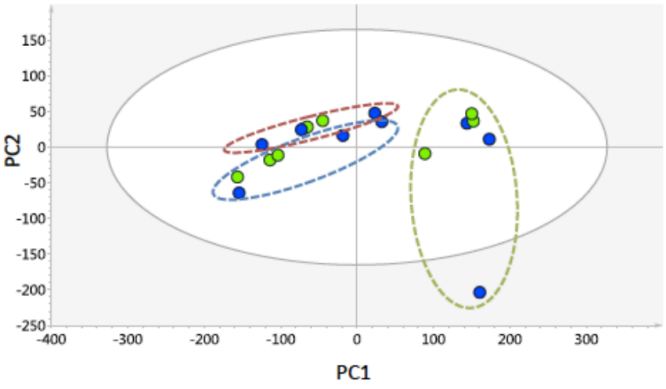
Cell extract		Cell media	
$ASS1^{U}$	$ASS1^{M}$	$ASS1^{U}$	$ASS1^{M}$
uridine	glutathione	arginine	glucose
uridine species	glutamine	lactate	glutamate
lactate	glutamate	pyruvate	
tyrosine		leucine	
choline		taurine	
taurine		3-hydroxy-isovalerate	
beta-alanine		isoleucine	
2-hydroxyl-valerate			
ribose			

3.2.9. ^{1}H NMR: Metabolic alteration upon ADI-PEG20 treatment

Having investigated samples at basal levels, metabolic profiles upon ADI-PEG20 treatment were next studied. PCA of $ASS1^{M}$ cells showed, that upon treatment, there was a clear separation in the global metabolic profile of cell extracts, and a marginal separation in cell media (figure 3.13).
This stood in contrast to observations in extract and media of $ASS1^{U}$ GBM cells, where there was no separation, indicating little global metabolic alteration upon treatment. These observations validated global trends observed in GC/TOF MS analysis (section A.2).
In astrocytes, ^{1}H NMR of cell media and cell extract showed that there was no separation upon ADI-PEG20 treatment, which stood in contrast to GC/TOF MS results. For both the PCA (figure 3.13) and cell count (figure 3.8), astrocytes followed the pattern observed in $ASS1^{U}$ (U87) cells.



(a)



(b)

Figure 3.13.: ^{1}H NMR: metabolic profile upon ADI-PEG20 treatment. PCA scores plots (PC1 vs PC2) from global metabolic profile of ASS1^{U} (U87), ASS1^{M} (SNB19) and non-GBM (astrocyte) cells ($n = 3$) at 48 hours in the presence and absence of ADI-PEG20 (1μg/ml) treatment from ^{1}H NMR analysis. Probabilistic quotient normalisation. (a) Cell extract; R^2=0.335, Q^2=0.130 and (b) Cell media; R^2=0.496, Q^2=0.077.

^{1}H NMR: OPLS-DA highlights discriminant metabolites upon ADI-PEG20 treatment

As described in the previous section (section 3.2.8), OPLS-DA was also applied to treated groups (eg: non-treated control versus ADI-PEG20 treated groups). Specific differences between metabolic profiles of groups were highlighted via colourimetric scale along spectral axis (figure 3.14).
All group comparisons passed model validation. OPLS-DA highlighted dis-

criminant metabolite peaks and those with high correlation coefficients were extracted. Figure 3.14 and 3.15 display representative OPLS-DA plots of cell extract and media accordingly in ASS1^{M} (SNB19) cells. Further OPLS-DA plots are found in the appendix (section A A.3). Metabolites were matched with the standards in the Chenomx spectral library (Chenomx NMR suite 8.1 Profiler, Canada) and discriminant metabolites are listed in table 3.7.

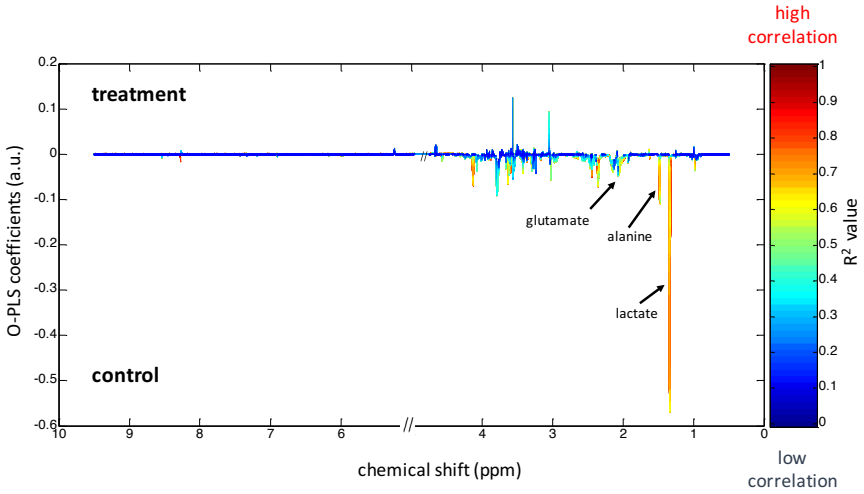


Figure 3.14.: ^{1}H NMR: Representative OPLS-DA correlation coefficient plot of cell extract in ASS1^{M} control versus treatment. OPLS-DA correlation coefficient plot from ^{1}H NMR spectra in ASS1^{M} (SNB19) cells harvested at 48 hours. Comparison of control and ADI-PEG20 treated (1μg/ml) cell extract samples ($n = 3$), highlighted discriminant metabolites including glutamate, alanine and lactate. Discriminatory metabolites were highlighted as indicated by colour scale of Pearson correlation coefficient R^2, where red indicated strong correlation and blue poor correlation. Upward pointing peaks are positively correlated with treated samples and downward pointing peaks are positively correlated with untreated control samples. Probabilistic quotient normalised. Cumulative values R^2=0.903 and Q^2=0.558. Key: A.u (arbitrary units), ppm (parts per million).

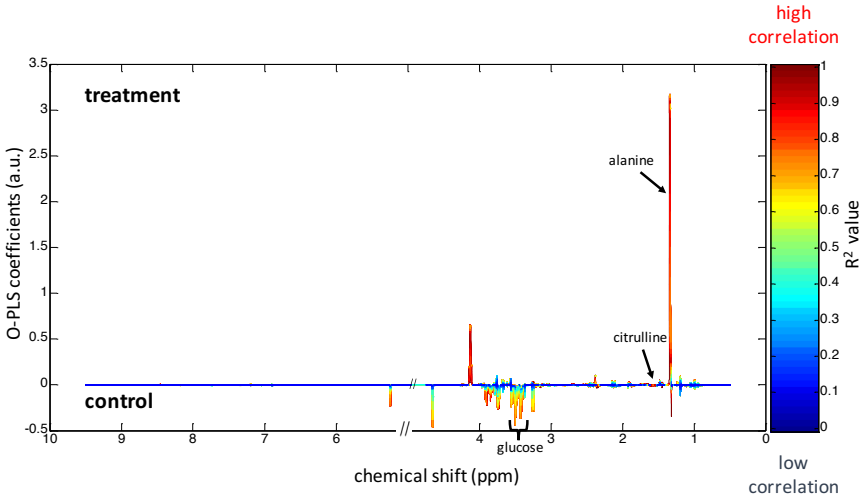


Figure 3.15.: ^{1}H NMR: Representative OPLS-DA correlation coefficient plot of cell media in ASS1^{M} control versus treatment. OPLS-DA correlation coefficient plot from ^{1}H NMR spectra in ASS1^{M} (SNB19) cells harvested at 48 hours. Comparison of control and ADI-PEG20 treated (1μg/ml) cell media samples ($n = 3$), showing discriminatory metabolites, including citrulline, alanine and glucose, as indicated by colour scale of Pearson correlation coefficient R^2, where red indicated strong correlation and blue poor correlation. Upward pointing peaks are positively correlated with treated samples and downward pointing peaks are positively correlated with control samples. Probabilistic quotient normalised. Cumulative values R^2=0.983 and Q^2=0.925. Key: A.u (arbitrary units), ppm (parts per million).

Table 3.7.: OPLS-DA: discriminant metabolites amongst ASS1 subtypes. Differential metabolites derived from OPLS-DA model of $ASS1^{M}$ (SNB19), $ASS1^{U}$ (U87) and non-GBM (astrocyte) cell extract and media from ^{1}H NMR analysis. Comparison in the presence and absence of ADI-PEG20 treatment (1μg/ml). Metabolites listed were positively correlated with groups (i.e: metabolites listed under control column were higher in control compared to treated group).

Cell line	Extract		Media	
	control	treatment	control	treatment
$ASS1^{M}$	glutathione	glycoproline	phenylalanine	citrulline
SNB19	lactate		glucose	thymine
	creatine		serine	alanine
	myo-inositol or AMP		3-methyl-2-oxovalerate	sn-glycero-3-phosphocholine
	alanine		choline	tyrosine
	aspartate		3-hydroxy-3-methylglutarate	citrate
	pyroglutamate		proline	succinate
	glutamate		pyroglutamate	proline
	glycoproline			valine
	threonine			lysine
				thymidine
				glycocholate
$ASS1^{U}$	UDP-glucose	citrulline	arginine	citrulline
U87	glycocholate		glucose	creatine phosphate
	glucose		glutamate	
	glutamate		methionine	
	succinate			
	glutamine			
Non-GBM	glycine	glutamate	arginine	citrulline
		3-hydroxyisovalerate		
Astro			glucose	thymidine
			lactate	
			proline	
			glutathionine	
			formate	
			valine	

3.2.10. Validation of trends in ASS1 GBM subtypes via ^{1}H NMR analysis

3.2.11. Experimental parameters

In order to verify ^{1}H NMR findings (section 3.2.6), enhance biological coverage and strengthen experimental parameters, an ^{1}H NMR validation experiment was performed. In addition to the cell lines used in previous ^{1}H NMR analysis (SNB19, U87 and astrocytes), further cell lines were added. For ASS1$^{\mathrm{M}}$ this included GAMG and LN229, and for ASS1$^{\mathrm{U}}$ this included U118. In order to strengthen statistical analysis, replicate samples were increased from $n = 3$ to $n = 9$.

Cell count of non-treated and ADI-PEG20 treated cells at 48 hour harvest for ^{1}H NMR analysis

Cells were plated and harvested at 48 hours, using optimal conditions established in previous ^{1}H NMR analysis (section 3.2.6). In line with earlier GC/TOF MS and ^{1}H NMR experiments, cell count was determined, parallel to harvest for metabolomic analysis.

Results of cell count confirmed ADI-PEG20 treatment effect, in decreasing viable cell count at 48 hours in ASS1$^{\mathrm{M}}$ cells and not ASS1$^{\mathrm{U}}$ cells (figure 3.16). Corresponding trends were demonstrated both in previously used cells (SNB19 and U87) and the added cell panel (GAMG, LN229 and U118).

Viable cell count of astrocytes significantly decreased upon ADI-PEG20 treatment. These results reflected the same trend observed in the previous ^{1}H NMR, SRB and GC/TOF MS analysis.

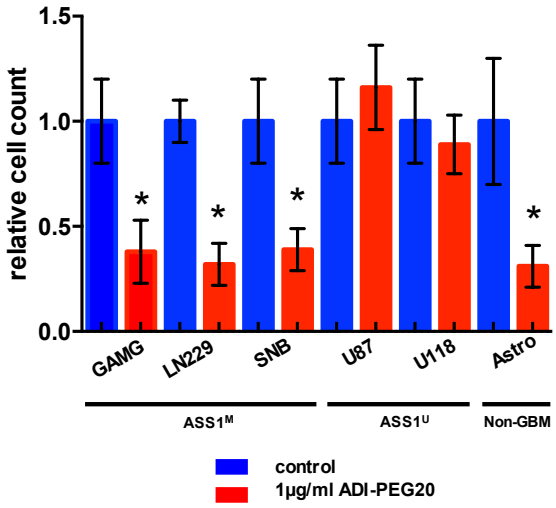


Figure 3.16.: Cell count determination at 48 hours in ASS1 GBM subtypes for ^{1}H NMR validation. ASS1$^{\mathrm{M}}$ (GAMG, LN229, SNB19), ASS1$^{\mathrm{U}}$(U87, U118), and non-GBM (astrocyte) cells ($n = 3$) were harvested at 48 hours in the presence and absence of ADI-PEG20 (1μg/ml) for ^{1}H NMR analysis. Cells were counted via a haemocytometer with use of trypan blue, showing that at 48 hours viable cell count of ASS1$^{\mathrm{M}}$ cells significantly decreased, whereas no significant change was observed in ASS1$^{\mathrm{U}}$ cells. Values shown are relative to control and error bars represent standard error $*p < 0.05$.

Profiling via ^{1}H NMR

^{1}H NMR spectra were acquired for each sample with both 1D NOESY and CPMG pulse sequence programmes. CPMG spectra were taken forward for subsequent analysis, as more metabolites could be detected. Representative spectra (figure 3.17) shows how protein suppression of the CPMG programme allowed for low-molecular weight metabolite metabolites such as tryptophan to be detected. In line with previous ^{1}H NMR analysis (section 3.2.6), spectra were normalised via probabilistic quotient normalisation.

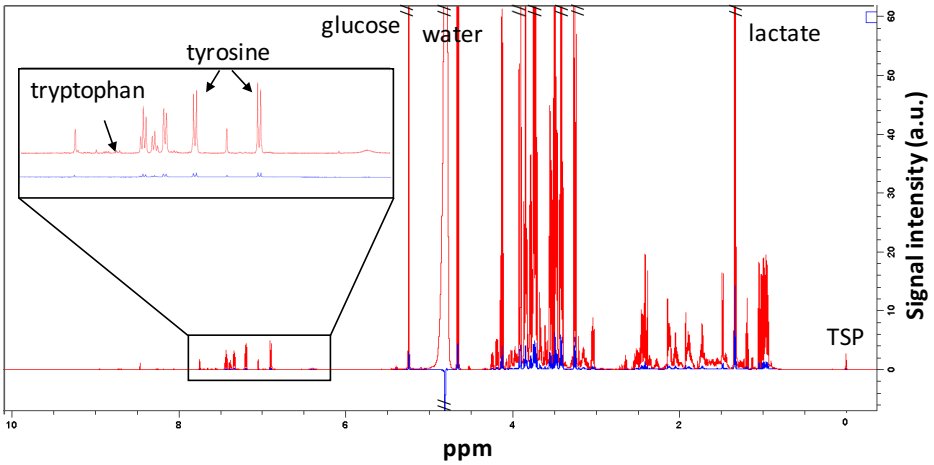


Figure 3.17.: Representative CPMG and 1D NOESY ^{1}H NMR spectra: Representative ^{1}H NMR spectra demonstrate CPMG spectra (red) allowed for more low-molecular weight metabolites such as tryptophan to be detected in GBM samples (from SNB19 media) than 1D NOESY (blue) pulse sequence programmes. A.u. (arbitrary units), ppm (parts per million).

Confirmation of ADI-PEG20 treatment effect

ADI-PEG20 treatment effect was further validated by interrogating arginine and citrulline levels. Blank and cell media samples confirmed that upon treatment, arginine decreased and citrulline increased at 48 hours (figure 3.18). LN229 (ASS1^{M}) cells, were however an exception, showing that arginine did not significantly decrease upon treatment. As outlined in section 3.2.7, this may be attributed to the fact that the amino-acid lysine rest at the same spectral region as arginine, and citrulline is a clearer indicator of ADI-PEG20 treatment effect via ^{1}H NMR in this *in vitro* model.

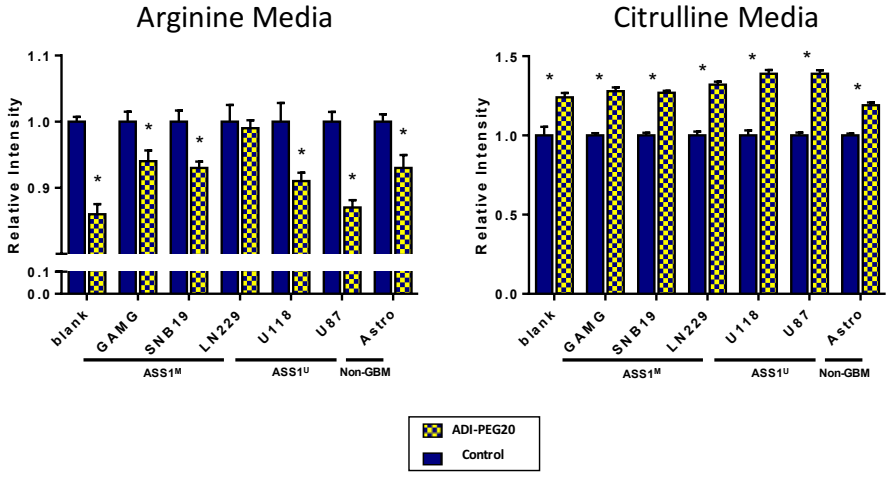


Figure 3.18.: ^{1}H NMR validation: Internal control of ADI-PEG20 effect. Arginine decreases and citrulline increases upon ADI-PEG20 treatment (1μg ADI-PEG20). Averages ($n = 9$) of integral intensities calculated at 48 hours in media of control and treated GBM cell line samples. Standard deviation marked with error bars and significance between treated and non-treated lines marked with $*p < 0.05$ for arginine and $*p < 0.001$ for citrulline.

3.2.12. ^{1}H NMR: Validation of global basal level trends in ASS1 subtypes

PCA analysis validated observations made in previous ^{1}H NMR analysis (section 3.2.6) and also provided further insights into global metabolic trends in ASS1 subtypes.

For the cell extract fraction, astrocytes were excluded from PCA, as sufficient information could not be gained from low spectra signal in these samples. This was due to lower count at harvest compared to other GBM lines and previous ^{1}H NMR analysis. These results highlight the limitations of using primary astrocyte cell lines in ^{1}H NMR analysis of cell extract studies, as large quantities of cells are required for detection (over $1x10^6$).

For the cell media fraction, PCA showed that the global profiles of GBM cell lines separated from non-GBM (astrocyte) cells (figure 3.19). In order

to interpret clustering trends amongst GBM lines and enhance visualisation, astrocytes were removed from cell media PCA plots.

Having excluded astrocytes, PCA showed that in the absence of treatment, the global profiles of SNB19 ($ASS1^{M}$) and U87 ($ASS1^{U}$) separated in both the cell extract and media fraction (figure 3.20). This was in-line with the observations of previous ^{1}H NMR and GC/TOF MS analysis. Further, $ASS1^{M}$ cells (SNB19, LN229, GAMG) clustered together, indicating similarities in their global profile amongst both cell extract and media sample fractions. Clustering of $ASS1^{M}$ cells was particularly pronounced in cell media samples.

PCA also showed that under normal growth conditions, U118 ($ASS1^{U}$) cells clustered with $ASS1^{M}$ cells (SNB19, LN229, GAMG), highlighting that in the presence of extra-cellular arginine not all ASS1 subtypes separate.

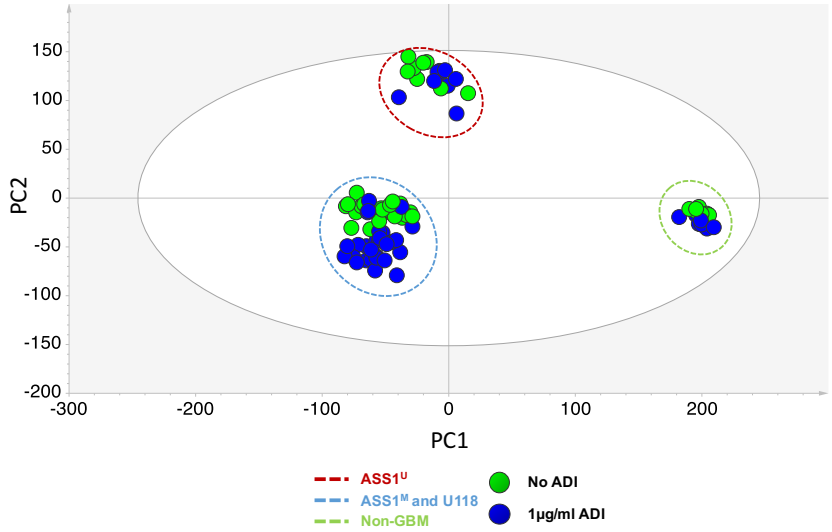
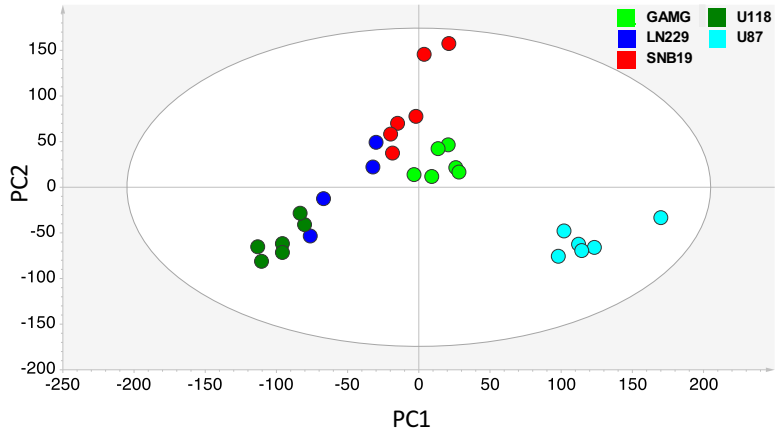
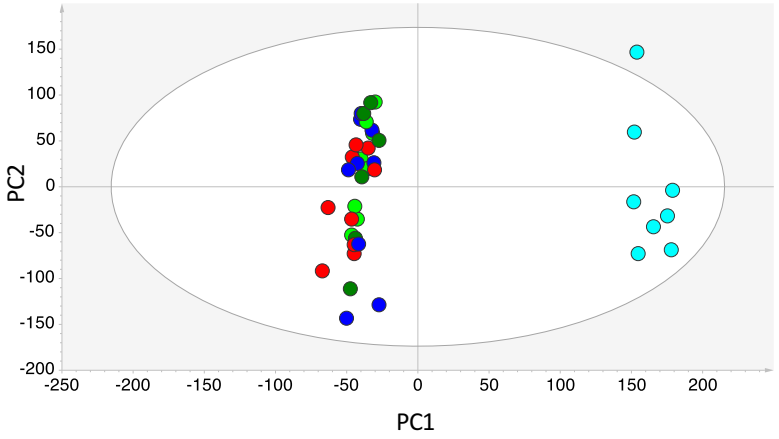


Figure 3.19.: ^{1}H NMR validation: PCA of metabolic profiles in media. PCA scores plots (PC1 vs PC2) from global metabolic profile of $ASS1^{U}$ (U87, U118), $ASS1^{M}$ (SNB19, GAMG, LN229) and non-GBM (astrocyte) cell media ($n = 4 - 9$) at 48 hours in the presence and absence of ADI-PEG20 (1μg/ml) from ^{1}H NMR analysis. R^2=0.386, Q^2=0.353. Probabilistic quotient normalisation.



(a)



(b)

Figure 3.20.: ^{1}H NMR validation: PCA of basal metabolic profiles. PCA scores plots (PC1 vs PC2) showing global metabolic profile of ASS1^{M} (SNB19, GAMG, LN229), ASS1^{U} (U87, U118) and non-GBM (astrocyte) cells ($n = 4-9$) at 48 hours in the absence of ADI-PEG20 and analysed via ^{1}H NMR. Probabilistic quotient normalisation. (a) Cell extract; R^2=0.264, Q^2=0.194 and (b) Cell media; R^2=0.292, Q^2=0.243.

^{1}H NMR: OPLS-DA highlights discriminant metabolites at basal levels

Specific differences between metabolic profiles of ASS1 subtypes were further explored using OPLS-DA. All group comparisons passed model validation as determined by positive Q^2 values.
At basal level, OPLS-DA of the cell extract highlighted more metabolic differences of high correlation between ASS1 subtypes (figure 3.21), than the cell media fraction (figure 3.22). Peaks of high correlation were all positively associated with $ASS1^{U}$ (U87, U118) cells, indicating they were metabolically more active than $ASS1^{M}$ cells.
Discriminant metabolites positively associated with $ASS1^{U}$ included uridine, uridine-associated metabolites (UDP-galactose, UDP-glucuronate, UDP-glucose, UDP-n-acetylglucosamine, y-glutamylphenylalanine), glucose, lactate and glutamate (table 3.8).

For cell media, OPLS-DA correlation coefficient plot showed there were limited metabolic alterations of high correlation between $ASS1^{M}$ (GAMG, SNB19, LN229) and $ASS1^{U}$ (U87, U118) GBM (figure 3.22). This reflected the trend observed via PCA (figure 3.20), where U118 clustered with $ASS1^{M}$ cells.

As indicated by colourimetric scale, metabolites of higher correlation were highlighted by the model and identities were assigned. These included alpha-ketoisovalerate and pyroglutamate. The former being a product of valine degradation, a compound not present in cell media or synthesised by human cells and was hence discarded as an artefact. The later, was positively correlated with $ASS1^{M}$ cells and is a metabolite associated with glutathionine (an antioxidant) synthase deficiency [100]. Methanol was also identified as a contaminant.

Discriminant metabolites matched with the standards in the Chenomx spectral library (Chenomx NMR suite 8.1 Profiler, Canada) are listed in table 3.8.

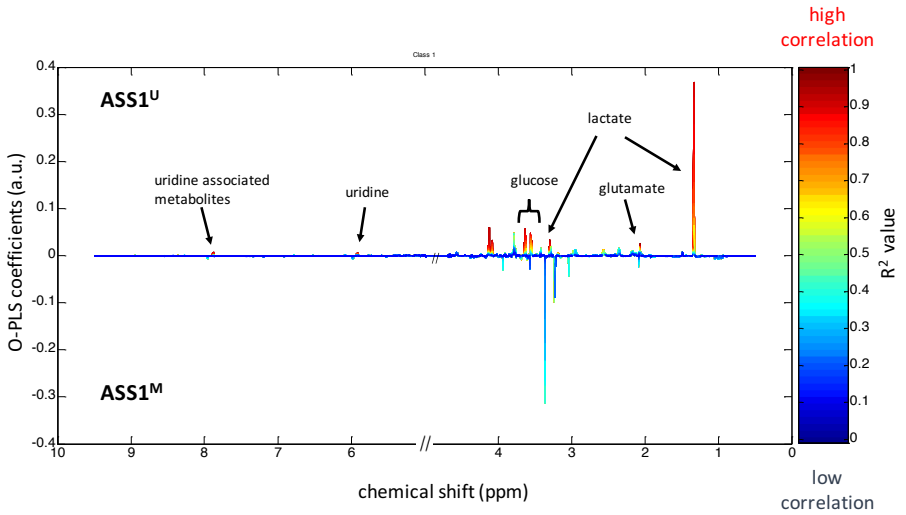


Figure 3.21.: ^{1}H NMR validation of extract: OPLS-DA correlation coefficient plot. OPLS-DA correlation coefficient plot obtained from ^{1}H NMR spectra. Comparison of ASS1^M (SNB19, LN229, GAMG) and ASS1^U (U87, U118) GBM cell extract at basal levels (absence of treatment), showing limited discriminatory metabolites as indicated by colour scale of Pearson correlation coefficient R^2. Harvest at 48 hours and probabilistic quotient normalised. Cumulative values R^2=0.862 and Q^2=0.560. Key: A.u (arbitrary units), ppm (parts per million).

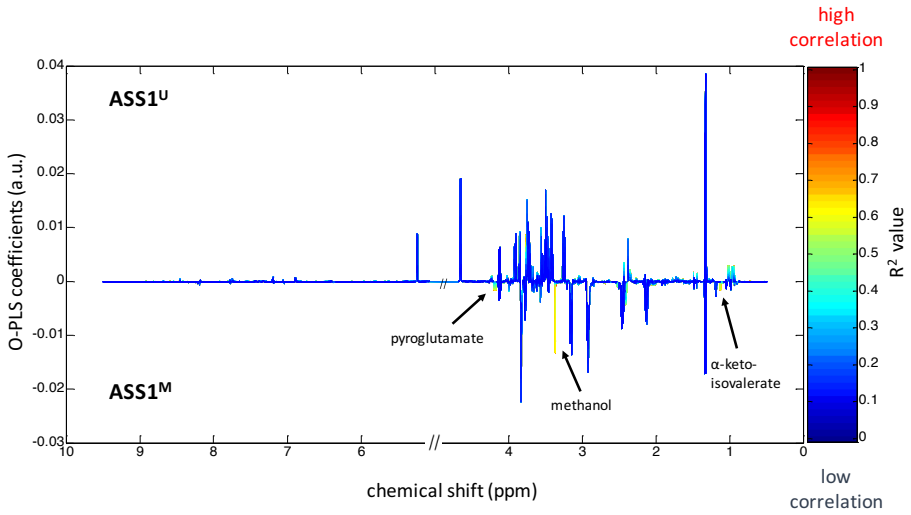


Figure 3.22.: ^{1}H NMR validation: OPLS-DA correlation coefficient plot of media from ASS1 subtypes. OPLS-DA correlation coefficient plot obtained from ^{1}H NMR spectra. Comparison of ASS1^{M} (SNB19, LN229, GAMG) and ASS1^{U} (U87, U118) GBM cell media at basal levels (absence of treatment), showing limited discriminatory metabolites as indicated by colour scale of Pearson correlation coefficient R^2. Harvest at 48 hours and probabilistic quotient normalised. Cumulative values R^2=0.545 and Q^2=0.680. Key: A.u (arbitrary units), ppm (parts per million).

Table 3.8.: OPLS-DA: discriminant metabolites amongst ASS1 subtypes at basal levels. Differential metabolites derived from OPLS-DA model of $ASS1^{M}$ (SNB19, LN229, GAMG) and $ASS1^{U}$ (U87, U118). Cell extract and media harvested at 48 hours and comparison was made at basal levels (absence of treatment) from ^{1}H NMR analysis. Metabolites listed were positively correlated with ASS1 subtypes.

Cell extract		Cell media	
$ASS1^{U}$	$ASS1^{M}$	$ASS1^{U}$	$ASS1^{M}$
2-deoxyadenosine	sn-3-glycerophospho-choline	citrate	pyroglutamate
uridine			3-methyl-oxovalerate
lactate			
myoinositol			
citrulline			
glutathionine			
glutamine			

Validation of ^{1}H NMR analysis trends: ASS1 subgroup comparison upon ADI-PEG20 treatment via PCA and OPLS-DA

Specific differences between metabolic profiles of groups (eg: control versus treatment) were further explored using PCA. All group comparisons passed model validation as determined by positive Q^2 values.
In order to allow for visualisation and explore clustering trends upon ADI-PEG20 treatment via PCA, groups were individually analysed. PCA of ^{1}H NMR showed, that upon treatment, global metabolic profiles of all ASS1^{M} cell extract (figure 3.23) and media (figure 3.24) separated from control cells. As observed in previous ^{1}H NMR and GC/TOF MS results, U87 (ASS1^{U}) cells did not separate upon treatment. U118 (ASS1^{U}) cells did also not separate in the extract fraction, yet interestingly there was a separation in cell media upon treatment.

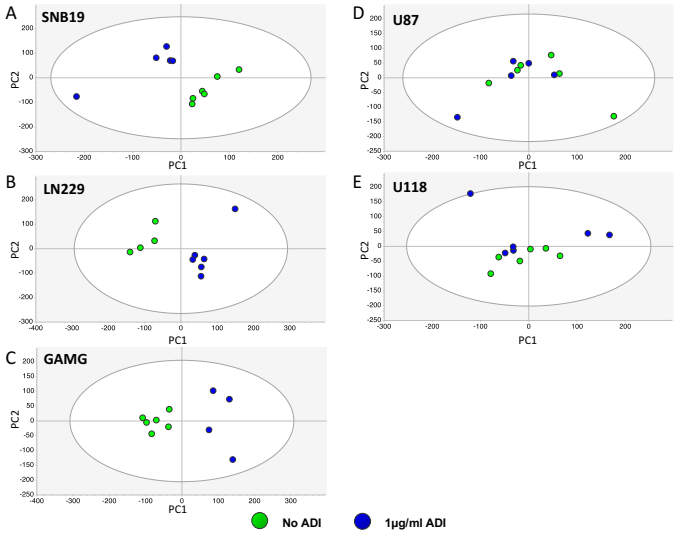


Figure 3.23.: ^{1}H NMR validation: PCA of extract group comparison upon ADI-PEG20 treatment: Individual PCA scores plot (PC1 vs PC2) of global metabolic profile in ASS1^{M} (GAMG, LN229, SNB19) and ASS1^{U} (U87 and U118) cells ($n = 4-9$) harvested at 48 hours in the presence and absence of ADI-PEG20 (1μg/ml). Probabilistic quotient normalisation. A. SNB19; R^2= 0.261, Q^2= 0.194, B. LN229; R^2= 0.449, Q^2= 0.016, C. GAMG; R^2= 0.393, Q^2= 0.027, D. U87; R^2= 0.350, Q^2= 0.102, E. U118; R^2= 0.333, Q^2= 0.062.

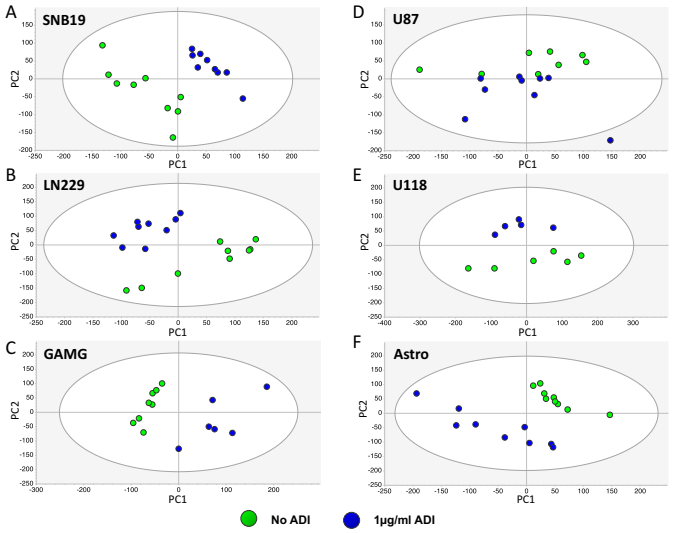


Figure 3.24.: ^{1}H NMR validation: PCA of media group comparison upon ADI-PEG20 treatment: Individual PCA scores plot (PC1 vs PC2) of global metabolic profile in ASS1$^{\mathrm{M}}$ (GAMG, LN229, SNB19) and ASS1$^{\mathrm{U}}$(U87 and U118) cells ($n = 6 - 9$) harvested at 48 hours in the presence and absence of ADI-PEG20 (1μg/ml). Probabilistic quotient normalisation. A. SNB19; R^2=0.287, Q^2=0.153 B. LN229; R^2=0.383, Q^2=0.195. C. GAMG; R^2=0.365, Q^2=0.071. D. U87; R^2=0.328, Q^2=0.067 E. U118; R^2=0.406, Q^2=0.058. F. Astro; R^2=0.350, Q^2=0.153.

^{1}H NMR validation: OPLS-DA highlights discriminant metabolites upon ADI-PEG20 treatment

GBM cell lines were individually analysed via OPLS-DA, in order to highlight discriminant metabolites between control and ADI-PEG20 treated samples. Representative plots of cell extract and media fractions can be seen in figure 3.25 and 3.26 accordingly, with further plots in appendix (section A.4). Highly correlated peaks were extracted and metabolites were matched with the standards in the Chenomx spectral library (Chenomx NMR suite 8.1 Profiler, Canada). Discriminant metabolites are separately listed for ASS1^{M} (table 3.9), ASS1^{U} (table 3.10) and non-GBM cells (table 3.11). In accordance with the expected treatment effect, all group comparisons showed that citrulline was positively correlated with treated samples.

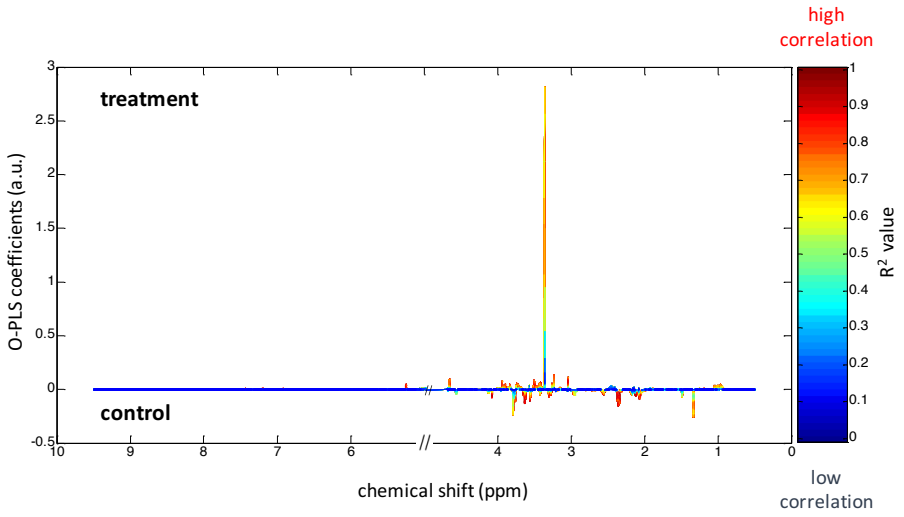


Figure 3.25.: Representative ^{1}H NMR: OPLS-DA correlation coefficient plot of cell extract upon treatment. OPLS-DA correlation coefficient plot from ^{1}H NMR spectra in ASS1^{M} (SNB19) cells harvested at 48 hours. Comparison of control and ADI-PEG20 treated (1μg/ml) cell extract samples ($n = 9$), showing discriminatory metabolites as indicated by colour scale of Pearson correlation coefficient R^2, where red indicated strong correlation and blue poor correlation. Upward pointing peaks are positively correlated with treated samples and downward pointing peaks are positively correlated with control samples. Probabilistic quotient normalised. Cumulative values R^2=0.988 and Q^2=0.770. Key: A.u (arbitrary units), ppm (parts per million).

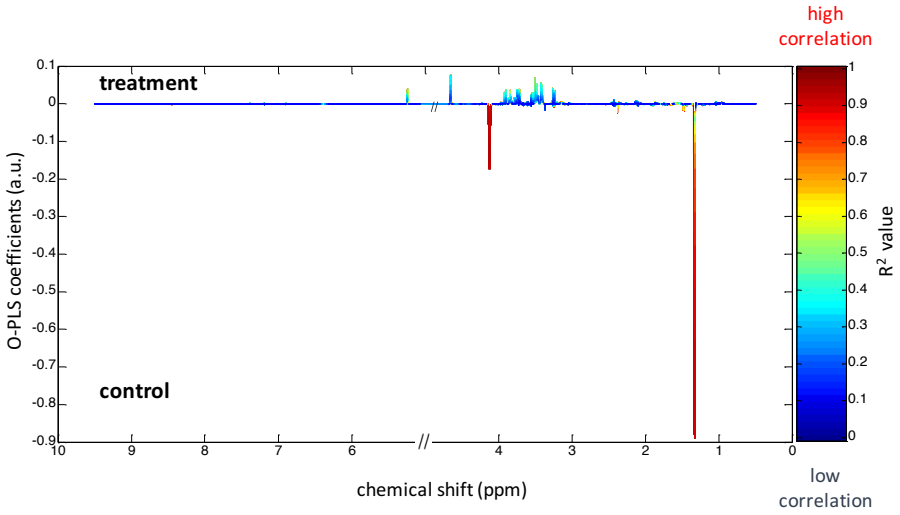


Figure 3.26.: Representative ^{1}H NMR: OPLS-DA correlation coefficient plot of cell media upon treatment. OPLS-DA correlation coefficient plot from ^{1}H NMR spectra in ASS1^{M} (SNB19) cells harvested at 48 hours. Comparison of control and ADI-PEG20 treated (1μg/ml) cell media samples ($n = 9$), showing discriminatory metabolites as indicated by colour scale of Pearson correlation coefficient R^2, where red indicated strong correlation and blue poor correlation. Upward pointing peaks are positively correlated with treated samples and downward pointing peaks are positively correlated with control samples. Probabilistic quotient normalised. Cumulative values R^2=0.982 and Q^2=0.838. Key: A.u (arbitrary units), ppm (parts per million).

Table 3.9.: OPLS-DA: discriminant metabolites amongst ASS1^{M} cells. Differential metabolites derived from OPLS-DA model of ASS1^{M} (SNB19, LN229, GAMG) cell extract and media from ^{1}H NMR analysis. Comparison in the presence and absence of ADI-PEG20 treatment (1μg/ml). Metabolites listed were positively correlated with groups (control or treatment).

Cell line	Extract		Media	
	control	treatment	control	treatment
ASS1^{M} SNB19	glutathionine	citrulline	arginine	citrulline
	threonine	tyrosine	formate	glucose
	lactate	glucose	lactate	
	aspartate	glycolate or galactarate	citrate	
	glutamate	glutathionine	pyruvate	
	alanine	sn-glycero-phosphocholine	alanine	
		creatine or creatinine		
		phenylalanine		
ASS1^{M} LN229	glutathione	citrulline	pyruvate	citrulline
	lactate	UDP glucose	formate	ribose
	myoinositol	glucose	lactate	glucose
	glutamate	sn-glycero-phosphocholine		galactonate
	taurine	glycolate		thymidine
	alanine	creatine		
	beta alanine	glycocolate		
	creatine	uracil		
	aspartate			
ASS1^{M} GAMG	arginine	citrulline	arginine	citrulline
	lactate	UDP-N-acetyl-glucosamine	formate	glucose
	myoinositol	proline	lactate	thymidine
	uridine	glycolate	alanine	
	glycine	glucose	glycine	
	beta-alanine	choline	glutamine	
	creatine	UDP-glucose	pyruvate	
	glutathionine	creatine		
	glutamate			
	isovalerate			
	lactate			

Table 3.10.: OPLS-DA: discriminant metabolites amongst ASS1^{U} cells. Differential metabolites derived from OPLS-DA model of ASS1^{U} (U87) cell extract and media from ^{1}H NMR analysis. Comparison in the presence and absence of ADI-PEG20 treatment (1μg/ml). Metabolites listed were positively correlated with groups (control or treatment).

Cell line	Extract		Media	
	control	treatment	control	treatment
ASS1^{U} U87	N-acetylglutamate	citrulline	arginine	citrulline
		triglycine	glucose	glutathionine
		beta-alanine		glutamine
ASS1^{U} U118	arginine	citrulline	arginine	citrulline
	myo-inositol		glucose	galactonate

Table 3.11.: OPLS-DA: discriminant metabolites amongst Non-GBM cells. Differential metabolites derived from OPLS-DA model of non-GBM (astrocyte) cell extract and media from ^{1}H NMR analysis. Comparison in the presence and absence of ADI-PEG20 treatment (1μg/ml). Metabolites listed were positively correlated with groups (control or treatment). N/A (non-applicable).

Cell line	Extract		Media	
	control	treatment	control	treatment
Non-GBM Astro	N/A		arginine	citrulline
			formate	3-methyl-2-oxovalerate
			lactate	inosine
			alanine	glucose
				pyruvate

3.3. Discussion

3.3.1. Basal profiles present limited metabolic differences amongst ASS1 subtypes in GBM cell lines

Overall, comparing $ASS1^{M}$ and $ASS1^{U}$ GBM cells in the absence of ADI-PEG20 via GC/TOF MS and ^{1}H NMR revealed limited specific metabolic differences amongst ASS1 subtypes via PLS-DA and OPLS-DA. These results were anticipated, as under normal growth conditions, where arginine is in ample supply in the media, large variation in the metabolic profile based on the methylation specific silencing of one gene was not expected. Studying GBM subtypes via GC/TOF MS and ^{1}H NMR, did however reveal that variation amongst GBM cell line profiles can be detected via metabolomic approaches, which has also been observed by others [27].

In the absence of ADI-PEG20 treatment, metabolic profiles (here forth also described as basal or control profiles) of cell extracts showed that metabolites including lactate, alanine and uridine were elevated in $ASS1^{U}$ cells, compared to $ASS1^{M}$ cells (table 3.12). Lactate and alanine are known biomarkers for increased glycolysis and cancer metabolism [3], indicating that these $ASS1^{U}$ cells were metabolically more active than $ASS1^{M}$ GBM. Further, with uridine being an important building-block of RNA, these findings could indicate that $ASS1^{U}$ cells analysed here were transcriptionally more active, which is interesting, given that $ASS1^{M}$ GBM have been found to be clinically more aggressive (Syed *et al.* [126]).

Basal level ^{1}H NMR analysis also displayed glutamate to be associated with media of $ASS1^{M}$ GBM cell lines. Extracellular glutamate release has been reported in GBM and other cancers [82] [159], and cellular glutamate excretion has been proposed as a contributing mechanism in cancer metastasis [121]. Consequently, it could be hypothesised that extracellular glutamate is a factor contributing towards aggressiveness and poorer survival in $ASS1^{M}$ cells, compared to $ASS1^{U}$ GBM [126]. Interestingly, ASS1 loss has also been associated with decreased metastasis-free survival in osteosarcoma [71] as well as more aggressive phenotypes in other cancers [62].

Table 3.12.: Comparative summary: Putative discriminant metabolites of GC/TOF MS and ^{1}H NMR analysis. Summary of top five putative differential metabolites derived from PLS-DA and OPLS-DA of GC/TOF MS and ^{1}H NMR analysis of ASS1^M (SNB19) versus ASS1^U (U87) cell extract and media samples (summary of table 3.1,3.6, 3.8).

Sample	GC/MS		^{1}H NMR		^{1}H NMR	validation
extract	malonic acid	l-valine	uridine	choline	2-deoxy-adenosine	myo-inositol
	l-threonine	l-proline	lactate	taurine	uridine	citrulline
	alanine		tyrosine		lactate	
media	n/a		arginine	leucine	citrate	
			lactate	taurine		
			pyruvate			

3.3.2. Arginine deprivation via ADI-PEG20 alters global metabolic profile in ASS1^{M} GBM cell lines

Analysis of GBM cell lines repeatedly demonstrated that upon ADI-PEG20 treatment there were global metabolic alterations in ASS1^{M} cells and not ASS1^{U} cells. Syed *et al.* [126] demonstrated that ASS1^{M} (and not ASS1^{U}) GBM cell lines undergo autophagy upon ADI-PEG20 treatment, hence findings presented here also reflect a snapshot of cells undergoing this metabolic process. Comparing the top discriminant metabolites of the GC/TOF MS and two ^{1}H NMR experiments, consistently showed elevated citrulline upon ADI-PEG20 treatment in cell media of ASS1^{M}, ASS1^{U} and astrocyte cells (table 3.13, 3.14, 3.15).

Interrogating specific metabolic alterations upon treatment showed that a higher number of metabolites were altered in ASS1^{M} than ASS1^{U} cell lines. Interestingly in GC/TOF MS analysis all metabolites that passed the cut-off criteria were higher in ADI-PEG20 treated samples for ASS1^{M} cells. Arginine deprivation is known to result in protein breakdown, mitochondrial damage and nuclear DNA leakage in cancer cells [128], and in an effort to maintain homeostasis, excretion of nucleosides has also been reported in other cells undergoing autophagy [61]. Trends observed via GC/TOF MS could therefore be attributed to stress induced by treatment, where ASS1^{M} cells released and ceases to consume metabolites, including those which are important for proliferation, such as pyrimidine, pyridine and purine.

Table 3.13.: ASS1^{M} comparative summary: Putative discriminant metabolites of GC/TOF MS and ^{1}H NMR analysis upon ADI-PEG20 treatment. Summary of top five putative differential metabolites derived from PLS-DA and OPLS-DA of GC/TOF MS and ^{1}H NMR analysis of GBM cell lines ASS1^{M} (SNB19, LN229, GAMG) cell extract and media samples (summary of table 3.2, 3.3, 3.7, 3.9).

Sample	GC/MS		^{1}H NMR		^{1}H NMR	validation
SNB19	malic acid	glucos-amine	glyco-proline		citrulline	glycolate
extract	malonic acid	l-valine			tyrosine	glutathio-nine
	cholesterol				glucose	
media	maltose	malonic acid	citrulline	glycero-phospho-choline	citrulline	
	galactose	l-proline	thymine	tyrosine	glucose	
	pyridine		alanine			
LN229	n/a		n/a		citrulline	glycolate
extract					glucose	creatine
					glycero-phospho-choline	
media	n/a		n/a		citrulline	galacto-nate
					ribose	thymidine
					glycose	
GAMG	n/a		n/a		citrulline	glycolate
extract					glucos-amine	glucose
					proline	
media	n/a		n/a		citrulline	
					glucose	
					thymidine	

Table 3.14.: ASS1^{U} comparative summary: Putative discriminant metabolites of GC/TOF MS and ^{1}H NMR analysis upon ADI-PEG20 treatment. Summary of top five putative differential metabolites derived from PLS-DA and OPLS-DA of GC/TOF MS and ^{1}H NMR analysis of GBM cell lines ASS1^{U} (U87, U118) cell extract and media samples (summary of table 3.4, 3.4, 3.7, 3.9).

Sample	GC/MS	^{1}H NMR	^{1}H NMR validation
U87 extract	n/a	citrulline	citrulline triglycine bete-alanine
media	tryptophan ribitol maltose malic acid glycine	citrulline creatine phosphate	citrulline glutathionine glytamine
U118 extract	n/a	n/a	citrulline
media	n/a	n/a	citrulline galactonate

Table 3.15.: Astrocyte comparative summary: Putative discriminant metabolites of GC/TOF MS and ^{1}H NMR analysis upon ADI-PEG20 treatment. Summary of top five putative differential metabolites derived from PLS-DA and OPLS-DA of GC/TOF MS and ^{1}H NMR analysis of astrocyte cell extract and media samples (summary of table 3.5, 3.7, 3.9).

Sample	GC/MS		^{1}H NMR	^{1}H NMR	validation
Astro	n/a		gluta-mate	n/a	
extract			3-hydroxy-isovalerate		
media	malonic acid	l-aspartic acid	citrulline	citrulline	glucose
	inosine	ribitol	thymi-dine	3-methyl-2-oxo-valerate	pyruvate
	glycine			inosine	

3.3.3. Modulation of arginine, glycolytic, citric acid, thymine and glutamine pathway in GBM cell lines upon ADI-PEG20 treatment

Discriminant metabolites identified by GC/TOF MS and ^{1}H NMR analyses demonstrated alterations in the arginine, glycolytic, citric acid, thymine and glutamine pathways. Changes observed in arginine pathway metabolites, namely via consistent arginine decrease and citrulline increase, were to be expected based on the ADI-PEG20 treatment effect (further detail section 3.3.4).

For ASS1^{M} subtypes, cell extract and media analysed by ^{1}H NMR (section 3.2.10) showed that metabolites of the glycolytic pathway, lactate and alanine, were continuously higher in control than ADI-PEG20 treated cells, indicating that these cells were metabolically more active. Glucose, a constituent of DMEM [34], was also continuously lower in control sample media, which indicated more glucose was being consumed, which further supported these observations.

GC/TOF MS also revealed that malic acid, an intermediate of the TCA cycle, decreased in extracts of ASS1^{U} cells upon treatment. ASS1^{M} showed the inverse, with malic acid increasing upon treatment. Interestingly succinate, a further intermediate of the TCA cycle was also found to be lower in ADI-PEG20 treated extract samples of ASS1^{U} cells, via ^{1}H NMR (section 3.2.6), though these results were not validated in subsequent ^{1}H NMR analysis (section 3.2.10). Observations made via malic acid and succinate in ASS1^{U} cells suggest that control cells were metabolically more active in this pathway and ADI-PEG20 treatment impacted the TCA cycle. Caneba *et al.* [20] showed that arginine deprivation led to decreased nitric oxide synthesis, and nitric oxide regulates TCA cycle flux in ovarian cancer cells. Though the ASS1 status of cells in the study by Caneba *et al.* are not known, it could be hypothesised that arginine deprivation perturbed the TCA cycle in ASS1^{U} cells via nitric oxide.

Thymidine, a metabolite important in DNA synthesis and cellular proliferation, was shown to also be perturbed, as demonstrated by elevated thymidine in the media of ADI-PEG20 treated ASS1^{M} cells. Allen *et al.* [4] also identified thymidine to be perturbed upon arginine-deprivation therapy in bladder cancer cell lines, though this was reported in the intracellular sam-

ples and not cell media. Interestingly, formate, a metabolite involved in purine nucleotide synthesis [2], also was elevated in control media of $ASS1^{M}$ and not $ASS1^{U}$ subtypes upon treatment. Extracellular thymidine could be attributed to nuclear DNA leakage [128] and excretion of thymidine and formate could be linked to cellular efforts to maintain homeostasis, prior the lead-up of ADI-PEG20 induced autophagy [61].
Glutamate, an intermediate of the glutamine metabolism [57], was elevated in cellular extracts of $ASS1^{M}$ GBM cells via ^{1}H NMR (section 3.2.10). These observations made at basal level suggest that $ASS1^{M}$ GBM cell lines are metabolically more active in the glutamine pathway, as indicated by glutamate. High glutamine consumption has been associated with highly proliferative cancer phenotypes [148], though comparisons made between metabolic profiles or proliferation rates (section 3.2.1) in ASS1 subtypes do not suggest differences in glutamate consumption or proliferation amongst GBM cell lines.

3.3.4. Metabolic techniques for studying ADI-PEG20 treatment response

Identifying clinical metrics for monitoring arginine-depleting treatment has been presented as a key aspect for determining success in cancer therapy [128]. This chapter presents use of chemometric approaches and two chemical instruments; GC/TOF MS and ^{1}H NMR for studying the effects of ADI-PEG20 treatment as an untargeted research tool. Observations in this chapter support and confirm the strength and suitability of applying these approaches for research studies into the metabolism of GBM cell lines. Further, by using two complementary instruments wider metabolic coverage was attained.
Despite advances being made, clinical application of metabolomic approaches remains limited. Lessons learned through these analyses, such as citrulline being a better indicator of ADI-PEG20 effect than arginine via ^{1}H NMR, could however help direct future application or development of cost-effective biochemical assays. Given further *in vivo* and clinical validation, observations made in these studies show potential for arginine deprivation treatment to be monitored via biochemical assays in the clinic.

3.3.5. Study limitations

Informative insights were gained from a total of six different cell lines in these anaylses. Enhancing the biological scope of cell line coverage would have been desirable, yet this was limited due to time and availability of resources. Further, despite efforts taken to minimise passage number in primary astrocyte cultures, the proliferative qualities of these cells have properties that distinguish them from their representative physiological counterpart as a control. Results observed in astrocytes were hence regarded with this consideration.

This chapter presents a snap-shot of metabolic profiles studied at 48-hours. Different time-points as well as isotopically labelled molecules (eg: ^{13}C glucose) would have been insightful for understanding dynamics of cellular metabolism upon ADI-PEG20 treatment.

The focus of this research was to detect metabolic alterations in a biological context, using several different cell lines. ASS1 knock-down studies in the same cell line would however have been insightful for better understanding mechanisms of arginine deprivation specifically attributed to the ASS1 gene. Finally, despite ADI-PEG20 being used in clinical trials for several cancers (www.clinicaltrials.gov) and there being substantial clinical interest, it does not currently form part of the standard of care in GBM patients [59]. For ADI-PEG20 to make it's way into the clinic for GBM, it will need to be integrated alongside existing standard of care; radio- and temozolomide chemotherapy. This study established fundamental findings of the metabolic profile in an *in vitro* GBM model, however profiling studies in combination with radio- and temozolomide chemo-therapy would provide further insights into possible combination treatments.

3.3.6. Conclusions

This chapter presents three main findings, contributing to the field of GBM and cancer metabolism research.

First, profiling the global intracellular and extracellular metabolism of GBM cells *in vitro* provides novel insights, contributing to the characterisation of ASS1 subtypes.
Second, identifying early metabolic alterations in ASS1 GBM subtypes upon arginine deprivation will be helpful in understanding underlying physiological processes (eg: autophagy) and cellular consequences of ADI-PEG20 treatment. Modulation of the arginine, glycolytic, thymine and glutamine pathways were identified so be associated with ADI-PEG20 treatment in GBM.
Third, two complementary techniques, GC/TOF MS and ^{1}H NMR, coupled with chemometric analysis approaches were shown to be a powerful research tool for studying GBM cells and treatment effects of ADI-PEG20 *in vitro*. Lessons learned, such as citrulline being a better indicator for detecting treatment response via ^{1}H NMR could help direct future application or development of cost-effective biochemical assays.

Taken together, these findings show that metabolic analysis can be employed for validating treatment effect of arginine deprivation in GBM cell lines and provides a basis for validating these observations *in vivo* and eventually the clinic.

4. Results: Transcriptional studies and metabolic pathway investigations

4.1. Introduction

Having identified early metabolic consequences of arginine deprivation via ADI-PEG20 in $ASS1^{M}$ and $ASS1^{U}$ GBM cell lines, potential regulators of perturbed pathways were investigated. GC/TOF MS and ^{1}H NMR studies from chapter 3 had highlighted alterations of the glycolytic, citric acid, thymine and glutamine pathway of ASS1 GBM subtypes upon treatment; all of which are important for cellular respiration, proliferation and metabolism. In order to elucidate potential modulators and further study altered pathways, enzymes associated with discriminant metabolites identified in chapter 3 were investigated transcriptionally with the ultimate purpose of identifying targets for therapy.

Some of the greatest advances in brain tumour research, including discovery of IDH 1 mutations, have been made through enzymatic studies. IDH1 mutations, associated with secondary GBM and low grade glioma, have been found to incur a metabolic switch from synthesis of alpha-ketoglutarate to 2-hydroxyglutarate [65]. Not only do IDH1 mutations result in widespread epigenetic changes, but they are also believed to be one of the most important mutations contributing towards oncogenesis in gliomas [156]. Further, understanding enzymatic expression has also demonstrated clinical utility for predicting treatment response in GBM, as demonstrated by O^{6}-alkylguanine DNA alkyltransferase (AGT). Expression of AGT has been associated with poor response to temozolomide (TMZ), whereas epigenetic silencing of MGMT, the gene encoding AGT, has been associated with

favourable response to TMZ [56].
RT-QPCR is a well established method for studying cellular mRNA signal in molecular biology. Combining the conversion of RNA to cDNA, PCR amplification and real time fluorescent detection has become the preferred method for RNA quantification[92]. In addition to sequence specificity, benefits also include speed of analysis, affordability (eg: compared to costs of antibodies required for Western blotting) and tailored probing [30].

Based on collective findings from chapter 3, the importance that enzymatic alterations play in GBM and the advantages of using RT-QPCR, enzymes associated with the glycolytic, citric acid and thymine pathway were transcriptionally studied in ASS1 GBM subtypes in response to ADI-PEG20 treatment.

4.1.1. Aims

RT-QPCR was employed to study *in vitro* GBM cell lines challenged with 48 hours of ADI-PEG20 treatment. The aims of studies presented here were to (*i*) identify changes in expression of enzymes involved in metabolic pathways altered by arginine deprivation, (*ii*) explore key enzymes in a biological context, focusing on therapeutic potential, (*iii*) elucidate enzymatic differences between $ASS1^{M}$ and $ASS1^{U}$ GBM subtypes.

4.1.2. Objectives

1. Probing mRNA of $ASS1^{M}$ (SNB19) and $ASS1^{U}$ (U87) cell lines via RT-QPCR for transcriptional expression from a panel of enzymes, comprising of those associated with the glycolytic, citric acid, thymine and glutamine pathway at basal levels and in response to ADI-PEG20 *in vitro*.
2. Comparing most significantly altered enzymes in ASS1 subtypes from the panel screen and providing a synthesis of information, comprising of public databases and literature review, with a focus on extracting information of biological significance, including enzyme function, links to cancer and available inhibitors.
3. Assess candidate enzyme transcriptional expression in a wider cell line panel of $ASS1^{M}$ (GAMG, SNB19, LN229), $ASS1^{U}$ (U118, U87) and non-cancer (astrocyte and melanocyte) cells in the presence and absence of ADI-PEG20.

4.2. Results

4.2.1. Transcriptional expression of enzymes associated with altered GBM metabolism

Consulting the KEGG database (http://www.genome.jp/kegg), enzymes associated with metabolic pathways perturbed upon ADI-PEG20 treatment in $ASS1^{M}$ and $ASS1^{U}$ cells were investigated using RT-QPCR. *In vitro* experimental parameters established for ^{1}H NMR analysis were applied for RT-QPCR analysis, harvesting cells after 48-hours of ADI-PEG20 treatment from 10-cm dishes. KEGG database provided information on which enzymes were associated with metabolic pathways identified in chapter 3, and a panel of enzymes were screened for their mRNA expression.

Transcriptional analysis showed that from the enzyme panel listed in figure 4.2, mRNA expression ranged from a fold-increase of 3.2 to fold-decrease of 0.89 upon ADI-PEG20 treatment in $ASS1^{M}$ cells. GPT2, an enzyme associated with glycolysis displayed the highest transcriptional increase, and TYMS, an enzyme associated with the thymine pathway presented the greatest decrease.
For $ASS1^{U}$ cells, RT-QPCR analysis showed that from the screened enzyme panel (figure 4.1), all mRNA levels increased upon ADI-PEG20 treatment by a fold-increase of 1 to 7. TK2, an enzyme of the thymine pathway had the greatest transcriptional increase, and AGXT2, an enzyme of the glycolytic pathway had the lowest increase.

These results highlight that the transcriptional induction of the screened gene panel was smaller by fold-change in $ASS1^{M}$ than $ASS1^{U}$ GBM cells *in vitro*.

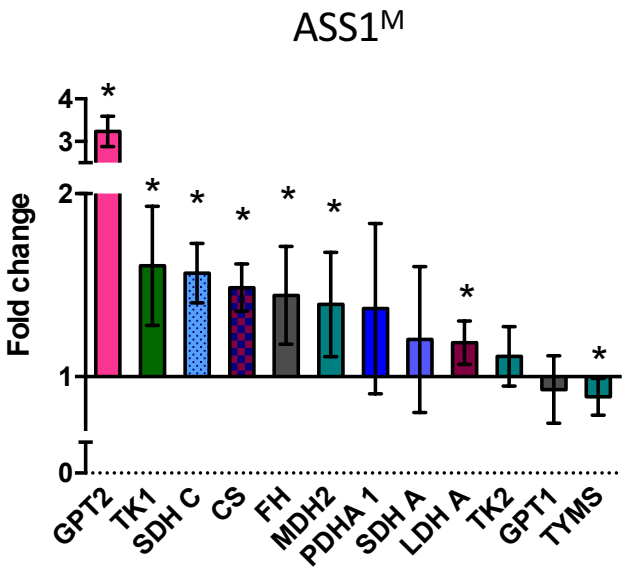


Figure 4.1.: ASS1^{M} RT-QPCR: ADI-PEG20 modulates expression of enzymes associated with citric acid, glycolytic and thymine pathways in ASS1^{M} cells. Enzymatic mRNA expression of ADI-PEG20 (1μg/ml) treated ASS1^{M} (SNB19) cells ($n = 3$), relative to non-treatment control at 48 hours. mRNA levels were determined by RT-QPCR and normalised to TBP1 expression. Error bars represent standard deviation, $*p < 0.05$. See table 4.1 and 4.2 for overview of enzyme function and pathway.

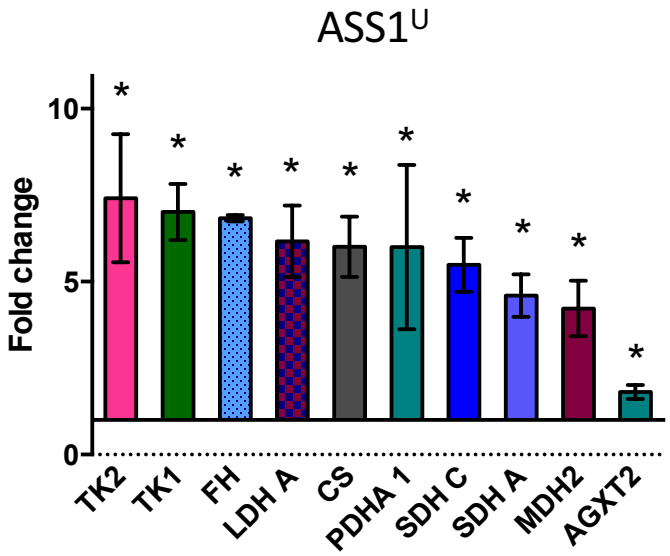


Figure 4.2.: ASS1^{U} RT-QPCR: ADI-PEG20 modulates expression of enzymes associated with citric acid, glycolytic and thymine pathways in ASS1^{U} cells. Enzymatic mRNA expression of ADI-PEG20 (1μg/ml) treated ASS1^{U} (U118) cells ($n = 3$), relative to non-treatment control at 48 hours. mRNA levels were determined by RT-QPCR and normalised to TBP1 expression. Error bars represent standard deviation, $*p < 0.05$. See table 4.1 and 4.2 for overview of enzyme function and pathway.

4.2.2. Biological interpretation

Having identified transcriptional alterations upon ADI-PEG20 treatment amongst GBM cell lines, enzymes were further interpreted, consulting publicly accessible databases and peer-reviewed literature.

Information on enzyme function, protein expression and other findings of biological significance (eg: associated therapies or inhibitors) was collected from UnitProtKB (www.unitprot.org), The Human Protein Atlas (www.proteinatlas.org), and Pubmed (www.ncbi.nlm.nih.gov/pmc) in a systematic manner. Table 4.1 provides an overview of findings from UnitProtKB and The Human Protein Atlas, and further synthesis of the literature review is found in table 4.2. Enzymes displaying the greatest alteration by fold-change in the RT-QPCR screen amongst ASS1 subtypes were first focused on and included GPT2, TYMS, TK2 and AGXT2.

GPT2 is a mitochondrial enzyme that can reversibly transfer an amino group between alanine + 2-oxoglutarate and glutamate + pyruvate, linking it to glycolysis and the TCA cycle [2]. Histological tissue staining from The Human Protein Atlas showed that in 8 out of 12 clinical glioma cases (11 of which high-grade), GPT2 protein expression was not detected, and the same was true for non-cancer sections (table 4.1). GPT2 expression has been reported in brain and muscle tissue [21], though relatively little is known about the enzyme. GPT2 is believed to be modulated by pyroxidine, a form of vitamin B_6, though clinical supplementation studies remain inconclusive [21].
TYMS is a key nuclear and mitchondrial enzyme of the thymine pathway, where it is responsible for *de novo* synthesis of deoxythymidylate monophosphate (dTMP), which is an essential building-block for DNA [83] [7]. Further, histological tissue staining from The Human Protein Atlas showed that most clinical glioma cases ($n = 12$, 11 of which high-grade) displayed moderate TYMS protein expression, whereas non-cancer sections did not detect protein expression (table 4.1). The literature review also highlighted TYMS to be the target of therapies including 5-fluorouracil, pemetrexed and raltitrexed (table 4.2).
TK2 is a mitochondrial enzyme involved in the salvage thymine pathway, converting thymidine to dTMP. Increased TK activity has been suggested to reflect enhanced DNA synthesis [53]. Histological tissue staining from The Human Protein Atlas uniformly showed no TK2 protein expression in gliomas, whereas non-cancer sections did display low protein expression (table 4.1).
AGTX2 is a mitochondrial enzyme with several functions, amongst which amino group transfer from alanine + glyoxylate to pyruvate + glycine [113], linking it to the glycolytic pathway. Isoenzyme AGTX1 has been well studied in relation to hyperoxaluria type I pathogenesis, though little is known about AGTX2 and links to cancer have not been reported. Interestingly, AGTX2 has also been proposed to act as a regulator of endogenous methylarginines which are derived from hydrolysis of cellular proteins [113]. Histological tissue staining from The Human Protein Atlas uniformly showed no AGTX2 protein expression in gliomas as well as non-cancer sections (table 4.1). Two inactivators, clinically used 5-fluorouracil and 6-azauracil, as well as several competitive endogenous inhibitors have been reported in as-

sociation with AGTX2 [72]. Competitive inhibitors include beta-alanine, (R)-3-aminoisobutyric acid, 5-aminolevulinic acid, methylarginine, and (S)-2-aminobutyric acid.

Combining results from chapter 3, the RT-QPCR screen (section 4.2.1), as well as the literature and database review, findings highlighted TYMS and the thymine pathway to be biologically altered and a promising target for therapy.
The RT-QPCR screen had shown TYMS to be the most down-regulated transcript by fold-change in the $ASS1^{M}$ enzyme panel (figure 4.1), and results in chapter 3 had also demonstrated increased extracellular thymidine upon treatment in parallel to arrested proliferation. Further, the database review presented TYMS protein expression to be higher in glioma cases compared to non-cancer sections, and the literature review highlighted several targets for therapy in TYMS and the thymine pathway. Based on these observations TYMS was selected for further transcriptional investigation and validation.

Table 4.1.: Overview of enzyme pathway, catalytic reaction and protein expression. Publicly accessible databases were reviewed. Information was extracted from: $_1$ UnitProtKB (www.unitprot.org) and $_2$ The Human Protein Atlas (www.proteinatlas.org). $_3$ tumour section $n = 12$ of which 11 high-grade and 1 low-grade, $_4$ non-cancer glial cell section.

	Enzyme	**Catalytic Reaction**$_1$	**Protein expression**$_2$	
			Glioma$_3$	**Non-cancer**$_4$
TCA cycle	SDH A	Succinate + a quinone = fumarate + a quinol	medium	low
	SDH C	electron transfer; succinate to ubiquinone (coenzyme Q)		
	CS	Acetyl-CoA + H2O + oxaloacetate = citrate + CoA	medium	medium
	FH	malate = fumarate + H2O	medium	low
	MDH2	malate + NAD+ = oxaloacetate + NADH	medium	medium
Glycolytic pathway	PDHA 1	Pyruvate + [dihydrolipoyllysine-residue acetyltransferase] lipoyllysine = [dihydrolipoyllysine-residue acetyltransferase] S-acetyldihydrolipoyllysine + CO2	not detected	low
	LDH A	lactate + NAD+ = pyruvate + NADH	low	low
	AGXT2	A. L-alanine + glyoxylate = pyruvate + glycine. B. (R)-3-amino-2-methylpropanoate + pyruvate = 2-methyl-3-oxopropanoate + L-alanine. C. Methylarginine + glyoxylate = alpha-keto-valeric acid + glycine [113]	not detected	not detected
	GPT1	L-alanine + 2-oxoglutarate = pyruvate + L-glutamate	not detected	not detected
	GPT2	L-alanine + 2-oxoglutarate = pyruvate + L-glutamate	not detected	not detected
Thymine pathway	TK1	ATP + thymidine = ADP + dTMP	not detected	not detected
	TK2	ATP + thymidine = ADP + dTMP	not detected	low
	TYMS	5,10-methylenetetrahydrofolate + dUMP = dihydrofolate + dTMP	medium	not detected

Abbreviations: succinate dehydrogenase (SDH), citrate synthase (CS), fumarate dehydrogenase (FH), malate dehydrogenase (MDH), pyruvate dehydrogenase (PDHA), lactate dehydrogenase (LDH), alanine-glyoxylate aminotransferase (AGXT), alanine aminotransferase (GPT), thymidine kinase (TK), Thymidylate synthase (TYMS), thymidine monophosphate (dTMP).

Table 4.2.: Synthesis of literature review: biological interpretation. Publicly accessible literature was systematically collected and reviewed, consulting Pubmed (www.ncbi.nlm.nih.gov/pmc).

Enzyme	Involvement in cancer	Inhibitors and modulators
SDH	tumour supressor [11] [68]	carboxin, thenoyltrifluoroacetone, and succinate-analogue inhibitors (malonate, malate, oxaloacetate) [149]
CS	knockdown defects respiration and decreases ATP, yet increases glycolysis [79]	high ratios of ATP:ADP, acetyl-CoA:CoA, NADH:NAD and succinyl-CoA, citrate [123]
FH	tumour suppressor [68] mutations associated with renal cell carcinoma	pyrvinium pamoate [115]
MDH	mutations linked to cancers (eg: prostate), overexpression linked to drug-resistance	thyroxine [138]
PDH	deficiency associated with better outcome in non-small cell lung carcinoma [74]	
LDH	expression associated with tumorigenesis. Inhibition decreases ATP and increase ROS, driving proliferation and DNA damage	oxomate and lipid oxidation, small molecule inhibitor; NHI-2 [5]
AGXT	none reported	inactivators (5-fluorouracil and 6-azauracil), and inhibitors; beta-alanine, (R)-3-aminoisobutyric acid, 5-aminolevulinic acid, methylarginine, and (S)-2-aminobutyric acid [72]
GPT	essential for anchorage independent growth in colon cancer cells [2]	pyroxidine [21]
TK	increased activity correlate with neoplasia and disease progression. TK serum levels used as measure of aggressivity of tumours (eg: NHL) [53] [8]	zidovudine [133], phytic acid [140]
TYMS	up-regulation associated with lung, breast, colon, cervical and bladder cancer [43]	5-fluorouracil, pemetrexed, raltitrexed [136][4][96]

Abbreviations: succinate dehydrogenase (SDH), citrate synthase (CS), fumarate dehydrogenase (FH), malate dehydrogenase (MDH), pyruvate dehydrogenase (PDHA), lactate dehydrogenase (LDH), alanine-glyoxylate aminotransferase (AGXT), alanine aminotransferase (GPT), thymidine kinase (TK), Thymidylate synthase (TYMS), reactive oxygen species (ROS), Non-Hodgkin lymphoma (NHL), methyl 1-hydroxy- 6-phenyl-4-(trifluoromethyl)-1H-indole-2-carboxylate (NHI-2).

4.2.3. Validating TYMS transcriptional expression

As outlined in the previous section, based on findings from section 4.2.2, section 4.2.1 and chapter 3, TYMS was selected for further investigation. In order to validate observations and enhance biological scope (i.e. number of cell lines analysed), further RT-QPCR experiments were performed. The enhanced cell line panel included $ASS1^{M}$ (GAMG, SNB19, LN229), $ASS1^{U}$ (U118, U87) and non-cancer (astrocyte and melanocyte) cells. It should be clearly noted that GBM do not arise from melanocytes and that these cells were included on the basis of providing information on non-cancer transcriptional expression. Both basal levels and ADI-PEG20 challenged cells were analysed for mRNA expression of TYMS.

4.2.4. Basal levels of TYMS in $ASS1^{M}$ and $ASS1^{U}$ GBM subtypes

Basal level transcriptional expression of TYMS was established in the cell line panel and showed that there was no significant trend between $ASS1^{M}$ and $ASS1^{U}$ GBM cells (figure 4.3). Both subtypes fluctuated, with GAMG and U87 showing low transcriptional expression and SNB19, LN229 and U118 showing higher expression. Non-cancer cells (astrocytes and melanocytes) also showed low basal level expression.

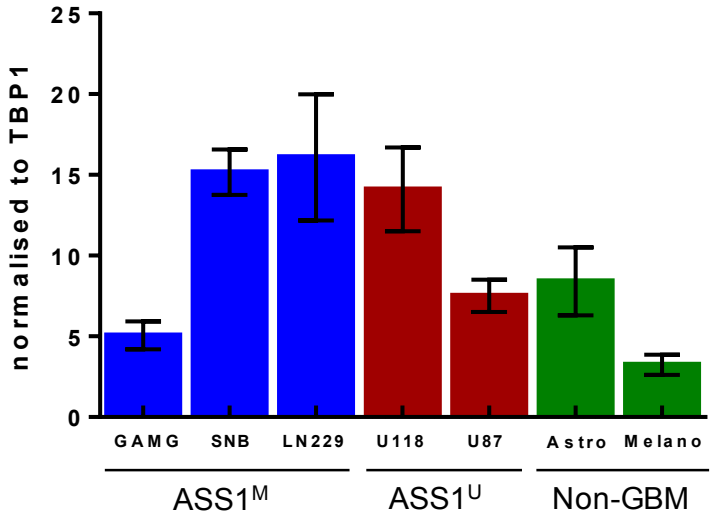


Figure 4.3.: Basal mRNA expression of TYMS determined by RT-QPCR. At basal levels, TYMS mRNA signal displayed no significant trend between ASS1 subtypes. ASS1^{M} (GAMG, SNB19, LN229), ASS1^{U} (U118, U87) and non-GBM (astrocyte and melanocyte) cell lines. TYMS mRNA levels were determined by RT-QPCR and normalised to TBP1 expression. $N = 3$ biological and technical triplicates harvested at 48 hours. Error bars represent standard deviation.

4.2.5. Downregulation of TYMS in ASS1^{M} subtypes upon ADI-PEG20 treatment

Having verified mRNA expression of TYMS at basal levels, transcriptional signal was next studied upon ADI-PEG20 treatment. RT-QPCR showed, that upon treatment mRNA signal significantly decreased by more than half in all ASS1^{M} cells, relative to non-treated basal levels (figure 4.4). Further, this experiment also validated observations made in the enzyme panel screen performed on SNB19 (section 4.2.1). ASS1^{U} treated cells (U87 and U118) did not follow the same trend, as demonstrated by no significant change between non-treated and treated samples. Both non-GBM cells (astrocytes and melanocytes) followed the same trend as ASS1^{M} cells, showing significant transcriptional down-regulation of TYMS upon ADI-PEG20 treatment.

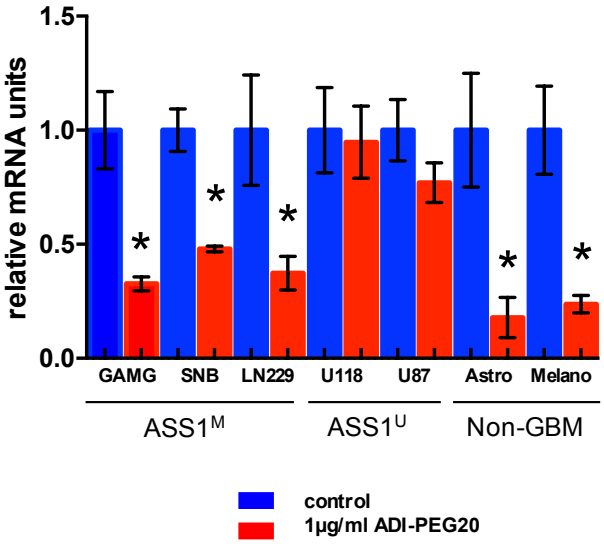


Figure 4.4.: RT-QPCR expression of TYMS upon ADI-PEG20 treatment. Upon ADI-PEG20 treatment (1μg/ml), ASS1^{M} GBM cells display significant down-regulation in transcriptional signal of TYMS, whereas ASS1^{U} remain unaltered. ASS1^{M} (GAMG, SNB19, LN229), ASS1^{U} (U118, U87) and non-GBM (astrocyte and melanocyte) cell lines. $N = 3$ biological and technical triplicates. Error bars represent standard error of the mean, $*p < 0.05$.

4.3. Discussion

4.3.1. Arginine deprivation alters transcriptional expression of metabolic enzymes in ASS1 subtypes

RT-QPCR studies in section 4.2.1 showed how ASS1 subtypes differentially alter mRNA expression of metabolic enzymes upon ADI-PEG20 treatment in GBM cell lines. Overall, both cell lines displayed an increase in transcription of almost all enzymes.

Uniform up-regulation was a surprising finding, particularly in $ASS1^{M}$ GBM. Transcriptional and translational processes are energy costly processes [141], hence it was anticipated that under cellular starvation and stress induced by ADI-PEG20 treatment cellular energy would be conserved.

Though arginine has been reported to modulate intestinal gene expression [18], little is known about transcriptional regulation and broad uniform modulation of enzymes in the glycolytic, citric acid and thymine pathway upon arginine deprivation. An *in vitro* rat hepatic tumour study by Leong *et al.* [77] showed that following 18-hours of arginine deprivation, 2175 genes were altered relative to control, representing 9-14% of rat genome. More than half of these genes analysed showed an increase in expression, highlighting that arginine deprivation induced broad, yet not genome wide transcriptional modulation. Based on these observations, it could be hypothesised that transcriptional induction upon ADI-PEG20 treatment is likely to be much larger than the small enzyme panel probed in section 4.2.1.

The glycolytic, citric acid and thymine pathway are evolutionary conserved metabolic processes [102], central to cellular metabolism. Uniform transcriptional induction of enzymes from these particular pathways (section 4.2.1) could be explained through cellular efforts to not only conserve but also enhance important metabolic processes in a bid to maintain homeostasis. The study by Leong *et al.* [77] also showed that upon arginine deprivation increased expression occurred in both cancer and normal cells. This, together with trends observed in section 4.2.1 could indicate that arginine deprivation induces broad transcriptional induction irrespective of ASS1 status.

Individual trends, including the fold-change and ranking of most to least altered enzyme upon treatment, were different amongst ASS1 subtypes. This was anticipated, given the distinctive proliferative and metabolic treatment effects observed in chapter 3. Enzymes displaying greatest modulation upon

treatment included GPT2, TYMS, TK2 and AGXT2, which are largely outlined in their biological context in section 4.2.2 and discussed in section 4.3.2.

Overall, results from section 4.2.1 show that differential enzymatic induction in ASS1 subtypes illustrates the complexity and versatility of stress induced by arginine deprivation upon ADI-PEG20 treatment.

4.3.2. Systematic database and literature review presents enzymatic roles in cancers and metabolic inhibitors

Systematic review of publicly accessible databases and peer-reviewed literature (section 4.2.2) provided an overview of enzymatic roles, insights into protein expression from clinical samples and highlighted available inhibitors. The most significantly altered transcripts from the RT-QPCR screen (section 4.2.1), GPT2, TYMS, TK2 and AGXT2, were first focused on and are largely outlined in section 4.2.2. Findings from the literature review identified that TYMS has been well studied in cancer, whereas little is known about GPT2 and AGTX2. Relatively little is known on TK2 in relation to cancer, though the enzymatic isoform TK1 has been well studied. It is also noteworthy, that TYMS was the only enzyme where studies in relation to arginine deprivation therapy have been reported [4].

TYMS was an interesting enzyme, as it showed the strongest down-regulated of mRNA signal upon ADI-PEG20 treatment in $ASS1^{M}$ cells. Studies by Szlosarek *et al.* [4] also identified down-regulation of TYMS both at transcriptional and protein level upon ADI-PEG20 treatment. The authors then went on to show that targeting TYMS and *de novo* thymine synthesis via pemetrexed potentiated ADI-PEG20 treatment effect in $ASS1^{M}$ bladder cancer.

Using publicly accessible information, via UnitProtKB and The Human Protein Atlas, was a helpful tool for interpreting biological findings (section 4.2.2). The Human Protein Atlas has been used to facilitate biomarker discovery [105], and findings from section 4.2.2 highlight and confirm the strength of the it's utility in a research capacity, particularly with regards to rapidly accessing information from clinical samples. Drawing on resources from a specialist central database not only ensures standardisation of histological tissue preparation and staining, but also brings time and resource

saving benefits, particularly with regards to antibody optimisation and validation. Despite the allowing for valuable information to be gained and inferences to be made, open access resources do not replace laboratory testing in a research setting. It is anticipated that researchers will increasingly draw on publicly accessible databases. Both UnitProtKB and The Human Protein Atlas are well established resources, yet a plethora of further databases exist. In order for these to be incorporated into routine research use, it would be recommendable for smaller, scattered databases to be united into a single resource that is easily accessible.

4.3.3. RT-QPCR validates transcriptional down-regulation of TYMS upon ADI-PEG20 treatment in ASS1^{M} cells

TYMS is transcriptionally expressed in GBM cells, irrespective of ASS1 status

RT-QPCR on an wider cell line panel (section 4.2.3) validated findings from TYMS in the enzyme panel screen (section 4.2.1) and provided further insights into TYMS mRNA expression in ASS1 subtypes.

Comparing basal level (absence of ADI-PEG20 treatment) TYMS expression in GBM cell lines showed no significant trend between ASS1 subtypes. This was no surprise, given the favourable growth conditions where arginine was in ample supply. With TYMS providing substrates required for DNA synthesis [1], it was hypothesised that transcriptional expression could be linked to cells with rapid doubling times. This was however not the case as U87 (ASS1^{U}), which had the fastest doubling time amongst GBM with only 22.4 hours, presented lower TYMS expression than LN229 (ASS1^{M}), which had the longest doubling time at 190.2 hours. It should also be noted that both of these cell lines originated from high-grade tumours, discarding potential differences on the basis of tumour grading.
Increased levels of TYMS have been identified in GBM and several cancers [43], [89]. Studies by Kallioniemi *et al.* [89] as well as Nelson *et al.* [134] reported transcriptional expression of TYMS in GBM, and results from this chapter substantiate these findings.
The study by Nelson *et al.* [134] showed higher transcriptional TYMS expression to be associated with GBM compared to astrocytomas, highlighting

this gene to be associated with more a aggressive and invasive phenotype. Interestingly, results in section 4.2.4 display mRNA expression in astrocytes to be comparable to that of GBM cell lines, contradicting these reports. As outlined in the previous chapter, astrocyte cell lines have several limitations compared to their physiological counterpart *in vivo*, and results should be interpreted accordingly. In the study by Kallioniemi *et al.* [89] transcriptional findings were also validated at the protein expression level, and histological tissue staining from The Human Protein Atlas also showed TYMS protein expression in glioma yet not non-cancer sections.
Taken together, these observations indicate that GBM express TYMS irrespective of ASS1 status.

Arginine deprivation transcriptionally down-regulates TYMS in ASS1^{M} GBM cells

Comparing TYMS transcriptional expression in GBM cell lines upon ADI-PEG20 treatment (section 4.2.5) not only validated TYMS findings in cells from the enzyme panel screen in section 4.2.1 but also provided further insights into cellular response to treatment in ASS1 subtypes.

RT-QPCR results showed significant transcriptional down-regulation of TYMS amongst all ASS1^{M} cells upon ADI-PEG20 treatment, whereas no significant change was noted amongst ASS1^{U} cells. A study by Szlosarek *et al.* [4] showed TYMS to be down-regulated upon ADI-PEG20 treatment in ASS1^{M} bladder cancer cells, corroborating findings made in ASS1^{M} GBM (section 4.2.5).
There is substantial research on TYMS in cancer, yet little is known about TYMS in relation to arginine deprivation in GBM. An overview of TYMS is already presented in section 4.2.2 and broadly discussed in section 4.3.2, yet validation of TYMS down-regulation in a wider ASS1^{M} GBM cell line panel warranted a deeper review and discussion.
As mentioned in the previous section, TYMS plays an important role in providing substrates for DNA synthesis via thymine pools, which comprises of the *de novo* and salvage pathway (figure 4.5). TYMS exerts it's function in the *de novo* route, contributing dTMP to the thymine pathway via catalysis

of dUMP and 5,10-methylenetetrahydrofolate [96].
Results in section 4.2.5 show, that under the stress induced by ADI-PEG20 treatment, TYMS is transcriptionally down-regulated in $ASS1^{M}$ cells. TYMS has been found to have a role in mitotic division [134], and results presented here substantiated this role, as arrested division ensued in $ASS1^{M}$ cells, as demonstrated in both the SRB and cell count assay in the previous chapter. Based on these observations it could be hypothesised that silencing of TYMS led to diminished *de novo* dTMP synthesis, contributed to arrested proliferation in $ASS1^{M}$ cells.
Interestingly, TK1 and TK2, both enzymes of the salvage pathway increased in $ASS1^{M}$ cells (section 4.2.1). Despite the salvage pathway also contributing to cellular dTMP pools, cellular proliferation was not maintained in $ASS1^{M}$ cells (chapter 3). Reports by Anderson *et al.* [7] have highlighted that the salvage pathway is not sufficient to maintain dTMP pools and *de novo* synthesis is needed, particularly to sustain mitochondrial DNA replication. Further, the authors also argue that depletion of dTTP pools from *de novo* pathway leads to deoxyuridine incorporation in mitochondrial and nuclear DNA, resulting in genome instability and severe mitochondrial dysfunction [7]. It should be noted that TK1 and TK2 were also transcriptionally induced in $ASS1^{U}$ cells. These results indicate that extracellular arginine deprivation resulted in salvage pathway modulation, yet through endogenous arginine synthesis and unaltered TYMS expression, these cells were able to continue proliferating.
Mechanisms through which arginine deprivation modulates TYMS, TK1 and TK2 expression in $ASS1^{M}$ cells have yet to be elucidated. Few mechanistic studies exist, though arginine and other amino-acids, including glutamine, have been reported to orchestrate regulation of gene expression through the activation of transcription factors, including the involvement of kinases [18]. Observations presented in this chapter could lead to the hypothesis that under stress induced by arginine deprivation via ADI-PEG20, *de novo* dTMP production is arrested through down-regulation of TYMS. Subsequently, salvage pathway up-regulation ensues via transcriptional induction of TK1 and TK2, in an attempt to maintain intracellular thymine pools. As supplied thymine is however not enough, uracil is incorporated into nuclear and mitochondrial DNA. Genomic instability and mitochondrial catastrophe follow, contributing towards arrested proliferation.

Taken together, findings presented in section 4.2.3 highlight that arginine deprivation via ADI-PEG20 alters the *de novo* thymine pathway through down-regulation of TYMS in $ASS1^{M}$ GBM cells, whereas $ASS1^{U}$ remain unaltered. To date, these are the first reports linking TYMS down-regulation in $ASS1^{M}$ GBM exposed to ADI-PEG20 treatment.

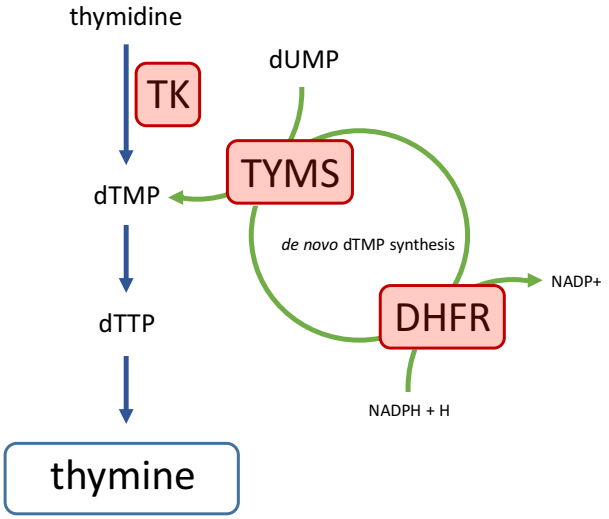


Figure 4.5.: TYMS and thymine synthesis pathway. Schematic representation of TYMS pathway. TYMS and TK synthesise the nucleotide dTMP and dTTP, which is then used to produce the nucleic acid thymine. Abbreviations: DHFR; dihydrofolate reductase, dTMP; deoxythymidylate monophosphate, dTTP; deoxythymidine triphosphate, dUMP; deoxyuridine monophosphate, TK; thymidine kinase, TYMS; thymidylate synthase. Figure adapted from Anderson *et al.* (2011) [7].

4.3.4. Study limitations

The enzyme screen (section 4.2.1) provided a small yet tailored view of transcriptional alteration in GBM cell lines upon arginine deprivation. Probing a larger enzyme panel and covering more isoforms would have been desirable, however this was limited by time and cost. Further, testing a larger scope of cell lines would have also added more strength to the enzyme panel analysis, yet selecting the most significantly altered enzyme followed with validation on more cell lines (section 4.2.3) proved to be a suitable approach.

Further, despite RT-QPCR investigations providing insightful information on transcriptional alteration, protein studies via Western blot would have provided further confirmation of post-translational expression. In the absence of a suitable antibody, inferences on protein expression were made from The Human Protein Atlas and literature searches.

Finally, as outlined in the previous chapter, astrocytes have notable limitations as a model for their physiological counterpart, yet were included with this consideration during analysis. Further, melanocytes were included to gain perspectives on TYMS expression in a further non-cancer cell line yet it should be noted that these cells arise from different cell lineages.

4.3.5. Conclusions

This chapter explored the complexity of metabolic pathways by studying enzymes associated with metabolites altered in chapter 3. Three main findings presented here contribute to knowledge on GBM and the cancer metabolism.

First, GPT2, TYMS, TK2 and AGXT2 were identified to be key altered enzymes upon ADI-PEG20 treatment in ASS1 subtypes. Probing the enzyme panel mRNA expression particularly added knowledge towards understanding transcriptional processes surrounding arginine deprivation in $ASS1^{M}$ cells.
Second, TYMS was shown to be transcriptionally expressed in GBM cell lines, irrespective of ASS1 status. The literature review determined TYMS and the *de novo* thymine pathway to play an important role in cellular proliferation and provided a synthesis of information on enzymatic function and

reported inhibitors. The database review also demonstrated the strength of using publicly accessible resources such as The Human Protein Atlas for research purposes.
Third, it was demonstrated that arginine deprivation incurs modulation of the thymine pathway via transcriptional down-regulation of TYMS and induction of TK1 and TK2 in $ASS1^{M}$ cells.

Taken together, results in this chapter link for the first time that ADI-PEG20 treatment results in transcriptional modulation of TYMS in $ASS1^{M}$ GBM cells. Findings could help direct further validation in clinical samples and results also present enzymes of the thymine pathway to be promising targets for treatment in GBM.

5. Results: IP6 arrests proliferation and enhances effect of ADI-PEG20 in ASS1^{M} GBM cells, while creatine promotes proliferation

5.1. Introduction

ADI-PEG20 arrests proliferation and compromises several metabolic processes, including the thymine and creatine pathway, in ASS1^{M} GBM cells. Thymine metabolism is an important pathway in cancer cells, supplying nucleic acids required to meet rapid proliferation demands [83] [7] [102]. Creatine metabolism, plays a role in cellular energy buffering, maintaining ATP levels together with phosphocreatine, essential in supplying energy for proliferating cells [143]. Given the importance of nucleic acid synthesis and efficient energy buffering in cancer, the thymine and creatine metabolism were investigated in order to target rapidly proliferating GBM cells.

As arginine deprivation via ADI-PEG20 arrested proliferation and down-regulated TYMS in the *de novo* thymine pathway of ASS1^{M} GBM cells, it was hypothesised that targeting the salvage thymine pathway could enhance arrest of proliferation in these cells. Further, rapid proliferation is a hallmark of cancer and failure of many chemotherapies has been attributed to lack of specificity towards cancers, whilst preserving healthy tissue [136]. It was therefore also hypothesised that compromising both thymine pathways and ultimately DNA synthesis would be a selective approach for targeting highly proliferative cancer tissues. Further, inhibition of TYMS in combination with other agents that assert their effect on the salvage pathway has also been

proposed to be of great clinical utility by Touroutoglou and Pazdur [133]. Several therapies asserting their action on the thymine pathway exist, including phytic acid and zidovudine, which have been associated with inhibition of TK in the salvage pathway [133] [140]. Phytic acid, also known as inositol hexakisphosphate (here forth referred to as IP6), is an organic phosphate with inhibitory effects via dephosphorylation into lower phosphates [140]. IP6 and other inositol phosphates are abundantly found in legumes and grains, where they acts as a phosphate reserve [66]. IP6 has been reported to exert effects against cancer in colon, leukaemic, liver, prostate and rhabdomyosarcoma cell lines [66]. Lower phosphates of IP6 have also been found to induce apoptosis and sensitise cells *in vitro* to chemotherapeutic agents (eg: cisplatin). *In vivo* ovarian carcinoma studies have shown anti-tumour and anti-angiogenic activity with no reported toxicity [88]. Further, substantial evidence exists, showing that IP6 has protective effects, including antioxidant properties via inhibition of free radical formation [140].
Zidovudine, also known as azidothymidine, is a thymidine analogue, that inhibits TK [133] as well as reverse transcriptase [25]. First synthesised in the 60's and developed in the 80's, it was one of the first chemotherapies widely used to treat and prevent HIV [28]. Successes seen in HIV treatment have however not been mirrored in cancer treatment. Despite initially promising clinical findings in leukaemia treatment [46], subsequent clinical studies resulted in treatment failure with substantial side-effects [28].
Based on the potential that IP6 has shown in pre-clinical cancer treatment and the limited success of zidovudine, IP6 was selected for further investigation in GBM.

Decreased intracellular creatine and arrested proliferation are associated with ADI-PEG20 treatment in $ASS1^{M}$ cells (section 3.2.6). Literature and KEGG database (http://www.genome.jp/kegg/pathway.html) reviews further highlighted creatine to be of biological interest, being one of the products of the arginine metabolism, functioning as an ATP buffer [143], exerting neuroprotective effects in neuroblastomas [26], [13] and reported protective effects from oxidative damage [69]. With ADI-PEG20 induced intracellular creatine reduction being associated with arrested cellular proliferation and it's role in buffering energy supplies, it was hypothesised that creatine was important in maintaining cellular proliferation and investigated in GBM.

5.1.1. Aims

Proliferation assay, RT-QPCR and luciferase assay were employed for studying treatment response of GBM cell lines exposed to IP6 or creatine alone and in combination with ADI-PEG20. The aims of studies presented here were to (*i*) explore effect of IP6 in ASS1 GBM subtype cells and investigate effect of IP6 and ADI-PEG20 combination treatment, (*ii*) elucidate enzymatic alterations in the *de novo* thymine pathway amongst ASS1 GBM subtypes, (*iii*) identify the role of creatine in GBM proliferation and intracellular energy modulation.

5.1.2. Objectives

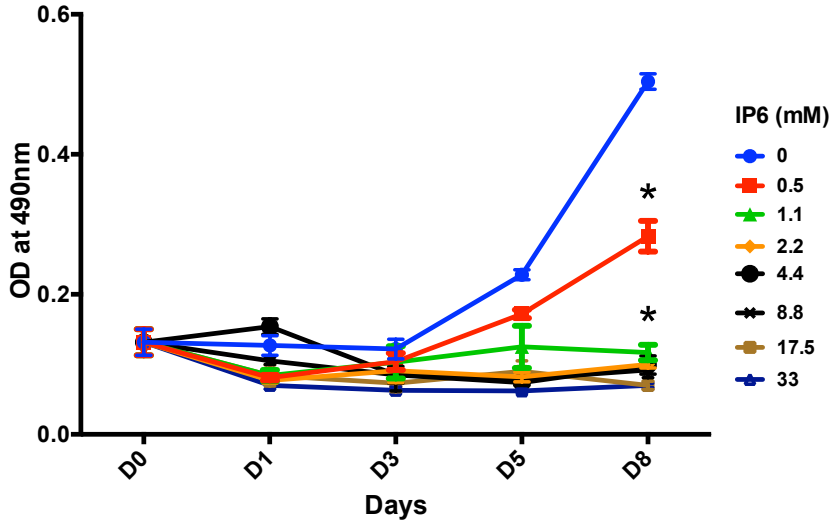
1. challenging GBM cells with dose-titrations of IP6 over time courses, alone and in combination with ADI-PEG20 *in vitro*, determining proliferative effects via SRB assay
2. assessing transcriptional expression of TYMS in $ASS1^{M}$ GBM cell lines exposed to IP6 and ADI-PEG20 combination treatment, using RT-QPCR
3. subjecting GBM cells to creatine titrations, determining proliferative effects via SRB assay and assessing intracellular ATP via luciferase assay.

5.2. Results

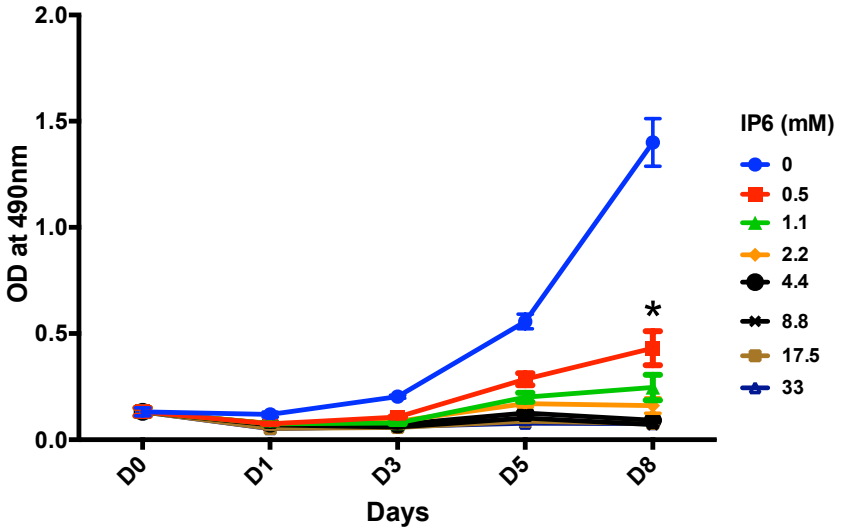
5.2.1. IP6 arrests proliferation of GBM cell lines

Prior to investigating combination treatments, GBM cells were exposed to solely IP6, as outlined in section 2.1.1, in order to determine stand-alone treatment effect and establish experimental parameters for combination treatment.

Results from the SRB proliferation assay showed (figure 5.1) that IP6 arrested proliferation in GBM cell lines irrespective of ASS1 subtype, in a time- and dose-dependent manner. Seven different dosages from $0.5 - 33.0$mM were applied, in-keeping with those used in the literature [67] [66], and effects became notable from 1mM. In order to test same time-points used in chapter 3 and chapter 4, as well as those within the literature [131], samples were harvested at regular intervals between 0 - 8 days. Proliferative effects were notable from day 3 and pronounced from day 5. A dosage of 1mM was selected for subsequent experiments to study IP6 treatment effect, as this compromised, yet did not completely arrest proliferation.



(a)



(b)

Figure 5.1.: IP6 titration: SRB proliferation assay. Showing IP6 arrests proliferation in GBM cells in a time- and dose-dependent manner, irrespective of ASS1 status. Cells ($n = 3$) exposed to IP6 titration $0-33$mM over $0-8$ days. Error bars represent standard error of the mean $*p < 0.01$ (a) ASS1^{M} (GAMG) and (b) ASS1^{U} (U87) cells.

5.2.2. Enhanced effect of ADI-PEG20 via IP6 in ASS1^{M} cell lines

In order to investigate if there was an enhanced treatment effect by ADI-PEG20 and IP6 combination treatment, concentrations that compromised, yet not completely arrested proliferation in GBM cell lines were selected to determine subtle proliferative effects. Based on results from section 3.2.1 and 5.2.1, ADI-PEG20 concentration of 0.01μg/ml and IP6 concentration of 1mM were selected to investigate combination treatment.

SRB proliferation assay showed (figure 5.2), that in ASS1^{M} cells, the combination of IP6 and ADI-PEG20 enhanced treatment effect, resulting in stronger proliferative arrest. For GAMG (ASS1^{M}) cells, at day 8 there was a 53% decrease in proliferation induced by the combination treatment compared to IP6 alone, and a 33% decrease compared to ADI-PEG20 alone. For SNB19 (ASS1^{M}) cells, arrested proliferation was also pronounced at day 8, with a 33% decrease resulting from the combination treatment compared to IP6 alone, and 17% decrease compared to ADI-PEG20 alone.

Amongst ASS1^{M} cells, GAMG cells were more sensitive to IP6 than SNB19 cells. Interestingly, ADI-PEG20 treatment effect was stronger than that of IP6 alone. Findings also confirmed ADI-PEG20 treatment effect in ASS1^{M} cells, in-line with previous results (section 3.2.1). For ASS1^{U} cells, as anticipated, ADI-PEG20 did not arrest or compromise proliferation.
The SRB proliferation assay also demonstrated that 1mM of IP6 treatment compromised proliferation in both ASS1 GBM subtypes. This validated findings made in the same cell lines used in section 5.2.1 (GAMG and U87), as well as further cell lines (SNB19 and U118). For both GBM cell lines, effects became notable at day 5 and pronounced at day 8.
Astrocytes were also sensitive to IP6 treatment, which was anticipated in view of known limitations these cells display in representing their true physiological counterpart (further detailed previously in section 3.2.1). Interestingly, astrocyte cells were less sensitive to IP6 than ADI-PEG20 treatment.

In summary, ADI-PEG20 and IP6 combination treatment enhanced arrested proliferation effect in ASS1^{M}, whereas ASS1^{U} GBM cells were only compro-

mised by IP6. Together these results show that effect of IP6 was not specific to either ASS1 subtype. In oder to determine if a higher ADI-PEG20 concentration could have synergistic effects with IP6 in $ASS1^{U}$ GBM, U118 and U87 were also exposed to 1 and 2μg/ml ADI-PEG20 in combination with 1mM IP6 (results not shown). No enhanced effect was observed.

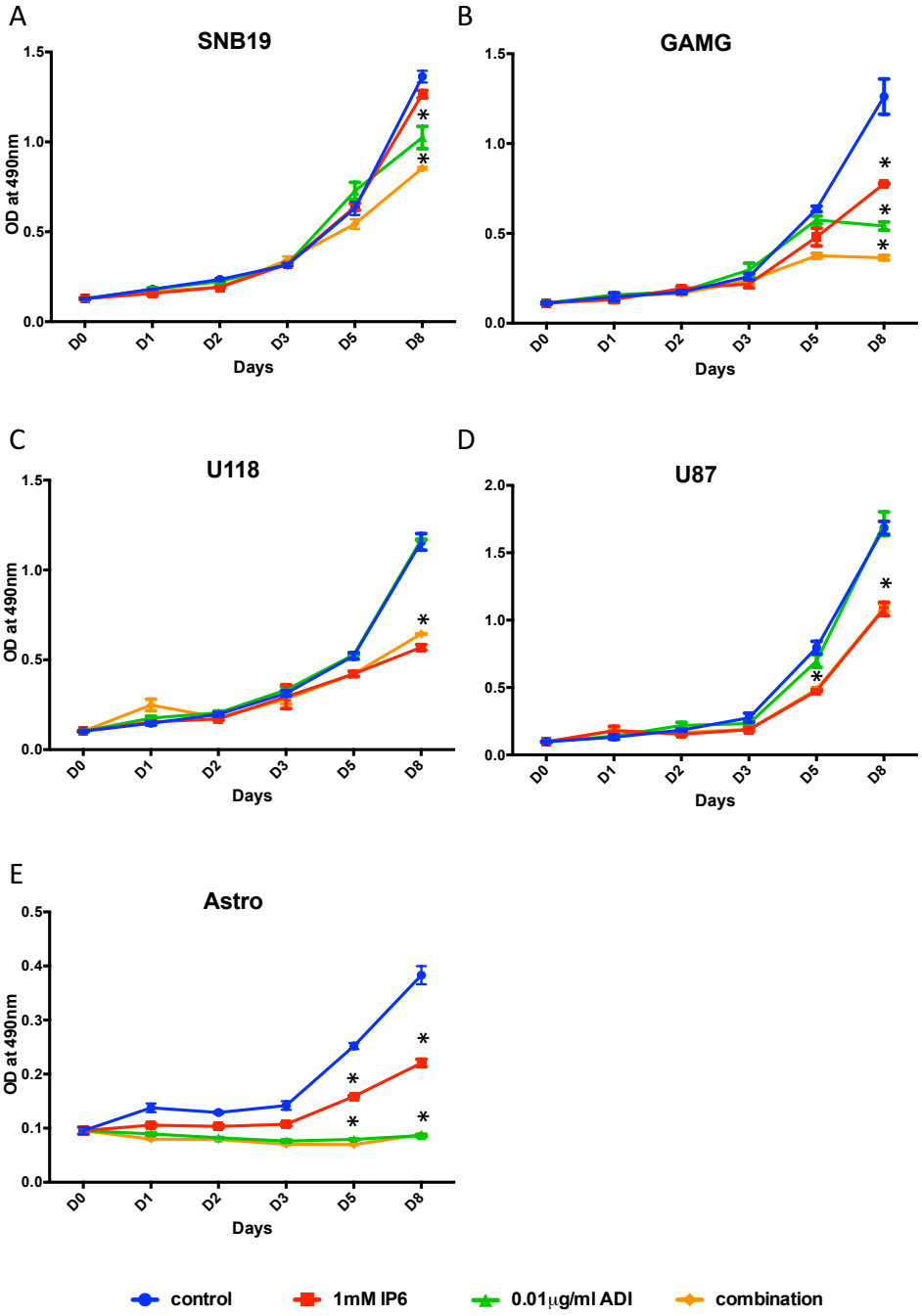


Figure 5.2.: IP6 and ADI-PEG20 combination treatment: SRB proliferation assay. IP6 and ADI-PEG20 combination treatment enhanced arrested proliferation effect in $ASS1^{M}$ GBM cells, whereas $ASS1^{U}$ were only compromised by IP6 alone. $ASS1^{M}$; A. SNB19, B. GAMG, $ASS1^{U}$; C. U118, D. U87 and E. non-GBM (astrocyte) cells ($n = 3$) exposed to IP6 (1mM) and ADI-PEG20 (0.01μg/ml) treatment over 0-8 days. These lower concentrations were chosen in oder to see treatment effect, as they compromised, yet not completely arrested proliferation. Cells were plated in triplicate and values shown are averages with standard error. Optical densities were read at 490nm and units are relative to day 0. Error bars represent standard error of the mean $*p < 0.01$.

5.2.3. Combination of ADI-PEG20 and IP6 potentiates further down-regulation of TYMS

Results in chapter 4 showed that ADI-PEG20 treatment down-regulates transcriptional expression of TYMS in the *de novo* thymine pathway. This finding, together with IP6 reported to affect the salvage thymine pathway via TK [133], led to the hypothesis that the *de novo* thymine synthesis pathway could also be modulated by IP6 via TYMS. In order to investigate early consequences, prior to the marked proliferative changes observed from day 3 (5.2.2), and compare transcriptional expression of results in chapter 4, cells were harvested after 48-hours of IP6 and ADI-PEG20 combination treatment and TYMS transcriptional expression was analysed via RT-QPCR.

For $ASS1^{M}$ cells (GAMG), ADI-PEG20 treatment significantly ($*p < 0.05$) compromised TYMS expression by more than half, validating results from chapter 4. TYMS was also significantly down-regulated by IP6 alone, though to a lesser extent than that incurred by ADI-PEG20. The combination treatment of ADI-PEG20 and IP6 also significantly down-regulated TYMS expression compared to (*i*) the control, (*ii*) ADI-PEG20 alone and (*iii*) IP6 alone. The difference between ADI-PEG20 alone and the combination treatment was significant ($*p < 0.05$) yet small, indicating that ADI-PEG20 contributed towards most of the observed effect.
In $ASS1^{U}$ (U87) cells, the three different treatments did not significantly alter TYMS transcriptional expression at 48-hours, relative to the non-treated control. For ADI-PEG20, this was anticipated, in-line with results from section 4.2.1 and section 4.2.3. Despite TYMS being significantly down-regulated by IP6 in GAMG ($ASS1^{M}$) cells and IP6 arresting proliferation in $ASS1^{U}$ cells (section 5.2.2), there was no transcriptional modulation of TYMS in U87 ($ASS1^{U}$) cells after 48-hours of treatment.
Taken together, these results show that in $ASS1^{M}$ (GAMG) cells, TYMS transcriptional expression is sensitive to ADI-PEG20, IP6 and combination treatment, whereas TYMS in $ASS1^{U}$ (U87) cells remains unaltered.

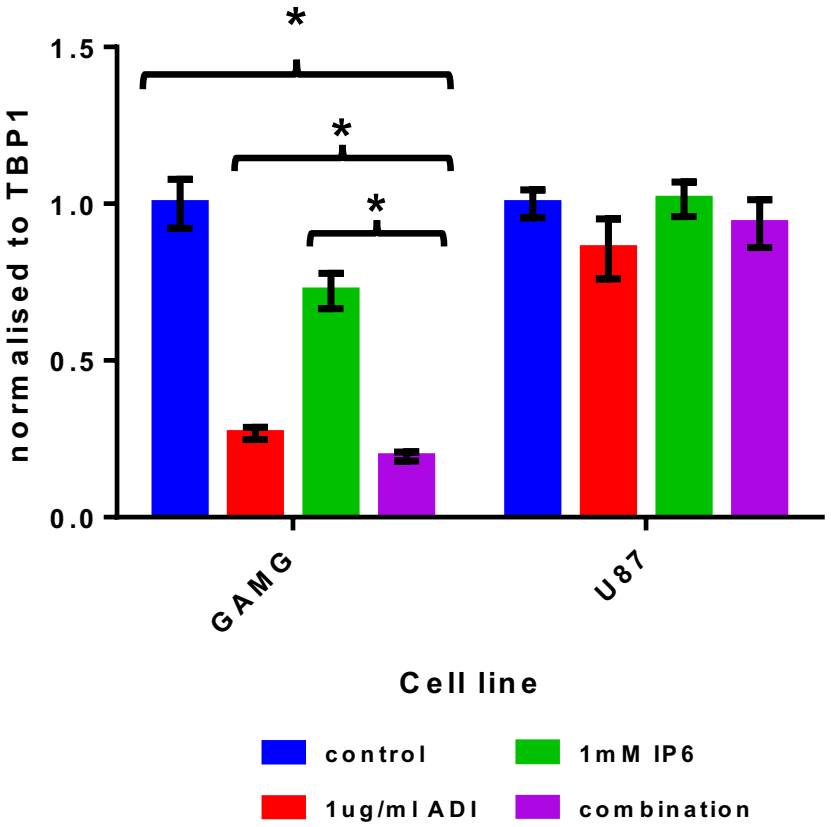


Figure 5.3.: RT-QPCR: Transcriptional down-regulation of TYMS in ASS1^{M}, yet not ASS1^{U} GBM cells upon IP6 and ADI-PEG20 combination treatment. mRNA of TYMS was down-regulated upon ADI-PEG20 alone (1μg/ml), IP6 alone (1mM) and combination treatment in ASS1^{M} (GAMG), whereas transcriptional expression in ASS1^{U} (U87) cells was not significantly altered. mRNA levels were determined by RT-QPCR and normalised to TBP1 expression. $N = 3$ biological and technical triplicates harvested at 48 hours. Values shown are relative to control. Error bars represent standard error of the mean $*p < 0.05$.

5.2.4. Arginine deprivation via ADI-PEG20 compromises the creatine pathway

Creatine was one of the discriminant metabolites identified to be altered upon ADI-PEG20 treatment intracellularly from ^{1}H NMR analysis (section 3.2.6). In ASS1^{M} (SNB19) cells, with a significant fold-decrease of 0.46 upon treatment, relative to the non-treated control (figure 5.4), creatine was the metabolite displaying the largest fold-decrease in ASS1^{M} cells. For ASS1^{U} (U87) cells there was a 0.77 fold decrease, and non-GBM cells (astrocytes) displayed a 1.46 fold-increase, both of which were non-significant.

In order to further investigate creatine pathway perturbations, intermediates and substrates of the arginine and creatine metabolism (figure 5.5) were reviewed, referring to discriminant metabolite findings from chapter 3. Under normal growth conditions, arginine and glycine are metabolised via arginine:glycine amidino-transferase (AGAT), which occurs up-stream of creatine synthesis in this pathway [19]. Referring to GC/TOF MS analysis (section 3.2.5), glycine had displayed a 4.1 fold-increase in ASS1^{M} cells. ASS1^{U} and astrocyte cells had shown a marginal fold-decrease and no-change, yet these results were however non-significant as determined by student's t-test.

Complimentary findings from ^{1}H NMR and GC/TOF MS facilitated analysis of the creatine pathway in ASS1^{M} cells. Results showed that there was an intracellular build-up of glycine, which were presumably not metabolised in the absence of arginine, as a consequence of arginine-deprivation via ADI-PEG20 and ASS1^{M} cells inability for *de novo* arginine synthesis, resulting in decreased creatine further downstream.

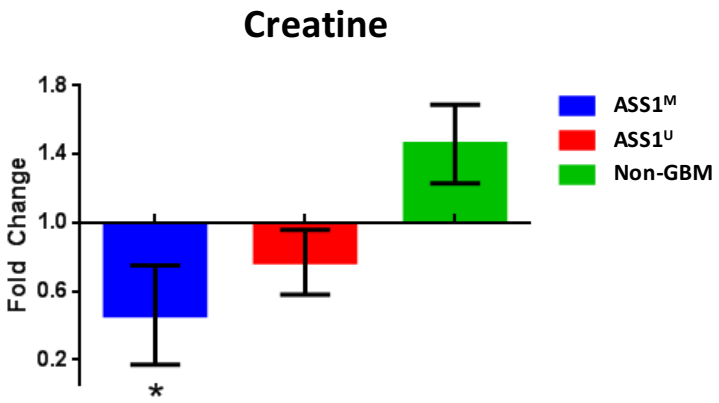


Figure 5.4.: ^{1}H NMR: Fold-decrease of creatine in ASS1$^{\mathrm{M}}$ GBM cells. Fold change of average values $n = 3$ per group of integral intensities calculated from featured creatine present at 48 hours in extract of ASS1$^{\mathrm{M}}$ (SNB19) and ASS1$^{\mathrm{U}}$ (U87) GBM and non-GBM (astrocytes) cell line samples exposed to ADI-PEG20 (1μg/ml) treatment or no treatment. Integral intensities represented. SEM marked with error bars. Significance between treated and non treated lines tested using student's t-test and marked at $*p < 0.01$ and $**p < 0.001$.

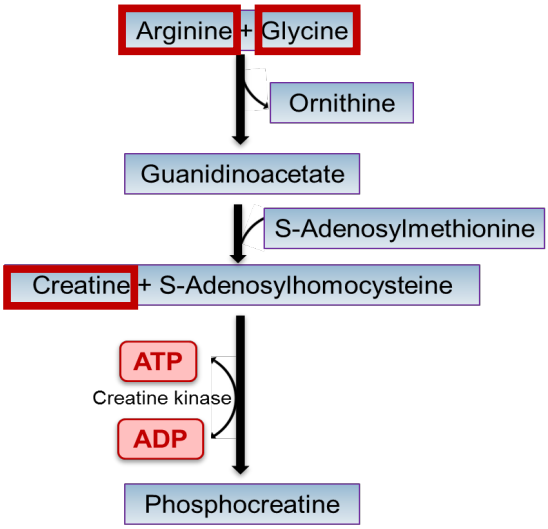


Figure 5.5.: Creatine metabolism via arginine and glycine. Creatine is a cellular energy reserve, synthesised via arginine and glycine. Use of two complimentary techniques, ^{1}H NMR and GC/TOF MS facilitated interpretation of GBM metabolic profiles. ^{1}H NMR identified decreased creatine, whereas GC/TOF MS identified increased glycine in ASS1^{M} cells.

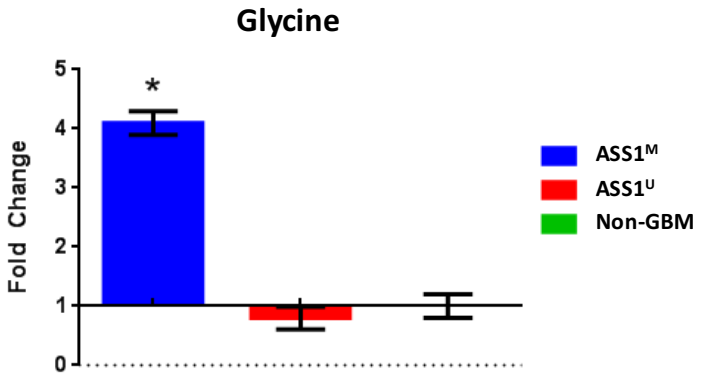


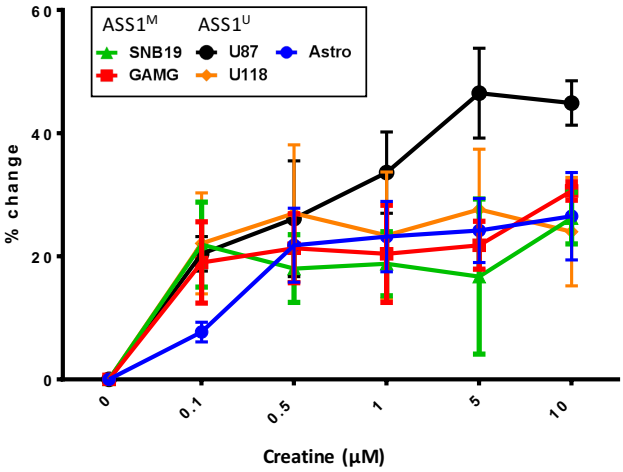
Figure 5.6.: GC/TOF MS: Fold-increase of glycine in ASS1^{M} GBM cells. Fold-change upon ADI-PEG20 (1μg/ml) treatment relative to non-treated control. Average values ($n = 3$ per group) of integral intensities calculated from featured creatine present at 48 hours in extract of ASS1^{M} (SNB19) and ASS1^{U} (U87) GBM and non-GBM (astrocyte) cells. SEM marked with error bars. Significance between treated and non treated lines tested using student's t-test and marked at $*p < 0.01$.

Creatine stimulates proliferation in GBM cell lines in a dose-dependent manner

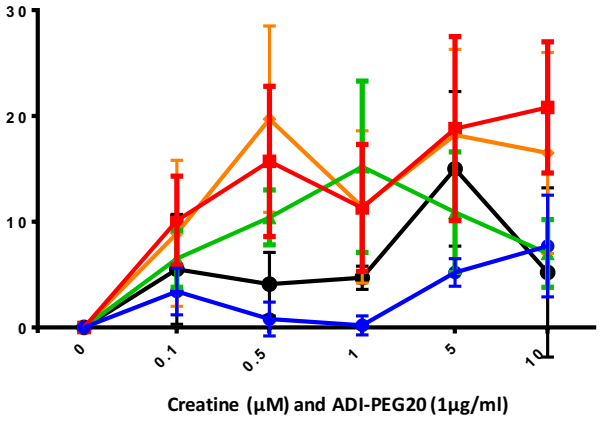
Having identified modulation of creatine pathway intermediates to be associated with arrested proliferation in ASS1^{M} cells, creatine was further investigated to understand it's role in proliferation and test it's protective effects in GBM. Media of GBM cell lines was supplemented with a creatine titration in the presence and absence of ADI-PEG20, in order to test if creatine supplementation could counteract the inhibitory effect of ADI-PEG20. In order to enhance biological scope, GBM cell lines (U118 and GAMG) were included in addition to cell lines presented in section 5.2.4.

Surprisingly, SRB proliferation assay showed (figure 5.7) that creatine supplementation not only rescued ASS1^{M} cells from ADI-PEG20 effect, but it also stimulated proliferation of all GBM by 8-20% beyond the ADI-PEG20 only control.

For cells exposed to creatine only (i.e. absence of ADI-PEG20), the boost in proliferation was even more pronounced with a 26-45% increase in proliferation. Again, this trend was observed not only $ASS1^{M}$ cells, but also $ASS1^{U}$ and astrocyte cells. Five different dosages from $0.1 - 10\mu$M were applied, in-keeping with those reported in the literature [26], and effects were notable from 0.1μM.



(a)



(b)

Figure 5.7.: Creatine supplementation boost proliferation in GBM cell: creatine titration and SRB proliferation assay. Creatine stimulates GBM cell line proliferation in a dose-dependent manner, demonstrating creatine had a role in GBM proliferation. In the absence of ADI-PEG20 proliferation was stimulated by 27-44% and in the presence of ADI-PEG20 by 8-20%. Percentage increase of cell lines from control with averaged values ($n = 3$) of SBR proliferation assay of $ASS1^{M}$ (GAMG, SNB19), $ASS1^{U}$ (U87, U118), and non-GBM (astrocytes) supplemented with creatine (0-10μM) over 5 days in the (a) absence and (b) presence ADI-PEG20. Error bars represent SEM.

Creatine supplementation does not affect intracellular ATP levels

In order to study the mechanism by which creatine stimulates proliferation and investigate the metabolite's reported [143] involvement in buffering cellular energy in GBM, ATP was measured via luciferase assay. The approach of using luciferase assay as an approximation of cellular energy was also applied by Berbeburg *et al.* [16].
Results show (figure 5.8) that relative to the control (media where no creatine was added), creatine supplementation did not yield significantly higher ATP content in GBM or non-GBM (astrocyte) cell lines. GBM cell lines (GAMG, LN229, SNB19, U87, U118 and astrocytes) were subjected to 10μM creatine. This was the concentration which had induced the highest boost in proliferation from the creatine titration (section 5.2.4). Further samples were harvested after 5-days of exposure, keeping the same conditions as in the previous SRB assay (section 5.2.4). These results show that despite creatine supplementation boosting proliferation, the mechanisms can not be directly attributed to enhanced ATP levels.

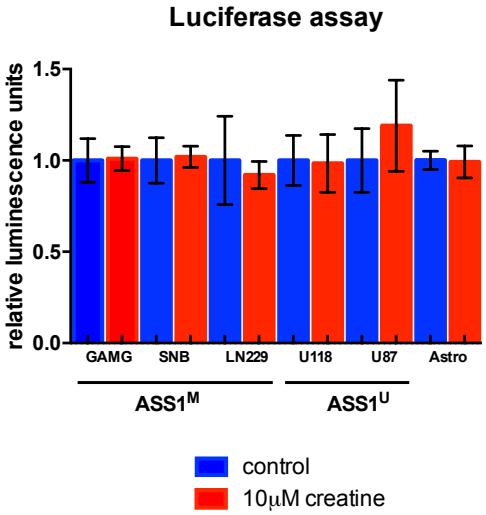


Figure 5.8.: Luciferase assay: ATP content is not enhanced by creatine supplementation in GBM cells. ASS1^{M} (GAMG, LN229, SNB19), ASS1^{U} (U87, U118), and non-GBM (astrocyte) cells were grown in the presence (10μM) and absence of creatine and harvested at day 5. Values shown are relative to the non-treated control and error bars represent SEM.

5.3. Discussion

5.3.1. IP6 arrests proliferation in GBM cell lines

Results in section 5.2.1 demonstrated that IP6 treatment arrested proliferation of GBM cell lines. These results corroborated the IP6 treatment effect observed by others in colon, leukaemic, liver, prostate and rhabdomyosarcoma and breast cancer cell lines [66] [131]. A study by Karmakar *et al.* [67] also found that IP6 arrested proliferation in the GBM cell line T98G. Results in this chapter substantiate observations made in a single cell line by these authors, demonstrating that IP6 arrested proliferation in four different GBM lines. IP6 is particularly attractive for use in GBM therapy, as no side effects have been reported and it can be administered through addition to drinking water [140]. Further, a pilot clinical study of IP6 in combination with inositol has even reported an amelioration in side-effects in breast cancer patients undergoing chemotherapy [10].

Time- and dose-dependent growth inhibition in GBM cell lines via IP6 corroborated findings made in other cancer cells [66] [131]. Treatment concentrations of 0.5mM IP6 and higher significantly decreased proliferation, which was also reported by Karmakar *et al.* [67] and in agreement with studies in other cancer cell lines [66]. Section 5.2.1 showed effect of IP6 was notable from day 3 and pronounced from day 5, which was in accordance with findings by Shamsuddin *et al.* [131] in breast cancer cell lines, though these authors also reported earlier effect from day 2.

Results presented here show that IP6 arrested proliferation in GBM cells, irrespective of ASS1 status, which are first reports of this to date. These observations were a surprise, given that ^{1}H NMR and RT-QPCR results from chapter 3 and 4 had shown ASS1^{M} cells to be more sensitive to perturbations in the thymine pathway. It had hence been anticipated that with IP6 affecting the *de novo* thymine pathway [140], ASS1^{M} cells would be also more sensitive to IP6 treatment than ASS1^{U} cells. It could therefore be hypothesised that in addition to IP6 effecting the *de novo* thymine pathway, further modes of action exist which have yet to be fully elucidated. Known and hypothesised modes of action are discussed in detail in section 5.3.3.

5.3.2. IP6 and ADI-PEG20 combination enhance arrested proliferation in ASS1^{M} cells but not ASS1^{U}

Findings in section 5.2.2 showed that IP6 and ADI-PEG20 combination treatment enhanced arrested proliferation in ASS1^{M} GBM cells, when compared to either treatment alone. To date, these are the first studies into this combination treatment in any cancer model. As previously mentioned (section 5.3.1), these two agents are attractive for use in GBM therapy, as both have been clinically tested in other cancers, with no reported side effects [10] [158].

For ASS1^{U} GBM cells it was anticipated that ADI-PEG20 would not have an enhanced effect, given results in previous chapters and the fact that these cells can synthesise their own arginine. These results did however confirm IP6 effect in ASS1^{U} cells, and that arrested proliferation observed under combination treatment could be attributed to IP6 effect alone in ASS1^{U} cells. Observations made in ASS1^{U} cells, highlight that there is merit for further investigating the incorporation of IP6 as a candidate in GBM treatment.

5.3.3. Combination treatment down-regulates TYMS mRNA expression in ASS1^{M} GBM cells

Transcriptional down-regulation of TYMS was significantly more pronounced by IP6 and ADI-PEG20 combination treatment than either treatment alone in ASS1^{M}, whereas mRNA was not significantly altered in ASS1^{U} cells in section 5.2.2. This suggested that ASS1^{M} GBM were more sensitive to perturbations the *de novo* thymine synthesis pathway, as indicated by TYMS. Enhanced suppression of TYMS by ADI-PEG20 in combination with thymine pathway targeting agent 5-fluorouracil has also been reported by Cheng *et al.* in hepatocellular carcinoma [23], corroborating findings made with ADI-PEG20 and IP6 combination treatment in GBM (section 5.2.2).

Section 5.2.1 and 5.2.2 had shown IP6 treatment effect, arresting proliferation in both ASS1 GBM subtypes. The mechanism by which IP6 asserts it's effect if not fully understood, however amongst other mechanisms, it has been reported to affect the salvage thymine pathway via inhibition of TK [133] [140]. Results in section 5.2.3 showed that the *de novo* thymine

pathway was modulated in $ASS1^{M}$ (GAMG) cells via down-regulation of TYMS, indicating that the thymine pathway in these cells is sensitive to IP6 treatment. Given further validation, IP6 would be an attractive candidate for TYMS targeted therapy in $ASS1^{M}$ cells, particularly as other TYMS targeting therapies such as pemetrexed have not progressed into clinical success in GBM [17]. Interestingly, $ASS1^{U}$ (U87) GBM cells did not reflect the same trend in TYMS mRNA expression as $ASS1^{M}$ (GAMG) cells. As arrested proliferation had however been observed in $ASS1^{U}$ cells, these findings indicate that IP6 asserts it's effect in $ASS1^{U}$ cells outside of TYMS.
Multiple modes of action have been reported in IP6, which are believed to result from dephosphorylation of IP6 into lower phosphates [140]. These include alteration of ion channel protein transfer, glucose transporter GLUT-4, endocytosis, exocytosis and nuclear mRNA transfer [140] [108]. Modulation of ion channel protein transfer and exocytosis could be of particular interest in GBM cells, given the metabolic alterations observed in chapter 3. *In silico* studies also propose IP6 activation of kinase and inositol 1,4,5-triphosphate receptor [66]. Karmakar *et al.* [67] report of up-regulation of mitochondria-dependent caspase cascade in GBM cell line T98G, and IP6-induced apoptosis via caspases have also been found in squamous cell carcinoma lines [64].

Taken together, these findings highlight TYMS modulation is induced by IP6 in $ASS1^{M}$, yet the precise mechanisms by which IP6 asserts it's proliferative inhibition in GBM cells has yet to be elucidated.

5.3.4. Creatine stimulates proliferation, yet mechanism can not be attributed to ATP changes

Results from section 5.2.4 demonstrated that creatine supplementation stimulates proliferation in GBM cell lines, yet this can not be attributed to enhanced ATP levels. As the reduction in creatine and arrested proliferation had been observed in $ASS1^{M}$ GBM under arginine-deprived conditions (section 5.2.4), and arginine is a precursor required for *de novo* creatine synthesis, it had been hypothesised that creatine supplementation could contravene the effect of ADI-PEG20. It was therefore a surprise, that creatine supplementation not only rescued but also boosted proliferation by 8-20% beyond the ADI-PEG20 treated control. The 26-45% enhanced proliferation

resulting from the creatine supplementation compared to the normal growth medium control was even more astonishing.

The role of creatine in cancer is not well understood. Of the few studies that exist on creatine in relation to cancer, Tang *et al.* [130] report that upon deprivation of the amino-acid methionine breast cancer cells transcriptionally activated the creatine biosynthesis pathway. These findings by Tang *et al.* [130] could indicate that GBM cells undergoing arginine deprivation also had a transcriptionally activated creatine biosynthesis pathway which was however not functional in the absence of arginine, hence displaying the metabolic alterations in creatine and glycine in section 5.2.4. Interestingly, dietary creatine and more specifically cyclocreatine was reported to inhibit tumour growth in human colon adenocarcinoma xenograft mice [75], which stands in stark contrast to results observed here, highlighting that more research is required in this area.

Despite lack of information on effects of creatine supplementation in relation to cancer, the amino-acid's role in buffering cellular energy, increasing muscle mass and performance as well as protective effects against cellular insults are well documented [142],[13]. Creatine together with phosphocreatine also buffer cellular energy (ATP) via the enzyme creatine kinase, and creatine supplementation has been found to help strengthen cellular energetics and enhance mitochondrial function in neurodegenerative diseases [142]. Increased cellular ATP due to creatine supplementation could have explained enhanced proliferation in GBM, however luciferase assay (section 5.2.4) did not show that this was the case in GBM cell lines, demonstrating that more research needs to be conducted into understanding the mechanism by which creatine boosts proliferation.

5.3.5. Study limitations

For SRB proliferation and RT-QPCR assays small panels of cell lines were studied, limited by time and resource constraints. Particularly the multiple time-points, dose-ranges and combination treatments limited feasibility of extending this, yet ideally a wider biological scope (i.e. more cell lines) would have been tested.

Further, despite RT-QPCR being a rapid, informative and widely used method for studying mRNA expression, it should be clearly noted that RT-QPCR provides information at transcriptional level. Further post-translational modifications such as protein ubiquitination or acetylation, which could have affected TYMS activity and that of the *de novo* thymine pathway were not investigated as they were outside the scope of this study, but would have provided helpful insights in section 5.2.3.
For section 5.2.4, luciferase was a fast and simple assay for testing cellular energy levels in relation to creatine exposure, however as cellular ATP levels are kept in homeostatic equilibrium and rapidly metabolised [16], which may limit use of luciferase as a cellular energy measure. ^{1}H NMR or radioactively labeled creatine experiments would help shed further insights into the mechanism by which creatine stimulates proliferation.

5.3.6. Conclusions

Studying the effects of IP6 treatment and creatine supplementation identified two opposite effects in GBM cell lines. Whereas IP6 arrested proliferation, creatine stimulated cell growth. Results shown here uniquely investigated ASS1 GBM subtypes and in the case of IP6 present novel treatment options. Findings further our knowledge on the effect that IP6 and creatine have on GBM and provide further insights and direction into the underlying mechanisms of action.

Effect of thymine pathway targeting agent IP6 alone, and combination with ADI-PEG20, was studied by investigating cellular proliferation and mRNA expression in GBM cell lines. Three key findings from results presented here contribute towards knowledge of IP6 treatment in GBM.
First, IP6 arrests proliferation in GBM cells irrespective of ASS1 status in a time- and dose-dependent manner. The mechanisms for this is not known, but demonstrates that IP6 asserts effects outside of the *de novo* thymine pathway.
Second, combination treatment of IP6 and ADI-PEG20 enhanced proliferative arrest in $ASS1^{M}$ GBM cells. These are the first studies into this combination treatment in any cancer model.
Third, it was shown that TYMS mRNA suppression was significantly enhanced by IP6 and ADI-PEG20 combination treatment in $ASS1^{M}$ cells, compared to either treatment alone. As TYMS modulation was specific to $ASS1^{M}$ GBM cells, yet arrested treatment effect was observed in both ASS1 subtypes, these results highlight that IP6 exerts it's effect via multiple modes of action.

Creatine supplementation studies are first reported investigations of this amino-acid's effect on GBM to date. The dose-dependent boost in proliferation demonstrate that creatine has a powerful effect on not just $ASS1^{M}$ but also $ASS1^{U}$ GBM in the presence and absence of ADI-PEG20. Despite the role of creatine in buffering intracellular energy supplies, ATP levels were not shown to be modulated via luciferase assay. Identifying inhibitors and understanding the mechanisms by which creatine boost proliferation will be key for furthering work in this area, however findings presented here high-

light the importance of the creatine pathway in GBM cells.

Returning the focus to IP6, which presents more immediate clinically relevant findings, results demonstrate that IP6 alone and in combination with ADI-PEG20, are novel candidates for therapy in GBM and should be investigated further. Findings are first investigations of this combination treatment and provide a base, directing further validation and mechanistic studies in GBM. Given further success in identifying mechanisms and demonstrating that IP6 and combination treatment improve patient outcome, there is strong reasoning for these therapies to be used clinically in GBM, as IP6 has already been safely used clinically as an adjuvant to breast cancer treatment [10]. Findings presented here identify IP6 as a prospective adjuvant to therapy for enhanced treatment outcome in GBM patients.

5.3.7. Future work

With the ultimate aim of IP6 reaching the clinic for GBM treatment, several steps lie ahead, and the most immediate would be to elucidate the mechanism by which IP6 arrests proliferation as observed via SRB assay and confirm IP6 and combination treatment effect on TYMS.

SRB proliferation assay (section 5.2.1 and 5.2.2) allowed for several doses and time-points to be tested on GBM cell lines, that enabled insights into effects of IP6 and ADI-PEG20 combination treatment. SRB is an efficient, robust and more cost-effective method compared to other colourimetric assays such as MTT [60], however measures are limited to cell proliferation, and further assays such as flow cytometry would provide further information on induction of cellular apoptosis as a result of treatment [111].
The down-regulation of TYMS via IP6 was identified through RT-QPCR, and ADI-PEG20 combination treatment at transcriptional level. Confirming down-regulation of TYMS at protein level via Western blot would validate findings and provide insights into protein expression. Further, 48-hours was selected for studying the early consequences of treatments on TYMS, showing effect in $ASS1^{M}$ yet not $ASS1^{U}$ GBM cells at this time-point. Probing TYMS transcriptional expression at different time-points will help determine changes at later time-points (day 5 and 8), when arrested proliferation was more pronounced.
Further, comparing and testing addition of IP6 and ADI-PEG20 combination treatment to temozolomide and radio-therapy, the GBM clinical standard of care [59], will also be important in demonstrating therapeutic advantage for GBM.

Studies presented here on creatine (section 5.2.4) focused on understanding the effect and mechanism by which the amino-acid boost proliferation, however the ultimate aim would be to inhibit this pathway and arrest proliferation in GBM. SRB proliferation assays (section 5.2.4) provided first insights into the action of creatine in GBM, however given further validation of findings, future work should focus on identifying suitable inhibitors. As there have been reports [130] of the creatine pathway being transcriptionally activated upon amino-acid deprivation, verifying this trend in GBM

subjected to arginine-deprivation could also help target specific enzymes in the creatine pathway.

6. Final discussion and concluding remarks

6.1. Summary of main findings

The overall aim of this PhD project was to characterise ASS1 GBM subtypes and identify novel treatment approaches. This was achieved by metabolic profiling, using two complimentary biochemical techniques, statistical analysis and molecular biology techniques. Treatment response ADI-PEG20 was determined and used to highlight cellular vulnerabilities to target with novel treatments. Metabolic analysis was also used as an explorative tool, directing pathway investigations, which were further studied by molecular biology techniques, in order to identify mechanisms and test possible treatment approaches.

Starting with a broad non-targeted approach, metabolic characteristics and alterations amongst ASS1 subtypes were established in GBM cells, including the glycolytic, uridine, citric acid, thymine and glutamine pathway. Following these alterations, focus was directed on these select pathways, identifying transcriptional modulations amongst subtypes. Finally investigations were centred on thymine and creatine pathways, demonstrating IP6 as a novel treatment approach in GBM that could be translated into clinical application.

6.1.1. Metabolic characterisation of ASS1 GBM subtypes

Characterisation of ASS1 GBM subtypes was achieved, using GC/TOF MS and ^{1}H NMR, analysing both intra- and extra-cellular metabolic profiles *in vitro* in the presence and absence of ADI-PEG20.

It was demonstrated that at basal level (no ADI-PEG20 treatment) there were limited difference between profiles of ASS1 GBM subtypes. This showed that under growth conditions where arginine is in ample supply, methylation-specific silencing of one gene does not exert drastic differences. More subtle differences in the glycolytic and uridine pathway were however identified, suggesting that ASS1^{U} GBM were metabolically and transcriptionally more active than ASS1^{M} GBM cells.
It was repeatedly shown that in ADI-PEG20 challenged ASS1^{M} GBM cell lines arginine-deprivation exerts extensive global metabolic alterations, whereas limited changes occur in ASS1^{U} GBM cells. Significantly modulated metabolites included those of the arginine, glycolytic, citric acid, thymine and glutamine pathway. Further, metabolically important metabolites required for proliferation, including pyrimidine, pyridine and purine were released or ceased to be consumed in ASS1^{M} GBM, manifesting homeostatic disequilibrium in these cells. Through metabolic analysis it was also shown that under normal growth conditions GBM are metabolically more active than when challenged with ADI-PEG20, with perturbations amongst intermediates of the TCA cycle.

The strength and potential of using GC/TOF MS and ^{1}H NMR analysis for characterising GBM metabolic profiles was confirmed, and these are the first report to date, demonstrating application of chemometric approaches for monitoring ADI-PEG20 treatment response in ASS1 GBM subtypes. It was also shown that these techniques are powerful as an untargeted research tool, and recognised that clinical application currently remains limited due to time and resource constraints. Clinical application of cost-effective biochemical assays should however be pursued, and findings presented here show that citrulline may be a better indicator for monitoring ADI-PEG20 treatment response than arginine.

6.1.2. Transcriptional studies and metabolic pathway investigations

It was demonstrated, using transcriptional studies, that ASS1 GBM differentially alter enzymatic mRNA expression upon ADI-PEG20 treatment. Despite there being no significant differences in TYMS expression at basal levels amongst ASS1 subtypes, it was shown that ADI-PEG20 treatment results in significant transcriptional down-regulation of TYMS in $ASS1^{M}$ and not $ASS1^{U}$ cell lines, which are first accounts of this in GBM. Interestingly, regarding a wider enzyme panel, RT-QPCR showed there to be an overall increase in transcriptional activity upon treatment, irrespective of ASS1 status. Significantly altered enzymes displaying greatest transcriptional modulation upon treatment including GPT2 and TYMS for $ASS1^{M}$ cells and TK2 and AGXT2 for $ASS1^{U}$ GBM.

Biological interpretations of altered enzymes and their associated pathways were made, guided by publicly accessible databases and systematic literature searches, highlighting the strength of using these resources in a research capacity. TYMS was identified to be of particular interest, given the fact that is was not only significantly down-regulated in $ASS1^{M}$ GBM cells upon ADI-PEG20 treatment, but also in view of it's biological significance, being closely linked to DNA synthesis, required for cellular proliferation [1].

It was repeatedly shown and confirmed, that TYMS was significantly down-regulated in $ASS1^{M}$ and not $ASS1^{U}$ GBM cells upon ADI-PEG20 treatment. TYMS and it's role in *de novo* thymine synthesis has been well studied in several cancers [43],[136],[4],[96], however results presented here are first accounts associating ADI-PEG20 with down-regulation in $ASS1^{M}$ GBM cells. Findings also demonstrate that $ASS1^{U}$ cells, which can endogenously synthesise arginine, were able to sustain proliferative activities and TYMS expression remained unaltered. It was shown that TYMS and the *de novo* thymine pathway play and important role in facilitating proliferation in GBM, yet the mechanisms by which arginine deprivation modulates TYMS have yet to be elucidated.

6.1.3. IP6 arrests proliferation and enhances effect of ADI-PEG20 in ASS1^{M} GBM cells, while creatine promotes proliferation

Targeting the *de novo* thymine and creatine metabolic pathway, it was demonstrated that IP6 treatment arrests proliferation, as evidenced by SRB proliferation assay, whereas creatine supplementation boosts growth. Studies were first of it's kind, investigating both treatments alone and in combination with arginine-deprivation via ADI-PEG20 in ASS1 GBM subtype cell lines. IP6 is particularly attractive for use in GBM as no clinical side-effects have been reported from application in other pathologies. Whilst IP6 studies focused on identifying therapeutic options by targeting the *de novo* thymine pathway, creatine investigations aimed to understand the effect and mechanism by which this amino-acid exerts it's effect in promoting proliferation.

It was established that IP6 treatment alone significantly arrests cellular proliferation in a time- and dose-dependent manner in GBM cells. This effect was identified to occur irrespective of ASS1 status, as shown by SRB proliferation assay.
Combining IP6 with ADI-PEG20 treatment was found to enhance arrested proliferation in ASS1^{M} GBM cells, compared to either treatment alone. Results also repeatedly confirmed that ADI-PEG20 does not affect ASS1^{U} GBM, yet IP6 alone does affect these cells. Studies were first investigations looking at IP6 and ADI-PEG20 combination treatment in any cell line model. Success of IP6 in ASS1^{U} GBM, which do not respond to ADI-PEG20, particularly merits further investigation as a candidate for GBM treatment.

Transcriptional down-regulation of TYMS was found to be significantly more pronounced through IP6 and ADI-PEG20 combination treatment in ASS1^{M} GBM than either treatment alone, yet ASS1^{U} cells remained unaltered. As indicated by TYMS, ASS1^{M} cells were therefore more sensitive to modulation of the *de novo* thymine synthesis pathway.
Despite TYMS down-regulation playing a role in arrested proliferation in ASS1^{M} GBM cells, it was demonstrated that IP6 also exerts it's mode of action outside of TYMS, as indicated by IP6 arresting proliferation in ASS1^{U}

GBM without significant TYMS modulation. Multiple modes of action have been reported in IP6 [140] [108], and results presented here corroborate these observations. Together, findings highlight that the precise mechanism by which IP6 acts in GBM has yet to be elucidated.

Creatine supplementation studies demonstrated that not only can this amino-acid contravene ADI-PEG20 treatment effect in $ASS1^{M}$ cells, but supplementation even boosted proliferation by 8-20%, as determined by SRB proliferation assay. Further, in the absence of ADI-PEG20 the effect was even more pronounced, boosting proliferation by 26-45%. As creatine has a role in buffering intracellular energy supplies [142],[13], it had been hypothesised that enhanced ATP levels could help explain this mechanism. It was however demonstrated via luciferase assay, that creatine supplementation does not significantly increase ATP levels in either ASS1 GBM subtypes. Results show that the mechanism by which creatine supplementation drives proliferation in GBM has yet to be elucidated.

6.1.4. Future directions

Following-on from this PhD research, three key areas have been identified for future work. First, next steps for demonstrating direct clinical translation, will require for characteristics of metabolic profiles identified from *in vitro* GBM cell lines to be validated in biological human samples. Validation of intracellular characteristics could be achieved, testing tumour biopsy samples, and those identified extracellularly through plasma. Further, as ADI-PEG20 progresses towards clinical application in GBM treatment, blood or plasma samples would provide a minimally invasive option for monitoring treatment response in $ASS1^{M}$ tumours. Citrulline had been identified as a marker for monitoring treatment response and it will be important to demonstrate that this can be detected amongst other metabolites present in complex human bio-systems.

Second, validating transcriptional modulation of enzymes in at protein level in GBM cell lines and tumour tissues. RT-QPCR was a cost-effective method for studying enzymatic alterations at mRNA level, and next steps would include probing protein expression via Western blot. Having focused on TYMS and it's association with arrested proliferation in $ASS1^{M}$ GBM cells, it would be interesting to further investigate this enzymes function in GBM, using siRNA in knock-down studies. Finally, TYMS had been focused on in view of it being one of the most significantly altered enzymes and it's biological relevance, however GPT2, TK2 and AGXT2 were also interesting enzymes and inhibitors identified in the literature review also merit further investigation through *in vitro* proliferation studies.

Third, validating proliferative effects of IP6 *in vivo* and identifying creatine pathway inhibitors, as well as determining mechanisms of action. IP6 showed great clinical potential, demonstrating arrested proliferation in both ASS1 subtypes. Given further successes, IP6 could be used to treat $ASS1^{U}$ cells, which do not respond to ADI-PEG20 treatment. In order to progress this work towards the clinic, xenograft mouse-models will be key for verifying that tumours also respond *in vivo*, and that dietary supplementation shows comparable potential as media supplementation. As there have not been reported toxicities from IP6 *in vivo* [88], making IP6 a strong candi-

date for therapy in GBM. Further, identifying the mechanism by which IP6 exerts it's action outside of TYMS will also be important to demonstrate IP6 targets.

Creatine's ability to boost proliferation raised many questions. Identifying the mechanism by which creatine exerts it's action will be important in directing further research. As enhanced ATP level generation was discarded as a possible mechanism of action, further mRNA or protein studies should look at induction or up-regulation of cell-cycle regulators. The ultimate aim would however be to identify novel therapies that inhibit proliferation, hence the real challenge will rest in identifying suitable therapeutic inhibitors and demonstrating their clinical utility.

6.1.5. Concluding remarks

This PhD research has directly contributed towards our knowledge and understanding of GBM, focusing on two different GBM subtypes. Findings firmly establish the central role that the arginine and other metabolic processes have in GBM, demonstrating significant characteristic differences amongst the cellular metabolism in ASS1 subtypes, showing enzymatic alterations and targeting specific pathways to arrest proliferation.

With an average GBM survival of only 15-months [49], GBM is one of the most fatal cancers and treatment outcome remains unacceptable. Despite advances, successes remain limited and novel treatment approaches are desperately needed. Complete GBM tumour resection in this anatomically difficult locations remains challenging and presence of the blood-brain-barrier can prevent drugs reaching it's target [90]. Metabolic therapies therefore present particularly attractive treatment approaches.

Findings of this PhD research identify IP6 as one novel treatment approach, and evidence further substantiates findings to help advance ADI-PEG20 treatment into the clinic in order to improve GBM patient outcome.

Bibliography

[1] E. A. Abdallah, M. F. Fanelli, M. E. C. Buim, M. C. Machado Netto, J. L. Gasparini Junior, V. Souza e Silva, A. L. A. Dettino, N. B. Mingues, J. V. Romero, L. M. M. Ocea, et al., Thymidylate synthase expression in circulating tumor cells: A new tool to predict 5-fluorouracil resistance in metastatic colorectal cancer patients, International Journal of Cancer, 137(6), (2015), pp. 1397–1405.

[2] C. S. Ahn, C. M. Metallo, Mitochondria as biosynthetic factories for cancer proliferation, Cancer Metab, 3(1), (2015), p. 1.

[3] M. J. Albers, R. Bok, A. P. Chen, C. H. Cunningham, M. L. Zierhut, V. Y. Zhang, S. J. Kohler, J. Tropp, R. E. Hurd, Y.-F. Yen, et al., Hyperpolarized 13C lactate, pyruvate, and alanine: noninvasive biomarkers for prostate cancer detection and grading, Cancer research, 68(20), (2008), pp. 8607–8615.

[4] M. D. Allen, P. Luong, C. Hudson, J. Leyton, B. Delage, E. Ghazaly, R. Cutts, M. Yuan, N. Syed, C. L. Nigro, et al., Prognostic and therapeutic impact of argininosuccinate synthetase 1 control in bladder cancer as monitored longitudinally by PET imaging, Cancer research, 74(3), (2014), pp. 896–907.

[5] S. Allison, J. Knight, C. Granchi, R. Rani, F. Minutolo, J. Milner, R. Phillips, Identification of LDH-A as a therapeutic target for cancer cell killing via (i) p53/NAD (H)-dependent and (ii) p53 independent pathways, Oncogenesis, 3(e102), (2014), pp. 1–11.

[6] A. Alonso, S. Marsal, A. Julià, Analytical methods in untargeted metabolomics: state of the art in 2015, Frontiers in bioengineering and biotechnology, 3.

[7] D. D. Anderson, C. M. Quintero, P. J. Stover, Identification of a de novo thymidylate biosynthesis pathway in mammalian mitochondria, Proceedings of the National Academy of Sciences, 108(37), (2011), pp. 15163–15168.

[8] S. Aufderklamm, T. Todenhöfer, G. Gakis, S. Kruck, J. Hennenlotter, A. Stenzl, C. Schwentner, Thymidine kinase and cancer monitoring, Cancer letters, 316(1), (2012), pp. 6–10.

[9] V. Babushok, P. Linstrom, J. Reed, I. Zenkevich, R. Brown, W. Mallard, S. Stein, Development of a database of gas chromatographic retention properties of organic compounds, Journal of Chromatography A, 1157(1), (2007), pp. 414–421.

[10] I. Bačić, N. Družijanić, R. Karlo, I. Škific, S. Jagić, Efficacy of IP 6+ inositol in the treatment of breast cancer patients receiving chemotherapy: prospective, randomized, pilot clinical study, Journal of Experimental & Clinical Cancer Research, 29(1), (2010), p. 1.

[11] C. Bardella, P. J. Pollard, I. Tomlinson, SDH mutations in cancer, Biochimica et Biophysica Acta (BBA)-Bioenergetics, 1807(11), (2011), pp. 1432–1443.

[12] G. A. Barding Jr, S. Béni, T. Fukao, J. Bailey-Serres, C. K. Larive, Comparison of GC-MS and NMR for metabolite profiling of rice subjected to submergence stress, Journal of proteome research, 12(2), (2012), pp. 898–909.

[13] M. F. Beal, Neuroprotective effects of creatine, Amino Acids, 40(5), (2011), pp. 1305–1313.

[14] K. P. Becker, J. Yu, Status quoâĂŤstandard-of-care medical and radiation therapy for glioblastoma, The Cancer Journal, 18(1), (2012), pp. 12–19.

[15] O. Beckonert, H. C. Keun, T. M. Ebbels, J. Bundy, E. Holmes, J. C. Lindon, J. K. Nicholson, Metabolic profiling, metabolomic and metabonomic procedures for NMR spectroscopy of urine, plasma, serum and tissue extracts, Nature protocols, 2(11), (2007), pp. 2692–2703.

[16] M. Berneburg, T. Gremmel, V. Kurten, P. Schroeder, I. Hertel, A. Von Mikecz, S. Wild, M. Chen, L. Declercq, M. Matsui, et al., Creatine supplementation normalizes mutagenesis of mitochondrial DNA as well as functional consequences, Journal of investigative dermatology, 125(2), (2005), pp. 213–220.

[17] M. Bischof, A. Abdollahi, P. Gong, C. Stoffregen, K. E. Lipson, J. ürgen Debus, K. J. Weber, P. E. Huber, Triple combination of irradiation, chemotherapy (pemetrexed), and VEGFR inhibition (SU5416) in human endothelial and tumor cells, International Journal of Radiation Oncology* Biology* Physics, 60(4), (2004), pp. 1220–1232.

[18] C. G. Brasse-Lagnel, A. M. Lavoinne, A. S. Husson, Amino acid regulation of mammalian gene expression in the intestine, Biochimie, 92(7), (2010), pp. 729–735.

[19] J. T. Brosnan, R. P. Da Silva, M. E. Brosnan, The metabolic burden of creatine synthesis, Amino acids, 40(5), (2011), pp. 1325–1331.

[20] C. Caneba, L. Yang, J. Baddour, R. Curtis, J. Win, S. Hartig, J. Marini, D. Nagrath, Nitric oxide is a positive regulator of the Warburg effect in ovarian cancer cells, Cell death & disease, 5(6), (2014), p. e1302.

[21] K. Celis, S. Shuldiner, E. V. Haverfield, J. Cappell, R. Yang, D.-W. Gong, W. K. Chung, Loss of function mutation in glutamic pyruvate transaminase 2 (GPT2) causes developmental encephalopathy, Journal of inherited metabolic disease, 38(5), (2015), pp. 941–948.

[22] E. C. Y. Chan, K. K. Pasikanti, J. K. Nicholson, Global urinary metabolic profiling procedures using gas chromatography-mass spectrometry, Nature protocols, 6(10), (2011), pp. 1483–1499.

[23] P. N.-M. Cheng, T.-L. Lam, W.-M. Lam, S.-M. Tsui, A. W.-M. Cheng, W.-H. Lo, Y.-C. Leung, Pegylated recombinant human arginase (rhArg-peg5, 000mw) inhibits the in vitro and in vivo proliferation of human hepatocellular carcinoma through arginine depletion, Cancer research, 67(1), (2007), pp. 309–317.

[24] P. Chinnaiyan, E. Kensicki, G. Bloom, A. Prabhu, B. Sarcar, S. Kahali, S. Eschrich, X. Qu, P. Forsyth, R. Gillies, The metabolomic signature of malignant glioma reflects accelerated anabolic metabolism, Cancer research, 72(22), (2012), pp. 5878–5888.

[25] T. Cihlar, A. S. Ray, Nucleoside and nucleotide HIV reverse transcriptase inhibitors: 25 years after zidovudine, Antiviral research, 85(1), (2010), pp. 39–58.

[26] M. Cunha, M. Martin-de Saavedra, A. Romero, E. Parada, J. Egea, L. Del Barrio, A. Rodrigues, M. Lopez, Protective effect of creatine against 6-hydroxydopamine-induced cell death in human neuroblastoma SH-SY5Y cells: involvement of intracellular signaling pathways, Neuroscience, 238, (2013), pp. 185–194.

[27] M. Cuperlovic-Culf, D. Ferguson, A. Culf, P. Morin, M. Touaibia, 1H NMR metabolomics analysis of glioblastoma subtypes correlation between metabolomics and gene expression characteristics, Journal of Biological Chemistry, 287(24), (2012), pp. 20164–20175.

[28] R. Danesi, A. Falcone, P. F. Conte, M. Del Tacca, Pharmacokinetic optimisation of the treatment of cancer with high dose zidovudine, Clinical pharmacokinetics, 34(2), (1998), pp. 173–180.

[29] B. Delage, D. A. Fennell, L. Nicholson, I. McNeish, N. R. Lemoine, T. Crook, P. W. Szlosarek, Arginine deprivation and argininosuccinate synthetase expression in the treatment of cancer, International Journal of Cancer, 126(12), (2010), pp. 2762–2772.

[30] S. Derveaux, J. Vandesompele, J. Hellemans, How to do successful gene expression analysis using real-time PCR, Methods, 50(4), (2010), pp. 227–230.

[31] K. Dettmer, P. A. Aronov, B. D. Hammock, Mass spectrometry-based metabolomics, Mass spectrometry reviews, 26(1), (2007), pp. 51–78.

[32] F. Dieterle, A. Ross, G. Schlotterbeck, H. Senn, Probabilistic quotient normalization as robust method to account for dilution of complex biological mixtures. Application in 1H NMR metabonomics, Analytical chemistry, 78(13), (2006), pp. 4281–4290.

[33] G. Dresemann, Temozolomide in malignant glioma, Onco Targets Ther, 3, (2010), pp. 139–46.

[34] R. Dulbecco, G. Freeman, Plaque production by the polyoma virus, Virology, 8(3), (1959), pp. 396–397.

[35] W. B. Dunn, D. I. Ellis, Metabolomics: current analytical platforms and methodologies, TrAC Trends in Analytical Chemistry, 24(4), (2005), pp. 285–294.

[36] C. M. Ensor, F. W. Holtsberg, J. S. Bomalaski, M. A. Clark, Pegylated arginine deiminase (ADI-SS PEG20, 000 mw) inhibits human melanomas and hepatocellular carcinomas in vitro and in vivo, Cancer research, 62(19), (2002), pp. 5443–5450.

[37] Y. Feng, D. He, Z. Yao, D. J. Klionsky, The machinery of macroautophagy, Cell research, 24(1), (2014), pp. 24–41.

[38] L. Feun, N. Savaraj, Pegylated arginine deiminase: a novel anticancer enzyme agent, Expert opinion on investigational drugs, 15(7), (2006), pp. 815–822.

[39] L. Feun, M. You, C. Wu, M. Kuo, M. Wangpaichitr, S. Spector, N. Savaraj, Arginine deprivation as a targeted therapy for cancer, Current pharmaceutical design, 14(11), (2008), p. 1049.

[40] O. Fiehn, Metabolomics–the link between genotypes and phenotypes, Plant molecular biology, 48(1-2), (2002), pp. 155–171.

[41] J. M. Fonville, S. E. Richards, R. H. Barton, C. L. Boulange, T. Ebbels, J. K. Nicholson, E. Holmes, M.-E. Dumas, The evolution of partial least squares models and related chemometric approaches in metabonomics and metabolic phenotyping, Journal of Chemometrics, 24(11-12), (2010), pp. 636–649.

[42] H. S. Friedman, R. E. McLendon, T. Kerby, M. Dugan, S. H. Bigner, A. J. Henry, D. M. Ashley, J. Krischer, S. Lovell, K. Rasheed, et al., DNA mismatch repair and O6-alkylguanine-DNA alkyltransferase analysis and response to Temodal in newly diagnosed malignant glioma., Journal of Clinical Oncology, 16(12), (1998), pp. 3851–3857.

[43] E. Furuta, H. Okuda, A. Kobayashi, K. Watabe, Metabolic genes in cancer: their roles in tumor progression and clinical implications, Biochimica et Biophysica Acta (BBA)-Reviews on Cancer, 1805(2), (2010), pp. 141–152.

[44] O. Gallego, Nonsurgical treatment of recurrent glioblastoma, Current Oncology, 22(4), (2015), p. e273.

[45] S. Ganti, S. L. Taylor, O. A. Aboud, J. Yang, C. Evans, M. V. Osier, D. C. Alexander, K. Kim, R. H. Weiss, Kidney tumor biomarkers revealed by simultaneous multiple matrix metabolomics analysis, Cancer research, 72(14), (2012), pp. 3471–3479.

[46] P. S. Gill, W. Harrington Jr, M. H. Kaplan, R. C. Ribeiro, J. M. Bennett, H. A. Liebman, M. Bernstein-Singer, B. M. Espina, L. Cabral, S. Allen, et al., Treatment of adult T-cell leukemia–lymphoma with a combination of interferon alfa and zidovudine, New England Journal of Medicine, 332(26), (1995), pp. 1744–1748.

[47] R. Goodacre, S. Vaidyanathan, W. B. Dunn, G. G. Harrigan, D. B. Kell, Metabolomics by numbers: acquiring and understanding global metabolite data, Trends in biotechnology, 22(5), (2004), pp. 245–252.

[48] E. Gottlieb, I. P. Tomlinson, Mitochondrial tumour suppressors: a genetic and biochemical update, Nature Reviews Cancer, 5(11), (2005), pp. 857–866.

[49] I. S. Group, et al., Brain tumour risk in relation to mobile telephone use: results of the INTERPHONE international case–control study, International journal of epidemiology, (2010), p. dyq079.

[50] A. M. Groves, T. Win, S. B. Haim, P. J. Ell, Non-[18 F] FDG PET in clinical oncology, The lancet oncology, 8(9), (2007), pp. 822–830.

[51] R. J. Haines, L. C. Pendleton, D. C. Eichler, Argininosuccinate synthase: at the center of arginine metabolism, International journal of biochemistry and molecular biology, 2(1), (2011), p. 8.

[52] J. M. Halket, D. Waterman, A. M. Przyborowska, R. K. Patel, P. D. Fraser, P. M. Bramley, Chemical derivatization and mass spectral li-

braries in metabolic profiling by GC/MS and LC/MS/MS, Journal of experimental botany, 56(410), (2005), pp. 219–243.

[53] B. M. Hannigan, Y. A. Barnett, D. B. A. Armstrong, V. J. McKelvey-Martin, P. G. McKenna, Thymidine kinases: the enzymes and their clinical usefulness, Cancer Biotherapy & Radiopharmaceuticals, 8(3), (1993), pp. 189–197.

[54] C. Haskell, G. Canellos, B. Leventhal, P. Carbone, J. Block, A. Serpick, O. Selawry, L-asparaginase: therapeutic and toxic effects in patients with neoplastic disease, New England journal of medicine, 281(19), (1969), pp. 1028–1034.

[55] M. E. Hegi, A.-C. Diserens, S. Godard, P.-Y. Dietrich, L. Regli, S. Ostermann, P. Otten, G. Van Melle, N. de Tribolet, R. Stupp, Clinical trial substantiates the predictive value of O-6-methylguanine-DNA methyltransferase promoter methylation in glioblastoma patients treated with temozolomide, Clinical Cancer Research, 10(6), (2004), pp. 1871–1874.

[56] M. E. Hegi, A.-C. Diserens, T. Gorlia, M.-F. Hamou, N. de Tribolet, M. Weller, J. M. Kros, J. A. Hainfellner, W. Mason, L. Mariani, et al., MGMT gene silencing and benefit from temozolomide in glioblastoma, New England Journal of Medicine, 352(10), (2005), pp. 997–1003.

[57] C. T. Hensley, A. T. Wasti, R. J. DeBerardinis, Glutamine and cancer: cell biology, physiology, and clinical opportunities, The Journal of clinical investigation, 123(9), (2013), pp. 3678–3684.

[58] P. Hore, Nuclear magnetic resonance, Oxford University Press, USA, 2015.

[59] A. F. Hottinger, R. Stupp, K. Homicsko, Standards of care and novel approaches in the management of glioblastoma multiforme, Chin J Cancer, 33(1), (2014), pp. 32–9.

[60] P. Houghton, R. Fang, I. Techatanawat, G. Steventon, P. J. Hylands, C. Lee, The sulphorhodamine (SRB) assay and other approaches to testing plant extracts and derived compounds for activities related to reputed anticancer activity, Methods, 42(4), (2007), pp. 377–387.

[61] H. Huang, T. Kawamata, T. Horie, H. Tsugawa, Y. Nakayama, Y. Ohsumi, E. Fukusaki, Bulk RNA degradation by nitrogen starvation-induced autophagy in yeast, The EMBO journal, (2014), p. e201489083.

[62] H.-Y. Huang, W.-R. Wu, Y.-H. Wang, J.-W. Wang, F.-M. Fang, J.-W. Tsai, S.-H. Li, H.-C. Hung, S.-C. Yu, J. Lan, et al., ASS1 as a novel tumor suppressor gene in myxofibrosarcomas: aberrant loss via epigenetic DNA methylation confers aggressive phenotypes, negative prognostic impact, and therapeutic relevance, Clinical Cancer Research, 19(11), (2013), pp. 2861–2872.

[63] G. Ivosev, L. Burton, R. Bonner, Dimensionality reduction and visualization in principal component analysis, Analytical chemistry, 80(13), (2008), pp. 4933–4944.

[64] S. C. Janus, B. Weurtz, F. G. Ondrey, Inositol hexaphosphate and paclitaxel: symbiotic treatment of oral cavity squamous cell carcinoma, The Laryngoscope, 117(8), (2007), pp. 1381–1388.

[65] G. Jin, Z. J. Reitman, I. Spasojevic, I. Batinic-Haberle, J. Yang, O. Schmidt-Kittler, D. D. Bigner, H. Yan, 2-hydroxyglutarate production, but not dominant negative function, is conferred by glioma-derived NADP+-dependent isocitrate dehydrogenase mutations, PloS one, 6(2), (2011), p. e16812.

[66] A. Joy, S. Balaji, Drug-likeness of Phytic Acid and Its Analogues, The Open Microbiology Journal, 9, (2015), p. 141.

[67] S. Karmakar, N. L. Banik, S. K. Ray, Molecular mechanism of inositol hexaphosphate-mediated apoptosis in human malignant glioblastoma T98G cells, Neurochemical research, 32(12), (2007), pp. 2094–2102.

[68] A. King, M. Selak, , E. Gottlieb, Succinate dehydrogenase and fumarate hydratase: linking mitochondrial dysfunction and cancer, Oncogene, 25(34), (2006), pp. 4675–4682.

[69] P. Klivenyi, R. J. Ferrante, R. T. Matthews, M. B. Bogdanov, A. M. Klein, O. A. Andreassen, G. Mueller, M. Wermer, R. Kaddurah-Daouk, M. F. Beal, Neuroprotective effects of creatine in a transgenic

animal model of amyotrophic lateral sclerosis, Nature medicine, 5(3), (1999), pp. 347–350.

[70] D. R. Knapp, Handbook of analytical derivatization reactions, John Wiley & Sons, 1979.

[71] E. Kobayashi, M. Masuda, R. Nakayama, H. Ichikawa, R. Satow, M. Shitashige, K. Honda, U. Yamaguchi, A. Shoji, N. Tochigi, et al., Reduced argininosuccinate synthetase is a predictive biomarker for the development of pulmonary metastasis in patients with osteosarcoma, Molecular cancer therapeutics, 9(3), (2010), pp. 535–544.

[72] Y. Kontani, M. Kaneko, M. Kikugawa, S. Fujimoto, N. Tamaki, Identity of D-3-aminoisobutyrate-pyruvate aminotransferase with alanine-glyoxylate aminotransferase 2, Biochimica et Biophysica Acta (BBA)-General Subjects, 1156(2), (1993), pp. 161–166.

[73] W. H. Koppenol, P. L. Bounds, C. V. Dang, Otto Warburg's contributions to current concepts of cancer metabolism, Nature Reviews Cancer, 11(5), (2011), pp. 325–337.

[74] M. I. Koukourakis, A. Giatromanolaki, E. Sivridis, K. C. Gatter, A. L. Harris, Tumor, A. R. Group, et al., Pyruvate dehydrogenase and pyruvate dehydrogenase kinase expression in non small cell lung cancer and tumor-associated stroma, Neoplasia, 7(1), (2005), pp. 1–6.

[75] C. Kristensen, N. Askenasy, R. Jain, A. Koretsky, Creatine and cyclocreatine treatment of human colon adenocarcinoma xenografts: 31P and 1H magnetic resonance spectroscopic studies, British journal of cancer, 79(2), (1999), p. 278.

[76] G. Y. Lee, P. M. Haverty, L. Li, N. M. Kljavin, R. Bourgon, J. Lee, H. Stern, Z. Modrusan, S. Seshagiri, Z. Zhang, et al., Comparative oncogenomics identifies PSMB4 and SHMT2 as potential cancer driver genes, Cancer research, 74(11), (2014), pp. 3114–3126.

[77] H. X. Leong, C. Simkevich, A. Lesieur-Brooks, B. W. Lau, C. Fugere, E. Sabo, N. L. Thompson, Short-term arginine deprivation results

in large-scale modulation of hepatic gene expression in both normal and tumor cells: microarray bioinformatic analysis, Nutrition & metabolism, 3(1), (2006), p. 1.

[78] M. V. Liberti, J. W. Locasale, The Warburg Effect: How Does it Benefit Cancer Cells?, Trends in biochemical sciences.

[79] C.-C. Lin, T.-L. Cheng, W.-H. Tsai, H.-J. Tsai, K.-H. Hu, H.-C. Chang, C.-W. Yeh, Y.-C. Chen, C.-C. Liao, W.-T. Chang, Loss of the respiratory enzyme citrate synthase directly links the Warburg effect to tumor malignancy, Scientific reports, 2.

[80] J. C. Lindon, J. K. Nicholson, Spectroscopic and statistical techniques for information recovery in metabonomics and metabolomics, Annu. Rev. Anal. Chem., 1, (2008), pp. 45–69.

[81] J. C. Lindon, J. K. Nicholson, E. Holmes, The handbook of metabonomics and metabolomics, Elsevier, 2011.

[82] S. A. Lyons, W. J. Chung, A. K. Weaver, T. Ogunrinu, H. Sontheimer, Autocrine glutamate signaling promotes glioma cell invasion, Cancer research, 67(19), (2007), pp. 9463–9471.

[83] A. J. MacFarlane, D. D. Anderson, P. Flodby, C. A. Perry, R. H. Allen, S. P. Stabler, P. J. Stover, Nuclear localization of de novo thymidylate biosynthesis pathway is required to prevent uracil accumulation in DNA, Journal of Biological Chemistry, 286(51), (2011), pp. 44015–44022.

[84] W. D. McElroy, The energy source for bioluminescence in an isolated system, Proc. Natl. Acad. Sci. USA, 33(11), (1947), pp. 342–345.

[85] P. McKinney, Brain tumours: incidence, survival, and aetiology, Journal of Neurology, Neurosurgery & Psychiatry, 75(suppl 2), (2004), pp. ii12–ii17.

[86] C. M. McPherson, M. Gerena-Lewis, J. C. Breneman, R. E. Warnick, Results of phase I study of a multi-modality treatment for newly diagnosed glioblastoma multiforme using local implantation of concurrent

BCNU wafers and permanent I-125 seeds followed by fractionated radiation and temozolomide chemotherapy, Journal of neuro-oncology, 108(3), (2012), pp. 521–525.

[87] S. Meiboom, D. Gill, Modified spin-echo method for measuring nuclear relaxation times, Review of scientific instruments, 29(8), (1958), pp. 688–691.

[88] E. Meuillet, Novel inhibitors of AKT: assessment of a different approach targeting the pleckstrin homology domain, Current medicinal chemistry, 18(18), (2011), p. 2727.

[89] J. P. Mpindi, H. Sara, S. Haapa-Paananen, S. Kilpinen, T. Pisto, E. Bucher, K. Ojala, K. Iljin, P. Vainio, M. Björkman, et al., GTI: a novel algorithm for identifying outlier gene expression profiles from integrated microarray datasets, PloS one, 6(2), (2011), p. e17259.

[90] M. M. Mrugala, Advances and challenges in the treatment of glioblastoma: a clinicianâĂŹs perspective, Discovery medicine, 15(83), (2013), pp. 221–230.

[91] P. Newsholme, J. Procopio, M. M. R. Lima, T. C. Pithon-Curi, R. Curi, Glutamine and glutamateâĂŤtheir central role in cell metabolism and function, Cell biochemistry and function, 21(1), (2003), pp. 1–9.

[92] T. Nolan, R. E. Hands, S. A. Bustin, Quantification of mRNA using real-time RT-PCR, Nature protocols, 1(3), (2006), pp. 1559–1582.

[93] H. Ohgaki, P. Kleihues, Epidemiology and etiology of gliomas, Acta Neuropathologica, 109(1), (2005), pp. 93–108.

[94] H. Ohgaki, P. Kleihues, Genetic pathways to primary and secondary glioblastoma, The American journal of pathology, 170(5), (2007), pp. 1445–1453.

[95] O. Olivares, J. H. M. Daebritz, A. King, E. Gottlieb, C. Halsey, Research into cancer metabolomics: Towards a clinical metamorphosis, in: Seminars in Cell & Developmental Biology, vol. 43, Elsevier, 2015, pp. 52–64.

[96] U. Ozer, K. W. Barbour, S. A. Clinton, F. G. Berger, Oxidative Stress and Response to Thymidylate Synthase-Targeted Antimetabolites, Molecular pharmacology, 88(6), (2015), pp. 970–981.

[97] P. Palma, G. Famiglini, H. Trufelli, E. Pierini, V. Termopoli, A. Cappiello, Electron ionization in LC-MS: recent developments and applications of the direct-EI LC-MS interface, Analytical and bioanalytical chemistry, 399(8), (2011), pp. 2683–2693.

[98] D. W. Parsons, S. Jones, X. Zhang, J. C.-H. Lin, R. J. Leary, P. Angenendt, P. Mankoo, H. Carter, I.-M. Siu, G. L. Gallia, et al., An integrated genomic analysis of human glioblastoma multiforme, Science, 321(5897), (2008), pp. 1807–1812.

[99] K. K. Pasikanti, P. Ho, E. Chan, Gas chromatography/mass spectrometry in metabolic profiling of biological fluids, Journal of Chromatography B, 871(2), (2008), pp. 202–211.

[100] A. Pastore, G. Federici, E. Bertini, F. Piemonte, Analysis of glutathione: implication in redox and detoxification, Clinica chimica acta, 333(1), (2003), pp. 19–39.

[101] S. Patel, S. Ahmed, Emerging field of metabolomics: big promise for cancer biomarker identification and drug discovery, Journal of pharmaceutical and biomedical analysis, 107, (2015), pp. 63–74.

[102] J. M. Peregrín-Alvarez, C. Sanford, J. Parkinson, The conservation and evolutionary modularity of metabolism, Genome biol, 10(6), (2009), p. R63.

[103] K. Petrecca, M.-C. Guiot, V. Panet-Raymond, L. Souhami, Failure pattern following complete resection plus radiotherapy and temozolomide is at the resection margin in patients with glioblastoma, Journal of neuro-oncology, 111(1), (2013), pp. 19–23.

[104] M. M. Phillips, M. T. Sheaff, P. W. Szlosarek, Targeting arginine-dependent cancers with arginine-degrading enzymes: opportunities and challenges, Cancer Research and Treatment, 45(4), (2013), pp. 251–262.

[105] F. Pontén, J. M. Schwenk, A. Asplund, P.-H. Edqvist, The Human Protein Atlas as a proteomic resource for biomarker discovery, Journal of internal medicine, 270(5), (2011), pp. 428–446.

[106] R. Possemato, K. M. Marks, Y. D. Shaul, M. E. Pacold, D. Kim, K. Birsoy, S. Sethumadhavan, H.-K. Woo, H. G. Jang, A. K. Jha, et al., Functional genomics reveal that the serine synthesis pathway is essential in breast cancer, Nature, 476(7360), (2011), pp. 346–350.

[107] N. Psychogios, D. D. Hau, J. Peng, A. C. Guo, R. Mandal, S. Bouatra, I. Sinelnikov, R. Krishnamurthy, R. Eisner, B. Gautam, et al., The human serum metabolome, PloS one, 6(2), (2011), p. e16957.

[108] K. Raina, K. Ravichandran, S. Rajamanickam, K. M. Huber, N. J. Serkova, R. Agarwal, Inositol hexaphosphate inhibits tumor growth, vascularity, and metabolism in TRAMP mice: a multiparametric magnetic resonance study, Cancer Prevention Research, 6(1), (2013), pp. 40–50.

[109] D. Reardon, J. Herndon, K. Peters, A. Desjardins, A. Coan, E. Lou, A. Sumrall, S. Turner, E. Lipp, S. Sathornsumetee, et al., Bevacizumab continuation beyond initial bevacizumab progression among recurrent glioblastoma patients, British journal of cancer, 107(9), (2012), pp. 1481–1487.

[110] D. Ricard, A. Idbaih, F. Ducray, M. Lahutte, K. Hoang-Xuan, J.-Y. Delattre, Primary brain tumours in adults, The Lancet, 379(9830), (2012), pp. 1984–1996.

[111] C. Riccardi, I. Nicoletti, Analysis of apoptosis by propidium iodide staining and flow cytometry, Nature protocols, 1(3), (2006), pp. 1458–1461.

[112] N. G. Richards, M. S. Kilberg, Asparagine synthetase chemotherapy, Annual review of biochemistry, 75, (2006), p. 629.

[113] R. N. Rodionov, N. Jarzebska, N. Weiss, S. R. Lentz, AGXT2: a promiscuous aminotransferase, Trends in pharmacological sciences, 35(11), (2014), pp. 575–582.

[114] C. M. Rubingh, S. Bijlsma, E. P. Derks, I. Bobeldijk, E. R. Verheij, S. Kochhar, A. K. Smilde, Assessing the performance of statistical validation tools for megavariate metabolomics data, Metabolomics, 2(2), (2006), pp. 53–61.

[115] C. Sakai, E. Tomitsuka, H. Esumi, S. Harada, K. Kita, Mitochondrial fumarate reductase as a target of chemotherapy: from parasites to cancer cells, Biochimica et Biophysica Acta (BBA)-General Subjects, 1820(5), (2012), pp. 643–651.

[116] J. H. Sampson, Alternating Electric Fields for the Treatment of Glioblastoma, JAMA, 314(23), (2015), pp. 2511–2513.

[117] A. Scalbert, L. Brennan, O. Fiehn, T. Hankemeier, B. S. Kristal, B. van Ommen, E. Pujos-Guillot, E. Verheij, D. Wishart, S. Wopereis, Mass-spectrometry-based metabolomics: limitations and recommendations for future progress with particular focus on nutrition research, Metabolomics, 5(4), (2009), pp. 435–458.

[118] C. Schummer, O. Delhomme, B. M. Appenzeller, R. Wennig, M. Millet, Comparison of MTBSTFA and BSTFA in derivatization reactions of polar compounds prior to GC/MS analysis, Talanta, 77(4), (2009), pp. 1473–1482.

[119] K. Schwartz, H. T. Chang, M. Nikolai, J. Pernicone, S. Rhee, K. Olson, P. C. Kurniali, N. G. Hord, M. Noel, Treatment of glioma patients with ketogenic diets: report of two cases treated with an IRB-approved energy-restricted ketogenic diet protocol and review of the literature, Cancer Metab, 3(3.10), (2015), p. 1186.

[120] J. A. Schwartzbaum, J. L. Fisher, K. D. Aldape, M. Wrensch, Epidemiology and molecular pathology of glioma, Nature clinical practice Neurology, 2(9), (2006), pp. 494–503.

[121] E. P. Seidlitz, M. K. Sharma, Z. Saikali, M. Ghert, G. Singh, Cancer cell lines release glutamate into the extracellular environment, Clinical & experimental metastasis, 26(7), (2009), pp. 781–787.

[122] L.-J. Shen, K. Beloussow, W.-C. Shen, Modulation of arginine

metabolic pathways as the potential anti-tumor mechanism of recombinant arginine deiminase, Cancer letters, 231(1), (2006), pp. 30–35.

[123] C. M. Smith, J. R. Williamson, Inhibition of citrate synthase by succinyl-CoA and other metabolites, FEBS letters, 18(1), (1971), pp. 35–38.

[124] R. Stupp, M. E. Hegi, W. P. Mason, M. J. van den Bent, M. J. Taphoorn, R. C. Janzer, S. K. Ludwin, A. Allgeier, B. Fisher, K. Belanger, et al., Effects of radiotherapy with concomitant and adjuvant temozolomide versus radiotherapy alone on survival in glioblastoma in a randomised phase III study: 5-year analysis of the EORTC-NCIC trial, The lancet oncology, 10(5), (2009), pp. 459–466.

[125] R. Stupp, E. T. Wong, A. A. Kanner, D. Steinberg, H. Engelhard, V. Heidecke, E. D. Kirson, S. Taillibert, F. Liebermann, V. Dbalỳ, et al., NovoTTF-100A versus physicianâĂŹs choice chemotherapy in recurrent glioblastoma: a randomised phase III trial of a novel treatment modality, European journal of cancer, 48(14), (2012), pp. 2192–2202.

[126] N. Syed, J. Langer, K. Janczar, P. Singh, C. L. Nigro, L. Lattanzio, H. Coley, E. Hatzimichael, J. Bomalaski, P. Szlosarek, et al., Epigenetic status of argininosuccinate synthetase and argininosuccinate lyase modulates autophagy and cell death in glioblastoma, Cell death & disease, 4(1), (2013), p. e458.

[127] B. D. Sykes, et al., Urine stability for metabolomic studies: effects of preparation and storage, Metabolomics, 3(1), (2007), pp. 19–27.

[128] P. W. Szlosarek, Arginine deprivation and autophagic cell death in cancer, Proceedings of the National Academy of Sciences, 111(39), (2014), pp. 14015–14016.

[129] P. W. Szlosarek, J. F. Spicer, T. Szyszko, G. J. Cook, P. Y. Chan, M. Hategan, D. Repana, J. P. Steele, P. Schmid, M. Diaz, et al., Phase I study of ADI-PEG 20 in combination with pemetrexed and cisplatin (TRAP) in patients with ASS1-deficient mesothelioma and non-squamous lung cancer., in: ASCO Annual Meeting Proceedings, vol. 33, 2015, p. TPS2612.

[130] X. Tang, M. M. Keenan, J. Wu, C.-A. Lin, L. Dubois, J. W. Thompson, S. J. Freedland, S. K. Murphy, J.-T. Chi, Comprehensive profiling of amino Acid response uncovers unique methionine-deprived response dependent on intact creatine biosynthesis, PLoS Genet, 11(4), (2015), p. e1005158.

[131] K. Tantivejkul, I. Vucenik, J. Eiseman, A. M. Shamsuddin, Inositol hexaphosphate (IP6) enhances the anti-proliferative effects of adriamycin and tamoxifen in breast cancer, Breast cancer research and treatment, 79(3), (2003), pp. 301–312.

[132] P. J. Taylor, Matrix effects: the Achilles heel of quantitative high-performance liquid chromatography–electrospray–tandem mass spectrometry, Clinical biochemistry, 38(4), (2005), pp. 328–334.

[133] N. Touroutoglou, R. Pazdur, Thymidylate synthase inhibitors., Clinical cancer research, 2(2), (1996), pp. 227–243.

[134] C.-L. Tso, W. A. Freije, A. Day, Z. Chen, B. Merriman, A. Perlina, Y. Lee, E. Q. Dia, K. Yoshimoto, P. S. Mischel, et al., Distinct transcription profiles of primary and secondary glioblastoma subgroups, Cancer research, 66(1), (2006), pp. 159–167.

[135] S. Turcan, D. Rohle, A. Goenka, L. A. Walsh, F. Fang, E. Yilmaz, C. Campos, A. W. Fabius, C. Lu, P. S. Ward, et al., IDH1 mutation is sufficient to establish the glioma hypermethylator phenotype, Nature, 483(7390), (2012), pp. 479–483.

[136] M. G. Vander Heiden, Targeting cancer metabolism: a therapeutic window opens, Nature reviews Drug discovery, 10(9), (2011), pp. 671–684.

[137] M. G. Vander Heiden, L. C. Cantley, C. B. Thompson, Understanding the Warburg effect: the metabolic requirements of cell proliferation, science, 324(5930), (2009), pp. 1029–1033.

[138] S. Varrone, E. Consiglio, I. Covelli, The nature of inhibition of mitochondrial malate dehydrogenase by thyroxine, iodine cyanide and molecular iodine, European Journal of Biochemistry, 13(2), (1970), pp. 305–312.

[139] V. Vichai, K. Kirtikara, Sulforhodamine B colorimetric assay for cytotoxicity screening, Nature protocols, 1(3), (2006), pp. 1112–1116.

[140] I. Vucenik, A. M. Shamsuddin, Cancer inhibition by inositol hexaphosphate (IP6) and inositol: from laboratory to clinic, The Journal of nutrition, 133(11), (2003), pp. 3778S–3784S.

[141] A. Wagner, Energy constraints on the evolution of gene expression, Molecular biology and evolution, 22(6), (2005), pp. 1365–1374.

[142] T. Wallimann, M. Tokarska-Schlattner, U. Schlattner, The creatine kinase system and pleiotropic effects of creatine, Amino acids, 40(5), (2011), pp. 1271–1296.

[143] T. Wallimann, M. Wyss, D. Brdiczka, K. Nicolay, H. Eppenberger, Intracellular compartmentation, structure and function of creatine kinase isoenzymes in tissues with high and fluctuating energy demands: the'phosphocreatine circuit'for cellular energy homeostasis., Biochemical Journal, 281(Pt 1), (1992), p. 21.

[144] O. Warburg, On respiratory impairment in cancer cells., Science (New York, NY), 124(3215), (1956), pp. 269–270.

[145] C. Wibom, I. Surowiec, L. Mörén, P. BergstroÌĹm, M. Johansson, H. Antti, A. T. Bergenheim, Metabolomic patterns in glioblastoma and changes during radiotherapy: a clinical microdialysis study, Journal of proteome research, 9(6), (2010), pp. 2909–2919.

[146] S. Wiklund, E. Johansson, L. Sjoestroem, E. J. Mellerowicz, U. Edlund, J. P. Shockcor, J. Gottfries, T. Moritz, J. Trygg, Visualization of GC/TOF-MS-based metabolomics data for identification of biochemically interesting compounds using OPLS class models, Analytical chemistry, 80(1), (2008), pp. 115–122.

[147] I. D. Wilson, R. Plumb, J. Granger, H. Major, R. Williams, E. M. Lenz, HPLC-MS-based methods for the study of metabonomics, Journal of Chromatography B, 817(1), (2005), pp. 67–76.

[148] D. R. Wise, C. B. Thompson, Glutamine addiction: a new therapeutic target in cancer, Trends in biochemical sciences, 35(8), (2010), pp. 427–433.

[149] L. Wojtczak, A. Wojtczak, L. Ernster, The inhibition of succinate dehydrogenase by oxaloacetate, Biochimica et Biophysica Acta (BBA)-Enzymology, 191(1), (1969), pp. 10–21.

[150] S. Wold, K. Esbensen, P. Geladi, Principal component analysis, Chemometrics and intelligent laboratory systems, 2(1-3), (1987), pp. 37–52.

[151] S. Wold, M. Sjöström, L. Eriksson, PLS-regression: a basic tool of chemometrics, Chemometrics and intelligent laboratory systems, 58(2), (2001), pp. 109–130.

[152] A. Wolf, S. Agnihotri, A. Guha, Targeting metabolic remodeling in glioblastoma multiforme, Oncotarget, 1(7), (2010), p. 567.

[153] B. Worley, R. Powers, Multivariate analysis in metabolomics, Current Metabolomics, 1(1), (2013), p. 92.

[154] J. F. Xiao, B. Zhou, H. W. Ressom, Metabolite identification and quantitation in LC-MS/MS-based metabolomics, TrAC Trends in Analytical Chemistry, 32, (2012), pp. 1–14.

[155] H. Yamamoto, H. Yamaji, Y. Abe, K. Harada, D. Waluyo, E. Fukusaki, A. Kondo, H. Ohno, H. Fukuda, Dimensionality reduction for metabolome data using PCA, PLS, OPLS, and RFDA with differential penalties to latent variables, Chemometrics and Intelligent Laboratory Systems, 98(2), (2009), pp. 136–142.

[156] H. Yan, D. W. Parsons, G. Jin, R. McLendon, B. A. Rasheed, W. Yuan, I. Kos, I. Batinic-Haberle, S. Jones, G. J. Riggins, et al., IDH1 and IDH2 mutations in gliomas, New England Journal of Medicine, 360(8), (2009), pp. 765–773.

[157] M. Yang, T. Soga, P. J. Pollard, Oncometabolites: linking altered metabolism with cancer, The Journal of clinical investigation, 123(9), (2013), pp. 3652–3658.

[158] T. Yang, S. Lu, Y. Chao, I. Sheen, C. Lin, T. Wang, S. Chen, J. Wang, L. Liao, J. Thomson, et al., A randomised phase II study of pegylated arginine deiminase (ADI-PEG 20) in Asian advanced hepatocellular

carcinoma patients, British journal of cancer, 103(7), (2010), pp. 954–960.

[159] Z.-C. Ye, H. Sontheimer, Glioma cells release excitotoxic concentrations of glutamate, Cancer research, 59(17), (1999), pp. 4383–4391.

[160] J. Zhou, K.-B. Atsina, B. T. Himes, G. W. Strohbehn, W. M. Saltzman, Novel delivery strategies for glioblastoma, Cancer journal (Sudbury, Mass.), 18(1).

A. Appendix

A.1. Appendix to section 2.2: Data set for GC/TOF MS analysis

Table A.1.: Raw data of GC/TOF MS: media. Showing analyte identification, mass, retention time (RT), and averaged integral ($n = 3$) of astrocytes (A), SNB19 (S) and U87 (U) GBM samples (t for ADI-PEG20 treated at 1μg/ml) harvested at 48 hours and quality control (QC). Cut-off criteria of co-efficient variant (CV) below 30%.

Analyte	Mass	RT	At	A	S	St	U	Ut	QC	CV
Benzoic acid, 4-isopropyl-, ethyl ester	177	792.5	2.46	1.33	0.26	0.82	0.48	0.45	0.57	0.36
Analyte 293	97	766.9	6.72	3.61	0.67	2.16	1.28	1.17	1.49	1.04
Benzoic acid, 3,5-bis(1,1-dimethylethyl)-4-hydroxy-, methyl ester	249	978.35	14.56	7.77	1.79	5.69	3.35	3.16	3.84	1.07
Silanamine, 1,1,1-trimethyl-N-(trimethylsilyl)-N-[2-[(trimethylsilyl)oxy]ethyl]-	174	428.85	58.37	32.98	8.84	22.53	10.18	8.49	13.81	1.39
Analyte 525	247	1226.45	19.98	9.97	2.37	7.45	4.46	4.10	5.06	1.43
Trimethyl[4-(1,1,3,3,-tetramethylbutyl)phenoxy]silane	207	716.7	8.16	4.45	0.88	2.85	1.63	1.49	1.94	1.54
Analyte 203	99	501.1	3.27	2.06	0.52	1.22	0.75	0.76	0.75	1.66
Unknown 75	264	890	0.65	0.36	0.07	0.22	0.14	0.13	0.15	1.84
Unknown 11	71	225.95	36.36	20.06	4.33	13.24	8.37	7.14	9.45	1.97
Pentasiloxane, dodecamethyl-:2	281	444.45	0.83	0.51	0.10	0.32	0.17	0.17	0.19	2.00
Silanamine, N-methoxy-1,1,1-trimethyl-N-(trimethylsilyl)-:2	116	221.4	1194.03	607.97	173.56	517.40	326.18	235.22	379.09	2.38
Analyte 187	188	448.75	0.47	0.29	0.07	0.20	0.09	0.08	0.12	2.50

Ronnel	287	851.8	0.62	0.32	0.06	0.21	0.12	0.10	0.15	2.61
Butanoic acid, 4-[bis(trimethylsilyl)amino]-, trimethylsilyl ester	174	391.45	0.62	0.39	0.06	0.24	0.14	0.12	0.15	2.76
Z-1,6-Tridecadiene	68	377.5	6.27	3.62	0.74	2.42	1.45	1.25	1.57	2.80
Analyte 309	235	797.8	0.79	0.40	0.08	0.25	0.15	0.13	0.17	3.01
Trifluoromethyl-bis-(trimethylsilyl)methyl ketone	187	225.7	2.96	1.64	0.35	1.01	0.67	0.56	0.75	3.05
2-Desoxy-pentos-3-ulose, bis(methoxime),O,O'-bis(trimethylsilyl)-:2	231	830.6	1.40	0.47	0.45	1.47	0.77	0.76	0.71	3.07
Trisiloxane, octamethyl-	221	195.55	3750.91	2123.58	464.68	1452.55	846.55	774.08	984.88	3.11
2-Desoxy-pentos-3-ulose, bis(methoxime),O,O'-bis(trimethylsilyl)-	231	809.75	7.80	2.54	1.80	5.93	3.12	3.11	3.13	3.36
Ethylbis(trimethylsilyl)amine	174	231.7	5549.49	3155.40	710.34	2105.50	1295.03	1096.84	1486.48	3.46
Analyte 43	237	229.1	2.05	1.21	0.25	0.76	0.47	0.42	0.54	3.59
L-Threonic acid, tris(trimethylsilyl) ether, trimethylsilyl ester	292	672.5	4.22	2.07	0.44	1.41	0.69	0.95	0.88	3.64
Ribitol, 1,2,3,4,5-pentakis-O-(trimethylsilyl)-:18	174	1068	0.75	0.42	0.26	0.49	0.42	0.33	0.55	3.96
Analyte 241	77	625.4	183.08	127.71	8.76	31.35	24.67	16.53	28.24	4.11
Ribitol, 1,2,3,4,5-pentakis-O-(trimethylsilyl)-:35	446	1217.25	11.53	3.30	0.72	1.62	1.23	0.89	2.97	4.11

Unknown 46	104	579.35	8.82	4.20	0.45	1.70	1.04	0.80	1.26	4.24
3,6,9,12-Tetraoxa-2,13-disilatetradecane, 2,2,13,13-tetramethyl-	117	618.8	4.02	2.13	0.36	1.44	0.64	0.57	0.78	4.36
L-Asparagine, N,N2-bis(trimethylsilyl)-, trimethylsilyl ester	116	737.25	75.99	9.29	0.03	0.15	0.02	0.02	1.15	4.37
2-Pyrrolidone-5-carboxylic acid, trimethylsilyl ester:3	174	633.3	7.93	1.93	2.12	9.51	2.66	1.91	3.20	4.41
Analyte 24	86	210.35	36.51	20.99	4.38	14.10	8.77	7.36	9.76	4.49
Analyte 243	237	633.05	1.39	0.78	0.13	0.44	0.23	0.22	0.33	4.64
Disiloxane, 1,3-bis(chloromethyl)-1,1,3,3-tetramethyl-	153	205.35	376.78	221.08	44.68	138.51	85.55	76.36	95.59	4.64
Cyclohexane, 1-methyl-2-propyl-	97	227.5	49.06	28.33	5.98	18.41	11.71	9.80	12.90	4.68
Butanoic acid, 2,4-bis[(trimethylsilyl)oxy]-, trimethylsilyl ester	103	565.1	1.50	0.61	0.63	0.70	0.55	1.06	0.30	4.69
1,2-Bis(trimethylsiloxy)ethane:3	207	293.85	6.88	3.87	0.66	2.29	1.22	1.15	1.70	4.80
Unknown 124	57	1677.75	7.45	4.02	0.87	2.62	1.78	1.53	1.91	5.07
Analyte 533	290	1257.1	0.12	0.04	0.06	0.16	0.20	0.15	0.14	5.18
Analyte 31	207	218.5	5.88	3.47	0.71	2.23	1.25	1.20	1.49	5.22
Butanoic acid, trimethylsilyl ester	145	192	3.02	1.81	0.56	2.01	0.81	0.64	0.79	5.23
Silanamine, N,1,1,1-tetramethyl-N-(trimethylsilyl)-:3	149	198.6	17.24	10.93	1.48	7.16	4.10	3.80	4.32	5.51

Unknown 4	69	205.25	23.38	14.19	2.90	9.08	5.47	4.95	6.14	5.55
d-Glucose, 2,3,4,5,6-pentakis-O-(trimethylsilyl)-, o-methyloxyme, (1E)-	160	904.55	7.98	3.96	2.51	7.24	3.46	4.10	3.34	5.57
1,3-Cyclopentanediol, cis-	83	211.8	47.63	28.08	5.82	17.57	11.09	9.71	12.18	5.58
Ethanone, 1-(1-methylcyclohexyl)-	97	214.3	45.03	26.70	5.54	16.87	10.44	9.20	11.64	5.59
Urea, N,N'-bis(trimethylsilyl)-	171	407.7	432.06	225.48	29.50	167.40	58.26	47.26	72.30	5.79
Silane, (2-ethoxyethoxy)trimethyl-	221	305.3	1.49	1.32	0.22	0.85	0.38	0.70	0.28	5.90
Analyte 48	151	232.75	22.59	14.16	3.61	9.74	6.91	7.01	5.21	6.04
Methyltris(trimethylsiloxy)silane	207	306.75	8.12	4.51	0.70	2.12	1.26	1.31	1.68	6.09
Alanine, phenyl-, trimethylsilyl ester, dl-	120	637.1	45.79	23.81	4.37	27.00	11.57	6.34	7.95	6.21
Butanoic acid, 2-[(trimethylsilyl)amino]-, trimethylsilyl ester	130	202.65	11.97	6.22	1.40	3.75	2.72	1.97	2.98	6.29
Analyte 266	156	684.8	2.61	1.24	0.13	0.30	0.24	0.16	0.52	6.51
Ribitol, 1,2,3,4,5-pentakis-O-(trimethylsilyl)-:32	446	1205.75	7.78	2.20	0.58	1.34	1.03	0.71	2.16	6.56
Analyte 141	174	333.8	1.46	1.24	0.16	0.97	0.28	0.34	0.32	6.58
1,2-Benzenedicarboxylic acid, diisooctyl ester	149	1197.7	2.38	1.14	0.14	0.46	0.42	0.31	0.46	6.65
Cholesterol trimethylsilyl ether	129	1468.9	12.25	5.72	1.11	3.47	2.67	2.04	2.54	6.92
Unknown 113	61	1226.7	2.69	1.26	0.55	1.76	1.15	0.87	1.06	6.94

Silanamine, N-methoxy-1,1,1-trimethyl-N-(trimethylsilyl)-:4	125	227	2.31	1.21	0.28	0.82	0.49	0.48	0.59	7.21
Unknown 72	74	885.4	4.11	5.72	1.30	3.39	1.76	2.27	1.65	7.30
Analyte 21	108	206	4.31	2.18	0.46	1.42	0.91	0.78	1.05	7.44
Analyte 151	232	353.55	0.48	0.29	0.18	0.53	0.39	0.21	0.25	7.59
l-Aspartic acid, bis(trimethylsilyl) ester:2	160	556.95	3.78	0.70	0.05	0.31	0.14	0.07	0.48	7.76
Cinnamic acid, m-(trimethylsiloxy)-, methyl ester	250	1199.75	1.11	0.64	0.05	0.12	0.08	0.27	0.25	7.97
Ribitol, 1,2,3,4,5-pentakis-O-(trimethylsilyl)-:7	117	846.65	9.64	4.40	0.71	2.44	1.32	1.13	1.53	7.99
2-Hexenal	55	253.5	148.53	90.10	18.44	54.91	35.02	30.08	36.65	8.20
4-Methyl-2-pentanol, trimethylsilyl ether	158	211.6	3.56	1.99	0.47	1.18	0.82	0.70	0.96	8.24
2-Isopropyl-3-ketobutyrate, bis(O-trimethylsilyl)-	273	578.5	1.39	0.64	0.10	0.20	0.15	0.19	0.09	8.36
Malonic acid, bis(2-trimethylsilylethyl ester	204	247.2	2.48	1.33	0.23	0.75	0.48	0.42	0.58	8.41
2-Pyrrolidone-5-carboxylic acid, trimethylsilyl ester:2	184	588.9	2.96	1.01	0.15	0.53	0.17	0.18	0.32	8.55
Analyte 237	110	617.15	1.91	1.08	0.32	0.94	0.53	0.55	0.61	8.55
Ribitol, 1,2,3,4,5-pentakis-O-(trimethylsilyl)-:37	132	1282.25	1.70	0.55	0.43	1.48	0.76	0.63	0.80	8.67
l-Cysteine, trimethylsilyl ester	194	1043.15	1.06	0.48	0.02	0.23	0.20	0.38	0.59	8.79
1,2-Bis(trimethylsiloxy)ethane	191	213.6	3.17	1.87	0.41	1.21	0.71	0.65	0.88	8.82

Acetic acid, [(trimethylsilyl)oxy]-, trimethylsilyl ester	177	299.95	1.51	0.71	0.23	0.57	0.27	0.48	0.29	8.86
Ribitol, 1,2,3,4,5-pentakis-O-(trimethylsilyl)-:38	132	1293.95	5.40	1.59	0.54	2.21	0.96	1.82	2.82	8.90
Ribitol, 1,2,3,4,5-pentakis-O-(trimethylsilyl)-:20	84	1101	8.52	2.93	1.98	7.72	3.90	2.91	4.44	8.91
Ribitol, 1,2,3,4,5-pentakis-O-(trimethylsilyl)-:40	179	1400.9	0.47	0.14	0.35	1.38	0.69	0.69	0.79	8.93
D-Fructose, 1,3,4,5,6-pentakis-O-(trimethylsilyl)-, O-methyloxime:3	217	895.2	350.92	170.02	53.65	196.39	82.52	84.60	89.39	8.98
Analyte 110	158	291.35	3.20	1.52	0.39	0.92	0.70	0.58	0.82	9.02
Silanamine, 1,1,1-trimethyl-N-(trimethylsilyl)-	146	358.8	1.19	0.69	0.10	0.26	1.02	0.15	0.26	9.02
Trimethylsilyl 3-pyridinecarboximidoate #	179	579.1	23.37	11.75	1.29	4.98	2.63	2.13	3.62	9.12
Analyte 102	97	281.1	1.70	1.02	0.20	0.62	0.38	0.33	0.42	9.24
4-Chlorobenzoic acid	111	235.95	11.49	5.99	1.35	3.76	2.56	2.09	2.76	9.35
Aminomalonic acid, tris(trimethylsilyl)-	218	601.6	0.45	0.22	1.14	5.27	2.70	1.76	1.21	9.44
Analyte 100	71	279.05	4.05	2.00	0.42	1.24	0.80	0.71	0.86	9.44
Analyte 491	144	1158.5	0.83	0.27	0.05	0.24	0.13	0.21	0.46	9.77
Analyte 72	69	249.3	1.84	0.87	0.21	0.69	0.39	0.36	0.47	9.80
1-Pentanol, 2-ethyl-	85	271.85	11.37	6.83	1.38	4.19	2.69	2.35	2.81	9.81
Sulfurous acid, di(cyclohexylmethyl) ester	97	272.7	7.62	4.47	0.92	2.79	1.77	1.54	1.89	9.89
(Z)-Bis-1,2-(trimethylsilyloxy)ethylene	204	239.45	0.45	0.15	0.04	0.07	0.07	0.08	0.26	9.90

Hept-2-ene, 2,4,4,6-tetramethyl-	97	260.15	5.95	3.77	0.71	2.19	1.37	1.18	1.46	10.07
3-Methyl-3-hexene	97	245	13.87	7.73	1.63	4.78	3.12	2.59	3.29	10.18
N-Acetyl glucosamine methoxime, tetrakis(trimethylsilyl):2	233	1296.5	1.71	0.30	0.02	0.17	0.04	0.14	0.29	10.23
1-Hexene, 4,5-dimethyl-	71	271.5	34.54	20.13	4.08	12.55	7.90	6.86	8.38	10.34
6-Amino-1-hexanol, N,o-bis(tert-butyldimethylsilyl)-	288	1172.4	0.33	0.20	1.20	2.38	1.96	1.18	0.43	10.35
d-Galactose, 2,3,4,5,6-pentakis-O-(trimethylsilyl)-, o-methyloxyme, (1E)-	319	912.5	1506.14	762.32	369.08	1333.54	725.66	557.34	705.26	10.47
Analyte 63	153	242	2.49	0.77	0.03	0.13	0.06	0.03	0.22	10.71
L-Norleucine, N-(trimethylsilyl)-, trimethylsilyl ester	202	665.4	0.96	7.06	1.13	8.46	2.39	4.15	2.40	10.74
Analyte 89	71	267.7	2.12	1.32	0.22	0.76	0.44	0.41	0.50	10.85
2,3,4-Trihydroxybutyric acid tetrakis(trimethylsilyl) deriv.	292	682.65	0.91	0.41	0.04	0.15	0.07	0.08	0.12	10.86
Pantothenic acid tritms	201	941.45	11.97	5.23	0.33	1.35	0.67	0.59	1.46	10.98
Cyclooctane, (1-methylpropyl)-	111	270.65	5.77	3.44	0.70	2.11	1.34	1.17	1.42	10.99

N,N-Diethyl-1,1,1-trimethylsilylamine	158	227.25	32.70	12.27	3.44	6.86	6.03	4.08	8.14	11.06
Ribitol, 1,2,3,4,5-pentakis-O-(trimethylsilyl)-:21	160	1125.4	0.90	0.44	0.11	0.47	0.23	0.54	0.95	11.07
Metoprolol di-TMS derivative	144	282.3	11.89	3.97	1.14	2.09	2.09	1.29	2.65	11.10
Diisoamylene	188	275.4	1.00	0.66	0.11	0.49	0.22	0.20	0.23	11.19
2-Buten-1-one, 1-(6,7,7-trimethyl-2,3-dioxabicyclo[2.2.2]oct-5-en-1-yl)-, [1R-[1Ãă(E),4Ãą]]-	125	259.65	1.43	0.83	0.16	0.52	0.33	0.29	0.35	11.21
d-Galactose, 2,3,4,5,6-pentakis-O-(trimethylsilyl)-, o-methyloxyme, (1Z)-	319	940.05	5.74	2.58	0.49	2.03	1.02	0.82	1.14	11.47
Analyte 81	162	257.45	1.13	0.49	0.13	0.48	0.27	0.20	0.30	11.49
Serine, bis(trimethylsilyl)-	116	435	72.86	46.24	8.67	27.10	17.10	11.84	17.91	11.54
[1,3]Dioxepino[5,6-c]pyridine, 1,5-dihydro-8-methyl-3-(1-methylethyl)-9-(2-propynyloxy)-	187	232	6.73	3.97	0.92	2.92	1.95	1.37	1.68	11.59
L-Norvaline, N-(trimethylsilyl)-, trimethylsilyl ester	144	234.8	4209.66	1479.13	441.32	820.81	805.23	501.68	995.03	11.66
Analyte 70	70	247.55	2.65	1.40	0.32	1.02	0.62	0.54	0.67	11.67

Pyrimidine, 2,4-bis[(trimethylsilyl)oxy]-	241	492.55	1.13	0.54	0.13	0.49	0.19	0.16	0.25	11.76
Cyclopentane, 2-isopropyl-1,3-dimethyl-	97	237.95	22.40	12.70	2.69	8.05	5.13	4.44	5.35	11.88
Propanoic acid, 2-[(trimethylsilyl)oxy]-, trimethylsilyl ester	117	293.25	5147.81	3060.69	1096.50	4650.52	2308.73	1845.85	1573.53	11.89
Ribitol, 1,2,3,4,5-pentakis-O-(trimethylsilyl)-:10	307	875.05	0.28	0.27	0.12	0.50	0.22	0.29	0.16	11.94
3-Ethyl-4-octene	85	260.55	3.45	2.05	0.41	1.26	0.79	0.70	0.83	12.03
L-Valine, N-(trimethylsilyl)-, trimethylsilyl ester:2	188	611.8	1.57	9.75	1.41	7.89	2.97	3.72	3.40	12.06
Analyte 489	418	1154.05	1.11	0.51	0.69	1.83	1.51	1.42	0.93	12.08
Ethanol, 2-methoxy-, acetate	58	240	13.62	8.02	1.53	3.03	1.76	2.15	2.49	12.15
Trimethylsilyl ether of glycerol	205	464.4	69.00	51.41	6.23	184.09	13.92	11.72	13.88	12.21
Analyte 68	137	246.55	1.24	0.71	0.15	0.44	0.29	0.24	0.30	12.27
Analyte 538	436	1263.15	0.23	0.07	0.12	0.31	0.25	0.23	0.15	12.29
Analyte 79	125	256.3	1.17	0.67	0.14	0.42	0.27	0.23	0.28	12.32

Pyridine, 2-methyl-3-(trimethylsilyloxy)-4,5-bis-[(trimethylsilyloxy)methyl]-	280	885.1	6.83	3.15	1.17	4.17	2.30	1.93	2.07	12.44
Analyte 80	160	256.6	1.29	0.78	0.17	0.51	0.30	0.26	0.33	12.45
Unknown 33	50	294.15	15.45	8.69	4.81	17.10	16.83	8.27	3.94	12.45
Analyte 55	237	236.45	5.94	3.32	0.73	2.11	1.32	1.19	1.43	12.66
Myo-Inositol, 1,2,3,4,5,6-hexakis-O-(trimethylsilyl)-	318	918.85	1.89	0.94	0.19	0.63	0.37	0.30	0.47	12.72
Analyte 87	70	264.3	3.03	1.75	0.36	1.13	0.68	0.60	0.75	12.76
1-Decene, 5-methyl-	111	258.45	11.67	6.98	1.46	4.23	2.77	2.31	2.90	12.77
I-Trimethylsiloxy-2-trimethylsilylaminoethane	190	240.6	2.67	1.03	0.33	0.62	0.57	0.37	0.70	12.82
Ribitol, 1,2,3,4,5-pentakis-O-(trimethylsilyl)-:22	205	1128.1	0.91	0.40	0.56	2.20	1.09	0.80	0.95	12.93
Ribitol, 1,2,3,4,5-pentakis-O-(trimethylsilyl)-:25	158	1165.45	0.05	0.02	0.16	0.54	0.25	0.20	0.10	12.98
Ribitol, 1,2,3,4,5-pentakis-O-(trimethylsilyl)-:39	205	1389.3	0.23	0.07	0.41	1.42	0.67	0.51	0.41	13.06
Cyclopropane, 3-chloro-1,1,2,2-tetramethyl-	97	269.2	10.69	6.25	1.33	3.98	2.53	2.23	2.61	13.08

Butanoic acid, 3-[(trimethylsilyl)oxy]-, trimethylsilyl ester	117	365.35	8.59	4.04	0.76	2.76	1.44	1.18	1.56	13.18
DL-Malic acid, O-trimethylsilyl-, bis(trimethylsilyl) ester	233	618	2.19	1.05	0.15	0.62	0.25	0.19	0.34	13.32
L-Proline, 5-oxo-1-(trimethylsilyl)-, trimethylsilyl ester	156	625.25	8705.99	5001.66	404.26	1446.60	820.64	658.70	1363.89	13.39
Glycine, N-benzoyl-, trimethylsilyl ester	105	818.8	7.43	3.06	0.37	1.83	0.91	0.59	1.15	13.41
Analyte 88	156	264.95	0.81	0.39	0.08	0.24	0.18	0.14	0.22	13.54
Analyte 207	224	508.55	0.52	0.20	0.01	0.07	0.02	0.02	0.10	13.58
Glycine, N-(trimethylsilyl)-, trimethylsilyl ester	102	332.65	14.49	5.18	1.81	5.06	3.52	2.57	5.46	13.66
l-Methionine, trimethylsilyl ester	104	537.2	13.90	9.31	2.82	10.28	5.36	3.82	5.11	13.76
D-Gluconic acid, 2,3,4,5,6-pentakis-O-(trimethylsilyl)-, trimethylsilyl ester	333	976.8	0.30	0.14	0.08	0.24	0.16	0.17	0.12	13.78
l-Leucine, trimethylsilyl ester	86	354.15	259.04	132.69	26.30	96.94	58.92	40.53	60.88	13.85
L-Proline, 1-(trimethylsilyl)-4-[(trimethylsilyl)oxy]-, trimethylsilyl ester, trans-	230	649.25	72.27	34.95	5.30	20.42	10.23	8.40	12.48	13.90

Myo-Inositol, 1,2,3,4,5,6-hexakis-O-(trimethylsilyl)-:2	217	1026.2	273.83	118.09	21.87	76.56	44.98	35.49	53.19	13.90
D-Turanose, heptakis(trimethylsilyl)-	361	1349.05	0.10	0.17	0.28	1.78	0.63	0.57	0.44	14.00
Inosine, tetrakis(trimethylsilyl) ether	230	1231.65	49.84	15.92	0.14	0.22	0.23	0.20	4.61	14.10
Thiosalicylic acid, S-(tert-butyldimethylsilyl)-, tert-butyldimethylsilyl ester	325	1185.5	30.73	9.36	0.09	0.48	0.21	0.39	3.03	14.12
Serine tritms	204	526.45	151.77	45.43	6.62	24.90	15.43	8.73	22.80	14.18
Hexadecanoic acid, trimethylsilyl ester	313	961.7	1.85	1.33	0.24	0.64	0.40	0.36	0.47	14.37
2-Butenedioic acid (E)-, bis(trimethylsilyl) ester	245	503.3	2.29	0.95	0.22	0.71	0.38	0.27	0.40	14.41
1,2,3-Propanetricarboxylic acid, 2-[(trimethylsilyl)oxy]-, tris(trimethylsilyl) ester	273	846.25	12.94	5.21	0.72	2.96	1.76	1.10	1.95	14.59
Butanoic acid, 4-[(tert-butyldimethylsilyl)amino]-, tert-butyldimethylsilyl ester:5	274	1154.85	1.93	0.85	0.30	0.82	0.48	0.52	0.42	14.61
Unknown 121	75	1349.7	0.92	1.95	0.75	7.36	1.78	3.14	1.87	14.63
Analyte 168	188	387.15	0.34	0.17	0.03	0.18	0.07	0.08	0.06	14.79

Butanoic acid, 4-[(trimethylsilyl)oxy]-, trimethylsilyl ester	147	419.35	3.53	2.66	0.33	1.31	0.63	0.57	0.68	14.92
Glycine, trimethylsilyl ester	132	209.9	0.76	0.49	0.09	0.22	0.22	0.15	0.45	14.94
Ribitol, 1,2,3,4,5-pentakis-O-(trimethylsilyl)-:5	217	808.25	5.41	2.15	0.43	1.62	0.99	0.83	1.02	15.14
Pentasiloxane, dodecamethyl-	281	401.6	17.77	12.17	0.62	3.13	1.23	1.17	2.67	15.40
Propanoic acid, 2,3-bis[(trimethylsilyl)oxy]-, trimethylsilyl ester	189	503.05	1.66	0.93	0.33	0.80	0.35	0.78	0.44	15.47
Analyte 534	127	1259.15	1.09	0.33	0.07	0.08	0.17	0.16	0.22	15.50
l-Cysteine, trimethylsilyl ester:2	174	1043.35	0.81	1.06	0.33	0.91	0.62	0.69	0.60	15.55
Creatinine enol N1,N3,O-tris(trimethylsilyl)	115	662.5	6.92	2.98	0.29	1.50	0.69	0.30	1.13	15.57
Silanol, trimethyl-, phosphate (3:1)	299	452.6	5.77	2.72	0.23	0.98	0.58	0.38	0.43	15.60
Benzoic acid trimethylsilyl ester	179	417.65	4.26	2.12	0.40	1.21	0.83	0.56	0.72	15.64
D-Fructose, 1,3,4,5,6-pentakis-O-(trimethylsilyl)-, O-methyloxime:4	307	900.6	89.50	46.42	14.61	57.54	22.10	22.96	24.74	15.66
Octadecanoic acid, trimethylsilyl ester	117	1066.9	14.82	11.27	2.21	6.12	3.76	3.55	3.70	15.71

2,2,4-Trimethyl-3-hexene	207	252.4	4.83	2.82	0.58	1.73	1.04	0.95	1.15	15.73
l-Threonine, O-(trimethylsilyl)-, trimethylsilyl ester	130	466.95	10.95	7.70	9.37	32.06	17.57	12.61	11.84	15.92
Analyte 557	452	1316.25	0.52	0.12	0.36	0.84	0.70	0.63	0.30	15.94
Analyte 497	418	1169.45	1.35	0.56	1.38	3.64	2.89	3.08	1.18	15.97
Inositol, 1,2,3,4,5,6-hexakis-O-(trimethylsilyl)-, scyllo-	318	991.2	2.17	0.97	0.18	0.61	0.36	0.28	0.44	15.99
Propanoic acid, 2-methyl-3-[(trimethylsilyl)oxy]-, trimethylsilyl ester	147	365.6	26.97	12.83	2.57	9.85	4.82	3.98	5.05	16.01
Glycoside, Ãă-methyl-trtrakis-O-(trimethylsilyl)-:9	204	1176.35	0.47	0.09	2.54	5.12	3.19	2.04	0.76	16.14
L-Aspartic acid, N-(trimethylsilyl)-, bis(trimethylsilyl) ester:2	232	640.6	21.28	1.94	0.23	1.00	0.54	0.36	2.68	16.19
Analyte 49	184	234.45	9.38	5.29	1.38	3.22	2.46	3.11	1.84	16.20
d-Galactose, 2,3,4,5,6-pentakis-O-(trimethylsilyl)-, o-methyloxyme, (1Z)-:2	319	943.8	89.35	40.21	7.68	29.08	16.79	13.30	18.34	16.34
Ribitol, 1,2,3,4,5-pentakis-O-(trimethylsilyl)-:17	257	1062.2	1.85	0.78	0.45	1.34	0.89	1.12	0.54	16.46

1H-Indole-2,3-dione, 1-(tert-butyldimethylsilyl)-7-(3-methylbutyl)-, 3-[O-(tert-butyldimethylsilyl)oxime]	404	1142.9	4.24	1.37	1.60	4.45	3.30	3.60	1.77	16.48
Disilathiane, hexamethyl-	163	228.45	8.91	4.16	1.57	5.72	2.20	2.70	1.24	16.48
Silanamine, N,N'-methanetetraylbis[1,1,1-trimethyl-	171	230.55	37.56	77.12	23.01	77.32	56.74	7.66	25.11	16.59
Unknown 9	159	214.45	0.84	0.34	0.45	1.86	0.26	0.32	0.23	16.82
Ribitol, 1,2,3,4,5-pentakis-O-(trimethylsilyl)-:33	287	1206.85	5.36	1.59	0.19	0.72	0.30	0.60	0.94	17.01
L-Homoserine, N,O-bis(trimethylsilyl)-, trimethylsilyl ester	218	751.8	38.89	11.16	0.46	2.40	0.43	0.23	2.97	17.05
2-Keto-d-gluconic acid, pentakis(O-trimethylsilyl)-	257	1088.65	0.48	0.26	0.32	0.88	0.65	0.80	0.28	17.14
Unknown 7	97	208	2.65	1.67	0.34	0.98	0.58	0.53	0.69	17.15
Silane, tetramethyl-	257	1075.85	0.61	0.32	0.30	0.84	0.60	0.75	0.34	17.23
Analyte 290	218	762.5	1.50	0.42	0.26	0.57	0.23	0.18	0.17	17.27
Unknown 32	84	293.4	25.99	13.12	5.07	20.62	13.21	9.28	6.57	17.29
Cyclotetrasiloxane, octamethyl-	281	254.95	3.45	1.94	0.42	1.29	0.78	0.67	0.83	17.39

Butanedioic acid, bis(trimethylsilyl) ester	247	474.5	11.15	4.91	0.89	3.31	1.72	1.33	2.00	17.66
Analyte 400	353	938.95	1.00	0.24	0.04	0.20	0.08	0.06	0.14	17.87
l-Valine, trimethylsilyl ester	72	304.6	655.36	372.38	34.91	132.77	73.46	49.29	110.31	18.00
4-Ketoglucose, bis(O-methyloxime), tetrakis(trimethylsilyl):2	84	1112	0.12	0.07	0.20	0.67	0.37	0.23	0.17	18.07
2,3,4-Trimethyl-hex-3-enal	123	251.85	2.40	1.39	0.29	0.86	0.57	0.48	0.55	18.10
Analyte 518	478	1207.7	0.06	0.02	0.61	1.90	1.14	1.14	0.17	18.36
Silanol, trimethyl-, 2-aminobenzoate	194	509.9	2.48	1.12	0.03	0.05	0.15	0.11	0.20	18.47
Analyte 77	131	254	1.58	0.92	0.24	0.55	0.36	0.28	0.38	18.51
Butanoic acid, 2-[(trimethylsilyl)oxy]-, trimethylsilyl ester	131	342.35	5.89	6.16	0.89	6.02	2.11	1.90	1.57	18.90
Analyte 61	184	240.4	1.40	0.92	0.25	0.54	0.33	0.29	0.33	19.11
Unknown 102	129	1154.35	0.83	0.30	0.19	0.92	0.41	0.45	0.45	19.34
Analyte 544	416	1281.25	0.95	0.83	0.19	0.81	0.38	1.50	0.52	19.46

Butylated Hydroxytoluene	205	616	5.32	2.37	0.48	1.85	0.77	0.67	1.00	19.63
Analyte 206	88	505.6	1.92	0.51	0.21	0.54	0.20	0.22	0.33	19.77
Tryptophan, bis(trimethylsilyl)- (mainlib)	202	1037.95	12.66	4.31	0.18	2.32	0.40	2.80	5.32	19.77
Ethanedioic acid, bis(trimethylsilyl) ester:2	147	332.2	10.34	6.87	0.59	1.55	1.15	0.82	2.43	20.50
Unknown 80	204	922.65	126.01	63.97	64.80	254.17	135.16	96.48	115.79	20.50
Trimethylsilyl ether of glycerol:2	204	561.3	0.74	0.12	0.21	0.34	0.38	0.51	0.23	20.63
Butanedioic acid, methyl-, bis(trimethylsilyl) ester	83	486.75	5.40	2.32	0.16	0.47	0.53	0.31	0.70	20.70
2-Keto-3-methylvaleric acid mo-tms pk2	89	385.95	4.02	1.27	1.84	7.96	2.05	1.64	0.96	20.70
2-Ketoisocaproic acid mo-tms	200	395.55	2.25	0.80	1.38	6.20	1.49	1.15	0.81	20.74
Ribitol, 1,2,3,4,5-pentakis-O-(trimethylsilyl)-:19	257	1085.6	1.90	0.42	0.33	0.94	0.68	0.65	0.44	20.83
2-Keto-d-gluconic acid, pentakis(O-trimethylsilyl)-:5	437	1376.35	0.12	0.02	0.05	0.13	0.09	0.09	0.05	20.89
Ribitol, 1,2,3,4,5-pentakis-O-(trimethylsilyl)-:13	361	932.05	2.88	1.24	1.23	4.41	2.51	1.81	2.11	20.95

Unknown 71	204	884.2	0.94	0.54	0.47	0.56	0.52	0.91	0.38	21.39
Maltose, octakis(trimethylsilyl)-:3	204	1327.15	0.07	0.03	0.04	62.45	0.10	0.01	2.63	21.78
N,O,O-Tris(trimethylsilyl)-L-threonine	218	549.25	20.85	7.27	9.90	42.86	22.24	12.40	21.34	22.02
Melibiose, octakis(trimethylsilyl)-	217	1334.3	0.03	0.01	0.10	7.25	0.25	0.24	0.36	22.04
N-Acetyl glucosamine methoxime, tetrakis(trimethylsilyl)	290	1288.75	0.02	0.01	0.07	0.17	0.16	0.14	0.03	22.39
1,2-Bis(trimethylsiloxy)ethane:2	147	245.45	6.36	3.40	0.81	2.07	1.66	1.42	1.65	22.43
L-Leucine, N-(trimethylsilyl)-, trimethylsilyl ester	158	456.3	665.74	234.01	41.59	182.18	95.27	54.87	113.28	22.53
Unknown 15	51	235	49.82	25.62	6.18	16.85	13.14	8.94	11.51	22.60
1-Propanol, 2-methyl-2-nitro-	89	244.15	13.26	7.25	0.88	3.44	2.84	1.81	2.71	22.67
d-Glucose, 2,3,4,5,6-pentakis-O-(trimethylsilyl)-, o-methyloxyme, (1Z)-	319	922.5	359.18	187.11	177.49	688.27	344.38	255.29	324.54	22.70
Glycine, N-formyl-N-(trimethylsilyl)-, trimethylsilyl ester:2	130	998.55	3.80	2.14	0.12	2.88	0.12	1.36	0.97	22.88
Ribitol, 1,2,3,4,5-pentakis-O-(trimethylsilyl)-:27	84	1175.8	2.60	0.47	1.05	2.43	1.94	0.97	1.43	22.97

Analyte 386	50	913	20.36	8.73	5.25	22.40	16.21	9.21	8.71	23.08
Maltose, octakis(trimethylsilyl)-:5	204	1413.5	0.17	0.09	0.12	0.48	0.30	0.20	0.17	23.41
Analyte 530	313	1242.35	2.08	0.43	0.05	0.15	0.10	0.14	0.50	23.43
Maltose, octakis(trimethylsilyl)-:4	361	1400.15	0.21	0.11	0.31	1.33	0.71	0.46	0.43	23.45
1-(2-(2-Hydroxyethoxy)ethyl)piperazine	99	477.65	4.96	3.41	0.58	2.31	0.83	0.76	1.86	23.51
N,O-Bis-(trimethylsilyl)phenylalanine	218	707.65	115.14	44.64	13.61	53.95	26.36	17.62	31.54	23.53
Ethanol, 2-(trimethylsilyl)-	167	288.4	2.28	0.55	0.03	0.18	0.03	0.02	0.19	23.61
Ribitol, 1,2,3,4,5-pentakis-O-(trimethylsilyl)-:6	217	836.8	0.87	0.34	0.69	1.12	1.69	1.36	0.35	23.72
Mannose, 6-deoxy-2,3,4,5-tetrakis-O-(trimethylsilyl)-, L-:3	204	1162.9	0.06	0.02	3.64	11.36	6.33	7.16	2.81	24.07
Propanoic acid, 2-oxo-3-(trimethylsilyl)-, trimethylsilyl ester	147	310.75	3.25	5.97	1.05	1.75	3.86	3.26	2.98	24.32
Glycoside, Ãă-methyl-trtrakis-O-(trimethylsilyl)-:13	204	1358.8	0.07	0.04	0.11	0.52	0.28	0.19	0.25	24.76
Glycoside, Ãă-methyl-trtrakis-O-(trimethylsilyl)-:7	361	1145.25	0.04	0.01	0.22	0.53	0.38	0.73	0.23	24.86

Analyte 280	214	720.25	0.62	0.16	0.02	0.08	0.20	0.07	0.13	24.95
2-Keto-d-gluconic acid, pentakis(O-trimethylsilyl)-:4	257	1270.2	0.39	0.09	0.07	0.17	0.15	0.13	0.08	25.70
Unknown 94	217	1075.2	2.55	0.75	0.74	1.94	1.40	2.68	2.01	25.90
L-Cysteine, N,S-bis(trimethylsilyl)-, trimethylsilyl ester	220	664.25	9.58	2.17	0.84	2.71	0.80	0.27	1.09	25.92
l-Isoleucine, trimethylsilyl ester	86	370.05	270.87	197.80	34.04	146.72	75.06	60.65	74.86	26.04
L-Isoleucine, N-(trimethylsilyl)-, trimethylsilyl ester	158	473.65	670.31	254.14	45.80	210.70	105.79	62.46	122.68	26.27
L-Methionine, N-(trimethylsilyl)-, trimethylsilyl ester	176	631.6	68.98	18.36	5.08	22.48	11.82	7.07	13.58	26.32
Analyte 452	298	1084.65	0.84	0.16	0.01	0.03	0.03	0.08	0.22	26.36
2-Keto-d-gluconic acid, pentakis(O-trimethylsilyl)-:3	437	1113.6	0.52	0.15	0.21	0.58	0.46	0.44	0.25	26.39
Lyxose, tetra-(trimethylsilyl)-ether:2	204	878.5	0.05	0.03	0.28	0.11	0.12	0.51	0.03	26.50
Ribitol, 1,2,3,4,5-pentakis-O-(trimethylsilyl)-:12	205	892.1	0.21	0.10	0.16	0.37	0.13	0.28	0.15	26.66
9-Octadecenamide, (Z)-	72	1296.85	4.92	1.48	0.08	0.97	0.31	0.60	0.69	26.74

Unknown 56	198	664.8	0.30	0.17	0.18	1.07	0.29	0.18	0.19	26.81
Mannose, 6-deoxy-2,3,4,5-tetrakis-O-(trimethylsilyl)-, L-	204	983.25	40.65	27.30	20.58	101.94	36.66	29.07	31.01	26.91
Ribitol, 1,2,3,4,5-pentakis-O-(trimethylsilyl)-:2	217	769.45	1.84	1.44	0.13	0.59	0.28	0.20	0.42	27.06
Analyte 173	91	403.3	2.48	1.34	0.26	0.62	0.43	0.37	0.71	27.12
Gluconic acid, Ãğ-lactone, 2-methoximine, tris(O-trimethylsilyl)-:4	350	1140.55	0.48	0.07	0.16	0.33	0.29	0.54	0.37	27.13
Pentanoic acid, 2-(methoxyimino)-3-methyl-, trimethylsilyl ester	113	371.8	1.07	0.38	0.70	3.32	0.81	0.59	0.47	27.19
Lyxose, tetra-(trimethylsilyl)-ether	204	841.6	0.12	0.04	0.09	0.08	0.13	0.15	0.05	27.38
Ribitol, 1,2,3,4,5-pentakis-O-(trimethylsilyl)-	217	644.1	12.33	2.75	0.40	0.72	0.85	0.26	1.26	27.63
Tris(trimethylsilyl)borate	221	257.75	6.26	3.22	0.76	2.46	4.27	1.06	1.25	27.65
Ribitol, 1,2,3,4,5-pentakis-O-(trimethylsilyl)-:15	220	963.05	0.16	0.10	0.10	0.41	0.18	0.14	0.15	27.71
N-Acetyl glucosamine methoxime, tetrakis(trimethylsilyl):3	204	1297.85	0.22	0.06	0.01	6.74	0.04	0.03	0.61	28.03
Analyte 409	84	956.25	1.09	0.75	2.08	4.02	3.94	5.61	2.12	28.09

Erythrose, O-methyloxime, tris-O-(trimethylsilyl)-	205	601.9	0.72	0.84	0.27	1.88	0.59	0.52	0.39	28.53
Gluconic acid, Ãğ-lactone, 2-methoximine, tris(O-trimethylsilyl)-:5	204	1167.85	1.17	0.11	1.93	3.74	2.53	1.84	1.06	28.79
N,o,o'-Tris-(trimethylsilyl)-6-hydroxy-2-aminohexanoic acid	246	1130.8	0.27	0.09	1.65	3.85	1.37	0.38	0.19	28.82
9H-Purine, 9-(trimethylsilyl)-6-[(trimethylsilyl)oxy]-	265	807.65	28.33	11.61	0.04	0.16	0.03	0.03	0.76	29.01
L-Valine, N-(trimethylsilyl)-, trimethylsilyl ester	144	413.1	1711.35	720.41	68.11	301.81	149.80	95.13	209.74	29.08
D-Fructose, 1,3,4,5,6-pentakis-O-(trimethylsilyl)-	204	865.6	88.57	23.85	18.88	27.13	23.43	32.91	19.33	29.27
Ribitol, 1,2,3,4,5-pentakis-O-(trimethylsilyl)-:8	217	854.3	27.36	20.20	11.07	15.13	13.64	23.50	6.37	29.51

Table A.2.: Raw data of GC/TOF MS: extract. Showing analyte identification, mass, retention time (RT), and averaged integral ($n = 3$) of astrocytes (A), SNB19 (S) and U87 (U) GBM samples (t for ADI-PEG20 treated at 1μg/ml) harvested at 48 hours and quality control (QC). Cut-off criteria of co-efficient variant (CV) below 30%.

Analyte	Mass	RT	A	At	S	St	U	Ut	QC	CV
Disiloxane, 1,3-diethoxy-1,1,3,3-tetramethyl-	207	218.7	2.75	5.05	0.63	2.23	1.20	1.20	1.45	1.66
1-Hexene, 3,4,5-trimethyl-	70	264.45	1.55	3.21	0.39	1.34	0.73	0.69	0.81	1.95
3-Hexadecyne	68	377.55	3.37	6.60	0.79	2.67	1.44	1.41	1.70	1.99
Ethylbis(trimethylsilyl)amine	86	231.9	1606.03	3189.75	373.50	1240.99	714.39	627.53	776.04	2.20
Sulfurous acid, di(cyclohexylmethyl) ester	97	272.85	3.94	8.40	0.98	3.31	1.85	1.71	2.02	2.45
Unknown 39	207	293.85	3.12	6.94	0.79	2.47	1.41	1.38	2.23	2.52
Unknown 114	247	1226.65	7.27	14.37	1.72	5.77	3.34	3.04	4.47	2.58
3-Penten-1-ol, 2,2,4-trimethyl-	97	269.35	5.41	11.48	1.33	4.59	2.53	2.32	2.84	2.66
2-Hexenal	83	253.65	24.81	54.14	6.30	21.80	12.08	11.09	13.15	2.70
1-Hexene, 4,5-dimethyl-	71	271.7	17.60	37.09	4.34	14.62	8.25	7.60	9.03	2.83
Unknown 15	125	227.15	1.19	2.47	0.29	0.95	0.52	0.51	0.61	2.97
Unknown 8	124	207.5	0.46	0.88	0.11	0.38	0.21	0.19	0.23	2.99
Dichloroacetic acid, 4-methylpentyl ester	84	279.15	2.47	5.10	0.58	2.02	1.11	1.01	1.15	3.18
1-Pentanol, 2-ethyl-	85	272	6.04	12.72	1.48	5.03	2.82	2.61	3.03	3.35
Unknown 28	207	252.45	2.21	4.91	0.56	2.05	1.13	1.03	1.21	3.36

Cyclohexane, 1-methyl-2-propyl-:2	96	227.75	3.89	7.64	0.91	3.09	1.75	1.55	1.79	3.42
Disiloxane, 1,3-bis(chloromethyl)-1,1,3,3-tetramethyl-	153	205.6	205.10	406.66	47.34	158.70	91.00	83.24	99.76	3.67
2-Propanamine, N,N'-methanetetraylbis-	111	270.8	3.02	6.33	0.75	2.49	1.41	1.28	1.53	3.99
Trifluoromethyl-bis-(trimethylsilyl)methyl ketone	187	225.9	1.45	2.96	0.34	1.12	0.66	0.57	0.76	4.12
Unknown 12	170	212.35	1.21	2.49	0.26	0.88	0.54	0.52	0.55	4.18
Unknown 7	86	205.85	6.34	12.31	1.46	4.90	2.78	1.61	3.19	4.24
2,4,4-Trimethyl-1-hexene	71	226.15	20.24	39.42	4.64	15.95	9.21	8.11	9.87	4.58
Cyclohexane, 1-methyl-2-propyl-	97	214.6	25.08	50.40	5.78	19.63	11.12	10.12	12.04	4.68
N-Ãă-Acetyl-L-Lysine, N,N-trimethylsilyl-, trimethylsilyl ester	174	857.8	0.08	0.13	0.03	0.11	0.04	0.14	20.43	4.69
9-Eicosyne	97	766.85	2.78	5.46	0.63	2.16	1.23	1.12	1.48	4.76
Unknown 11	83	212.05	26.69	53.03	6.14	20.54	11.85	10.69	12.63	4.89
Cyclotetrasiloxane, octamethyl-	281	255.1	1.77	3.99	0.46	1.54	0.88	0.78	0.99	4.92
Unknown 24	137	246.8	0.65	1.34	0.15	0.53	0.30	0.27	0.32	4.96
trans-2,4-Dimethylthiane, S,S-dioxide	56	253.8	9.02	19.91	2.34	8.76	4.32	4.54	4.70	5.01
Unknown 34	71	267.8	1.55	3.23	0.37	1.32	0.76	0.70	0.66	5.16
3-Isopropyl-5-methyl-hex-4-en-2-one:2	85	260.75	1.71	3.73	0.43	1.51	0.84	0.77	0.90	5.19
Cyclopentane, 2-isopropyl-1,3-dimethyl-	97	238.15	12.19	24.41	2.80	9.67	5.48	4.93	5.83	5.51

Silanamine, N-methoxy-1,1,1-trimethyl-N-(trimethylsilyl)-:2	150	220.3	16.38	32.58	4.01	10.73	7.64	5.25	7.62	5.76
Unknown 90	287	851.85	0.25	0.50	0.06	0.21	0.11	0.11	0.13	5.77
Benzoic acid, 3,5-bis(1,1-dimethylethyl)-4-hydroxy-, methyl ester	249	978.4	5.54	10.83	1.27	4.30	2.46	2.28	3.52	6.08
4-Decene, 6-methyl-, (E)-	97	245.2	7.39	14.95	1.70	5.90	3.36	2.98	3.54	6.14
Hept-2-ene, 2,4,4,6-tetramethyl-:2	97	281.2	0.90	1.88	0.22	0.75	0.41	0.37	0.46	6.19
Unknown 59	99	501.2	1.44	2.83	0.30	1.12	0.61	0.67	0.70	6.41
Unknown 2	149	198.8	8.29	16.85	1.97	7.13	3.67	3.67	4.60	6.45
Butane, 1,2,3-tris(trimethylsiloxy)-	117	846.85	1.11	1.86	0.44	1.19	1.05	0.89	1.56	6.57
6-Isopropyl-2,3-dihydropyran-2,4-dione	154	252.6	3.08	6.57	0.75	2.10	1.51	1.41	1.70	6.61
Unknown 80	177	792.35	1.02	1.96	0.23	0.78	0.44	0.41	0.55	6.63
4-Octene, 2,3,6-trimethyl-	125	259.8	0.71	1.58	0.18	0.64	0.36	0.33	0.38	6.64
Unknown 29	172	254.15	0.32	0.73	0.07	0.25	0.15	0.14	0.14	7.30
Mesalamine	108	206.3	2.41	4.81	0.54	1.82	1.08	0.94	1.17	7.43
3-Isopropyl-5-methyl-hex-4-en-2-one	111	258.65	5.96	13.36	1.52	5.23	2.89	2.65	3.13	7.50
Unknown 66	110	617.15	0.98	2.01	0.24	0.86	0.47	0.45	0.61	8.07
Benzoic acid, 4-[(2,4-dimethoxy-6-pentylbenzoyl)oxy]-2-methoxy-6-pentyl-, methyl ester	235	797.7	0.31	0.60	0.07	0.24	0.13	0.12	0.17	8.14
Trimethyl[4-(1,1,3,3,-tetramethylbutyl)phenoxy]silane	57	716.6	0.87	1.76	0.20	0.67	0.38	0.35	0.49	8.15
Unknown 30	125	256.5	0.76	1.69	0.20	0.68	0.38	0.34	0.41	8.39

Ribitol, 1,2,3,4,5-pentakis-O-(trimethylsilyl)-:20	446	1217.7	0.02	0.04	0.01	0.02	0.01	0.04	2.17	8.40
Unknown 10	86	210.6	19.79	38.89	4.51	15.02	8.62	7.34	9.88	8.51
L-Proline, 5-oxo-1-(trimethylsilyl)-, trimethylsilyl ester	156	625.25	58.12	58.39	12.81	52.19	23.38	19.66	1243.70	8.58
Unknown 84	161	824.8	0.39	0.75	0.09	0.30	0.17	0.16	0.21	8.75
t-Butyldiphenyl(prop-2-ynyloxy)silane	237	229.35	1.11	2.24	0.25	0.86	0.49	0.44	0.53	8.76
Unknown 13	193	221.1	257.42	502.65	58.95	164.93	113.58	75.86	116.56	8.89
3,6,9,12-Tetraoxa-2,13-disilatetradecane, 2,2,13,13-tetramethyl-	117	618.7	1.08	1.99	0.32	1.03	0.51	0.42	0.79	9.58
Alanine, phenyl-, trimethylsilyl ester, dl-	120	637.05	0.38	0.64	0.55	2.18	0.93	0.74	9.50	9.61
L-Isoleucine, N-(trimethylsilyl)-, trimethylsilyl ester	158	473.7	0.48	0.79	0.35	1.12	0.50	0.43	62.71	10.07
Methyltris(trimethylsiloxy)silane	207	306.75	4.22	8.44	0.96	3.34	1.82	1.73	2.11	10.43
2,4-Thiazolidinedione	117	330.85	0.08	0.14	0.02	0.09	0.04	0.02	2.31	10.55
Unknown 25	70	247.7	1.47	2.88	0.35	1.20	0.59	0.64	0.74	11.11
Silanamine, N,N'-methanetetraylbis[1,1,1-trimethyl-	171	230.75	11.90	20.39	2.75	8.83	4.81	4.05	32.12	11.12

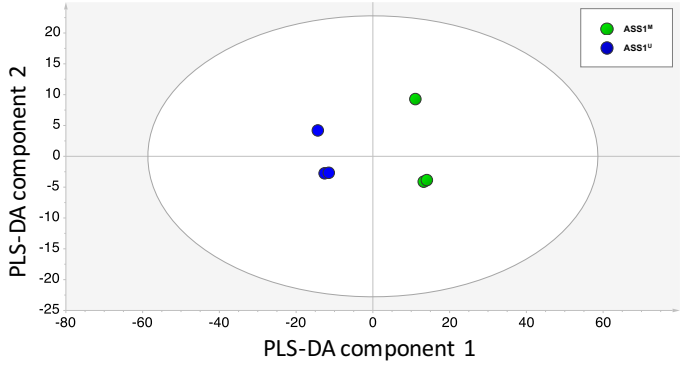
2-Pyrrolidone-5-carboxylic acid, trimethylsilyl ester	84	586.7	17.69	15.83	4.13	13.86	7.05	5.13	85.38	11.54
Isotridecanol-	188	275.55	0.34	0.78	0.09	0.38	0.18	0.14	0.25	11.74
Unknown 118	57	1677.25	3.94	8.47	0.98	3.03	1.72	1.66	2.04	11.76
1,2-Bis(trimethylsiloxy)ethane	191	213.95	1.71	2.49	0.39	1.26	0.75	0.65	0.82	11.78
Unknown 53	174	391.4	0.30	0.61	0.07	0.25	0.14	0.11	0.17	11.86
Unknown 67	77	625.4	1.51	1.72	0.39	1.58	0.78	0.69	34.00	12.11
Unknown 20	237	236.7	3.03	6.01	0.69	2.35	1.34	1.19	1.45	12.35
Unknown 1	144	197.6	223.32	443.69	51.21	164.33	103.14	77.89	105.59	12.44
Unknown 31	160	256.8	0.67	1.49	0.17	0.57	0.33	0.28	0.35	12.44
l-Threonine, O-(trimethylsilyl)-, trimethylsilyl ester	130	466.8	0.16	0.27	1.17	5.43	2.12	1.52	11.73	13.01
Malonic acid, bis(2-trimethylsilylethyl ester	204	247.3	1.23	2.61	0.28	0.94	0.56	0.45	0.60	13.18
Unknown 4	197	199.55	0.91	2.01	0.23	0.73	0.44	0.32	0.44	13.36

Unknown 40	112	294.1	0.71	1.57	0.18	0.65	0.34	0.31	0.55	13.39
L-Valine, N-(trimethylsilyl)-, trimethylsilyl ester	144	413.1	1.23	2.16	0.57	1.85	0.79	0.73	124.58	15.09
Urea, N,N'-bis(trimethylsilyl)-	171	407.15	0.29	0.45	0.09	0.32	0.11	0.17	37.34	15.12
Glycine, N-(trimethylsilyl)-, trimethylsilyl ester	102	332.8	1.13	0.99	0.50	1.47	0.55	0.33	6.82	15.15
Unknown 60	245	503.3	0.20	0.20	0.10	0.27	0.10	0.07	0.34	15.45
1,2-Bis(trimethylsiloxy)ethane:2	69	293.65	5.05	10.13	1.20	4.07	2.18	2.04	7.85	15.93
Silanamine, 1,1,1-trimethyl-N-(trimethylsilyl)-	119	358.85	0.67	1.38	0.16	0.52	0.30	0.25	0.24	16.40
Unknown 9	97	208.2	1.75	3.41	0.36	1.36	0.79	0.70	0.74	16.67
n-Butylamine, N,N-bis(trimethylsilyl)	128	333.75	0.19	0.46	0.05	0.32	0.11	0.12	0.19	17.61
DL-Malic acid, O-trimethylsilyl-, bis(trimethylsilyl) ester	233	617.9	0.24	0.20	0.15	0.43	0.13	0.08	0.29	18.08
l-Valine, trimethylsilyl ester	72	304.7	2.78	6.02	1.31	5.22	1.96	2.18	95.72	18.19
Cyclohexane, 1-ethyl-1,3-dimethyl-, cis-	111	236.1	5.87	11.82	1.33	4.51	2.72	2.18	2.69	18.25

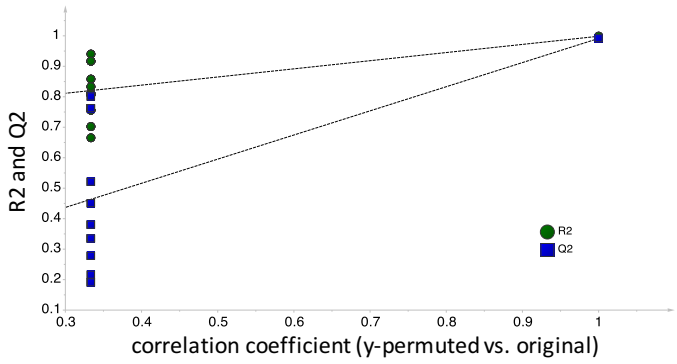
N-Acetyl glucosamine methoxime, tetrakis(trimethylsilyl)	61	1227.1	0.84	1.72	0.20	0.69	0.40	0.36	1.15	18.37
1,2-Benzenedicarboxylic acid, diisooctyl ester	149	1197.8	2.15	4.35	0.52	1.58	1.01	1.01	0.62	19.34
Acetamide, 2,2,2-trifluoro-N-methyl-N-(trimethylsilyl)-	134	283.6	0.37	0.97	0.11	0.41	0.15	0.12	0.29	19.50
Unknown 68	185	643.85	0.03	0.03	0.01	0.02	0.01	0.01	0.17	20.10
Ãą-Alanine, N,N-bis(trimethylsilyl)-, trimethylsilyl ester	174	574.65	0.12	0.06	0.11	0.64	0.37	0.36	0.33	20.56
Pentasiloxane, dodecamethyl-:2	73	444.45	0.73	1.21	0.20	0.84	0.25	0.65	1.03	21.09
Benzoic acid trimethylsilyl ester	179	417.75	0.90	1.87	0.21	0.70	0.37	0.39	0.88	21.63
Unknown 17	152	232.7	2.00	4.39	0.49	1.73	0.93	0.88	1.30	22.11
Unknown 32	162	257.55	0.97	2.09	0.23	0.54	0.44	0.27	0.41	23.17
Cholesterol trimethylsilyl ether	129	1468.9	6.32	9.27	3.60	13.01	5.29	4.48	3.48	23.57
l-Leucine, trimethylsilyl ester	86	354.15	0.94	2.01	0.94	3.87	1.68	1.52	49.87	23.64
Glycoside, Ãă-methyl-trtrakis-O-(trimethylsilyl)-	204	983.2	0.06	0.06	0.03	0.06	0.04	0.16	45.78	23.74

d-Galactose, 2,3,4,5,6-pentakis-O-(trimethylsilyl)-, o-methyloxyme, (1E)-	217	912.4	1.18	1.03	0.56	1.38	0.94	4.13	628.10	23.88
Unknown 70	89	665.2	0.07	0.07	0.05	0.16	0.09	0.06	1.03	24.32
Pentasiloxane, dodecamethyl-	281	401.3	2.05	3.65	0.40	1.39	0.74	0.72	2.92	25.00
Silanamine, 1,1,1-trimethyl-N-(trimethylsilyl)-N-[2-[(trimethylsilyl)oxy]ethyl]-	174	428.85	29.73	60.54	5.85	19.79	12.82	12.10	10.78	25.44
L-Leucine, N-(trimethylsilyl)-, trimethylsilyl ester	158	456.25	0.47	0.79	0.33	1.10	0.56	0.42	49.97	26.41
Propanedioic acid, (acetylamino)methyl-, diethyl ester	116	239.2	0.69	1.24	0.14	0.46	0.29	0.22	0.28	27.00
Unknown 71	185	665.35	0.09	0.09	0.03	0.12	0.05	0.03	0.91	27.13
Butanedioic acid, bis(trimethylsilyl) ester	247	474.4	0.07	0.12	0.02	0.06	0.02	0.02	1.42	27.66
Unknown 95	172	912.75	0.06	0.05	0.03	0.07	0.05	0.20	70.51	27.91
Glycine, N,N-bis(trimethylsilyl)-, trimethylsilyl ester	174	484.6	12.59	13.20	3.72	15.38	4.71	3.85	57.46	30.49

A.2. Appendix to section A.2: GC/TOF MS: Metabolic characterisation of ASS1 GBM subtypes



(a)



(b)

Figure A.1.: GC/TOF MS: PLS-DA and permutation test of $\mathbf{ASS1^M}$ and $\mathbf{ASS1^U}$ media at basal levels. (a) PLS-DA was used to investigate the metabolic profiles of $ASS1^M$ (SNB19) and $ASS1^U$ (U87) cells from the cell media at basal levels. (b) Permutation test (100 permutations) was used for validating PLS-DA model, as determined here, where Q^2 values of permuted data were higher than those of the original data sets and Q^2 values trending towards intersection of the y-axis below zero.

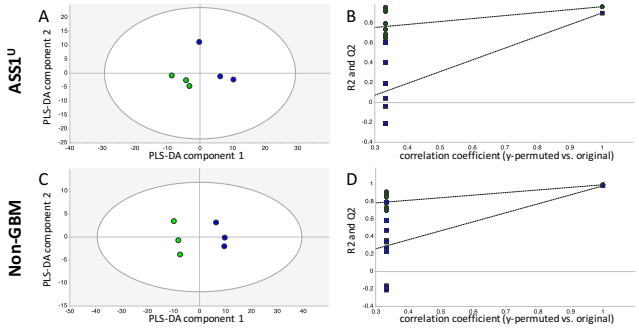


Figure A.2.: GC/TOF MS: Cell extract PLS-DA plots and permutation validation upon ADI-PEG20 treatment. PLS-DA plots (left) and y-permuted model validation (right) for group comparison of treated (ADI-PEG20, 1μg/ml) versus non-treated cell line samples. Showing ASS1$^{\mathrm{U}}$ (U87, figure A and B) and non-GBM (astrocytes, figure C and D) group comparison.

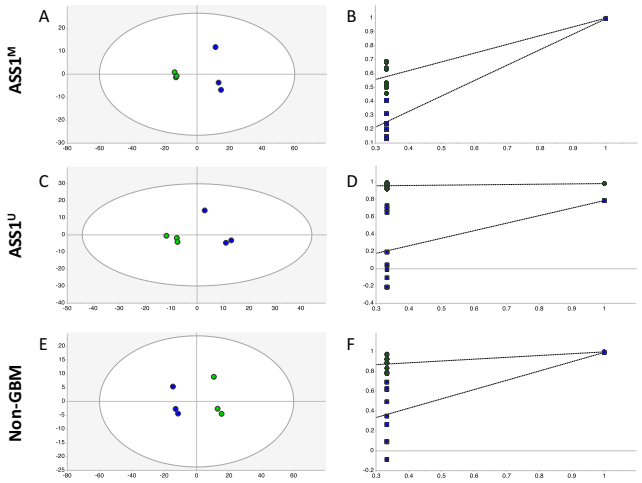


Figure A.3.: GC/TOF MS: Cell media PLS-DA plots and permutation validation upon ADI-PEG20 treatment PLS-DA plots (left) and Y-permuted model validation (right) for group comparison of treated (ADI-PEG20, 1μg/ml) versus non-treated cell line samples. Showing ASS1$^{\mathrm{M}}$ (SNB19, figure A and B), ASS1$^{\mathrm{U}}$ (U87, figure C and D) and non-GBM (astrocyte, figure E and F) group comparison.

A.3. Appendix to section 3.2.6: ^{1}H NMR: Complementary metabolic characterisation of ASS1 GBM subtypes

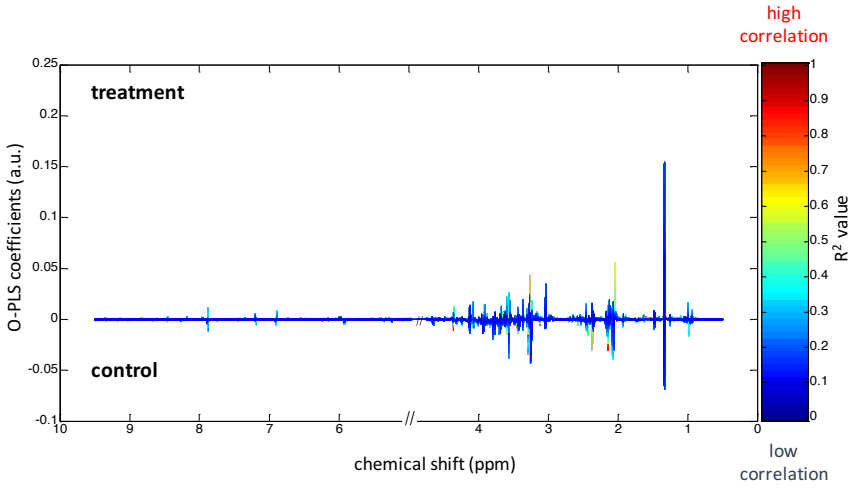


Figure A.4.: Extract ^{1}H NMR: OPLS-DA correlation coefficient plot of ASS1^{U} control versus treatment. OPLS-DA correlation coefficient plot from ^{1}H NMR spectra in ASS1^{U} (U87) cells harvested at 48 hours. Comparison of control and ADI-PEG20 treated (1μg/ml) cell extract samples ($n = 3$), showing discriminatory metabolites as indicated by colour scale of Pearson correlation coefficient R^2, where red indicated strong correlation and blue poor correlation. Upward pointing peaks are positively correlated with treated samples and downward pointing peaks are positively correlated with control samples. Probabilistic quotient normalised. Probabilistic quotient normalised. Cumulative values R^2=0.988 and Q^2=0.035. Key: A.u (arbitrary units), ppm (parts per million).

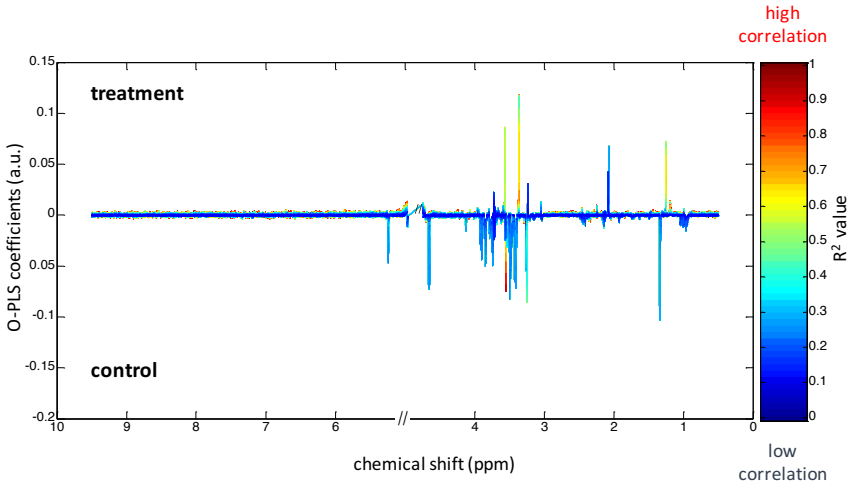


Figure A.5.: Extract ^{1}H NMR: OPLS-DA correlation coefficient plot of non-GBM control versus treatment. OPLS-DA correlation coefficient plot from ^{1}H NMR spectra in non-GBM (astrocyte) cells harvested at 48 hours. Comparison of control and ADI-PEG20 treated (1μg/ml) cell extract samples ($n = 3$), showing discriminatory metabolites as indicated by colour scale of Pearson correlation coefficient R^2, where red indicated strong correlation and blue poor correlation. Upward pointing peaks are positively correlated with treated samples and downward pointing peaks are positively correlated with control samples. Probabilistic quotient normalised. Cumulative values R^2=0.072 and Q^2=0.387. Key: A.u (arbitrary units), ppm (parts per million).

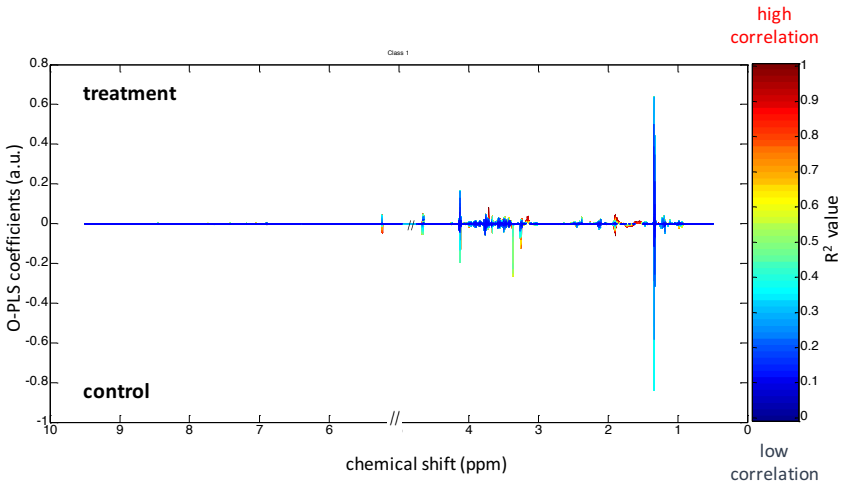


Figure A.6.: Media ^{1}H NMR: OPLS-DA correlation coefficient plot of ASS1^{U} control versus treatment. OPLS-DA correlation coefficient plot from ^{1}H NMR spectra in ASS1^{M} (U87) cells harvested at 48 hours. Comparison of control and ADI-PEG20 treated (1μg/ml) cell media samples ($n = 3$), showing discriminatory metabolites as indicated by colour scale of Pearson correlation coefficient R^2, where red indicated strong correlation and blue poor correlation. Upward pointing peaks are positively correlated with treated samples and downward pointing peaks are positively correlated with control samples. Probabilistic quotient normalised. Cumulative values R^2=0.987 and Q^2=0.685. Key: A.u (arbitrary units), ppm (parts per million).

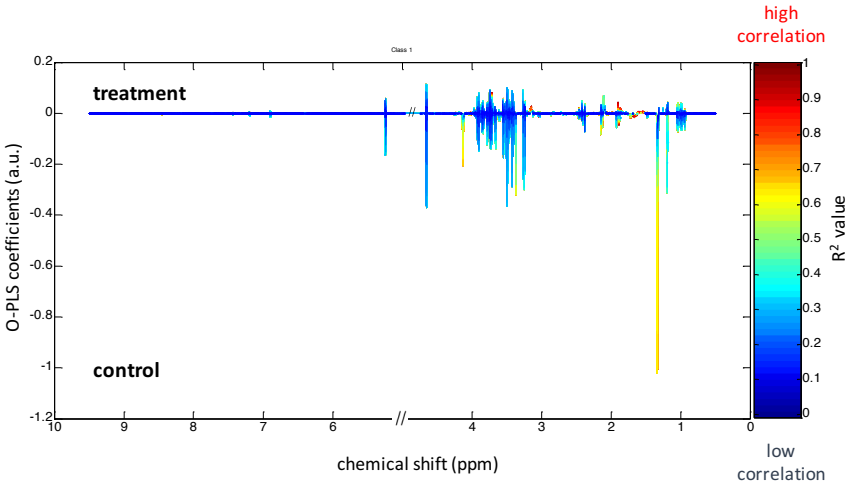


Figure A.7.: Media ^{1}H NMR: OPLS-DA correlation coefficient plot of non-GBM control versus treatment. OPLS-DA correlation coefficient plot from ^{1}H NMR spectra in non-GBM (astrocyte) cells harvested at 48 hours. Comparison of control and ADI-PEG20 treated (1μg/ml) cell media samples ($n = 3$), showing discriminatory metabolites as indicated by colour scale of Pearson correlation coefficient R^2, where red indicated strong correlation and blue poor correlation. Upward pointing peaks are positively correlated with treated samples and downward pointing peaks are positively correlated with control samples. Probabilistic quotient normalised. Probabilistic quotient normalised. Cumulative values R^2=0.991 and Q^2=0.534. Key: A.u (arbitrary units), ppm (parts per million).

A.4. Appendix to section 3.2.10: Validation of trends in ASS1 GBM subtypes via ^{1}H NMR analysis

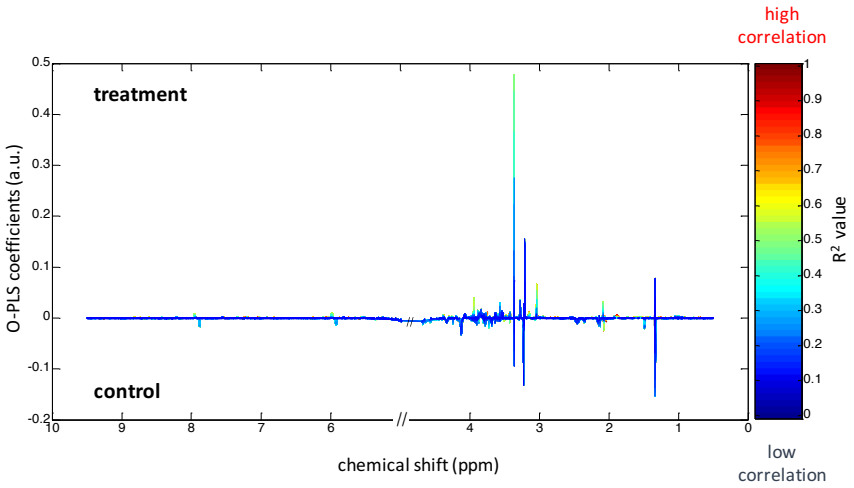


Figure A.8.: ^{1}H NMR validation: OPLS-DA correlation coefficient plot of U87 extract. OPLS-DA correlation coefficient plot from ^{1}H NMR spectra in ASS1^{U} (U87) cells harvested at 48 hours. Comparison of control and ADI-PEG20 treated (1μg/ml) cell extract samples (n = 9), showing discriminatory metabolites as indicated by colour scale of Pearson correlation coefficient R^2, where red indicated strong correlation and blue poor correlation. Upward pointing peaks are positively correlated with treated samples and downward pointing peaks are positively correlated with control samples. Probabilistic quotient normalised. Cumulative values R^2=0.990 and Q^2=0.247. Key: A.u (arbitrary units), ppm (parts per million).

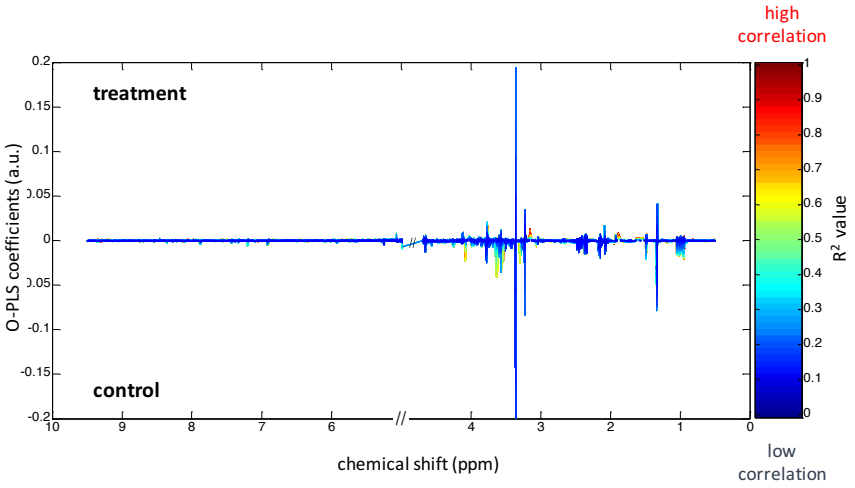


Figure A.9.: ^{1}H NMR validation: OPLS-DA correlation coefficient plot of U118 extract. OPLS-DA correlation coefficient plot from ^{1}H NMR spectra in ASS1^{U} (U118) cells harvested at 48 hours. Comparison of control and ADI-PEG20 treated (1μg/ml) cell extract samples ($n = 9$), showing discriminatory metabolites as indicated by colour scale of Pearson correlation coefficient R^2, where red indicated strong correlation and blue poor correlation. Upward pointing peaks are positively correlated with treated samples and downward pointing peaks are positively correlated with control samples. Probabilistic quotient normalised. Probabilistic quotient normalised. Cumulative values R^2=0.963 and Q^2=0.168. Key: A.u (arbitrary units), ppm (parts per million).

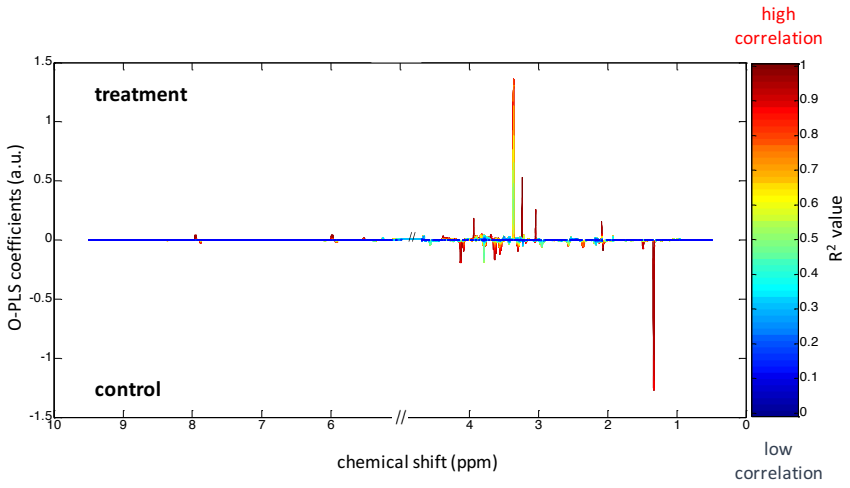


Figure A.10.: ^{1}H NMR validation: OPLS-DA correlation coefficient plot of GAMG extract. OPLS-DA correlation coefficient plot from ^{1}H NMR spectra in ASS1^{M} (GAMG) cells harvested at 48 hours. Comparison of control and ADI-PEG20 treated (1μg/ml) cell extract samples ($n = 9$), showing discriminatory metabolites as indicated by colour scale of Pearson correlation coefficient R^2, where red indicated strong correlation and blue poor correlation. Upward pointing peaks are positively correlated with treated samples and downward pointing peaks are positively correlated with control samples. Probabilistic quotient normalised. Probabilistic quotient normalised. Cumulative values R^2=0.982 and Q^2=0.813. Key: A.u (arbitrary units), ppm (parts per million).

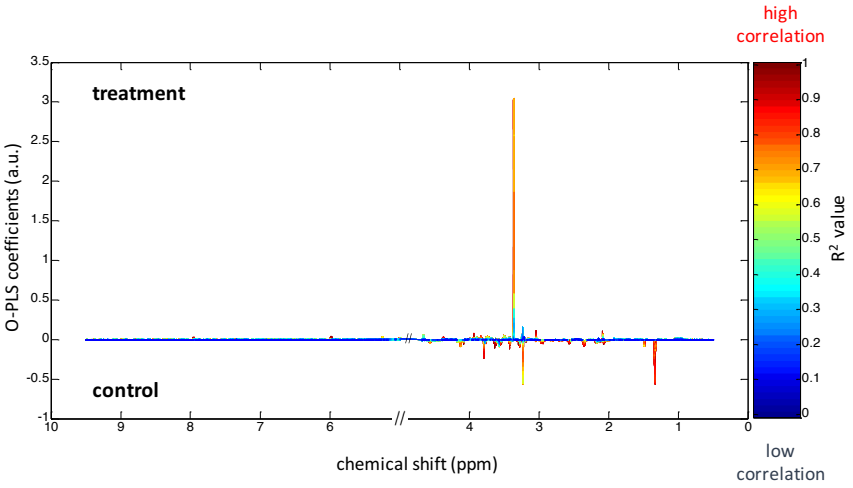


Figure A.11.: ^{1}H NMR validation: OPLS-DA correlation coefficient plot of LN229 extract. OPLS-DA correlation coefficient plot from ^{1}H NMR spectra in ASS1^{M} (LN229) cells harvested at 48 hours. Comparison of control and ADI-PEG20 treated (1μg/ml) cell extract samples (n = 9), showing discriminatory metabolites as indicated by colour scale of Pearson correlation coefficient R^2, where red indicated strong correlation and blue poor correlation. Upward pointing peaks are positively correlated with treated samples and downward pointing peaks are positively correlated with control samples. Probabilistic quotient normalised. Probabilistic quotient normalised. Cumulative values R^2=0.988 and Q^2=0.823. Key: A.u (arbitrary units), ppm (parts per million).

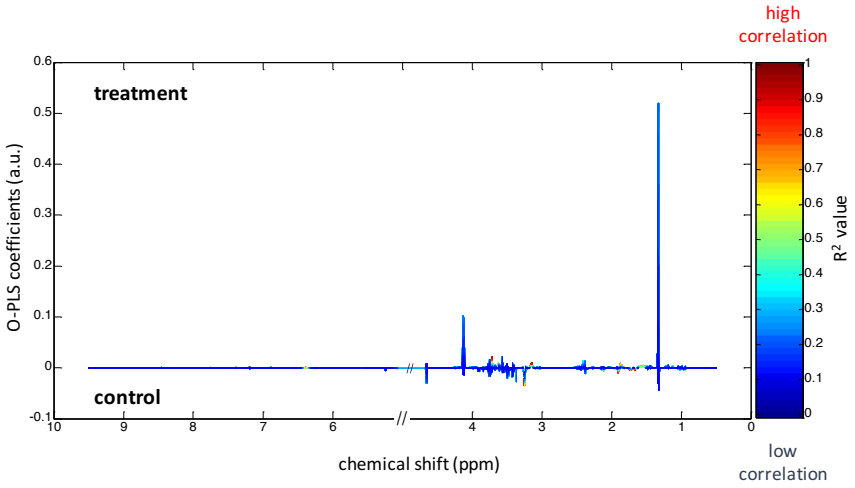


Figure A.12.: ^{1}H NMR validation: OPLS-DA correlation coefficient plot of U87 media. OPLS-DA correlation coefficient plot from ^{1}H NMR spectra in ASS1^{U} (U87) cells harvested at 48 hours. Comparison of control and ADI-PEG20 treated (1μg/ml) cell media samples (n = 9), showing discriminatory metabolites as indicated by colour scale of Pearson correlation coefficient R^2, where red indicated strong correlation and blue poor correlation. Upward pointing peaks are positively correlated with treated samples and downward pointing peaks are positively correlated with control samples. Probabilistic quotient normalised. Probabilistic quotient normalised. Cumulative values R^2=0.936 and Q^2=0.655. Key: A.u (arbitrary units), ppm (parts per million).

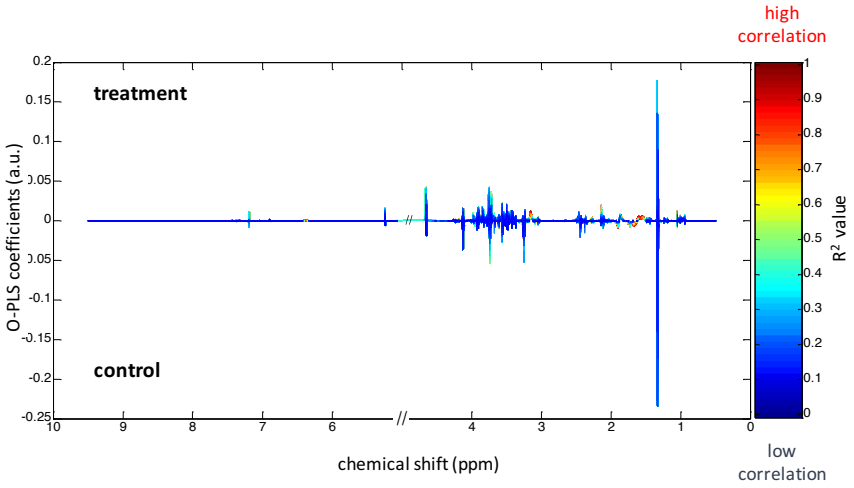


Figure A.13.: ^{1}H NMR validation: OPLS-DA correlation coefficient plot of U118 media. OPLS-DA correlation coefficient plot from ^{1}H NMR spectra in ASS1^U (U118) cells harvested at 48 hours. Comparison of control and ADI-PEG20 treated (1μg/ml) cell media samples (n = 9), showing discriminatory metabolites as indicated by colour scale of Pearson correlation coefficient R^2, where red indicated strong correlation and blue poor correlation. Upward pointing peaks are positively correlated with treated samples and downward pointing peaks are positively correlated with control samples. Probabilistic quotient normalised. Probabilistic quotient normalised. Cumulative values R^2=0.916 and Q^2=0.536. Key: A.u (arbitrary units), ppm (parts per million).

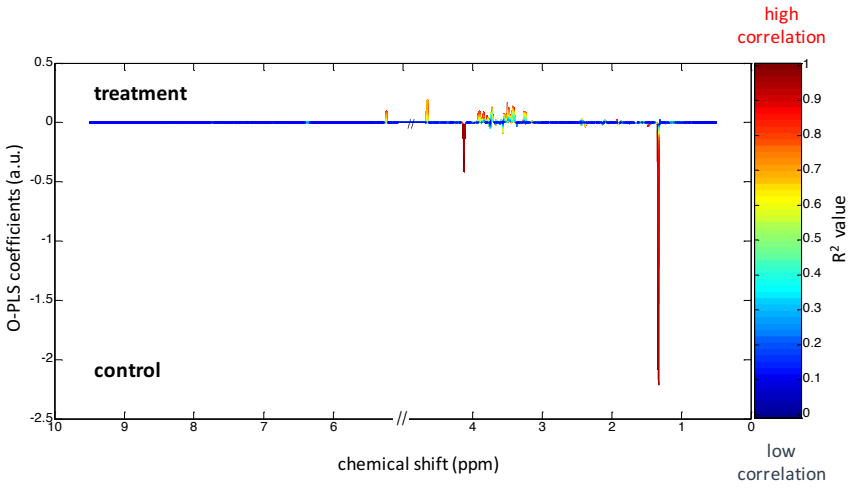


Figure A.14.: ^{1}H NMR validation: OPLS-DA correlation coefficient plot of GAMG media. OPLS-DA correlation coefficient plot from ^{1}H NMR spectra in ASS1^{M} (GAMG) cells harvested at 48 hours. Comparison of control and ADI-PEG20 treated (1μg/ml) cell media samples ($n = 9$), showing discriminatory metabolites as indicated by colour scale of Pearson correlation coefficient R^2, where red indicated strong correlation and blue poor correlation. Upward pointing peaks are positively correlated with treated samples and downward pointing peaks are positively correlated with control samples. Probabilistic quotient normalised. Probabilistic quotient normalised. Cumulative values R^2=0.975 and Q^2=0.838. Key: A.u (arbitrary units), ppm (parts per million).

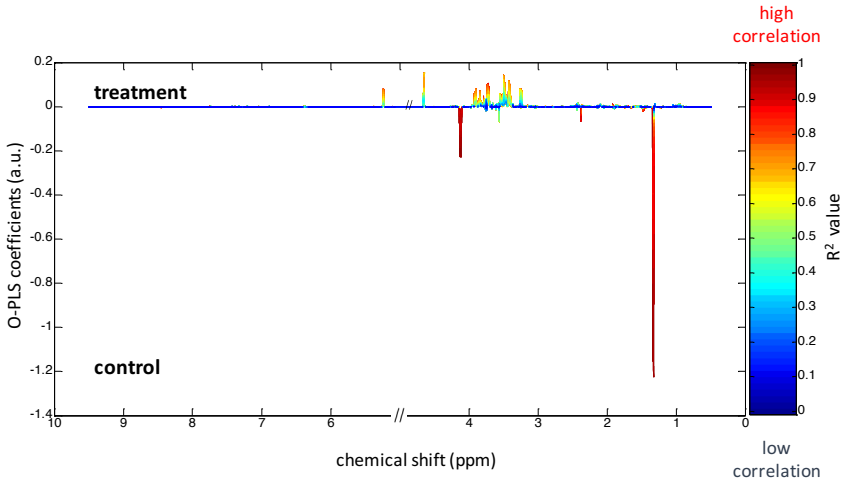


Figure A.15.: ^{1}H NMR validation: OPLS-DA correlation coefficient plot of LN229 media. OPLS-DA correlation coefficient plot from ^{1}H NMR spectra in ASS1^{M} (LN229) cells harvested at 48 hours. Comparison of control and ADI-PEG20 treated (1μg/ml) cell media samples (n = 9), showing discriminatory metabolites as indicated by colour scale of Pearson correlation coefficient R^2, where red indicated strong correlation and blue poor correlation. Upward pointing peaks are positively correlated with treated samples and downward pointing peaks are positively correlated with control samples. Probabilistic quotient normalised. Probabilistic quotient normalised. Cumulative values R^2=0.978 and Q^2=0.863. Key: A.u (arbitrary units), ppm (parts per million).

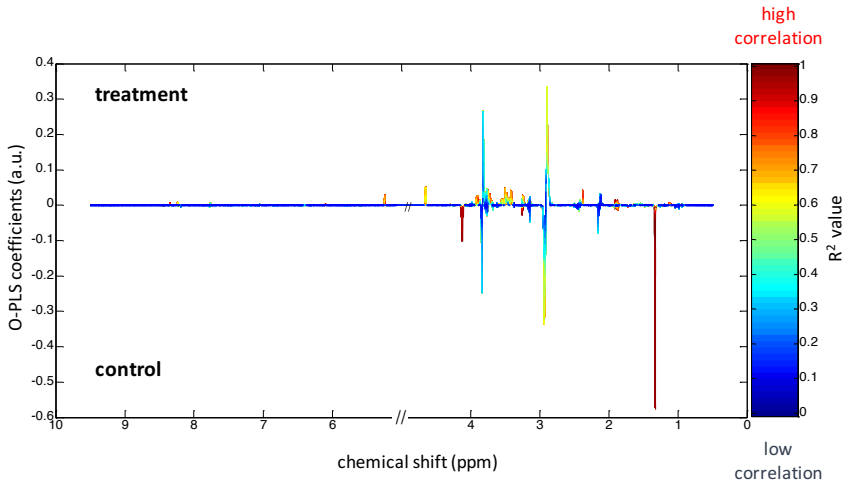


Figure A.16.: ^{1}H NMR validation: OPLS-DA correlation coefficient plot of astrocyte media. OPLS-DA correlation coefficient plot from ^{1}H NMR spectra in non-GBM (astrocyte) cells harvested at 48 hours. Comparison of control and ADI-PEG20 treated (1μg/ml) cell media samples ($n = 9$), showing discriminatory metabolites as indicated by colour scale of Pearson correlation coefficient R^2, where red indicated strong correlation and blue poor correlation. Upward pointing peaks are positively correlated with treated samples and downward pointing peaks are positively correlated with control samples. Probabilistic quotient normalised. Probabilistic quotient normalised. Cumulative values R^2=0.976 and Q^2=0.914. Key: A.u (arbitrary units), ppm (parts per million).